

# Signal and Spectrum Coordination for Next Generation DSL Networks

**Rodrigo B. Moraes**

Dissertation presented in partial  
fulfillment of the requirements for the  
degree of Doctor in Engineering  
Science

January 2014



# Signal and Spectrum Coordination for Next Generation DSL Networks

**Rodrigo B. MORAES**

Supervisory Committee:  
Prof. dr. ir. Y. Willems, chair  
Prof. dr. ir. M. Moonen, supervisor  
Dr. ir. P. Tsiiaflakis, co-supervisor  
Prof. dr. ir. G. Gielen  
Prof. dr. ir. S. Pollin

Prof. dr. ir. P. Ödling  
(Lund University)  
Prof. dr. ir. M. Moeneclaey  
(UGent)  
Dr. J. Maes  
(Alcatel-Lucent Bell Labs)

Dissertation presented in partial  
fulfillment of the requirements for  
the degree of Doctor  
in Engineering Science

January 2014

© KU Leuven – Faculty of Engineering Science  
Kasteelpark Arenberg 10 postbus 2440, B-3001 Heverlee (Belgium)

Alle rechten voorbehouden. Niets uit deze uitgave mag worden vermenigvuldigd en/of openbaar gemaakt worden door middel van druk, fotocopie, microfilm, elektronisch of op welke andere wijze ook zonder voorafgaande schriftelijke toestemming van de uitgever.

All rights reserved. No part of the publication may be reproduced in any form by print, photoprint, microfilm or any other means without written permission from the publisher.

D/2014/7515/15  
ISBN 978-94-6018-791-9

# Preface

The plot is well-known. This one starts in October 2009: A newly graduated Masters student arrives in the city of Leuven for a period of four years. In his overweight luggage, a local map, some Engineering books and some rather inadequate clothing for the local weather. In his head, the ambition to do a PhD at the KU Leuven. In his pocket... well, not much.

That was four years ago. I won't even bother to say that it was kind of tough in the beginning. Coming to live in a country for four years where you do not know a living soul and where you do not speak the local language (initial inquiries included "Why do they have some many buses going to *Geen Dienst* if nobody ever wants to go there?") is not always a walk in the park. Fortunately, I am not the kind of person to say no to an adventure, especially to this kind of adventure. Doing a PhD had been my dream and ambition ever since I took the first timid steps in the world of research. KU Leuven was my absolute favorite place to come. And here I am now, affirming with all my conviction that these four years have been some of the most rewarding, interesting and fun years in my life so far. It is now the time to thank the people who have contributed to this.

The first thanks is rather abstract. I would like to thank the city of Leuven, which I have learned to love and care about to the point that I find myself speaking of "We in Leuven" when introducing the city to foreign friends. I like to see the lights in the Oude Markt at night, I like the pubs and restaurants (all hail the Namaste!), I like to be nice and cosy at home when there is snow outside and I like the Arenberg campus. Wherever I go, these places will always be warmly remembered.

My promotor Marc Moonen has been a constant source of ideas and inspiration throughout my PhD, and I owe him enormously. It is a great pleasure to work with Marc and I have learned continuously. I thank him for trusting in me since the very beginning, for the continued support and for putting me back on

the right track when it was necessary (I can think of a few moments here). Our discussions have been extremely fruitful, his attention to detail has improved my papers greatly and your experience in making difficult decisions has not failed me once.

I am extremely grateful to my co-promotor, Paschalis Tsiaflakis. Throughout the PhD, Paschal was the person I turned to when I needed advice in both small and large matters. Without his experience and assistance, this whole project would have been much more difficult. He was a source of tranquility during turbulent times and a source of enthusiasm when new ideas surfaced. Our technical discussions have sometimes saved me 6 months of dead end research. That just cemented the respect I have for Paschal as a professional. Our non-technical discussion have been great, and I am happy to be able to count Paschal not only as my co-promotor, but also as a dear friend.

I am grateful to the members of the committee for reading this text and for providing suggestions and criticism that certainly have made this work improve in a number of ways. Prof. G. Gielen, Prof. S. Pollin, Prof. P. Ödling, Prof. M. Moeneclae and Dr. J. Maes, thank you.

During the course of the PhD I have been warmly welcomed in the beautiful city of Vienna by Martin Wolkerstorfer and Driton Statovci. Big thanks to the two of you. I enjoyed all the Wiener Schnitzels I had (yes, that is a plural) and I appreciated the various technical discussions we had on the black board. I had a great time in my visit to FTW and the research results were top notch.

This preface would be impossible without mentioning Aldebaro Klautau. It all began there, in a warm summer afternoon when we met in the Signal Processing laboratory at UFPA and I almost immediately had (kind of) a research assistant position in one of his projects. His energy, competence and trust in me have made a huge impact in my career. I owe a lot to the opportunities that were offered to me by him. Cheers to my friends from the good old days of UFPA, Guillermo, Marcel and Müller.

I thank Raimundo Sampaio for so much during our collaboration of a little bit more than one year. I have gained a lot of scientific maturity at that time, and his passion for teaching and tutoring are always remembered. The people of CETUC were wonderful, with special mentions to Aline, Fabian, Mauro and Tiago.

A score of friends have made my life in this city not only rewarding but also very pleasant. I thank Joelle, my oldest friend in Leuven, and Wouter, a fan of river monsters, for the epic Pictionary battles; Joe and Goele (whose getting together was so painstakingly planned), for having helped me defend my girl's honor; Els and Adrian, for the inimitable taste in pants; Bruno, for going into

a concert with me without paying; Gabriel, for the good old party days; and Aldona, for making me a crocodile slayer in the eyes of her son.

I thank my colleagues for making such a pleasant and involving work environment. Alexander, Amin, Amir, Beier, Bram, Enzo (hope you don't regret the iPad), Gert ('the legend'), Giacomo, Giuliano (sorry for never coming to the Italian party), Javier (previous football superstar), Hanne, Jorge (thanks for all those goals), Kim (who introduced me to Belgian beer), Kristian, Marijn, Nejem, Niccolo, Pepe, Rodolfo (thanks for all those goals, sorry for the blanket), Toon (thanks for all the info about your pets and the tools) and Wouter, I enjoyed our nights out, our end-of-the-year steaks (keep the tradition alive!), our lunches in Alma, our coffee breaks, the birthday cakes, the parties, the conferences and so many more moments. And I say three cheers for the finally victorious DSP football team!

*Agradeço a minha família, em especial meus pais e meus irmãos. Sem o apoio e o carinho de vocês eu nunca teria chegado aqui. Como sempre, agradeço em especial a minha mãe. Mãe, és de longe a pessoa que mais contribuiu para o meu sucesso. Sempre estiveste comigo nas horas em que precisava, não importa o quão difícil era estar lá. Sempre me estendeste a mão com carinho e amor quando eu mais precisei. Sempre me ensinaste a ter ambição e disciplina, a me esforçar e a acreditar em mim. Essas lições formaram meu caráter, e carrego-as em mim todo o tempo. São elas que me fizeram chegar até aqui.*

*De Vandenbussches waren het beste surrogaat-gezin dat ik mij kon indenken. Frits, Lien en Wannes, bedankt voor de gastvrijheid, de vriendschap, de zorg, het eten, de roddels, de uitstapjes, de tamdems, de gezelschapsspelletjes, de bezoeken in Leuven en zo veel meer.*

Finally, there are no words to thank Inge. This whole project would have been so much more difficult without her. She was the one who picked me up when I was down and pulled me down when my feet left the ground. She came to the office to work with me so that I would not get bored. She discovered the big cat lover in me. She shares rainy days and sunny days, and the good thing is that with her both of them end up being fun. This thesis pales in comparison to my greatest achievement during these four years, which is to have met her.

Rodrigo B. Moraes

January 2014



# Abstract

The ability to easily exchange and access data has transformed the way we work, study, inform and entertain ourselves. In particular, the Internet has had an effect on people's lives in the past two decades that is profound.

Profound as this effect may be, people seem not to grow tired of it. On the contrary: as of today, the Internet revolution is far from over. The thirst for bigger amounts of data at higher speeds and ubiquitous connectivity seem not to abate.

This thirst for more, faster and better quality data is both a huge challenge and a huge opportunity for the broadband access industry. The opportunity lies on the fact that, as of the end of 2012, there were 600 million subscribers to broadband services around the world. Plus, even though the market is already enormous, it still has big growth potential. The challenge lies on the connections between the network backbone and the user, the so-called *local loop*. In the local loop the network thins out and usually consists of lower quality channels in comparison to the network backbone.

Of the technologies currently available to bridge this local loop, digital subscriber lines (DSL) is by far the market leader. This technology uses twisted copper pairs, the same used for decades for standard telephony services. If on the plus side the telephone network infrastructure is ubiquitous through the globe, making costs of installation very small, on the minus side DSL operates in a medium not initially designed for broadband communications. One of the consequences of this is severe levels of multi-user interference, commonly known as crosstalk.

In this thesis, we develop signal and spectrum coordination techniques that aim at avoiding, minimizing or even profiting from crosstalk. The collection of these techniques is commonly known in the literature as dynamic spectrum management (DSM). DSM has repeatedly been shown to provide formidable gains in the performance of DSL networks. It is an enabler for next generation

DSL services and it is the unifying topic of this thesis.

In Part I of this thesis, we focus on spectrum coordination. Here we focus on a single input, single output (SISO) interference channel. The goal is to come up with a fair power allocation through frequency so that every user strikes a balance between maximizing its own data rate and minimizing interference to others. We propose two algorithms for the solution of the weighted rate sum maximization problem subject to per-user power constraints. Both approaches start with the re-writing of the problem with different variables. The classical way to represent the design variables of this problem is with cartesian vector coordinates, where each position of the vector denotes the power allocation of one user. We use spherical coordinates, which consists of representing the design variables with a radius and a direction vector with a norm constraint. Spherical coordinates allow us to find a surprising amount of structure in this problem, which can be used to save considerably on computational complexity. Our first proposed algorithm can be up to 100 times faster than the relevant previous proposal. Our second algorithm is 2-15 times faster than the relevant previous proposal.

In Part II, we focus on combined signal and spectrum coordination. First, we focus on a scenario that is referred to as the discrete multitone multiple-input, multiple-output interference channel (DMT MIMO IC). This scenario consists of multiple interfering users, each operating a distinct number of transceivers as a MIMO system. Coordination is done both on the signal level (with per-user MIMO techniques) and on the spectrum level (with multi-user power allocation). We propose two algorithms for the DMT MIMO IC weighted rate sum maximization problem. We focus both on per-user and on per-transceiver power constraints. In the first algorithm, we profit from recent work showing the close relation between the weighted rate sum maximization problem and the weighted minimum mean squared error (MMSE) minimization problem. We show that with a simple extension, we can adapt the previous work to the scenario of interest. In the second algorithm, the signal and spectrum coordination parts are solved separately. For the signal coordination part, we obtain multiple independent single tone MIMO IC's, which allows us to leverage on the previous work on the topic. For the spectrum coordination part, one of the interesting results of our analysis is a generalization of the waterfilling power allocation formula for the multiple input, multiple output (MIMO) interference channel. This formula takes into account the matrix structure of the channel and includes a penalty for the user that causes excessive interference. Simulation results demonstrate that both algorithms obtain significant gains when compared to pure spectrum coordination algorithms.

Still in Part II, we develop a general system framework that encompasses the whole complexity of DSL networks. Our framework includes every other

previously studied situation as a special case, including all other scenarios mentioned in this thesis. We also propose an algorithm that uses this framework and works for all cases, including any number of users, any number of transceivers, any number of tones, any kind of coordination on both the transmitter and on the receiver sides, and synchronous or asynchronous transmission.



# Beknopte samenvatting

De mogelijkheid om eenvoudig data uit te wisselen en toegang toe te hebben heeft de manier waarop we werken, studeren en informeren veranderd. Het Internet bijvoorbeeld heeft in de afgelopen decennia een diepgaand effect gehad op het leven van mensen.

Hoe diepgaand dit effect ook is, mensen lijken het niet beu te worden. Integendeel: de internetrevolutie is vandaag nog lang niet voorbij. De honger naar grotere hoeveelheden data met hogere snelheden en alomtegenwoordige verbinding vermindert niet.

Deze honger naar meer, snellere en meer kwalitatieve data is zowel een enorme uitdaging als een enorme kans voor de breedband-industrie. Deze kans situeert zich in het feit dat, op het einde van 2012, waren er 600 miljoen abonnees op breedbanddiensten over de hele wereld. Daarnaast heeft de markt, hoewel ze al enorm is, nog steeds een groot groeipotentieel. De uitdaging ligt vooral in de verbindingen tussen de netwerk-backbone en de gebruiker, de zogenaamde *local loop*. In de *local loop* wordt het netwerk dunner en bestaat het meestal uit lagere kwaliteit kanalen in vergelijking met de netwerk-backbone.

Van de technologieën die momenteel beschikbaar zijn voor de overbrugging van de *local loop*, is *digital subscriber lines* (DSL) veruit de marktleider. Deze technologie maakt gebruik van getwiste koper paren, die al tientallen jaren worden gebruikt voor standaard telefoniediensten. Een voordeel hiervan is dat de telefoonnetwerkinfrastructuur alomtegenwoordig is in de hele wereld, waardoor de kosten van de installatie zeer klein worden. Een nadeel daarentegen is dat DSL opereert in een medium dat niet in eerste instantie ontworpen is voor breedbandcommunicatie. Het gevolg hiervan is ernstige meerdere-gebruikers interferentie, algemeen bekend als *overspraak*.

In deze thesis ontwikkelen we signaal- en spectrumcoördinatietechnieken die gericht zijn op het vermijden, minimaliseren of zelfs exploiteren van overspraak. De collectie van deze technieken is in de literatuur bekend als

*dynamic spectrum management* (DSM). DSM heeft herhaaldelijk spectaculaire performantiewinsten van DSL netwerken aangetoond. DSM technieken spelen een belangrijke rol voor de volgende generatie DSL-diensten en ze zijn het algemene thema van deze thesis.

In Deel I van deze thesis, richten we ons op spectrumcoördinatie. Hier richten we ons op een *single input, single output* (SISO) interferentiekanaal. Het doel is om te komen tot een eerlijke vermogenallocatie, zodat elke gebruiker een evenwicht vindt tussen het maximaliseren van de eigen snelheid en het minimaliseren van interferentie aan anderen gebruikers. Wij stellen twee algoritmen voor voor de oplossing van het gewogen snelheidsmaximalisatieprobleem rekening houdend met per-gebruiker vermogenbeperkingen. Beide benaderingen vertrekken van het herschrijven van het probleem met verschillende variabelen. De klassieke manier om de ontwerpparameters van dit probleem te vertegenwoordigen is met een Cartesische coördinaten vector, waarbij elke positie van de vector de vermogentoekening van een gebruiker aanduidt. We gebruiken daarentegen sferische coördinaten, waarbij de ontwerpparameters worden aangeduid met een straal en een richting vector met een normbeperking. Met sferische coördinaten kunnen we verrassend veel structuur in dit probleem vinden, die de berekeningscomplexiteit aanzienlijk kan verminderen. Een van onze voorgestelde algoritmen kan tot 100 keer sneller werken dan het vorige relevante voorstel. De tweede voorgestelde algoritme werkt 2-15 keer sneller dan het vorige relevante voorstel.

In deel II, richten we ons op gecombineerde signaal- en spectrumcoördinatie. Eerst richten we ons op een scenario dat wordt aangeduid als *discrete multitone multiple-input, multiple-output interference channel* (DMT MIMO IC). Dit scenario bestaat uit meerdere gebruikers, die elk een verschillend aantal zendontvangers als een MIMO-systeem gebruiken. De coördinatie gebeurt zowel op het signaalniveau (met per-gebruiker MIMO technieken) als op het spectrumniveau (met meerdere gebruiker vermogenallocatie). Wij stellen twee algoritmes voor voor de DMT MIMO IC gewogen snelheidsmaximalisatieprobleem. Wij richten ons zowel op per-gebruiker als de per-zendontvanger vermogenbeperkingen. In het eerste algoritme, gebruiken we recent werk die de nauwe relatie tussen de gewogen snelheid som maximalisatie probleem en de gewogen *minimum mean squared error* (MMSE) minimalisatie probleem aantoon. We laten zien dat, met een eenvoudige uitbreiding, eerdere werk kan aangepast worden tot onze concrete situatie. In het tweede algoritme, worden de signaal- en spectrumcoördinatie delen afzonderlijk opgelost. Voor het signaalcoördinatiedeel, krijgen we meerdere onafhankelijke MIMO IC's, die ons in staat stellen om gebruik te maken van eerder werk. Voor het spectrumcoördinatiedeel, is een van de interessante uitkomsten van onze analyse een generalisatie van de waterfilling vermogenallocatie voor het MIMO

interferentie kanaal. Deze formule houdt rekening met de matrixstructuur van het kanaal en omvat een strafparameter voor de gebruiker die excessieve interferentie veroorzaakt. Simulaties tonen aan dat beide algoritmen een aanzienlijke winst belonen in vergelijking met pure spectrumcoördinatie algoritmen.

Nog in deel II, ontwikkelen we een algemeen systeemkader dat de hele complexiteit van DSL netwerken omvat. Ons kader omvat elke andere eerder bestudeerde situatie als een speciaal geval, met inbegrip van alle andere in dit proefschrift vermelde scenario's. We stellen ook een algoritme voor dat dit kader gebruikt voor alle mogelijke gevallen, inclusief elk aantal gebruikers, elk aantal zendontvangers, elk aantal tonen, elke vorm van afstemming op de zender en aan de ontvangstzijde, en synchrone of asynchrone transmissie.



# Abbreviations

2B1Q	2-binary, 1-quartenary
2SB	semiblind spectrum alancing
ADSL	asymmetrical digital subscriber line
ANSI	American National Standards Institute
AWG	American wire gauge
AWGN	additive white Gaussian noise
BC	broadcast channel
BER	bit error rate
CM	common mode
CO	central office
CP	cyclic prefix
CPE	customer premisses equipment
DC	difference of concave
DFT	discrete Fourier transform
DM	direct mode
DMT	discrete multitone
DP	distribution point
DSB	distributed spectrum balancing
DSL	digital subscriber lines
ETSI	European Telecommunications Standards Institute
FDM	frequency division multiplexing
FEXT	far end crosstalk
FFT	fast Fourier transform
FTTB	fiber to the basement
FTTC	fiber to the cabinet
FTTdp	fiber to the distribution point
FTTH	fiber to the home
GDFE	generalized decision feedback equalization
GDSB	generalized distributed spectrum balancing

---

GF-WMMSE-GDSB	generalized framework WMMSE-GDSB
GP	geometric program
HDSL	high-bit-rate digital subscriber line
HFC	hybrid fiber-coax
IBI	inter-block interference
IA	interference alignment
IC	interference channel
ICI	inter-carrier interference
ISB	iterative spectrum balancing
ISI	inter-symbol interference
IDFT	inverse discrete Fourier transform
IFFT	inverse fast Fourier transform
ISB	iterative spectrum balancing
ISDN	integrated service digital network
IWF	iterative waterfilling
KKT	Karush-Kuhn-Tucker
LMMSE	linear minimum means squared error
MAC	multiple access channel
MIMO	multiple input, multiple output
MIW	modified waterfilling
ML	maximum likelihood
MMSE	minimum mean squared error
MSE	mean squared error
NEXT	near end crosstalk
OFDM	orthogonal frequency division multiplexing
OSB	optimal spectrum balancing
OSB-SC	optimal spectrum balancing with spherical coordinates
PAM	pulse amplitude modulation
PAPR	peak to average power ratio
PC	power constraint
pdf	probability distribution function
PM	phantom mode
PON	passive optical networks
POTS	plain old telephone service
PSD	power spectral density
PSTN	public switched telephone network
RR	rate region
SCALE	successive convex approximation for low complexity
SISO	single input, single output
SNR	signal to noise ratio

---

SVD	singular value decomposition
SW	split wire
TaSSO	taxicab spherical coordinates spectrum optimization
WMMSE	weighted minimum mean squared error
WRS	weighted rate sum
VDSL	very-high-bit-rate digital subscriber line
xDSL	the collection of all DSL standards
ZF	zero forcing



# List of Symbols

## Mathematical Notation

$x$	scalar
$\mathbf{x}$	column vector
$\mathbf{X}$	matrix
$\mathcal{X}$	set
$\mathbb{R}$	set of real numbers
$\mathbb{R}_+$	set of non-negative real numbers
$\mathbb{C}$	set of complex numbers
$\mathbb{H}^{A \times A}$	set of hermitian matrices of size $A$
$(\cdot)^*$	conjugate
$(\cdot)^T$	transpose
$(\cdot)^H$	Hermitian transpose
$(\cdot)^{-1}$	matrix inverse
$E[\cdot]$	expectation operator
$\text{tr}\{\cdot\}$	trace
$ x $	absolute value
$ \mathbf{X} $	determinant
$\text{adj}\{\mathbf{X}\}$	adjugate
$\mathbf{X} \succeq 0$	$\mathbf{X}$ is positive semi-definite
$\text{diag}\{\mathbf{x}\}$	matrix with a vector $\mathbf{x}$ in the main diagonal
$\ \cdot\ _2$	$\ell_2$ or Euclidean norm
$\ \cdot\ _1$	$\ell_1$ or taxicab norm
$\log(\cdot)$	natural logarithm
$\log_{10}(\cdot)$	base 10 logarithm
$\log_2(\cdot)$	base 2 logarithm
$\text{unif}(a, b)$	uniform random variable in the interval $[a, b]$
$\mathbf{I}_A$	identity matrix of size $A$
$\mathbf{0}_{A \times B}$	matrix of zeros whose dimensions are $A \times B$

$\mathbf{e}_i$	vector of zeros with a '1' in the $i$ th position
$O(\cdot)$	order
$\max(a, b)$	maximum of scalars $a$ and $b$
$\min(a, b)$	minimum of scalars $a$ and $b$
$\text{sgn}\{\}$	sign function

## Fixed Symbols

$A_n$	number of transceivers of user $n$
$\mathcal{A}_n$	set of transceivers of user $n$
$b_n^k$	data rate of user $n$ on tone $k$
$\mathbf{F}$	DFT matrix
$\mathbf{F}^H$	IDFT matrix
$h_{n,j}^k$	channel gain from transmitter of user $n$ to receiver of user $j$ on tone $k$
$\mathbf{H}_{n,j}^k$	channel matrix from transmitter of user $j$ to receiver of user $n$ on tone $k$
$L$	Lagrangean
$\mathbf{M}_n^k$	noise covariance matrix for user $n$ on tone $k$
$n$	user index
$N$	number of users
$\mathcal{N}$	set of users
$p_n^k$	power allocation for user $n$ on tone $k$
$P_n^{\max}$	power constraint for user $n$
$\mathbf{p}^k$	vector with power allocation of all users on tone $k$
$\mathbf{P}$	matrix with power allocation for all users, tones and transceivers
$k$	tone index
$K$	number of tones
$\mathcal{K}$	set of tones
$r_n$	total data rate of user $n$
$\mathbf{R}_n^k$	receive matrix for user $n$ on tone $k$ (also known as equalizer)
$\mathcal{R}$	set with receive matrices for all user and all tones
$\mathbf{T}_n^k$	transmit matrix for user $n$ on tone $k$ (also known as precoder)
$\mathcal{T}$	set with transmit matrices for all user and all tones
$x_n^k$	transmitted symbol for user $n$ on tone $k$
$\mathbf{x}_n^k$	transmitted symbol vector for user $n$ on tone $k$
$y_n^k$	received symbol for user $n$ on tone $k$

$\mathbf{y}_n^k$	received symbol vector for user $n$ on tone $k$
$z_n^k$	circularly symmetric zero mean Gaussian noise for user $n$ on tone $k$
$\mathbf{z}_n^k$	circularly symmetric zero mean Gaussian noise vector for user $n$ on tone $k$
$\alpha_{n,j}^k$	normalized crosstalk channel between the transmitter of user $j$ to the receiver of user $n$ on tone $k$
$\Delta_f$	tone spacing
$\lambda$ or $\mu$	vectors of Lagrange multipliers
$\Gamma$	SNR gap
$\sigma_n^k$	normalized noise power for user $n$ on tone $k$

## Spherical Coordinates

$\rho \mathbf{d}$	spherical coordinates in Euclidean geometry, where $\rho$ is the radius and $\ \mathbf{d}\ _2 = 1$
$\theta_{[j]}$	$j$ th angle for spherical coordinates in Euclidean geometry
$\eta \mathbf{v}$	spherical coordinates in taxicab geometry, where $\eta$ is the radius and $\ \mathbf{v}\ _1 = 1$
$\phi_{[j]}$	$j$ th angle for spherical coordinates in taxicab geometry

## Asynchronous Transmission

$\mathbf{A}_{n,j}^{k,s}$ and $\mathbf{B}_{n,j}^{k,s}$	matrices representing inter-carrier interference gain from user $j$ to user $n$ and from $s$ to tone $k$
$\mathbf{C}$	matrix that inserts the cyclic prefix
$\tilde{\mathbf{C}}$	matrix that removes the cyclic prefix
$L_g$	length of the impulse response of the channel
$L_{cp}$	length of the cyclic prefix
$\mathbf{S}_{(1)}$ and $\mathbf{S}_{(2)}$	matrices that capture asynchronous transmission offset between the reception of DMT blocks of users $n$ and $j$
$\beta_{n,j}$	



# Contents

<b>Abstract</b>	<b>v</b>
<b>Abbreviations</b>	<b>xiii</b>
<b>List of Symbols</b>	<b>xvii</b>
<b>Contents</b>	<b>xxi</b>
<b>1 Introduction</b>	<b>1</b>
1.1 The DSL Network . . . . .	6
1.2 A Brief History of DSL . . . . .	6
1.3 Transmission Modes . . . . .	8
1.4 The DSL Channel . . . . .	11
1.5 DMT Modulation . . . . .	13
1.5.1 SISO Case . . . . .	14
1.5.2 MIMO Case . . . . .	21
1.6 The Crosstalk Problem . . . . .	25
1.7 Multiuser Information Theory . . . . .	28
1.8 Dynamic Spectrum Management . . . . .	31
1.9 Thesis Overview and Contributions . . . . .	35

<b>I</b>	<b>Spectrum Coordination</b>	<b>38</b>
<b>2</b>	<b>Spectrum Coordination with Spherical Coordinates</b>	<b>39</b>
2.1	Introduction . . . . .	39
2.2	System Model and Previous Work . . . . .	41
2.3	Spectrum Coordination with Spherical Coordinates—Exhaustive Search for the Angles . . . . .	43
2.3.1	Algorithm . . . . .	46
2.3.2	Complexity . . . . .	47
2.3.3	Precision . . . . .	47
2.4	Spectrum Coordination with Spherical Coordinates in Taxicab Geometry—Iterative Search for the Angles . . . . .	51
2.4.1	Solving for the Radius . . . . .	53
2.4.2	Solving for the Angles . . . . .	54
2.4.3	Exhausting the Sum Power . . . . .	57
2.4.4	Algorithm . . . . .	57
2.4.5	Computational Complexity and Convergence . . . . .	58
2.5	Simulation Results . . . . .	59
2.5.1	OSB vs. OSB-SC . . . . .	59
2.5.2	Random Downstream ADSL . . . . .	61
2.5.3	Upstream VDSL . . . . .	63
2.6	Conclusion . . . . .	63
<b>II</b>	<b>Combined Signal and Spectrum Coordination</b>	<b>66</b>
<b>3</b>	<b>DMT MIMO IC</b>	<b>67</b>
3.1	Introduction . . . . .	67
3.2	Problem Statement . . . . .	69

3.3	Algorithm 1: DMT WMMSE Minimization . . . . .	73
3.3.1	WMMSE vs. WRS . . . . .	73
3.3.2	Algorithm . . . . .	76
3.3.3	Convergence and Computational Complexity . . . . .	77
3.4	Algorithm 2: WMMSE-GDSB . . . . .	78
3.4.1	Solving the problem in two parts . . . . .	78
3.4.2	Solving for $\mathbf{T}_n^k$ . . . . .	79
3.4.3	Solving for $\mathbf{P}$ . . . . .	80
3.4.4	Solving (3.27) . . . . .	82
3.4.5	Algorithm . . . . .	87
3.4.6	Convergence and Complexity . . . . .	88
3.5	Simulation Results . . . . .	90
3.5.1	Downstream ADSL . . . . .	90
3.5.2	Upstream VDSL . . . . .	93
3.6	Conclusion . . . . .	94
<b>4</b>	<b>DMT MIMO IC with Per-Transceiver Power Constraints</b>	<b>96</b>
4.1	Introduction . . . . .	96
4.2	Problem Statement . . . . .	98
4.3	DMT-WMMSE with Per-Transceiver Power Constraints . . . . .	101
4.4	WMMSE-GDSB with Per-Transceiver Power Constraints . . . . .	103
4.4.1	The Limitations of the Traditional Approach . . . . .	105
4.4.2	Exhaustive Search in $\mathbf{p}_n^k$ . . . . .	107
4.4.3	Changing $\mathbf{p}_n^k$ to Spherical Coordinates—Exhaustive Search for the Direction Vector . . . . .	108
4.4.4	Changing $\mathbf{p}_n^k$ to Spherical Coordinates in Taxicab Geometry— Iterative Search for the Direction Vector . . . . .	111
4.4.5	Convergence . . . . .	116

4.5	Simulation Results . . . . .	117
4.5.1	Downstream ADSL . . . . .	118
4.5.2	Upstream VDSL . . . . .	120
4.6	Conclusion . . . . .	122
<b>5</b>	<b>General Framework</b>	<b>123</b>
5.1	Introduction . . . . .	123
5.2	System Model and Problem Statement . . . . .	125
5.2.1	System Model and Notation—Synchronous Case . . . . .	125
5.2.2	System Model and Notation—Asynchronous Case . . . . .	129
5.3	Proposed Solution . . . . .	135
5.3.1	Solving for $\mathcal{T}$ . . . . .	137
5.3.2	Solving for $\mathbf{P}$ . . . . .	138
5.3.3	Algorithm . . . . .	139
5.4	Simulation Results . . . . .	141
5.4.1	Downstream ADSL . . . . .	141
5.4.2	Upstream G.fast . . . . .	144
5.5	Conclusion . . . . .	147
<b>6</b>	<b>Conclusion</b>	<b>149</b>
<b>A</b>	<b>Appendices to Chapter 2</b>	<b>155</b>
A.1	$N$ -dimensional Sphere Formulas . . . . .	155
A.2	Proof of Proposition 2.2 . . . . .	156
A.3	Proof of Propositions 2.3 and 2.4 . . . . .	159
<b>B</b>	<b>Appendix to Chapter 3</b>	<b>162</b>
B.1	Proof of Proposition 3.2 . . . . .	162

<b>C Appendices for Chapter 4</b>	<b>166</b>
C.1 General Formulas for $\rho_n^k$ , $\theta_{n,[i]}^k$ and $\eta_n^k$ , $\phi_{n,[i]}^k$ . . . . .	166
C.2 Proof of Proposition 4.1 . . . . .	167
<b>D Appendix to Chapter 5</b>	<b>169</b>
D.1 Derivation of the ICI Matrices for Fixed $\beta_{n,j}$ . . . . .	169
<b>Bibliography</b>	<b>173</b>



# Chapter 1

## Introduction

Making data travel used to be difficult. From today's standpoint, where uncountable terabytes of data are exchanged by the minute, it seems difficult to imagine (or to remember) how it was when, just two decades ago, the state-of-the-art transmission worked with 14.4 Kb/s and people were creating their first e-mail accounts. The ability to easily exchange and access data has profoundly transformed the way we work, study, inform and entertain ourselves.

Perhaps the biggest catalyst for this transformation we witnessed in the last decades is the popularization of the Internet. With it, people around the world have been able to experience business, news, studies, culture and entertainment in a new way. The Internet allows for information to reach people almost instantaneously from anywhere around the globe, at the click of a mouse, while for generation of their parents having access to the same information depended on waiting for the mailman, going to the closest newspaper shop or consulting the dusty pages of an outdated encyclopedia.

This Internet revolution is far from over. Perhaps it has not even peaked, and it has no turning back. Numerous new applications appear every year and continue to influence the world at large. As of today, the thirst for bigger amounts of data at higher speeds and ubiquitous connectivity seem not to abate. On the contrary, it still seems to be growing at a fast pace.

For the industry and the research community, this insatiable thirst for more, faster and higher quality data access is both an enormous opportunity and an enormous challenge. The broadband access market counted more than 600

million subscribers around the world at the end of 2012 [90]. Given the fast development and the large population of countries like India and China, this number still tends to grow a lot.

Broadband access uses two very distinct transmission channels to connect two points in the world wide network. One of them is the network backbone. The network backbone is responsible for making uncountable terabytes travel around the globe in a fast and reliable way. It consists of satellites, optical fiber, submarine cables, etc., all of which characterize high quality transmission channels. Because these technologies are relatively mature and cost effective, the network backbone has the potential to be upgraded to match virtually any increase in demand [87]. This means that the bottleneck of transmission is the second kind of transmission channels, the so-called *local loop*, i.e. the connection from the network backbone to the user. The local loop is comprised of usually severely lower quality transmission channels. It consists of the couple of kilometers to hundreds of meters when the network thins out so as to reach houses, offices and buildings. Following the parlance of the field, in this thesis the interface to the network backbone is represented by the central office (CO) of the network operator and the end user is referred to as the customer premises equipment (CPE), which includes both home and business users. The local loop exists thus between the CO and the CPE. Bridging the local loop in an efficient and cost effective way while maintaining high transmission rates is *the* challenge that needs to be addressed in the broadband access industry in the next years.

There are four main broadband access technologies today competing for the bridging of the local loop [30]. They are fixed wireless or satellite; cable modems; optical fiber; and digital subscriber lines (DSL). We comment on each of the four in the following paragraphs.

*Fixed wireless or satellite* broadband access is not such a commercial success. As of the end of 2012, it has less than 3 % share of the worldwide market [90]. The main issues with this technology are the scarcity of the radio spectrum and the fact that the wireless channel has higher loss than wireline channels (notice that the three competitors use some kind of physical, wireline connection). Although they have other considerable advantages, such as higher mobility and needs of simpler infrastructure, the wireless connections intrinsically waste power and bandwidth because the transmission channel is free space. This stands in contrast with the wireline counterparts, where transmission is restricted to a waveguide. The issue of interference is also much more worrying in the wireless case. To be sure, channels like the ones in DSL also experience interference. However, due to the fact that in DSL the transmission of each user is done on its own waveguide and interference is characterized by the signal that leaks from one waveguide to the next limits the damage of interference in a way that is unattainable in wireless communications. Because of these

factors, wireless broadband access is inherently more unstable and expensive than the alternatives. It is envisioned that this technology will attend the needs of some niche markets, such as large rural areas, areas with no pre-existing wireline infrastructure or areas where installing such wireline infrastructure is too costly. Its utilization for a broader market is and will probably continue to be hindered by the disadvantages just described.

Broadband access using *cable modem* is one of the main competitors in today's market, and as of 2012 it has a share of 20 % of the connections worldwide [90]. This technology uses the same coaxial cables utilized for cable television. The transmission channel is of much better quality in terms of useful bandwidth and isolation than, for example, DSL channels. Some combined operation with fiber is possible, and characterizes what is called hybrid fiber-coax (HFC). With HFC the coaxial cables bridge the last couple of kilometers from a fiber-fed distribution point to the CPE, which allows the fiber reach of the network to progress in a slow, evolutionary way. However, this technology has not experienced fast growth in the past years. This is so for a couple of reasons. First, the infrastructure already in place today for this kind of technology lags considerably behind that of some competitors, like DSL. Second, because the initial application was cable television, this kind of technology was conceived to be a one way communication channel, whereas broadband access requires two way exchanges. Thus the use of coaxial cable carries the extra cost of installation of equipment for bidirectional communications. Lastly, the coaxial cable is a shared channel, i.e. the total data rate is shared by a number of users in 'cake cutting' way. Hence, as more users sign in the network the per-user data rate decreases.

*Optical fiber* connections to the CPE have been a goal of the telecommunication industry for decades now. With optical fiber or the so-called passive optical networks (PON), a single data stream originates from the CO and is splitted in ever smaller pieces as the network branches out until it reaches the CPE. The transmission channel has considerably better quality than the three big competitors, and it is able to deliver the gigabits per second speeds that every home user dreams of. Optical fiber has time and again been predicted to dominate the market in the next couple of years in the sense that it would connect directly to the CPE—since the end of the 1980, some have considered fiber to the home (FTTH) to be the next big thing [6, 50]. These predictions, however, have not turned into reality: At the end of 2012, FTTH counted only 3 % of the worldwide broadband market. The predictions were overly optimistic because they have overlooked at least three different but interconnected facts. First, they have not properly considered that deployment of fiber is a prohibitively complicated and expensive operation. Optical fiber is a delicate material, and needs to be handled with proper care. The initial

investment necessary for deployment of fiber to every home around the globe is enormous (it has been estimated to be 250 billion US dollars in the USA alone, and trillions worldwide [91]). Furthermore, most home users do not like technicians around to dig and run cables in their gardens or living rooms [19]. Second, and as a consequence of the high cost implied by the first fact, the fiber network is expanding towards the CPE in an evolutionary rather than a revolutionary way. Given that fiber deployment is an expensive and somewhat complex endeavor, network operators have expanded the reach of the fiber network in a step-by-step way. With each step, the fiber gets closer to the CPE. In this fashion, instead of directly going for FTTH, what is observed is that the connections are going through a sequence of steps commonly known as FTTx, where the 'x' can stand for a cabinet in the street (FTTC), the basement of a large building (FTTB) or the last distribution point (FTTdp) [19, 25, 114]. Finally, the third fact is that, if fiber reaches the last distribution point (DP) or a basement, there are other options for transmission in the remaining hundreds of meters (i.e. from the DP to the CPE) that provide data rates in the neighborhood of 1 Gb/s but come at only a fraction of the cost of full fiber deployment.

The fourth type of connection is *DSL*. It is by far the most widespread means for high speed broadband access worldwide, with a 70 % share of the market (more than 450 million users worldwide). Probably the most fundamental reason for DSL's success is the use of pre-existing infrastructure. This technology uses twisted copper pairs, the same used for decades for standard telephony services (known as plain old telephone services [POTS]). If on the plus side this infrastructure is ubiquitous through the globe, making costs of installation very small, on the minus side DSL operates in a communication channel with worse characteristics in comparison to optical fiber and coaxial cable. In fact, although DSL uses a bandwidth that is several times larger than that of POTS, still it has to operate in a more modest bandwidth when compared to coaxial cable, for example. Moreover, and partly because of the use of very high frequencies, the interference problem becomes a serious one. When a signal travels through a DSL line (i.e. a twisted copper pair), it radiates electromagnetically. Typically, a collection of several DSL lines are bundled together in a *cable binder*. Because of electromagnetic radiation, the signal of one line leaks to the neighboring lines. This characterizes interference, commonly known as *crosstalk*. Crosstalk has recurrently been identified as the main source of performance degradation for DSL transmission.

Still, even with these disadvantages DSL is thriving. There are perhaps three main reasons for that. First, it is difficult to overstate the importance of the existing infrastructure. The telephone network reaches hundreds of millions of users around the globe. All these users have the basic infrastructure for

DSL service already in place. Second, new standards of DSL arise in tandem with the development of the optical fiber network. As FTTx is deployed and the last fiber-fed terminal and the CPE become closer, DSL is responsible for bridging distances that become every time shorter. Accordingly, international standardization bodies standardized the asymmetrical DSL (ADSL) in 1998, operating at 6 km lines and with transmission rates of 6 Mb/s; the very-high-bit-rate DSL (VDSL) in 2004, operating on lines approximately 1 km long and providing something between 20-52 Mb/s; and there is ongoing work on the G.fast [93], which works with lines a couple of hundred meter long and is able to provide 1 Gb/s. G.fast is predicted to reach the market in 2016. The evolution of line length versus date of standardization is clear. And, third, there is dynamic spectrum management (DSM). DSM deals with smart signal processing techniques that aims at mitigating (or even profiting from) the effect of multi-user interference, i.e. crosstalk. DSM works both on spectrum and on signal level processing of the signals and it has been repeatedly shown to provide formidable gains in performance. In this thesis, DSL empowered by DSM constitutes what is called *next generation DSL*. DSM is the unifying topic of this thesis.

If some decades ago it was thought that fiber connection to the CPE was within the grasp of the next generation of broadband access, today it is generally accepted that FTTH is not around the corner [23, 70, 91]. It remains the ultimate goal of broadband access, but the time for it to become a reality is counted in decades rather than years. In the meantime, fiber approaches the CPEs in a gradual albeit steady rhythm. For the reasons outlined above and developed throughout this thesis, DSL technology, specially when empowered by smart signal and spectrum coordination techniques, is perfectly poised for the bridging of the local loop. DSL has today not only the largest share of the market but also the fastest per-year growth, in particular in the hybrid FTTx scenarios. It will most likely continue to be a major player in this already massive and still growing market.

In the remainder of this chapter, we describe the main principles of DSL transmission. We cite the main characteristic of DSL networks in Section 1.1; provide a brief history of data transmission over the telephone network in Section 1.2; list the transmission modes of DSL in Section 1.3; describe models for the attenuation of the DSL channels in 1.4; describe the basics of discrete multitone (DMT) modulation in Section 1.5; discuss the crosstalk problem in Section 1.6; discuss some concepts of multi-user information theory in Section 1.7; describe the main principles of DSM in Section 1.8; and, finally, outline the organization and the contributions of this thesis in Section 1.9.

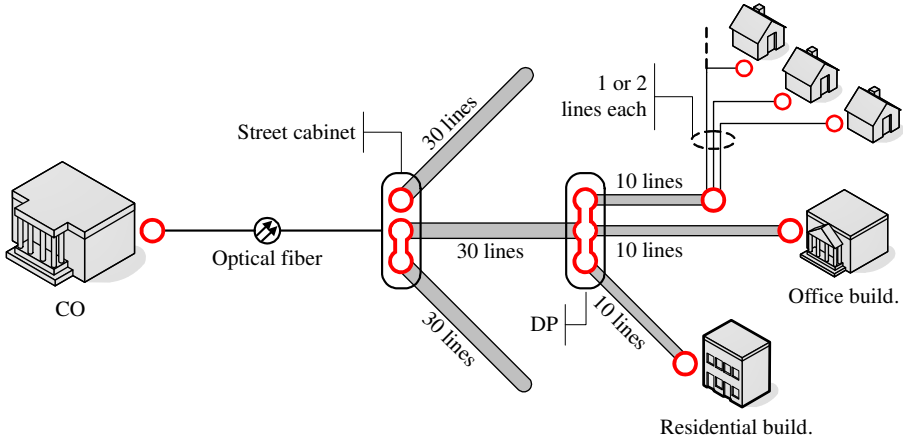


Figure 1.1: A typical DSL network with a tree topology.

## 1.1 The DSL Network

DSL uses the twisted copper pair utilized for more than a century to carry voice signals, i.e. telephone services. The telephone network has its origin with the invention of the analog telephone transmission by A. G. Bell in 1876. Today it is commonly referred to as public switched telephone network (PSTN). Voice transmission over copper use a 4 kHz bandwidth channel. DSL transmission extends this bandwidth greatly, sometimes to several MHz. The necessary infrastructure has been built during decades, and today there are literally hundreds of millions users connected around the globe. An important characteristic of these networks is that they typically have a *tree topology*. See Fig. 1.1 for an illustration. Departing from the CO or from a fiber-fed terminal, a large number of telephone (or DSL) lines are collected in a cable binder. This collection of lines becomes smaller as the network branches out to reach the CPEs, their destination. Notice that, for the DSL case, the advance of optical fiber towards the CPE does not change this tree topology. With FTTx, only the finer branches are serviced by DSL. The tree topology has important consequences when it comes to DSM, which we detail in Section 1.8.

## 1.2 A Brief History of DSL

Transmission of data other than voice in telephone lines goes back a long way, with the first attempts being carried out in the 1950's. Back then, the

applications included for example the facsimile. In the following, we provide a very brief history of data transmission over the telephone lines and outline the main different types of DSL technology, but we do not go so far back in time (to see more details on this history, see [30, 87]). We remark that the different flavors of DSL are sometimes collectively referred to as xDSL.

Before we proceed, we first add that DSL standards are classified as *symmetrical* or *asymmetrical*. For the former, transmission on the upstream (i.e. from CPE to CO) and on the downstream (i.e from the CO to the CPE) have the same bandwidth. For the latter, there is an imbalance between the bandwidths for upstream and downstream transmission. Symmetrical service is mainly important for business applications, such as teleconferencing. When applications such as web and video browsing are more popular, such as for home use, higher bandwidth for the downstream (i.e asymmetry benefiting the downstream transmission) is justified.

Our starting point is the basic rate *integrated service digital network* (ISDN), which is considered the first type of DSL standard. The technological concept was developed in the 1970's and first trials were carried out in the 1980's. ISDN uses 2-binary, 1-quaternary pulse amplitude modulation (2B1Q PAM) and provides services of both voice and data with symmetrical transmission and rates of 160 Kb/s. Service was provided to lines up to 5.5 km long. ISDN had at its peak more than 6 million users worldwide.

*High-bitrate DSL* (HDSL) was developed in the beginning of the 1990's. HDSL used one or two DSL lines for transmission of rates of 1.544 Mb/s. HDSL did not allow simultaneous operation of POTS. This standard was popular in North America, where typically two twisted pairs, each carrying half of the total data rate, serviced a single CPE. Transmission is symmetrical and uses 2B1Q PAM. HDSL can operate in lines about 4 km long. Some improvements in the forms of the standards HDSL2 and HDSL4 were developed towards the end of the 1990's.

*Asymmetrical DSL* (ADSL) was developed in the early 1990's with the aim of providing video on demand to residential customers, but focus quickly changed to broadband access. The technology hit the market at the end of the 1990's and it was a success: ADSL is both the most popular DSL standard and the most widely deployed single standard for broadband access, with more than 350 million subscribers worldwide as of the end of 2012. As the name suggests, transmission is asymmetric—ADSL was the first DSL standard to adopt asymmetric transmission. While downstream transmission can have data rates of 8 Mb/s, upstream transmission is limited to at most 1 Mb/s. To give an idea of how this imbalance looks like, we give the example of frequency division multiplexing (FDM) ADSL, where the up- and downstream bands do

not overlap. The upstream band starts at 25 kHz and goes up to 138 kHz. The downstream band starts at 180 kHz and goes up to 1.104 MHz. Unlike HDSL, ADSL allows for the concurrent utilization of POTS. It services CPE's with line lengths up to 6 km. Importantly, ADSL adopts discrete multitone (DMT) modulation—also the first DSL standard to do so. DMT is today the transmission scheme at the core of almost all important DSL types. We detail DMT modulation in Section 1.5. Because of DMT, ADSL is capable of using variable constellation sizes and some simple bit allocation through the sub-channels (i.e. tones). Important variants of ADSL include the ADSL2 and the ADSL2+. For the ADSL2+, for example, the bandwidth goes up to 2.2 MHz.

ADSL is the incumbent technology, but it is rapidly losing ground to the *very-high-bit-rate DSL* (VDSL). As of the end of 2012, VDSL had more than 100 million subscribers worldwide. The success of VDSL is strongly related to the enlargement of the fiber network. Accordingly, VDSL is primarily designed to connect the CPE from a fiber-fed terminal, i.e. a FTTx scenario, and hence to operate on lines with less than 1 km of length. Most deployments are asymmetric, with bandwidth going up to 12 MHz for first generation VDSL (VDSL1) and 30 MHz for second generation VDSL (VDSL2). Upstream rates are around 6.4 Mb/s and downstream rates are 52 Mb/s. VDSL also uses DMT, and some standards include advanced signal coordination techniques (more details on that in Section 1.8).

Finally, we mention that the development of the next generation DSL standard is ongoing at the time of writing. The *G.fast* will transmit in up to 200 MHz at line lengths of 250 m or less. Data rates are expected to go up to 1 Gb/s in short loops [94]. *G.fast* is expected to fill the gap between VDSL and full fledged fiber deployment [70]. It is expected to enter the market in 2016.

In this thesis, we focus on the two incumbent technologies, i.e. ADSL and VDSL, and the *G.fast*, the upcoming one. All simulations in these work consider one of these three standards.

## 1.3 Transmission Modes

POTS and classic DSL transmission use *differential mode* (DM) signals as means of communications. The DM signal is the standard transmission mode. It is the difference of voltages between the two wires of a twisted pair, as illustrated in Fig. 1.2-(a). If we consider the voltage on wire 1 to be  $v_1(t)$  and the voltage of wire 2 to be  $v_2(t)$ , the DM signal is given by  $d(t) = v_1(t) - v_2(t)$ .

There are, however, some alternatives for additional signaling. These stem from

the fact that standard DSL transmission of *one* signal is done on a twisted wire *pair*. Hence there can be unexplored transmission modes. Research on alternative transmission modes has been gaining some momentum in the past couple of years, see e.g. [39, 55, 56, 76].

One such alternative is the *common mode* (CM)—see e.g. [23, 39, 55, 56]. While the DM signal is the difference of voltages of the two wires, the CM signal, denoted as  $c(t)$  in Fig. 1.2, is their average., i.e.  $c(t) = 0.5(v_1(t) + v_2(t))$ . The CM signal is readily available in any copper pair, and can be extracted from the center tap of the transformer on both sides of the network. See Fig. 1.2-(b). With the use of the CM, a cable binder of  $N$  twisted copper pairs has  $2N$  transmission channels between transmitter and receiver. The CM can be also utilized for things other than signaling. In [56], the CM is used not as transmission mode but as a means to gather information about the background noise. The CM signal is correlated with the desired DM signal and with the observed background noise on the DM. If these correlation coefficients are known, the observation of the CM signal is a way to reduce noise and further enhance reception.

Another option is split wire (SW) signaling [23, 47]. In this kind of transmission, one wire is taken as a reference. The difference from the remaining wires to the reference wire constitutes the useful signal, denoted as  $s_i(t)$ . If we consider the voltage on the reference wire to be  $v_r(t)$  and the voltage of wire  $i$  to be  $v_i(t)$ , the  $i$ th SW signal is given by  $s_i(t) = v_i(t) - v_r(t)$ . See Fig. 1.2-(c), where the reference wire is taken to be the bottom one. In this case, a cable binder of  $N$  twisted copper pairs has  $2N - 1$  transmission channels between transmitter and receiver. It can also be that the metallic sheath, the outer protection of the cable binder, is used as the reference. In this case, there are  $2N$  transmission channels between transmitter and receiver.

One last option is the phantom mode (PM) [76]. The PM signal is the difference of the CM signal of two twisted copper pairs. See Fig. 1.2-(d), where the PM signal is denoted by  $p(t)$  and given by  $p(t) = c_1(t) - c_2(t)$ . With the use of the PM, there are  $2N - 1$  transmission channels between transmitter and receiver.

At first sight, there are some problems in the utilization of these alternative transmission modes, i.e. the CM, the SW and the PM. It is well-known, for example, that they cause and capture a lot of noise—much more than the traditional DM [23]. This should come as no surprise, because after all there is a reason the two wires are twisted in the first place. The twisting of the wires is a lesser-known invention of A. G. Bell himself, and it works as a way to reduce both ingress and egress of undesirable signals into the wire pair. It has been known for decades that twisting the wires leads to improved transmission. CM, SW and PM transmissions cause and receive very large levels of interference,

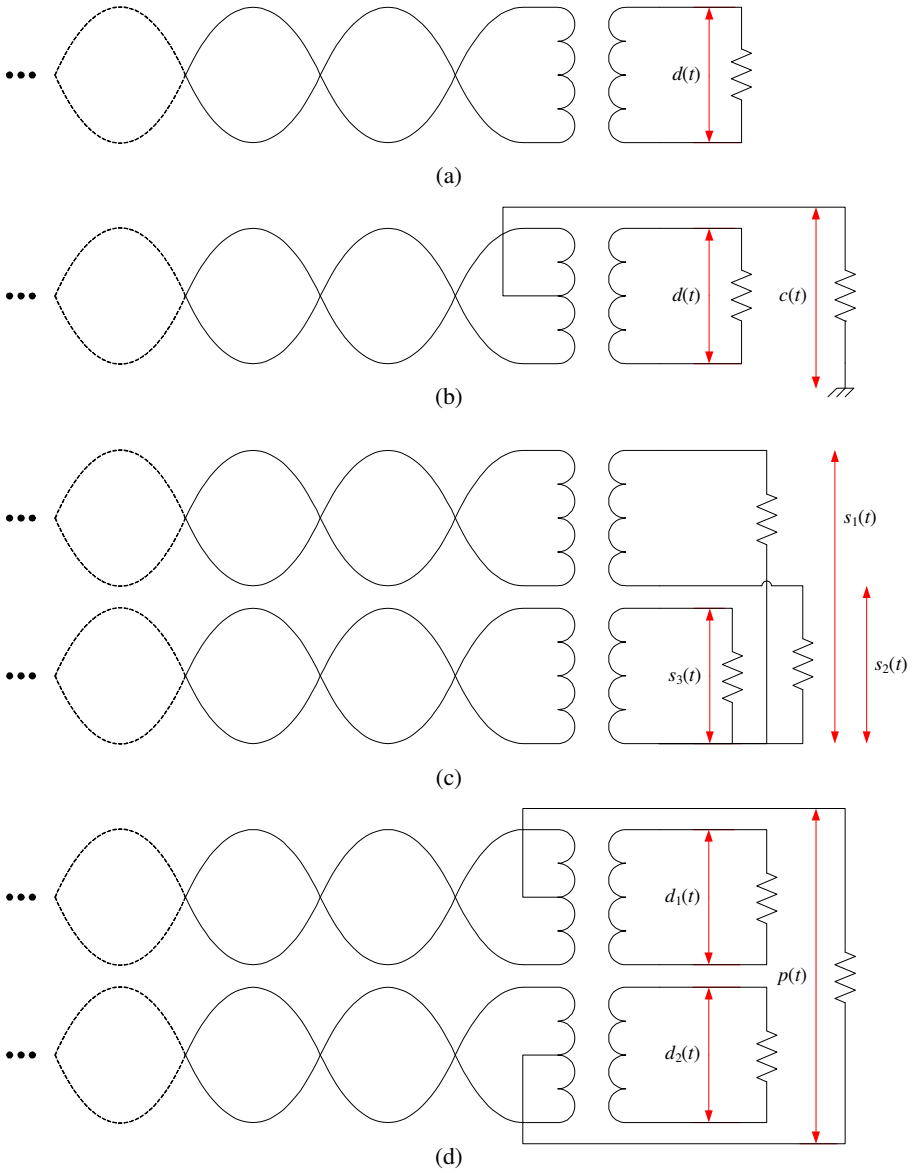


Figure 1.2: Transmission modes. (a) differential mode (DM); (b) common mode (CM); (c) split-wire (SW); and (d) phantom mode (PM).

i.e. crosstalk.

However, as we shall see in Part II of this thesis, crosstalk contains signal energy that can be observed on the other side of the communications channel. It is the processing of such signals that defines whether crosstalk is beneficial or detrimental to performance. With correct processing of crosstalk signals, the alternative transmission modes outlined above might be of practical interest. We mention that there has been successful tests with the PM, where a 390 Mb/s data rate was achieved with two DSL lines of length 400 m. The transmission used the two DMs and the PM [76].

## 1.4 The DSL Channel

There exist models to characterize the transfer function of the DSL channel through frequency. Because the DSL channels are wireline they are much more predictable than wireless channel, and reasonably good models for the behavior of these channels can be derived. For the DM, these models are well-known and have been treated carefully in [12,87,88,95] for both the direct channel and the crosstalk channel between two DSL lines. Unless otherwise stated, we use these models throughout this thesis (in one of the experiments we use measured channels). We now very briefly describe these channel models.

For the direct channels, accurate models can be obtained with the so-called RLCG model. The resistance (in  $\Omega/\text{Km}$ ), the inductance (in  $\text{H}/\text{km}$ ), the capacitance (in  $\text{F}/\text{km}$ ) and the conductance (in  $\text{Mho}/\text{km}$ ) of a DSL line are given respectively by

$$\begin{aligned} R^f &= (r_{0c}^4 + a_c f^2)^{0.25} \\ L^f &= (l_0 + l_\infty (f/f_m)^b) (1 + (f/f_m)^b)^{-1} \\ C^f &= c_\infty \\ G^f &= g_0 f^{g_e} \end{aligned}$$

These parameters depend on frequency (denoted by the superscript  $f$ ) in Hz. The constants  $r_{0c}$ ,  $a_c$ ,  $l_0$ ,  $l_\infty$ ,  $f_m$ ,  $b$ ,  $c_\infty$ ,  $g_0$  and  $g_e$  depend on the cable diameter and material. Several such constants are listed for different kinds of cable in [87]. The transfer function for the direct channel with DM transmission is given by

$$h^f(D) = \frac{Z_L + Z_S}{(Z_L + Z_S) \cosh(\gamma^f D) + (Z_0^f + Z_S Z_L (Z_0^f)^{-1}) \sinh(\gamma^f D)}, \quad (1.1)$$

where  $D$  is the line length in km. Here, we also define the propagation constant and the characteristic impedance respectively as

$$\gamma^f = \sqrt{(R^f + j2\pi fL^f)(G^f + 2j\pi fC^f)}$$

$$Z_0^f = \sqrt{\frac{R^f + j2\pi fL^f}{G^f + 2j\pi fC^f}}$$

Still in (1.1),  $Z_L$  and  $Z_S$  are the source impedance and the load impedance of the transmitting and receiving modems.

The model for the crosstalk channel between two DSL lines considers a 1 % worst case situation. This means that in practice 99 % of crosstalk channels are less severe than the model. The crosstalk channel transfer function with DM transmission between a interfering user  $j$  and a victim user  $n$  is given by

$$h_{n,j}^f = K_{\text{xf}}(f/f_0)\sqrt{D_{\text{xt}}}|h^f(D_{\text{xt}})|. \quad (1.2)$$

Here the constants are given by  $K_{\text{xf}} = 0.0056$  and  $f_0 = 1$  MHz and  $D_{\text{xt}}$  is the coupling distance, i.e. the distance in km in which the two users share the cable binder.

A couple of remarks are in order:

- We note that while for (1.1) we have information for both absolute value and phase, for (1.2) we only have information for absolute value. This is a slight problem. For multiple input, multiple output (MIMO) transmission, knowing the phase of the crosstalk channel between two DSL lines is relevant. We circumvent this difficulty by assuming that the phase of  $h_{n,j}^f$  in (1.2) is the same as that of  $h^f(D_{\text{xt}})$ . For MIMO transmission, we thus use

$$h_{n,j}^f = K_{\text{xf}}(f/f_0)\sqrt{D_{\text{xt}}}h^f(D_{\text{xt}}). \quad (1.3)$$

We comment more to this issue when we describe MIMO transmission in Section 1.5.2.

- We emphasize that all the models just presented treat DM transmission. There have also been some efforts to characterize the attenuation of the DSL channel in the other transmission modes [39, 46].
- Finally, we also remark that the model in (1.2) is not an accurate representation of crosstalk channels. This model is a worst case, and in most cases the actual crosstalk channels are less severe. Crosstalk

channel estimation is an active area of research, e.g. [34, 54]. The impact of errors in the channel estimation in the performance of DSM algorithms are the focus of [49, 106].

- In this work we always assume perfect channel knowledge at both the transmitter and receiver sides of the network.

## 1.5 DMT Modulation

This section aims at briefly presenting the main characteristics of discrete multitone (DMT) modulation. More complete expositions can be found in, for example, [1, 87]. DMT is a kind of block transmission scheme where the available bandwidth is subdivided in  $K$  narrowband sub-channels or tones. All modern DSL standards, from ADSL onwards and including the G.fast, use DMT as the core of their transmission techniques.

DMT is a type of orthogonal frequency division multiplexing (OFDM) [1, 60, 104, 115]. The only significant difference between the two is that the former is able to adapt the modulation type of each tone depending on the channel conditions. That is why DMT modulation is more suitable to wireline communications, where the channel is almost static. In DSL, for example, there can be some changes due to temperature fluctuations, but these make the channel change slowly in time. Because of this mostly static channel, adaptive modulation for each tone makes sense and can deliver substantial gains in performance. For wireless communication, the channel changes much faster and as such adaptive per-tone modulations are much more difficult.

In the remainder of this section, we discuss the basics of DMT modulation, always focusing on a single user (multi-user DMT transmission is treated in Section 1.6). We emphasize that we always assume that the channel is known perfectly at the transmitter and at the receiver. We outline the basic principles of DMT modulation in Section 1.5.1. Here we focus on a single DSL line as a single input, single output (SISO) channel. First, we look at the block diagram of the transmission and detail each of the steps. We then discuss some advantages and disadvantages of DMT and discuss dynamic power allocation.

In Section 1.5.2, we discuss a situation where a user has a number of DSL lines for transmission. In this situation, a DMT multiple input, multiple output (MIMO) transmission applies. For DMT MIMO, we consider that full two-sided coordination is available on both sides of the network. We present the optimal transmission strategy and discuss the gains obtained with MIMO transmission.

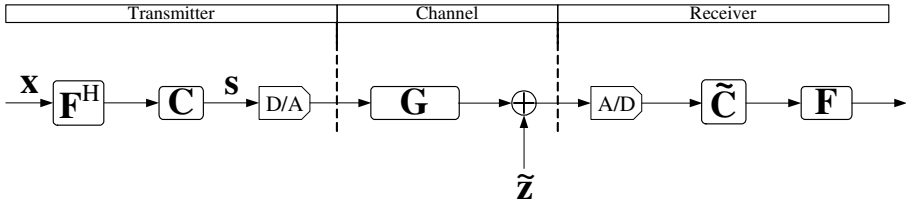


Figure 1.3: Block diagram for DMT modulation for the SISO case.

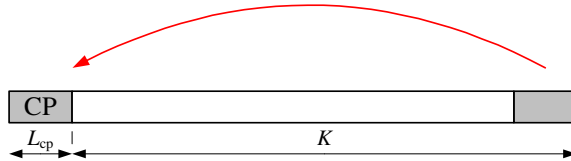


Figure 1.4: Inserting the cyclic prefix.

### 1.5.1 SISO Case

In this section, we focus on DMT transmission on a single DSL line. We refer to this type of transmission as DMT SISO.

Being a block transmission scheme, DMT transmits symbols simultaneously instead of sequentially. The symbol vector to be transmitted at the  $i$ th time instant is denoted by  $\mathbf{x} = [x^1 \ \dots \ x^K]^T \in \mathbb{C}^K$ , where  $x^k$  is the symbol for tone  $k$ . The processing of this vector is shown in Fig. 1.3, with the transmitter on the left-hand side and the receiver on the right-hand side.

The symbol vector  $\mathbf{x}$  is first multiplied by the IDFT matrix  $\mathbf{F}^H \in \mathbb{C}^{K \times K}$ , whose  $(i, j)$ th element is given by  $\mathbf{F}^H(i, j) = 1/K \exp(j2\pi(i-1)(j-1)/K)$ ,  $i, j = 1, \dots, K$ . Still on the transmitter side, the *cyclic prefix* (CP) is added. The CP consists in attaching the last  $L_{cp}$  symbols of  $\mathbf{F}^H \mathbf{x}$  to the beginning of the symbol, as illustrated in Fig. 1.4. This operation is done by the multiplication with the matrix  $\mathbf{C} \in \mathbb{R}_+^{K+L_{cp} \times K}$ , where  $L_{cp}$  is the length of the CP. This matrix is defined as

$$\mathbf{C} = \begin{bmatrix} \mathbf{0}_{L_{cp} \times (K-L_{cp})} & \mathbf{I}_{L_{cp}} \\ \mathbf{I}_K \end{bmatrix}$$





property that their eigenvectors are independent of the specific coefficients. The eigenvectors of circulant matrices are always complex exponential, and if organized in a matrix, they produce a DFT matrix. This is why circulant matrices are diagonalized by pre- and post multiplication by IDFT and DFT matrices, respectively [31, 88]. This is why we reach (1.8), where  $\mathbf{h} = [h^1 \dots h^K]^T \in \mathbb{C}^K$  is the channel frequency response. For the simulations in this thesis, this channel is obtained with (1.1). Notice that here we use the tone index  $k$  as superscript.

The operation of adding and removing the CP help diagonalize the channel matrix, which means that all tones are orthogonal to each other. Hence, the second function of the CP is to eliminate inter-symbol interference (ISI). We write the  $k$ th element of  $\mathbf{y}$  in (1.8) as

$$y^k = h^k x^k + z^k. \quad (1.9)$$

This represents a standard additive white Gaussian noise (AWGN) scalar channel. For symbol detection, we first compensate for the effects of the channel by calculating

$$\hat{x}^k = \frac{y^k}{h^k} = x^k + \frac{z^k}{h^k}.$$

The choice of the symbol is then done with a simple maximum likelihood (ML) detector.

Because the  $k$ th per-tone symbol comes multiplied by the corresponding frequency response  $h^k$ , it justifies the usual interpretation of DMT/OFDM systems: that of dividing the available bandwidth into a number of  $K$  narrowband sub-channels or tones. With OFDM/DMT modulation, given an available bandwidth of  $B$  Hz, each tone has width of  $\Delta_f = B(K)^{-1}$  Hz.

We remark that the same kind of orthogonality between the tones could be achieved with the use of a bank oscillators in the transmitter and matched filters to these oscillators on the receiver (see e.g. [88]). This, however, means bandpass filtering, which adds complexity to the transmission. The advantage of the transmission strategy depicted in Fig. 1.3 is that everything is done with baseband digital signal processing techniques, such as FFT and IFFT. The savings in computational complexity of DMT in relation to the scheme with the bank of oscillators are very significant.

Given the same bandwidth of  $B$  Hz, it would also be possible to design a single carrier (SC) transmission system with the same data rate as that of DMT. Symbols would be transmitted sequentially instead of simultaneously. Unlike DMT, each symbol would be of short duration in time and wide in frequency. The advantages of DMT in relation to single carrier transmission

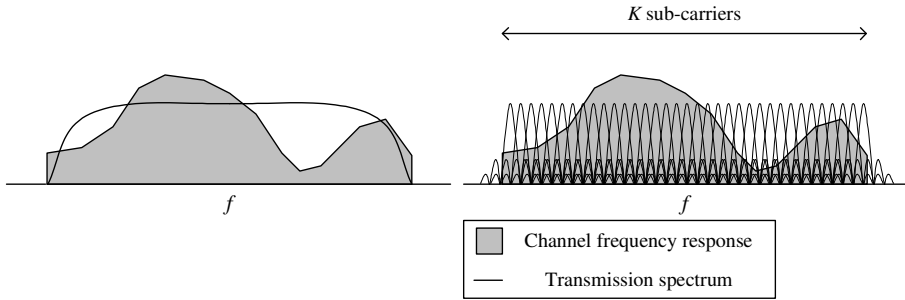


Figure 1.5: On the left, illustration of the transmission of a single carrier system. The signal is distorted in a frequency selective way. On the right, illustration of transmission with DMT modulation, where the tones are orthogonal. Each tone experiences approximately flat fading in frequency.

are various. For DMT, symbols have long duration, which makes the effects of channel spreading limited and adds robustness against impulse noise. Plus, because each tone has the characteristics of a scalar AWGN channel (see (1.9)), equalization at the receiver is performed with a simple one-tap equalizer, i.e.  $\hat{x}^k = y^k (h^k)^{-1}$ . For SC transmission, ISI is a much more serious issue, and needs to be combated with complex, multi-tap equalizers. The higher the effect of ISI, the more complex the equalizer needs to be. This difference between DMT and SC systems can be best visualized with the aid of Fig. 1.5. Because  $\Delta_f$  is small compared to  $B$ , each DMT sub-carrier experiences an approximately flat channel in frequency, whereas the SC signal suffers from frequency selective distortion.

Moreover, DMT opens the possibility of dynamic power allocation through the tones. Since transmission on one tone is independent of all others and since tones have different channel qualities, it is possible to allocate power (hence bits) so as to maximize data rate. This is particularly suitable for wireline, static channels such as DSL. The optimal way to perform this dynamic power allocation is with the well-known waterfilling formula. We briefly describe the derivation of the waterfilling formula in the next couple of paragraphs.

Our starting point is to consider  $\tilde{\sigma}^k = \text{E}[z^k(z^k)^*]$  to be the noise spectral density for tone  $k$  and  $p^k = \text{E}[x^k(x^k)^*]$  to be the power spectral density (PSD) for tone  $k$ . The maximum data rate of tone  $k$  for this channel is given by the

classic Shannon capacity formula, written as

$$\begin{aligned} c^k &= \Delta_f \log_2(1 + \text{SNR}^k) \\ &= \Delta_f \log_2\left(1 + \frac{p^k |h^k|^2}{\tilde{\sigma}^k}\right). \end{aligned} \quad (1.10)$$

Every practical and implementable coding scheme transmits below the theoretical capacity. How close it comes to the theoretical maximum shown in (1.10) is determined by the SNR gap  $\Gamma$  [87], which takes into account the coding gain, the noise margin and a desired bit error rate (BER). We thus rename  $c^k$  as  $b^k$  and re-write (1.10) as

$$\tilde{b}^k = \Delta_f \log_2\left(1 + \frac{p^k |h^k|^2}{\Gamma \tilde{\sigma}^k}\right) \quad (1.11)$$

In this thesis, we do two simplifications on (1.11). First, we always exclude the constant  $\Delta_f$  and consider the natural logarithm, denoted by  $\log(\cdot)$ . Second, we normalize the background noise power by defining  $\sigma^k = \Gamma \tilde{\sigma}^k |h^k|^{-2}$ . Thus, we re-write (1.11) as

$$b^k = \log\left(1 + \frac{p^k}{\sigma^k}\right) \quad (1.12)$$

We call both (1.11) and (1.12) the data rate on tone  $k$ , but use only (1.12) throughout this text. Notice that they are related by a simple constant, i.e.  $b^k = \log(2)(\Delta_f)^{-1} \tilde{b}^k$ . We remark that, throughout this thesis, we ignore the practical constraint of discrete bit allocation, i.e. we consider  $b^k$  to be a continuous variable.

Next, define the vector  $\mathbf{p} = [p^1 \ \dots \ p^K]^T \in \mathbb{R}_+^K$ . This vector represents the power allocation through the tones, i.e. this is the decision variable for the dynamic power allocation. Also, define the set of tones to be  $\mathcal{K} = \{1, 2, \dots, K\}$ . To maximize the total data rate of the DMT system we have to solve the following optimization problem:

$$\begin{aligned} \max_{\mathbf{p}} \quad & \sum_{k \in \mathcal{K}} b^k \\ \text{subject to} \quad & \sum_{k \in \mathcal{K}} p^k \leq P^{\max} \end{aligned} \quad (1.13)$$

The goal here is to find a vector  $\mathbf{p}$  that maximizes the total data rate (i.e. the sum of the per-tone data rates) while respecting a power constraint (PC)  $P^{\max}$  (i.e. the sum of the per-tone powers should not exceed  $P^{\max}$ ).

To solve this optimization problem, we use the fact that the sum of logarithms in the form of (1.13) is a concave function [7]. Because the constraint in (1.13) forms a convex set, the optimization problem is concave. That makes it easy to solve. To arrive at the solution, we can use the well-known Karush-Kuhn-Tucker (KKT) conditions. Towards this end, we first write the Lagrangean of (1.13) as

$$L(\mathbf{p}, \lambda) = \sum_{k \in \mathcal{K}} b^k - \lambda \left( \sum_{k \in \mathcal{K}} p^k - P^{\max} \right)$$

Here  $\lambda$  is a Lagrange multiplier. Because of concavity, the optimal solution can be found by taking the derivative of  $L(\mathbf{p}, \lambda)$  in  $\mathbf{p}$ , setting it to zero and solving for  $p^k$  [7, 51]. After a few simple manipulations, we find

$$p^k = \max\left(\frac{1}{\lambda} - \sigma^k, 0\right) \quad (1.14)$$

This is the well-known *waterfilling formula*.

The power allocation described by (1.14) can be interpreted as pouring water in a bowl whose bottom is uneven. The term  $\lambda^{-1}$  is the water level and the bottom of the bowl is stairs-like with  $K$  levels, with the  $k$ th level having height of  $\sigma^k$ . The power assigned to tone  $k$  is then the difference from the water level to the  $k$ th bottom height. Notice that negative values of power are not permitted, hence the  $\max(a, 0)$  operator. With (1.14), channels with low  $\sigma^k$  get more power than channels with high  $\sigma^k$ —notice that the previously defined  $\sigma^k = \Gamma \bar{\sigma}^k |h^k|^{-2}$  is the inverse channel-to-noise ratio. The water level depends on the Lagrange multiplier  $\lambda$ . To find the optimal  $\mathbf{p}$ , an appropriate  $\lambda$  should be found so that the power constraint is respected. This can be done with a simple bisection search due to the monotonous relation between  $\lambda$  and the total allocated power  $\sum_{k \in \mathcal{K}} p^k$ .

The waterfilling algorithm is very efficient, see, for example [10]. It also provides good gains in comparison to, for example, a situation where power is uniformly distributed through the tones. The ability of dynamical power allocation through the tones is another significant advantage of DMT in comparison to SC systems.

DMT modulation has also some disadvantages. We cite the example of the peak to average power ratio (PAPR): the sum of  $K$  exponentials with different frequencies can lead to peaks that, when passing through a power amplifier, generate distortion and waste of energy. See e.g. [79, 107]. However, we ignore this difficulty.

One additional fact is that DSL is actually a baseband transmission technology, which means that the signals that travel through the channel are real. In this section and in this thesis, we always use complex signals. Real signals can be

obtained by imposing complex conjugate symmetry in the transmitted signal vector  $\mathbf{x}$  and by performing IDFT/DFT operations with matrices that are twice as large—i.e. with  $\mathbf{F}, \mathbf{F}^H \in \mathbb{C}^{2K \times 2K}$  [102]. The need for real signals is a constraint that can be accommodated in the system model described in this section. The fact that we consider complex signals does not alter the resource allocation problems that are the focus of this thesis.

## 1.5.2 MIMO Case

MIMO has constituted a paradigm shift in the way communication systems are designed. It has captured the attention of researchers and the telecommunication industry since the 1990's, when it was first studied. The technology is an undeniable success, and within a decade it has evolved from a theoretical concept to practical implementation [3, 28, 72, 89]. MIMO is very popular in wireless communications, and most of the research and standardization activities when it comes to this technology have focused on wireless transmission. However, the same paradigm can be applied to any multi-transceiver scenario where there are cross channel gains between all transmitters and all receivers. Because of crosstalk, this is exactly the situation we find in a DSL cable binder.

Quite often it happens that several DSL lines terminate on the same equipment on both CO and CPE sides. For example, it can happen that several DSL servicing a small building depart together from the CO, travel together in the cable binder and arrive at the CPE at the same equipment (for example, an access multiplexer in the basement of said small building). If the signals can be collected and processed jointly on both sides of the network, this allows for MIMO transmission.

We remark that MIMO transmission on DSL encompasses the possible utilization of not only the DM, but also the alternative transmission modes discussed in Section 1.3. For example, a cable binder with 10 copper pairs (terminating on the same equipment on both the CPE and the CO sides) can have 19 communication channels, corresponding to 10 DMs and 9 PMs. Henceforth we will only use the term ‘transceiver’—we use it as a generalization of ‘line’. We define a transceiver to be connected to a physical communications channel, which can be a differential or a common mode of a DSL line, a phantom mode of two copper pairs, or a split-wire. In wireless, a similar terminology would be antenna.

MIMO achieves increases in data rate in relation to SISO systems due to the exploitation of three different gains: The *beamforming gain*, the *diversity gain* and the *multiplexing gain* [5]. The beamforming gain arises from combining

the multiple replicas of the transmitted signal in a coherent way so that the SNR is improved. The diversity gain applies more to wireless communications. It arises from the fact that, given all the replicas of the transmitted signal, it is unlikely that all of them experience deep fades simultaneously. The multiplexing gain arises from the use of extra dimensions opened up by the use of multiple transceivers. These extra dimensions can carry simultaneous symbols through the channel, leading to a linear increase in capacity. For the DSL case, both beamforming and multiplexing gains can be exploited.

In this section, we focus on the DMT MIMO transmission on a collection of DSL lines that can be coordinated on both the transmitter and the receiver sides. In the literature, it is often called a *MIMO point-to-point* system. In the DSL literature, DMT MIMO is sometimes called *bonding* [47, 76]. DSL with bonding can provide impressive gains in data rate, with 4 bonded DSL lines using DM providing something close to 1 Gb/s with 100 m line lengths.

Consider that the cable binder has  $A$  transceivers and define the set  $\mathcal{A} = \{1, \dots, A\}$ .<sup>1</sup> Each transceiver uses DMT modulation. After the standard DMT steps described in Section 1.5.1, transceiver  $i$  sees  $\mathbf{x}_{(i)} \in \mathbb{C}^K$ , with the element on tone  $k$  being  $x_{(i)}^k$ . By concatenating the symbols of all transceivers on tone  $k$  in the vector  $\mathbf{x}^k = [x_{(1)}^k \ \dots \ x_{(A)}^k]^\top \in \mathbb{C}^A$ , we write the received signal vector for tone  $k$  as

$$\mathbf{y}^k = \mathbf{H}^k \mathbf{x}^k + \mathbf{z}^k \quad (1.15)$$

Here  $\mathbf{x}^k = [x_{(1)}^k \ \dots \ x_{(A)}^k]^\top \in \mathbb{C}^A$  is the transmitted symbol vector for tone  $k$ ;  $\mathbf{z}^k \in \mathbb{C}^A$  represents circularly symmetric zero mean complex Gaussian noise vector for tone  $k$ ; and  $\mathbf{H}^k \in \mathbb{C}^{A \times A}$  represents the channel matrix for tone  $k$ . Notice that the diagonal elements of  $\mathbf{H}^k$  represent ‘direct’ channels, i.e. from the transmitter of transceiver  $i$  to the receiver of the same transceiver  $i$ . For the simulations in this thesis, these channels are obtained with (1.1). The off-diagonal elements represent crosstalk channels, i.e. from the transmitter of transceiver  $j$  to the receiver of the transceiver  $i$ ,  $i \neq j$ . As we remark in Section 1.3, to circumvent the problem of having a crosstalk channel without a phase, for the simulations in this thesis that involve MIMO transmission we obtain the crosstalk channels with (1.3). Notice that in  $\mathbf{H}^k$  we use the tone index  $k$  as superscript.

MIMO uses processing on both sides of the transmission channel. Processing on the transmitter side is done by the matrix  $\mathbf{T}^k \in \mathbb{C}^{A \times A}$ , the *transmit matrix* for tone  $k$ . Before transmission, the symbol vector is multiplied by  $\mathbf{T}^k$ . This

---

<sup>1</sup>We remark that we consider that the  $A$  transceivers are available for transmission on both sides of the network. In wireless, this is equivalent to saying that the user has  $A$  transmit antennas and  $A$  receive antennas.

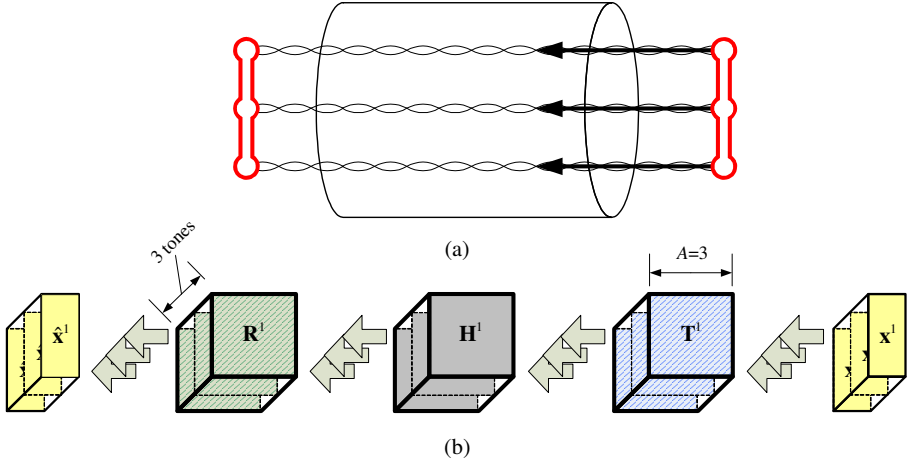


Figure 1.6: (a) Cable binder with three transceivers (three DM) and two-sided coordination; (b) Block diagram for the DMT MIMO for a scenario with 3 tones. The user has 3 transceivers. For simplicity, the zero mean Gaussian noise is not shown.

entails that we substitute  $\mathbf{x}^k$  in (1.15) by  $\mathbf{T}^k \mathbf{x}^k$  and re-write it as

$$\mathbf{y}^k = \mathbf{H}^k \mathbf{T}^k \mathbf{x}^k + \mathbf{z}^k \quad (1.16)$$

Processing on the receiver side is done by  $\mathbf{R}^k \in \mathbb{C}^{A \times A}$ , the *receive matrix* for tone  $k$ .<sup>2</sup> The received symbol vector is multiplied by  $\mathbf{R}^k$ . With these changes we write the estimated symbol vector on tone  $k$  as

$$\hat{\mathbf{x}}^k = \mathbf{R}^k \mathbf{H}^k \mathbf{T}^k \mathbf{x}^k + \mathbf{R}^k \mathbf{z}^k \quad (1.17)$$

Eq. (1.17) is the model for DMT MIMO transmission on tone  $k$ . We illustrate the block diagram of transmission in Fig. 1.6 for a system with three transceivers and three tones.

Our goal is to maximize the data rate of the transmission given by (1.17). We consider, without loss of generality, the noise covariance matrix on tone  $k$  to be  $\mathbb{E}[\mathbf{z}^k (\mathbf{z}^k)^H] = \tilde{\sigma}^k \mathbf{I}_A$ . Also, we define  $\mathbf{Q}^k = \mathbb{E}[\mathbf{x}^k (\mathbf{x}^k)^H] \in \mathbb{C}^{A \times A}$ , with  $\mathbf{Q}^k \succeq 0 \forall k$ , as the transmit covariance matrix on tone  $k$ ;  $\mathcal{T} = \{\mathbf{T}^k \mid k \in \mathcal{K}\}$  as the set of all transmit matrices;  $\mathcal{R} = \{\mathbf{R}^k \mid k \in \mathcal{K}\}$  as the set of all receive matrices; and  $\mathcal{Q} = \{\mathbf{Q}^k \mid k \in \mathcal{K}\}$  as the set of all transmit covariance matrices.

<sup>2</sup>Sometimes in the literature,  $\mathbf{T}^k$  is called a precoder and  $\mathbf{R}^k$  is called an equalizer.

In contrast to the SISO case, where only the power allocation through the tones can be optimized, in the MIMO case the decision variables are  $\mathcal{T}$ ,  $\mathcal{R}$  and  $\mathcal{Q}$ .

The optimal transmission strategy for MIMO in (1.17) consists in diagonalizing the channel matrix  $\mathbf{H}^k$  [89]. In order to do so, consider the singular value decomposition (SVD) of this matrix as  $\mathbf{H}^k = \mathbf{U}^k \text{diag} \left\{ \left[ \gamma_{(1)}^k \ \dots \ \gamma_{(A)}^k \right] \right\} (\mathbf{V}^k)^H \in \mathbb{C}^{A \times A}$ . Here  $\mathbf{U}^k$  and  $\mathbf{V}^k$  denote respectively the matrices of left and right singular vectors. The matrices  $\mathbf{U}^k$  and  $\mathbf{V}^k$  are unitary, i.e.  $\mathbf{V}^k (\mathbf{V}^k)^H = \mathbf{U}^k (\mathbf{U}^k)^H = \mathbf{I}_A$ . The vector  $\boldsymbol{\gamma} = \left[ \gamma_{(1)}^k \ \dots \ \gamma_{(A)}^k \right]^T \in \mathbb{R}^A$  is the vector of singular values of the channel matrix. We remark that throughout this thesis we always consider  $\mathbf{H}^k$  to be full rank.

In order to diagonalize  $\mathbf{H}^k$ , we set  $\mathbf{R}^k = (\mathbf{U}^k)^H$  and  $\mathbf{T}^k = \mathbf{V}^k$  for all tones. Then we can re-write (1.17) as

$$\hat{\mathbf{x}}^k = \text{diag} \{ \boldsymbol{\gamma} \} \mathbf{x}^k + (\mathbf{U}^k)^H \mathbf{z}^k. \quad (1.18)$$

Here, because  $\mathbf{U}^k$  is unitary, the noise covariance matrix is not altered.

In (1.18), because of the diagonalization of the channel matrix, all signals are coherently combined so as to provide improved SNR. This corresponds to the beamforming gain. Notice that the off-diagonal elements of  $\mathbf{H}^k$ , i.e. the ‘crosstalk’ channels, actually help transmission. After all, these crosstalk signals contain energy that can be detected on the other side of the network. Because of two-sided MIMO transmission, they become beneficial.

Also note in (1.18) how the channel is decomposed in  $A$  separate sub-channels or dimensions, commonly known as the channel eigenmodes. In our model, each transceiver corresponds to an eigenmode. We can use these transceivers or eigenmodes to simultaneously transmit  $A$  interference-free symbols or streams. This corresponds to the multiplexing gain.

Because of the diagonalized channel matrix, the optimal  $\mathbf{Q}^k$  is also diagonal for every tone. By considering  $p_{(i)}^k = \mathbb{E}[(x_{(i)}^k)^* x_{(i)}^k]$  to be the power allocated for transceiver  $i$  on tone  $k$ , the data rate for tone  $k$  is written as

$$\begin{aligned} b^k &= \sum_{i \in \mathcal{A}} \log \left( 1 + \frac{p_{(i)}^k (\gamma_{(i)}^k)^2}{\Gamma \tilde{\sigma}^k} \right) \\ &= \sum_{i \in \mathcal{A}} \log \left( 1 + \frac{p_{(i)}^k}{\sigma_{(i)}^k} \right) \end{aligned} \quad (1.19)$$

We again remark that, throughout this thesis, we ignore the practical constraint of discrete bit allocation, i.e. we consider  $b^k$  to be a continuous variable. In

(1.19), we define, similarly to Section 1.5,  $\sigma_{(i)}^k \triangleq (\gamma_{(i)}^k)^2 (\Gamma \bar{\sigma}^k)^{-1}$ . Now consider  $\mathbf{p} = [p_{(1)}^1 \ \dots \ p_{(A)}^K]^T \in \mathbb{R}_+^{K \cdot A}$  to be power allocation vector through tones and transceivers. The rate maximization problem for the DMT MIMO case thus reduces to

$$\begin{aligned} & \max_{\mathbf{p}} \sum_{k \in \mathcal{K}} b^k \\ & \text{subject to } \sum_{k \in \mathcal{K}} \sum_{i \in \mathcal{A}} p_{(i)}^k \leq P^{\max} \end{aligned} \tag{1.20}$$

Here, the problem is again about power allocation. However, this time power should be allocated through the tones and the transceivers. The optimal power allocation uses the waterfilling formula, which we write as

$$p_{(i)}^k = \max\left(\frac{1}{\lambda} - \sigma_{(i)}^k, 0\right). \tag{1.21}$$

The interpretation of (1.21) is the same as that of (1.14). As in (1.14), the Lagrange multiplier  $\lambda$  should be chosen so that the power constraint in (1.20) is respected.

## 1.6 The Crosstalk Problem

The DSL lines interfere with each other. Interference, also known as crosstalk, occurs when the electromagnetic radiation that is the consequence of signal transmission on one line creates an undesirable signal on neighboring lines. Hence, if two lines share the same cable binder, they can ‘see’ each other’s signals in their own lines. Crosstalk is familiar to many POTS users. It occurs when, instead of hearing the desired person on the other side of the telephone line, the user hears his neighbor. While for POTS crosstalk is but a mild annoyance, for DSL it is much more severe. That is so mainly because the technology uses much larger bandwidth than POTS and because crosstalk tends to increase with frequency. Crosstalk has been repeatedly been identified as the main source of performance degradation in DSL [17, 85].

There are two types of crosstalk, commonly known as near end crosstalk (NEXT) and far end crosstalk (FEXT). NEXT occurs when both the transmitter of the interferer and the receiver of the victim are on the same side of the network, i.e. both on the CO or both on the CPE side. FEXT occurs when transmitter of the interferer and the receiver of the victim are on opposite sides of the network, e.g. when the transmitter is on the CO side

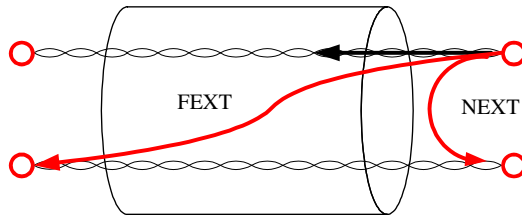


Figure 1.7: NEXT and FEXT.

and the receiver on the CPE side of the network. We illustrate the difference between the two in Fig. 1.7

NEXT is usually much stronger than FEXT. That is so because with NEXT there is close proximity from the transmitter of the interferer to the receiver of the victim. With FEXT, the interferer's signal has to travel the whole extent of the lines before it reaches the victim. The attenuation suffered by crosstalk with NEXT is much smaller than that suffered by crosstalk with FEXT.

Usually, NEXT is avoided altogether in modern DSL standards. In ADSL and VDSL, there is typically some frequency division duplexing between the upstream and downstream transmission bands, which means that the NEXT signal can be easily ignored. In G.fast, it is envisioned that some time division duplexing will separate upstream and downstream transmission. On this thesis, we only consider FEXT. From now on, when we refer to crosstalk we mean only FEXT.

In the previous section, we described DMT modulation for a single user in both SISO and MIMO cases. Since crosstalk effectively transforms the DSL cable binder into a multi-user channel, we have to focus on a multi-user version of DMT.

Consider the set of users to be  $\mathcal{N} = \{1, \dots, N\}$ . For the SISO case, let  $h_{n,j}^k$  be the channel gain between the transmitter of user  $j$  and receiver of user  $n$  at tone  $k$ ;  $x_n^k$  be the transmitted symbol for user  $n$  on tone  $k$ ; and  $z_n^k$  be circularly symmetric zero mean complex Gaussian noise for user  $n$  on tone  $k$ . The received signal for user  $n$  on tone  $k$  is obtained by re-writing (1.9) as

$$y_n^k = h_{n,n}^k x_n^k + \sum_{\substack{j \in \mathcal{N} \\ j \neq n}} h_{n,j}^k x_j^k + z_n^k$$

For symbol detection, we first compensate for the effects of the channel by calculating

$$\hat{x}_n^k = \frac{y_n^k}{h_{n,n}^k} = x_n^k + \sum_{\substack{j \in \mathcal{N} \\ j \neq n}} \frac{h_{n,j}^k}{h_{n,n}^k} x_j^k + \frac{z_n^k}{h_{n,n}^k}. \quad (1.22)$$

For the MIMO case, consider that user  $n$  has  $A_n$  transceivers. Let  $\mathbf{H}_{n,j}^k \in \mathbb{C}^{A_n \times A_j}$  be the channel matrix between the transmitter of user  $j$  and receiver of user  $n$  on tone  $k$ ;  $\mathbf{T}_n^k \in \mathbb{C}^{A_n \times A_n}$  to be the transmit matrix of user  $n$  on tone  $k$ ;  $\mathbf{x}_n^k$  be the transmitted symbol vector for user  $n$  on tone  $k$ ; and  $\mathbf{z}_n^k$  be circularly symmetric zero mean complex Gaussian noise vector for user  $n$  on tone  $k$ . The received signal vector for user  $n$  on tone  $k$  is obtained by re-writing (1.16) as

$$\mathbf{y}_n^k = \mathbf{H}_{n,n}^k \mathbf{T}_n^k \mathbf{x}_n^k + \sum_{\substack{j \in \mathcal{N} \\ j \neq n}} \mathbf{H}_{n,j}^k \mathbf{T}_j^k \mathbf{x}_j^k + \mathbf{z}_n^k.$$

For symbol detection, we first compensate the effects of the channel with the multiplication by  $\mathbf{R}_n^k$ , the receive matrix for user  $n$  on tone  $k$ , i.e.

$$\hat{\mathbf{x}}_n^k = \mathbf{R}_n^k \mathbf{H}_{n,n}^k \mathbf{T}_n^k \mathbf{x}_n^k + \mathbf{R}_n^k \sum_{\substack{j \in \mathcal{N} \\ j \neq n}} \mathbf{H}_{n,j}^k \mathbf{T}_j^k \mathbf{x}_j^k + \mathbf{R}_n^k \mathbf{z}_n^k. \quad (1.23)$$

We remark that both (1.22) and (1.23) represent *synchronous* multi-user transmission. Synchronous transmission is characterized by perfect receiver synchronization of the DMT blocks from all users. That means that, at reception, DMT blocks of different users begin and end at precisely the same instant. This leads to crosstalk that is decoupled across tones, which significantly simplifies the underlying resource allocation problem. In this thesis, we later focus on *asynchronous* multi-user transmission, i.e. the situation when the different DMT blocks arriving at a given receiver are not perfectly aligned in time. The consequence of the asynchronous transmission is inter-carrier interference (ICI). With ICI, the crosstalk decoupling is broken: a tone of an interfering user affects not only the corresponding tone of a victim user, but all neighboring tones too. We focus on asynchronous transmission in Chapter 5. Unless otherwise stated, we assume synchronous transmission.

Eqs. (1.22) and (1.23) are of fundamental importance because they represent the systems that we want to optimize. Notice that the elements in the summations in (1.22) and (1.23) represent interference, i.e. crosstalk. Needless to say that, because of multi-user interference, the single user strategies described for the SISO case in Section 1.5.1 and for the MIMO case in Section 1.5.2 are no longer optimal. If these strategies were applied to each user

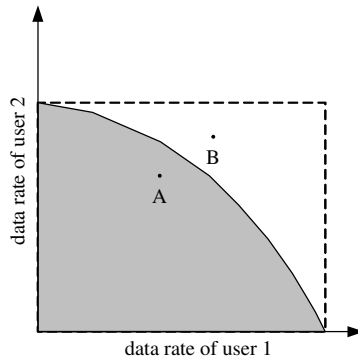


Figure 1.8: A typical RR. Point A is feasible, point B is not.

individually in the multi-user case, the network performance would suffer greatly. With interference, a wholly different set of transmission strategies is necessary.

## 1.7 Multiuser Information Theory

The multi-user transmission described in (1.22) and (1.23) are identified in information theory as an *interference channel* (IC). For decades now there have been efforts to characterize the capacity of these channels.

Because of the multi-user aspect, the characterization of the IC capacity contains  $N$  dimensions, whereas the capacity of single user channels can be described by a single number. The classical way to represent the capacity of multi-user channels is with a *rate region* (RR). The RR describes the tradeoff that is inherent of the sharing of the transmission channel by the various users. Generally speaking, the transmission channel can be construed as a limited collection of resources that all users have to share or compete for. On the one hand, as one of the users, say  $n$ , grabs more resources, its data rate increases. On the other hand, when user  $n$  does so, there is automatically less resources to all other users, which means that their data rates decrease.

A typical rate region is depicted in Fig. 1.8 for a case with two users. All points on the gray shaded area are feasible. Note that, if there were no interference, the RR would be a rectangular region.

We identify roughly three main approaches that have been taken in the literature so as to manage interference and characterize the RR of the IC [9,38].

- Decode: this approach is used in [11, 35] and applies to the case when interference is very strong. In this case, the interfering signal can be decoded first. Because interference is very strong, the detection of the interfering signal is almost perfect. The interfering signal is then subtracted from the received signal. The desired signal is in an ideal case free of interference. The channel capacity (at least for the two user case) is the sum of the interference-free per-user capacities, i.e. the RR is rectangular. In the literature, this approach is considered to be of limited practical applicability.
- Orthogonalize: This consists of the division of the resources of the channel between the users so that they are separated and hence do not interfere with each other. This separation can be done in the time, frequency or space dimensions, for example. Frequency or time separation is known to lead to poor performance. Recently, space separation of the users has been investigated with the concept of *interference alignment* [8, 9], which does provide good results given that all users operate with high SNR.
- Treat as noise: this option is a pragmatic way to deal with resource allocation problem in the IC. In this case, interference is treated as Gaussian noise, which leads to simpler designs for receivers and transmitters.

Throughout this thesis, we always treat interference as Gaussian noise. This is both the most pragmatic and the most common way in the literature to manage interference.

Notice here that the underlying assumption in the ‘treat as noise’ option is that interference is considered to be *Gaussian* noise. Some papers have attempted to ground this assumption more solidly with theoretical analyses. Ref. [41], for example, focuses on HDSL and shows that NEXT is very nearly Gaussian even for a case with only four interferers. In [82], a transmission scheme that treats interference as Gaussian noise achieves capacity under certain conditions that are typically satisfied in DSL networks. Hence, for DSL the assumption that interference is Gaussian noise is reasonably well justified.

With this assumption in hands, we consider, for the SISO case, the signal for user  $n$  on tone  $k$  in (1.22) and re-write the data rate equation in (1.12) as

$$b_n^k = \log \left( 1 + \frac{p_n^k}{\sigma_n^k + \sum_{\substack{j \in \mathcal{N} \\ j \neq n}} \alpha_{n,j}^k p_j^k} \right)$$

Here, we define  $p_n^k = \mathbb{E} [x_n^k (x_n^k)^*]$  as the power allocated for user  $n$  on tone  $k$ ; as before, we define  $\sigma_n^k = \Gamma \tilde{\sigma}_n^k |h_{n,n}^k|^{-2}$  as the normalized background noise

power, where  $\tilde{\sigma}_n^k = \mathbb{E} [z_n^k (z_n^k)^*]$ ; and

$$\alpha_{n,j}^k = \frac{\Gamma |h_{n,j}^k|^2}{|h_{n,n}^k|^2}, \quad n, j \in \mathcal{N}, \quad n \neq j$$

as the normalized crosstalk channel gain from the transmitter of user  $j$  to the receiver of user  $n$  on tone  $k$ . In the simulations in this thesis, we calculate  $h_{n,j}^k$  with (1.2).

Furthermore, we consider, for the MIMO case, the signal for user  $n$  on tone  $k$  in (1.23) and write the data rate equation as

$$b_n^k = \log \left| \mathbf{I}_{A_n} + (\mathbf{T}_n^k)^H (\mathbf{H}_{n,n}^k)^H (\mathbf{M}_n^k)^{-1} \mathbf{H}_{n,n}^k \mathbf{T}_n^k \right|.$$

where

$$\mathbf{M}_n^k = \Gamma \left( \sum_{\substack{j \in \mathcal{N} \\ j \neq n}} \mathbf{H}_{n,j}^k \mathbf{T}_j^k (\mathbf{T}_j^k)^H (\mathbf{H}_{n,j}^k)^H + \tilde{\sigma}_n^k \mathbf{I}_{A_n} \right) \quad (1.24)$$

is the noise covariance matrix of user  $n$  on tone  $k$ . For the simulations in this thesis, the  $(l, i)$ th element of  $\mathbf{H}_{n,j}^k$ ,  $l = 1, \dots, A_n$  and  $i = 1, \dots, A_j$ , is obtained with (1.3). We consider  $\mathbb{E} [\mathbf{z}_n^k (\mathbf{z}_n^k)^H] = \tilde{\sigma}_n^k \mathbf{I}_{A_n}$  and we fix  $\mathbf{Q}_n^k = \mathbb{E} [\mathbf{x}_n^k (\mathbf{x}_n^k)^H] = \mathbf{I}_{A_n} \quad \forall n, k$ . For the sake of conciseness, we usually re-write (1.24) as

$$\mathbf{M}_n^k = \sum_{\substack{j \in \mathcal{N} \\ j \neq n}} \mathbf{H}_{n,j}^k \mathbf{T}_j^k (\mathbf{T}_j^k)^H (\mathbf{H}_{n,j}^k)^H + \mathbf{I}_{A_n} \quad (1.25)$$

Here the crosstalk channel matrices  $\mathbf{H}_{n,j}^k$ ,  $j \neq n$  already include the SNR gap  $\Gamma$  and the background noise covariance is considered to be  $\mathbb{E} [\mathbf{z}_n^k (\mathbf{z}_n^k)^H] = \mathbf{I}_{A_n}$ . Notice that (1.24) and (1.25) amount to the same thing.

We again remark that, throughout this thesis, we ignore the practical constraint of discrete bit allocation, i.e. we consider  $b_n^k$  to be a continuous variable. Also, we sometimes use

$$r_n = \sum_{k \in \mathcal{K}} b_n^k$$

as the total data rate of transmission for user  $n$ . Moreover, for the MIMO case we only consider linear transmitters and receivers.

It is important to notice that now, for the SISO case, the per-tone data rate  $b_n^k$  depends not only on  $p_n^k$ , but on all other  $p_j^k$ ,  $j \neq n$  as well. In other words,  $b_n^k$  is now a function of the vector  $\mathbf{p}^k = [p_1^k \quad \dots \quad p_N^k]^T \in \mathbb{R}_+^N$ , which represents the power allocation of all users on tone  $k$ . As a simple example, consider a network with two users. If user 2 acts selfishly and allocates too much power

on tone  $k$ , its own data rate increases. At the same time, the data rate of user 1 decreases due to increased interference. How big this decrease is relates to (among other things) how large the normalized crosstalk channel gain  $\alpha_{1,2}^k$  is. This is exactly the type of competitive tradeoff for the resources of the system that is conveyed by the RR.

For the MIMO case, the per-tone data rate  $b_n^k$  depends not only on  $\mathbf{T}_n^k$ , but on all other  $\mathbf{T}_j^k$ ,  $j \neq n$  as well (note that we have fixed the transmit covariance matrix as  $\mathbb{E}[\mathbf{x}_n^k(\mathbf{x}_n^k)^H] = \mathbf{I}_{A_n} \forall n, k$ ). In other words,  $b_n^k$  is now a function of the set  $\mathcal{T}^k = \{\mathbf{T}_n^k \mid n \in \mathcal{N}\}$ . The goal of these transmit matrices is to use the extra dimensions provided by MIMO to perform the *spatial separation* (also known as spatial multiplexing) of the different signals. The ideal spatial separation is one which the desired signal vector seen at the receiver of one given user, say  $n$ , is perfectly orthogonal to all interferer's signal vectors, i.e. all  $j \neq n$ . As a simple example, consider again a two user network. If user 2 acts selfishly and uses its own channel eigenmodes for transmission, then, as explained in Section 1.5.2, its data rate is maximized. However, most likely the signal vectors of user 2 align badly at the receiver of user 1, which can lead to excessive interference and a decrease in data rate for the latter. Again, this represents the competitive tradeoff for the resources of the system that is conveyed by the RR.

## 1.8 Dynamic Spectrum Management

Generally speaking, in a communications system where multiple users have competing utilities, the intelligent allocation of the system resources offers the system designer a chance to significantly improve the network performance. With proper resource allocation, the competing users can be coordinated such that the transmission of each user is designed so as to maximize its own utility while being as little detrimental as possible to the transmission of all others. The system designer can count with a wide range of options so as to perform this coordination, such as the dimensions of power, code, space, frequency, time and waveform.

*Dynamic spectrum management* (DSM) classically focuses on the dimensions of frequency, power and space (i.e. transceivers) [85]. DSM looks for improvements by means of multi-user spectrum and/or signal coordination techniques. The main objective is to avoid, cancel or even profit from crosstalk. In the past ten to fifteen years, theoretical research has shown that data rate improvements achievable with DSM can be formidable.

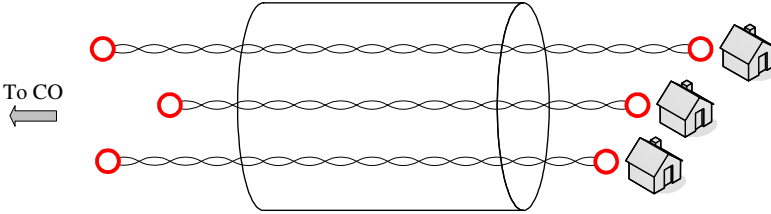


Figure 1.9: A typical scenario for spectrum coordination DSM.

DSM has typically been classified in levels ranging from zero to 3, with the amount of coordination increasing with each level. DSM level 0 is the situation with no coordination at all, DSM levels 1 and 2 use spectrum coordination and DSM level 3 uses (sometimes two-sided) signal coordination. This classification, however, is somewhat unnatural. It can be that a given scenario demands both signal and spectrum coordination. In this thesis, we classify DSM techniques according to their use of signal or spectrum coordination.

*Spectrum coordination* aims to allocate transmit power to the multiple users in the available spectrum so that crosstalk is avoided or minimized. It classically applies to the multi-user SISO IC scenario. A typical scenario is depicted in Fig. 1.9. Previous work on this topic includes [15–17, 57–59, 73, 96, 105, 106, 109, 110]. Spectrum coordination does not deliver the same gains as signal coordination does, but it profits from simplified requirements on infrastructure and smaller online complexity. For spectrum coordination, users do not necessarily have to have physically co-located transmitters and receivers, and a number of algorithms optimize a network in which little or no message exchanges between users take place. Spectrum coordination algorithms are in use today in the forms of waterfilling-based bit loading, downstream power back-off and upstream power back-off. Spectrum coordination is the topic of Part I of this thesis.

*Signal coordination*, also known as vectoring, involves multiple-input, multiple-output (MIMO) processing, either two-sided or single-sided. Previous work includes [13, 14, 26, 27, 29, 39, 44, 46, 47, 47, 48]. With signal coordination, requirements on infrastructure are considerably higher. For signal coordination, users have to have some physically co-located transmitters and/or receivers at the same equipment, and knowledge of all signals and all channel gains involved is usually required. On the plus side, signal coordination is able to deliver substantial gains in comparison to spectrum coordination, eliminating most or all crosstalk and sometimes even using crosstalk for its benefit. Note that the fact that crosstalk can be beneficial can be interpreted as a beamforming gain (see Section 1.5.2).

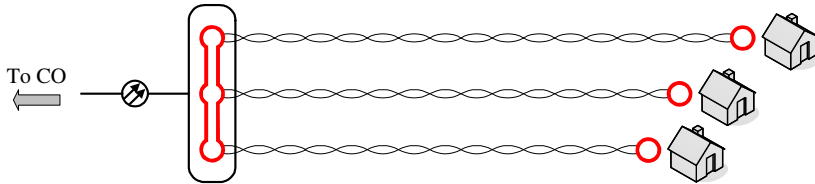


Figure 1.10: This is the most common scenario considered so far for signal coordination. In the upstream, we have a multiple access channel (MAC); and in the downstream, we have a broadcast channel (BC).

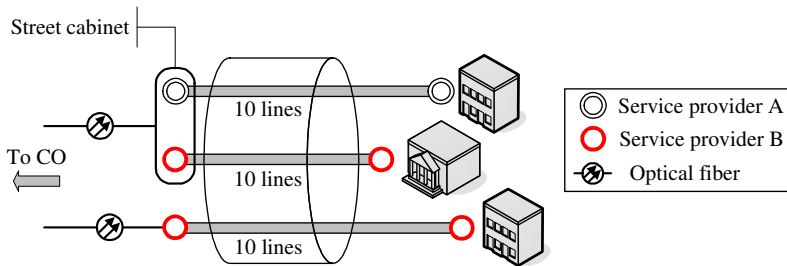


Figure 1.11: A typical scenario for combined signal and spectrum coordination DSM.

Hitherto most previous work in the literature have applied signal coordination in two distinct situations. The first situation is one with full, two-sided coordination. In our nomenclature, this is a single user system with bonding (i.e. MIMO point-to-point, see Section 1.5.2). The second situation is the one that is considered by the majority of papers in the DSM signal coordination literature. It is the one where each user uses one DSL and there is full coordination on the CO side of the network but no coordination on the CPE side of the network. We add that by saying that coordination is on the CO side of the network we mean that coordination can be done on the CO itself or in a cabinet, basement, or DP. This situation arises when several independent and geographically spread CPEs, each with one DSL line, have their lines arriving at the same location on the CO side of the network. This kind of scenario leads to a situation where, in the upstream, the transmitting CPEs are not coordinated but all signals can be collected on the CO side and jointly processed—i.e. a *multiple access channel* (MAC); and in the downstream, the signals can be jointly processed before transmission on the CO side but the receiving CPEs are not coordinated—i.e. a *broadcast channel* (BC). An example of such situation can be seen in Fig. 1.10. In the figure, we see many DSL lines starting from the same node to service several geographically dispersed houses.

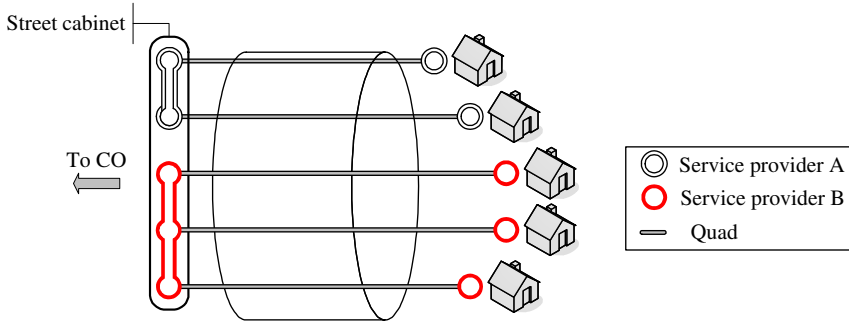


Figure 1.12: Another typical scenario for combined signal and spectrum coordination DSM.

In this thesis, we consider that applying signal coordination to only two types of scenarios to be too restrictive. We observe that such assumptions on the organization of the network are too limited and do not encompass all the complexity of DSL networks. We give two examples to illustrate our point.

For the first example, consider a situation where a set DSL lines start from a node on the CO side of the network to service a building. Consider that all lines arrive together on same equipment on the basement of said building. This allows for signal coordination on both sides of the network. We refer to this connection as a branch in the network. More specifically, we define a branch as a collection of DSL lines that start from the one single node and arrive at another single node. Now consider that several such branches share the same cable binder. See Fig. 1.11 for an illustration. Within each branch, two-sided signal coordination is theoretically possible. However, whenever some branches terminate on different nodes or when local loop unbundling is regulatory required, signal coordination among all the users is not possible, and so part of the coordination should be done on the spectrum level.

For the second example, consider that each of the houses in Fig. 1.12 operates with two DSL lines. We remind that all lines start from the same node on a DP (i.e. the CO side of the network). Consider that these houses are serviced by two different service providers. Furthermore, consider that the lines belonging to the same service provider can be coordinated on the signal level, but also take into account that local loop unbundling is regulatory required, so no inter-service-provider coordination is possible. So the situation is: inter-user coordination is possible on the DP for the users that belong to the same service provider; inter-user coordination is not possible on the CPE side because the

houses are geographically dispersed; and inter-service-provider coordination is not possible. In this scenario, both signal and spectrum coordination should be applied.

Notice that the scenarios in the two examples are complex but consistent with the tree topology of DSL networks. These scenarios do not fit perfectly in the classical situations where signal and spectrum coordination are applied. In these scenarios, both signal and spectrum coordination have to be used.

## 1.9 Thesis Overview and Contributions

This thesis aims at developing and analyzing signal and spectrum coordination techniques with an eye on the next generation of DSL networks. In a nutshell, the goal of this thesis is to contribute to make data travel even less difficult.

This introductory chapter outlined the main characteristics of DSL transmission and introduced the basic concepts that are used throughout this thesis. In this chapter, we have mentioned a couple of assumptions that we use in this thesis. We summarize them as follows:

- crosstalk is FEXT;
- the channel is perfectly known at both the transmitter and the receiver;
- we consider continuous data rates;
- imperfections of DMT (such as the PAPR problem) are ignored;
- for the MIMO case, we only focus on linear transmitters and receivers;
- interference is treated as Gaussian noise.

We remark that all these assumptions are standard in the DSL literature.

We now outline the organization and contributions of this thesis.

As mentioned, in Part I we focus on *spectrum coordination*. Here, every user uses one DSL line, which is treated as a SISO system (e.g. the scenario in Fig. 1.9). The goal is to come up with a fair sharing of the resources of the channel with dynamic power allocation. Towards this end, in Chapter 2, we first cast the power allocation problem as a weighted rate sum (WRS) maximization problem subject to per-user power constraints. We propose two algorithms for the solution of this problem. Both approaches start with the re-writing of the problem with different variables. The classical way to represent the

decision variables of the problem is with Cartesian vector coordinates, with each position of the vector denoting the power allocation of one user. We use spherical coordinates, which consists of representing the decision variables with a radius and a direction vector with a norm constraint. Spherical coordinates allow us to find a surprising amount of structure in the problem. With the first proposed algorithm, called OSB-SC, we find structure on the radius dimension. The remaining variables are solved with an exhaustive search. With the second algorithm, called TaSSO, we solve the problem in a block coordinate descent fashion, i.e. we solve a sequence of line searches. TaSSO uses a coordinate system that can be interpreted as spherical coordinates in taxicab geometry. We provide conditions for finding structure for each of the sub-problems. The two proposed algorithms save quite significantly in computational complexity. For example, we see that the OSB-SC can be up to 100 times faster than the relevant previous proposal. TaSSO can be 2-15 times faster than the relevant previous proposal. The contributions of Part I have been published as [67] and submitted for publication as [68]. Related material to spectrum coordination that is not discussed on this thesis has been published as [65,66].

In Part II, we focus on combined signal and spectrum coordination. This part of the thesis is divided in three chapters. In this part, each chapter pick up where the previous one has stopped and adds generality to the problem.

Chapter 3 focuses on a scenario that we call *DMT MIMO IC*. In this situation, some of the infrastructure required for full two-sided signal coordination is available, but not all. This scenario consists of multiple interfering users, each operating a distinct subset of transceivers as a MIMO system. Coordination is done both on the signal level (with MIMO techniques) and on the spectrum level (with multi-user power allocation). An example of such scenario is depicted in Fig. 1.11. We propose two algorithms for the DMT MIMO IC WRS maximization problem. In the first algorithm, called DMT-WMMSE, we profit from recent work showing the close relation between the WRS maximization problem and the weighted minimum mean squared error (MMSE) MMSE minimization problem. We show that with a simple extension, we can adapt the previous work to the scenario of interest. In the second algorithm, called WMMSE-GDSB, the signal and spectrum coordination parts are solved separately. For the signal coordination part, we obtain multiple independent single tone MIMO ICs, which allows us to leverage on the previous work on the topic. For the spectrum coordination part, one of the interesting results of our analysis is a generalization of the distributed spectrum balancing (DSB) [96] power allocation formula for the DMT MIMO IC scenario. Simulation results demonstrate that both algorithms obtain significant gains when compared to pure spectrum coordination algorithms.

In Chapter 4, we still focus on the DMT MIMO IC. However, while Chapter 3

considers per-user power constraints, in Chapter 4 we consider *per-transceiver* power constraints. Per-transceiver power constraints are more realistic, but they also add more complexity to the WRS maximization problem. We adapt the two algorithms of Chapter 3 to the per-transceiver case. First, we straightforwardly adapt the DMT-WMMSE algorithm. Second, we adapt the WMMSE-GDSB, in which we separate the problem in signal and spectrum coordination parts. For the spectrum coordination part, we show that the problem can be solved more efficiently with a change of coordinates: we use a coordinate system consisting of a radius and a direction vector with  $\ell_1$  norm equal to 1. This can be interpreted as spherical coordinates in taxicab geometry. It is observed that for the radial dimension the problem can be made concave after approximations and it is thus easy to solve. The remaining dimensions are solved with a sequence of line searches. Simulation results show that the WMMSE-GDSB converges faster.

In Chapter 5, we focus on the development of a *general framework* that includes all previous situations as a special case. By developing this framework, we can include not only the SISO IC or the DMT MIMO IC but also situations with any kind of inter-user coordination on both sides of the network. For example, this unified framework also accommodates BCs, MACs, ICs or anything in between, e.g. the scenario depicted in Fig. 1.12. Here we also focus on asynchronous transmission. We consider that different users in the network may have their DMT blocks not be perfectly aligned, which given rise to ICI. In this chapter, we first accurately model asynchronous transmission, then propose an algorithm, called GF-WMMSE-GDSB, that works for any number of users, any number of transceivers, any number of tones, any kind of coordination on both the transmitter and on the receiver sides, and synchronous or asynchronous transmission. The algorithm is seen to perform very well and with polynomial computational complexity.

The contributions of Part II have been published as [62, 64, 66] and submitted for publication as [61, 63]. Related material to combined signal and spectrum coordination that is not discussed on this thesis has been published as [98].

In Chapter 6, we draw final conclusions and discuss interesting future research directions.

## **Part I**

# **Spectrum Coordination**

## Chapter 2

# Spectrum Coordination with Spherical Coordinates

### 2.1 Introduction

In a communications system where multiple users have competing utilities, the intelligent allocation of the system resources offers the system designer means to significantly improve the network performance. With proper resource allocation, the competing users can be coordinated such that the transmission of each user is designed so as to maximize its own utility while being as little detrimental as possible to the transmission of all other users. The system designer can count on a wide range of options so as to perform this coordination, such as the dimensions of power, code, space, frequency, time and waveform.

In this part of the thesis, we focus on the dimensions of frequency and power. More specifically, we treat a SISO multi-user, multitone interference channel (IC) where the goal is to judiciously allocate power throughout frequency such that the weighted rate sum (WRS) of the users is maximized. Each user is subject to a power constraint (PC), which complicates the problem further.

The applications of this problem are numerous, and include both wireless and wireline systems. For the latter, the continued research activities to find efficient and high performance solutions to the power/frequency resource

allocation problem is referred to as spectrum coordination dynamic spectrum management (DSM), and its focus is usually on digital subscriber line (DSL) networks.

In the past ten to fifteen years extensive theoretical research [2, 16, 17, 36, 52, 53, 59, 62, 73, 83, 96, 99, 105, 109, 110, 112] has shown that spectrum coordination DSM leads to formidable gains in performance. In this chapter, we propose two algorithms for the solution of the spectrum coordination WRS maximization problem in DSL. Both algorithms exploit structure in order to save on computational complexity. Our approach is based on a change of variables. For a network of  $N$  users, the classical way to represent the decision variables of the problem is to define a vector  $\mathbf{p}^k = [p_1^k \ \cdots \ p_N^k]^T \in \mathbb{R}_+^N$  for each tone (i.e. sub-channel)  $k$ , where  $p_n^k$  is the power allocated for user  $n$  on tone  $k$ . The problem then consists in optimizing  $\mathbf{p}^k$  for every tone while respecting the per-user PCs. For the first algorithm, we change the decision variables as follows: we re-write  $\mathbf{p}^k$  in spherical coordinates, i.e.  $\mathbf{p}^k = \rho^k \mathbf{d}^k$ , with  $\|\mathbf{d}^k\|_2 = 1$ . Here  $\|\cdot\|_2$  is the  $\ell_2$  or Euclidean norm,  $\rho^k$  is the radius and  $\mathbf{d}^k$  is a direction vector—if  $N = 2$ , we have  $\mathbf{d}^k = [\cos \theta^k \ \sin \theta^k]^T$ ,  $\theta^k \in [0, \pi/2]$ . By observing that the WRS maximization problem is concave in the radius  $\rho^k$ , we propose an algorithm that optimizes the power allocation with an exhaustive search on the direction vector while concurrently optimizing for the radius by line search. The benchmark here is the optimal spectrum balancing (OSB) algorithm [17], which is built upon similar concepts but does an exhaustive search on the original, Cartesian coordinates vector. Because we exploit the structure in the radial dimension, we save considerably on computational complexity. We observe that our proposal can be 60 times faster than OSB.

For the second algorithm, we do yet another change of variables. We re-write the decision variables as  $\eta^k \mathbf{v}^k$ , where  $\|\mathbf{v}^k\|_1 = 1$ . Here  $\|\cdot\|_1$  is the  $\ell_1$  or taxicab norm,  $\eta^k$  is the radius and  $\mathbf{v}^k$  is a direction vector—if  $N = 2$ , we have  $\mathbf{v}^k = [(1 - \phi^k) \ \phi^k]^T$ ,  $\phi^k \in [0, 1]$ . This can be interpreted as spherical coordinates in taxicab geometry [43] (as opposed to Euclidean geometry). We show that with this coordinate system it is easier to use a block coordinate descent method, i.e. a sequence of line searches. As in the Euclidean spherical coordinates, concavity on the radial dimension still holds. We show that there is also structure to be exploited in the angle dimensions, i.e. the variables in the direction vector  $\mathbf{v}^k$ : we identify situations where the line searches for each of the angles are concave or convex. The structure in both the radial and in the angle dimensions are exploited in the second proposed algorithm with good savings in computational complexity. The benchmark here is the iterative spectrum balancing (ISB) algorithm [16], which also uses a block coordinate descent method but does not exploit structure. Through numerous simulations, it is observed that our

algorithm performs at least as well as ISB while being 2-15 times faster.

This chapter is organized as follows: in Section 2.2 we formalize the notation, present the problem in mathematical form and briefly discuss previous work. In Section 2.3 we present the first proposed algorithm, followed by analyses of computational complexity and precision. In Section 2.4.4 we present the second algorithm, along with an exposition on how to explore structure on the radial and on the angle dimensions. Section 2.5 presents some numerical experiments and finally Section 2.6 presents final remarks.

## 2.2 System Model and Previous Work

Consider an  $N$  user discrete multitone (DMT) system with  $K$   $\Delta_f$ -spaced tones. We define the set of users as  $\mathcal{N} = \{1, 2, \dots, N\}$  and the set of tones as  $\mathcal{K} = \{1, \dots, K\}$ . Let  $\mathbf{P} = \{p_n^k\} \in \mathbb{R}_+^{K \times N}$  be a matrix in which  $p_n^k$  is the transmit power of user  $n$  on tone  $k$ . We also define  $\mathbf{p}^k \in \mathbb{R}_+^N$  as the vector containing the powers of all users on tone  $k$ , i.e.  $\mathbf{p}^k = [p_1^k \dots p_N^k]^T \in \mathbb{R}_+^N$  and  $\mathbf{p}_n \in \mathbb{R}_+^K$  as the vector containing the powers of user  $n$  over all tones, i.e.  $\mathbf{p}_n = [p_n^1 \dots p_n^K]^T \in \mathbb{R}_+^K$ . Let  $h_{n,j}^k$  be the channel gain between the transmitter of user  $j$  and receiver of user  $n$  on tone  $k$ . The received signal for user  $n$  on tone  $k$  is given by

$$y_n^k = h_{n,n}^k x_n^k + \sum_{\substack{j \in \mathcal{N} \\ j \neq n}} h_{n,j}^k x_j^k + z_n^k. \quad (2.1)$$

Here, we consider the simplifying assumption of perfect DMT block synchronization between users [18, 66, 109]. Also, in our scenario every user operates with single input, single output (SISO) transmission. In (2.1),  $x_n^k$  and  $y_n^k$  are respectively the transmitted and received symbols for user  $n$  on tone  $k$  and  $z_n^k$  represents circularly symmetric zero mean complex Gaussian noise. We define  $p_n^k = \mathbb{E}[x_n^k (x_n^k)^*]$  as the transmit power and  $\tilde{\sigma}_n^k = \mathbb{E}[z_n^k (z_n^k)^*]$  as the Gaussian noise power, both relating to user  $n$  on tone  $k$ .

We remind that in this thesis, we consider all interference to be Gaussian noise. The data rate for user  $n$  on tone  $k$  is given by

$$b_n^k = \log \left( 1 + \frac{p_n^k}{\sigma_n^k + \sum_{\substack{j \in \mathcal{N} \\ j \neq n}} \alpha_{n,j}^k p_j^k} \right), \quad (2.2)$$

where  $\alpha_{n,j}^k = \Gamma |h_{n,j}^k|^2 |h_{n,n}^k|^{-2}$  is the normalized interference channel gain from user  $j$  to user  $n$  on tone  $k$  and  $\sigma_n^k = \Gamma \tilde{\sigma}_n^k |h_{n,n}^k|^{-2}$  is the normalized Gaussian

noise power. Also  $\Gamma$  accounts for the SNR gap to capacity, the noise margin and the coding gain [87]. We consider continuous data rates. The data rate of user  $n$  in bits per second is given by  $r_n = f_s / \log(2) \sum_{k \in \mathcal{K}} b_n^k$ , where  $f_s$  is the symbol rate.

The problem we focus on is that of maximizing the WRS of the participating users in the network while respecting their per-user PCs. Mathematically, we write

$$\begin{aligned} & \max_{\mathbf{P}} \quad \sum_{n \in \mathcal{N}} \sum_{k \in \mathcal{K}} u_n b_n^k \\ & \text{subject to} \quad \sum_{k \in \mathcal{K}} p_n^k \leq P_n^{\max}, \quad n \in \mathcal{N} \end{aligned} \tag{2.3}$$

Here,  $P_n^{\max}$  is the PC for user  $n$  and the  $u_n$  are weights assigned to the users. We call (2.3) the *spectrum coordination problem*. It can be shown that this problem is NP-hard [53].

As mentioned in the introduction, several works have focused on the spectrum coordination problem. Refs. [2, 36, 52, 53, 99, 112] focus primarily on theoretical analyses. These papers are important because they attempt to find structure in the spectrum coordination problem, which in turn can be used in the algorithms. In [53, 112] perhaps the most important characteristic of the spectrum coordination problem is rigorously formulated: it is established that, although the original problem is non-concave, its duality gap vanishes as the number of tones  $K$  increases to infinity. In the same vein, [52] provides an estimate of the duality gap. Ref. [36] provides conditions for the optimal solution of the problem to have a frequency division characteristic. In [2] some situations that allow for concave representation are identified. Some papers use a leakage or spillage criterium [20, 80]. In [99], it is shown that if the interference channel gains are weak enough, the spectrum coordination problem can be solved as a geometric program (GP).

Regarding the algorithms, several proposals are available, e.g. [16, 17, 59, 62, 73, 96, 105, 110]. The algorithms in [17] and [16] are of special interest to this chapter. In [17], the optimal spectrum balancing (OSB) algorithm is presented. This algorithm formulates the Lagrange dual of (2.3) and performs a per-tone exhaustive search for the powers, i.e. it exhaustively finds a  $\mathbf{p}^k$  that maximizes the per-tone Lagrangean. This per-tone exhaustive search is done on an  $N$ -dimensional grid. If the axes are sampled each with  $Q$  points, the total grid has  $Q^N$  points. The Lagrangean is then calculated for all grid points and the point that maximizes it is picked. On the minus side the applicability of OSB is hindered for large networks due to the exponentially increasing computational complexity (the grid size increases exponentially with  $N$ ). On

the plus side the two main elements of OSB (the per-tone exhaustive search and the vanishing duality gap in problems with large number of tones) make it approach optimality.

Of the lower computational complexity algorithms proposed so far the iterative spectrum balancing (ISB) algorithm [16] is a well-known example. In this algorithm, the objective function is maximized with a block coordinate descent method, i.e. when optimizing for a given user  $n$ , all other users have their powers fixed. The process repeats until convergence. Unlike the algorithms in [73, 96, 109], ISB does not do any approximation of the objective function. ISB has been shown time and again to perform very close to OSB for small and medium scenarios with only a fraction of the computational complexity.

## 2.3 Spectrum Coordination with Spherical Coordinates —Exhaustive Search for the Angles

As in [17], we write the Lagrangean of (2.3) as

$$L(\mathbf{P}, \boldsymbol{\lambda}) = \sum_{n \in \mathcal{N}} \sum_{k \in \mathcal{K}} u_n b_n^k - \sum_{n \in \mathcal{N}} \lambda_n \left( \sum_{k \in \mathcal{K}} p_n^k - P_n^{\max} \right). \quad (2.4)$$

Here  $\boldsymbol{\lambda} = [\lambda_1 \ \dots \ \lambda_N]^T \in \mathbb{R}_+^N$  is the vector of Lagrange multipliers associated with the per-user PCs. We formulate the dual problem as

$$\min_{\boldsymbol{\lambda}} \max_{\mathbf{P}} L(\mathbf{P}, \boldsymbol{\lambda}),$$

where appropriate values for  $\boldsymbol{\lambda}$  should be searched for so that the PCs are respected.

By re-writing (2.4) as

$$L(\mathbf{P}, \boldsymbol{\lambda}) = \sum_{k \in \mathcal{K}} L(\mathbf{p}^k, \boldsymbol{\lambda}) + \sum_{n \in \mathcal{N}} \lambda_n P_n^{\max},$$

where

$$L(\mathbf{p}^k, \boldsymbol{\lambda}) = \sum_{n \in \mathcal{N}} u_n b_n^k - \sum_{n \in \mathcal{N}} \lambda_n p_n^k, \quad (2.5)$$

we can see that the per-tone maximization of  $L(\mathbf{p}^k, \boldsymbol{\lambda})$  also leads to the maximization of (2.4). We can thus focus on the per-tone maximization of  $L(\mathbf{p}^k, \boldsymbol{\lambda})$ .

As is well known, the function  $L(\mathbf{p}^k, \boldsymbol{\lambda})$  is not concave in  $\mathbf{p}^k$  in general. When interference gains  $\alpha_{n,j}^k$  are very small, it can be that  $L(\mathbf{p}^k, \boldsymbol{\lambda})$  is concave. If

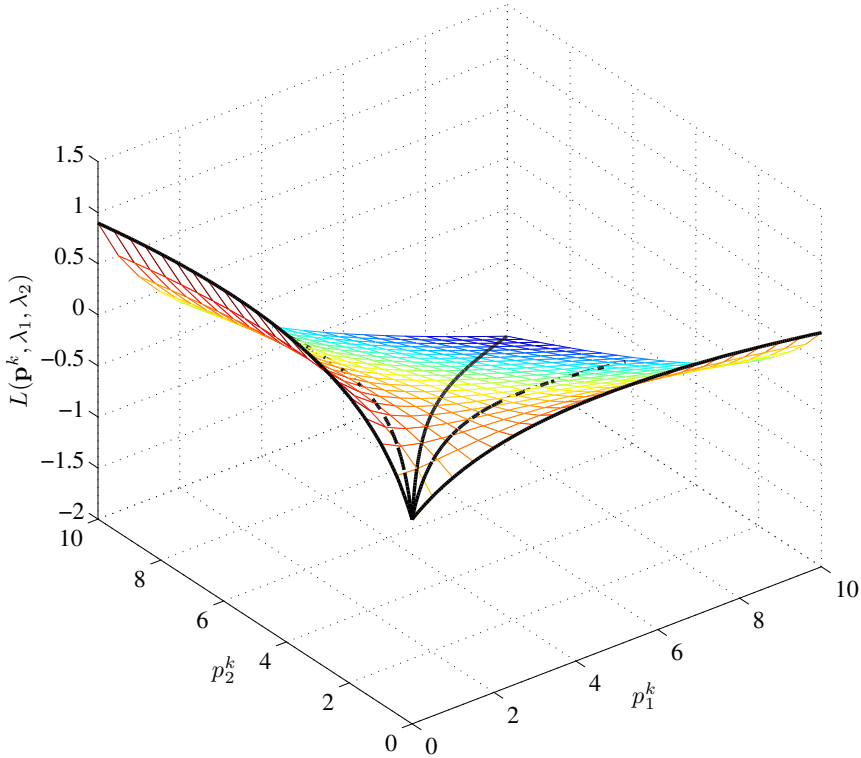


Figure 2.1: Illustration of non-concavity of  $L(\mathbf{p}^k, \boldsymbol{\lambda})$  for a two user case. We choose  $u_1 = u_2 = 0.5$ ,  $\alpha_{1,2}^k = \alpha_{2,1}^k = 1$ ,  $\sigma_1^k = 2$ ,  $\sigma_2^k = 1$ ,  $\lambda_1 = \lambda_2 = 0.15$ .

interference is sufficiently strong, then  $L(\mathbf{p}^k, \boldsymbol{\lambda})$  is maximized with only one active user [36]. We give an example of the latter case in Fig. 2.1, where  $N = 2$ . To find the  $\mathbf{p}^k$  that maximizes  $L(\mathbf{p}^k, \boldsymbol{\lambda})$  for the  $N = 2$  case, OSB discretizes the  $p_1^k$ - $p_2^k$  plane with  $Q^2$  points, calculates  $L(\mathbf{p}^k, \boldsymbol{\lambda})$  on the grid points and picks the best one.

Our approach is different. The first step is to do a change of variables. We write  $\mathbf{p}^k$  in spherical coordinates, i.e.

$$\mathbf{p}^k = \rho^k \mathbf{d}^k, \quad \rho^k \geq 0, \quad \|\mathbf{d}^k\|_2 = 1, \quad (2.6)$$

where  $\rho^k$  is the radius and  $\mathbf{d}^k = [d_1^k \ \dots \ d_N^k] \in \mathbb{R}_+^N$  is a direction vector. Eq. (2.6) describes the positive quadrant of an  $N$ -dimensional sphere. As a more

concrete example, consider that  $N = 3$ . Eq. (2.6) is written as

$$\mathbf{p}^k = \rho^k \begin{bmatrix} \cos \theta_{[1]}^k & \cos \theta_{[2]}^k \\ \cos \theta_{[1]}^k & \sin \theta_{[2]}^k \\ \sin \theta_{[1]}^k & \end{bmatrix}, \quad \rho^k \geq 0, \quad \theta_{[1]}^k, \theta_{[2]}^k \in \left[0, \frac{\pi}{2}\right]. \quad (2.7)$$

We write the spherical coordinates representation of a general  $N$ -dimensional vector in Appendix A.1 in (A.1), (A.2) and (A.3).

We make two important remarks about (2.6). First, it is very natural to associate the variables of the spectrum coordination problem with users, i.e.  $p_1^k$  for user 1 until  $p_N^k$  for user  $N$ , and literally all previous work has done so.<sup>1</sup> This is not the case with the spherical coordinates. In (2.7) for example, by changing the radius  $\rho^k$ , all user's powers change (in the Cartesian vector). By changing the angle  $\theta_{[1]}^k$ , the powers of users 1 and 2 change. This motivates our choice not to use subscripts for  $\rho^k$  and to use bracketed subscripts for the angles, e.g.  $\theta_{[2]}^k$  and  $\theta_{[2]}^k$  in (2.7). For the angles, the bracketed subscripts are best interpreted as directions, not users. Second, notice that although  $\mathbf{d}^k$  is  $N$ -dimensional, it has only  $N - 1$  free variables, i.e.  $\theta_{[1]}^k, \theta_{[2]}^k, \dots, \theta_{[N-1]}^k$  (see, for example, (2.7) or, for the general case, (A.1)-(A.3)). This is a direct consequence of the  $\ell_2$  norm constraint in (2.6).

We continue by redefining some formulas. We re-write (2.2) and (2.5) as

$$b_n^k = \log \left( 1 + \frac{\rho^k d_n^k}{\sigma_n^k + \sum_{\substack{j \in \mathcal{N} \\ j \neq n}} \alpha_{n,j}^k \rho^k d_j^k} \right) \quad (2.8)$$

$$L(\rho^k, \boldsymbol{\theta}^k, \boldsymbol{\lambda}) = \sum_{n \in \mathcal{N}} u_n b_n^k - \sum_{n \in \mathcal{N}} \lambda_n \rho^k d_n^k.$$

Here we define  $\boldsymbol{\theta}^k = [\theta_{[1]}^k \ \dots \ \theta_{[N-1]}^k]^\top \in \mathbb{R}_+^{N-1}$ ,  $\theta_{[i]}^k \in [0, \pi/2]$ ,  $i = 1, \dots, N-1$ .

The advantage of using spherical coordinates is that, while keeping  $\mathbf{d}^k$  fixed, there is structure to be found on the radial dimension.

**Proposition 2.1.** *For a fixed direction  $\mathbf{d}^k$ ,  $L(\rho^k, \boldsymbol{\theta}^k, \boldsymbol{\lambda})$  is strictly concave in  $\rho^k$ .*

---

<sup>1</sup>In Chapter 4 we also use spherical coordinates to solve the DMT MIMO IC WRS maximization problem with per-transceiver PCs.

*Proof.* It suffices to calculate the second derivative in  $\rho^k$  and show that

$$\frac{\partial^2 L(\rho^k, \boldsymbol{\theta}^k, \boldsymbol{\lambda})}{\partial (\rho^k)^2} = - \sum_{n \in \mathcal{N}} \frac{u_n d_n^k \sigma_n^k \left( 2I_n^k \rho^k (d_n^k + I_n^k) + 2I_n^k \sigma_n^k + d_n^k \sigma_n^k \right)}{(I_n^k \rho^k + \sigma_n^k)^2 \left( (I_n^k + d_n^k) \rho^k + \sigma_n^k \right)^2} < 0. \quad (2.9)$$

Here

$$I_n^k = \sum_{\substack{j \in \mathcal{N} \\ j \neq n}} \alpha_{n,j}^k d_j^k. \quad (2.10)$$

Since  $d_n^k \geq 0 \forall n$ , all variables in (2.9) are non-negative. Hence each term of the summation in  $n$  is non-negative. Because  $\|\mathbf{d}^k\| = 1$ , at least one term in the sum is strictly positive. Hence the sum is strictly positive. Because of the minus sign, the second derivative is, for  $\rho^k \geq 0$ , always strictly negative.  $\square$

The consequence of Proposition 2.1 is illustrated in Fig. 2.1. In the figure, the dark lines show  $L(\rho^k, \boldsymbol{\theta}^k, \boldsymbol{\lambda})$  for fixed angles  $\boldsymbol{\theta}^k = \{0, \pi/8, \pi/4, \pi/6, \pi/2\}$ . One interesting way to interpret this result is the following: for  $\boldsymbol{\theta}^k = 0$  and  $\boldsymbol{\theta}^k = \pi/2$ , it is well known that  $L(\rho^k, \boldsymbol{\theta}^k, \boldsymbol{\lambda})$  is concave in  $\rho^k$ . After all, these two cases represent situations with a single user. With Proposition 2.1 we generalize concavity for all other angles  $\boldsymbol{\theta}^k \in [0, \pi/2]$ .

### 2.3.1 Algorithm

Because of the concavity in the radial dimension, we can save considerably on computational complexity. In this section, we describe a per-tone exhaustive search algorithm that uses the spherical coordinates formulation. Our strategy consists of an exhaustive search only in the variables of the direction vector, i.e. in  $\theta_{[1]}^k, \theta_{[2]}^k, \dots, \theta_{[N-1]}^k$ . We construct an  $(N-1)$ -dimensional grid with each of the continuous axes (in  $[0, \pi/2]$ ) sampled with  $Q$  points. A point in this grid corresponds to a vector  $\mathbf{d}^k$ , hence a direction. For a fixed direction, since optimizing for the radius is a concave line search problem, we write  $L(\hat{\rho}^k(\mathbf{d}^k), \mathbf{d}^k, \boldsymbol{\lambda})$ , where  $\hat{\rho}^k(\mathbf{d}^k)$  is the optimal radius for  $\mathbf{d}^k$ .

A pseudocode is provided in Algorithm 2.1. We name the algorithm OSB with spherical coordinates (OSB-SC). In line 2, the  $(N-1)$ -dimensional vector space  $[\theta_{[1]} \ \dots \ \theta_{[N-1]}]^T$ , with  $\theta_{[i]} \in [0, \pi/2] \forall i$ , is sampled with  $Q$  points on each axis. It is natural to do so uniformly when all axes are in dB scale [17]. In line 4 we calculate the optimal radius for each fixed direction and fixed  $\boldsymbol{\lambda}$ . Since this is a one dimensional concave problem, we can solve it with the Newton method. In line 5 the exhaustive search is performed and in line 6 we transform back to Cartesian coordinates—here  $\mathbf{d}^k(\hat{\boldsymbol{\theta}}^k)$  is the vector that corresponds to  $\hat{\boldsymbol{\theta}}^k$  for

---

**Algorithm 2.1:** OSB-SC

---

- 1 Initialize  $\lambda$ ;
  - 2  $\mathcal{D} \leftarrow$  discretized  $\theta$ -space, with  $\theta_{[i]} \in [0, 1] \forall i$ ;
  - 3 **repeat**
  - 4     Obtain  $\hat{\rho}^k(\boldsymbol{\theta}^k)$ ,  $\boldsymbol{\theta}^k \in \mathcal{D}$ ,  $k \in \mathcal{K}$ ;
  - 5      $\hat{\boldsymbol{\theta}}^k = \operatorname{argmax}_{\boldsymbol{\theta}^k \in \mathcal{D}} L(\hat{\rho}^k(\boldsymbol{\theta}^k), \boldsymbol{\theta}^k, \lambda)$   $k \in \mathcal{K}$ ;
  - 6      $\mathbf{p}^k = \hat{\rho}^k(\hat{\boldsymbol{\theta}}^k) \mathbf{d}^k(\hat{\boldsymbol{\theta}}^k)$ ,  $k \in \mathcal{K}$ ;
  - 7      $\lambda_n = \max(\lambda_n + \epsilon(\sum_{k \in \mathcal{K}} p_n^k - P_n^{\max}), 0)$ ,  $n \in \mathcal{N}$ ;
  - 8 **until** convergence
- 

tone  $k$ . In line 7, the Lagrange multipliers are adjusted ( $\epsilon$  is a step size). The process repeats until convergence.

### 2.3.2 Complexity

The computational complexity of the OSB-SC algorithm is dominated by the exhaustive search for the angles. Since there is one separate search for each tone, the computational complexity is given by  $O(KQ^{N-1})$ . As a comparison, OSB has computational complexity given by  $O(KQ^N)$ .

It should be noted that both OSB and OSB-SC are restricted to cases with small  $N$ . For  $N > 5$ , both algorithms become intractable. This is a direct consequence of the fact that the computational complexity of both algorithms grow exponentially with  $N$ . However, with OSB-SC the search is in one less dimension, which means a significant computational complexity reduction.

### 2.3.3 Precision

Empirically we observe that OSB-SC is more precise than OSB. To understand why this is the case, consider Fig. 2.2. Here, we depict for a two user case the sampling of the  $\bar{p}_1^k$ - $\bar{p}_2^k$  plane for both algorithms. In the figure, both axes are in dB scale. For this section we use a bar for variables that are represented in dB scale, i.e.  $\bar{p}_n^k$ . Variables in linear scale are represented without a bar. We use  $Q = 5$ . OSB samples the space with 25 points in total, shown as the dots in the figure. OSB-SC samples the angle dimension with five angles in total, represented by the vectors  $\mathbf{d}_1$  to  $\mathbf{d}_5$ . While for OSB the search space is restricted to the dots, OSB-SC can use all points on the lines. This is so because the radial dimension is not discretized. The lines cover the continuous

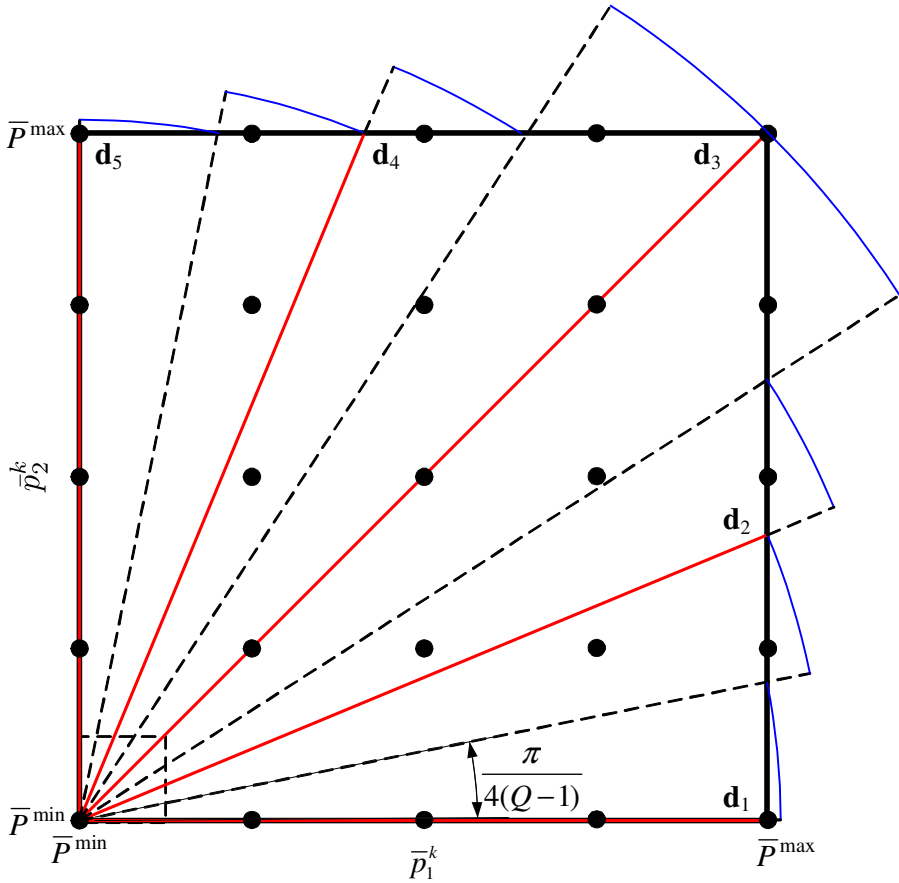


Figure 2.2: Per-tone distribution of  $Q^2$  points (for OSB) and  $Q$  lines (for OSB-SC) for  $Q = 5$ . The lines are represented by  $\mathbf{d}_1, \dots, \mathbf{d}_5$ . Both axes are in dB scale. The dotted lines demarcate the set of points closer to one line. The square on the lower left corner represent the set of points closer to the point at the origin.

plane on average better than the dots. We can quantify this with the following proposition.

**Proposition 2.2.** Consider  $N = 2$ . Consider two uniformly distributed, independent random vectors  $\bar{\mathbf{p}}_1 \in \mathbb{R}^K$  and  $\bar{\mathbf{p}}_2 \in \mathbb{R}^K$  with probability distribution

function (pdf) defined by

$$f(\bar{\mathbf{p}}_n) = \begin{cases} \text{constant, } \bar{p}_n^k \geq \bar{P}^{\min} \text{ and } \sum_{k \in \mathcal{K}} 10^{\bar{p}_n^k/10} \leq P^{\max} \\ 0, & \text{otherwise} \end{cases} \quad (2.11)$$

for  $n = 1$  and  $n = 2$  (for simplicity we consider that both users have the same  $P^{\max}$ ). Define  $\bar{P}^{\max} = 10 \log_{10} P^{\max}$  with  $\bar{P}^{\max} > \bar{P}^{\min}$ . For each tone, the  $\bar{p}_1^k$ - $\bar{p}_2^k$  plane is sampled with  $Q^2$  uniformly distributed grid points and  $Q$  uniformly spaced lines. The collection of grid points is represented by the set  $\mathcal{Y} = \{\mathbf{y}_1, \dots, \mathbf{y}_{Q^2}\}$ ,  $\mathbf{y}_i \in \mathbb{R}^2 \forall i$  and the lines are represented by  $\mathcal{D} = \{\mathbf{d}_1, \dots, \mathbf{d}_Q\}$ ,  $\mathbf{d}_i \in \mathbb{R}^2 \forall i$ . Now we define our measure for precision. Consider, respectively, the average squared distance from the random variables to the grid points and from the random variables to the lines.

$$\mathbb{E} [d_{\text{points}}^2] = \mathbb{E} \left[ \frac{1}{K} \sum_{k \in \mathcal{K}} \min_{\mathbf{y} \in \mathcal{Y}} \|\mathbf{y} - \bar{\mathbf{p}}^k\|_2^2 \right] \quad (2.12)$$

$$\mathbb{E} [d_{\text{lines}}^2] = \mathbb{E} \left[ \frac{1}{K} \sum_{k \in \mathcal{K}} \min_{\mathbf{d} \in \mathcal{D}} \|(\mathbf{d}^T \bar{\mathbf{p}}^k) \mathbf{d} - \bar{\mathbf{p}}^k\|_2^2 \right]. \quad (2.13)$$

Here  $\bar{\mathbf{p}}^k = [\bar{p}_1^k \ \bar{p}_2^k]^T$  and, in (2.13),  $(\mathbf{d}^T \bar{\mathbf{p}}^k)$  is the optimal radius for a given  $\bar{\mathbf{p}}^k$  (i.e. the projection of  $\bar{\mathbf{p}}^k$  in  $\mathbf{d}$ ). Eq. (2.12) can be upper bounded by

$$\mathbb{E} [d_{\text{points}}^2] \leq \frac{\bar{P}^2}{6(Q-1)^2} \quad (2.14)$$

and (2.13) is upper bounded by

$$\mathbb{E} [d_{\text{lines}}^2] < \bar{P}^2 \left( \frac{1}{4} - \frac{Q-1}{2\pi} \sin\left(\frac{\pi}{2(Q-1)}\right) \right) \frac{\sum_{i=0}^{Q-2} \cos^{-4}\left(\frac{(i+1)\pi}{4(Q-1)}\right)}{\sum_{i=0}^{Q-2} \cos^{-2}\left(\frac{(i+1)\pi}{4(Q-1)}\right)}, \quad (2.15)$$

where  $\bar{P} = \bar{P}^{\max} - \bar{P}^{\min}$ .

The derivations of (2.14) and (2.15) are given in Appendix A.2. The derivation of (2.14) is straightforward if we decorrelate the per-tone variables. To arrive at (2.15), we do two relaxations: First, we decorrelate the per-tone variables and, second, we extend the radial dimension to ease the calculation of an integral.

To demonstrate Eqs. (2.14) and (2.15), we perform a Monte Carlo simulation. We generate random variables as in (2.11), a grid with  $Q^2$  equally spaced points and a set of  $Q$  equally spaced lines. For the random variables, we consider, without loss of generality,  $\bar{P}^{\min} = 0$  and  $\bar{P}^{\max} = 100$  (i.e. a per-tone random

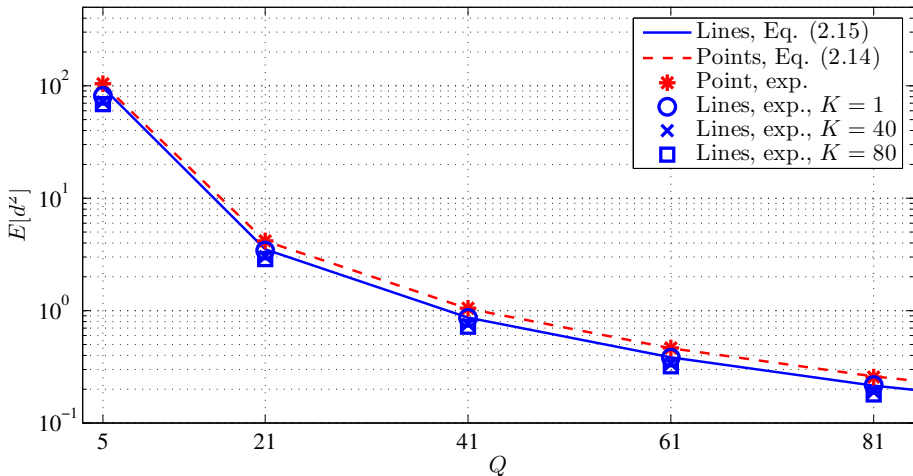


Figure 2.3: Average squared distance from random variables to point and lines, with results from both theory and Monte Carlo simulation. Data pertaining to the experiments are identified with ‘exp’. For the points, results for different values of  $K$  are practically the same, so only one result per  $Q$  is shown.

variable  $\bar{p}_n^k$  can have values in the range  $[0, 100]$ ). We calculate the squared distance from the random variables to the points and to the lines and average them over  $10^4$  realizations. The results of the experiment are given in Fig. (2.3) (indicated with ‘exp’), along with the theoretical results of (2.14) and (2.15), for different values of  $Q$  and of  $K$ . We make two remarks about this experiment. First, we find that the lines (i.e. the OSB-SC grid) are more precise than the points (i.e. the OSB grid). Second, the error for the lines decreases as  $K$  increases, while the error for the points remains approximately the same (this is why only two curves are shown for the points in Fig. 2.3, one curve with the experimental results and one with the upper bound in (2.14)). That is so because, since the tones are coupled through a total PC, the more tones there are, the less power each individual tone has on average. The error becomes smaller because the lines cover the lower values of power better than larger ones, whereas the points have no spatial preference. This can be seen in Fig. 2.2, where in the lower left corner of the figure the coverage of the lines is at its best.

We can also look at the complexity/precision tradeoff from a different perspective: we can compare OSB and OSB-SC with the same computational complexity and measure precision with (2.14) and (2.15). Towards this end,

we use  $Q^2$  points for OSB and  $Q^2$  lines for OSB-SC. By doing so, the time complexity of the two algorithms is approximately the same, but OSB-SC is significantly more precise. With, say  $Q = 40$ , we obtain  $E[d_{\text{points}}^2] \leq 1.0417$  and  $E[d_{\text{lines}}^2] < 4.8582 \times 10^{-4}$ .

Although Proposition 2.2 is restricted to the  $N = 2$  case (the analysis for larger cases is too complicated), we have experimental evidence that point to the fact that the qualitative conclusions of the this section hold for  $N > 2$  as well.

## 2.4 Spectrum Coordination with Spherical Coordinates in Taxicab Geometry—Iterative Search for the Angles

Even tough OSB-SC is faster than OSB, the fact remains that it is too complex for large number of users. In view of this, this section presents a lower complexity algorithm that still maintains good performance. Our starting point is to solve the problem with a block coordinate descent method, i.e. instead of jointly optimizing for all variables, we perform a sequence of line searches for each variable at a time. It is an approach that is used, e.g. in the ISB algorithm [16]. To emphasize the differences between our proposal and ISB, we briefly describe the latter in the following paragraph.

Consider the per-tone Lagrangean as a function of, say,  $p_1^k$ , and for fixed  $\lambda_1$

$$L(p_1^k, \lambda_1) = u_1 b_1^k + \sum_{\substack{j \in \mathcal{N} \\ j \neq 1}} u_j b_j^k - \lambda_1 p_1^k. \tag{2.16}$$

Maximizing (2.16) in  $p_1^k$  corresponds to a so-called *difference of convex* (DC) programming structure: the term  $b_1^k$  is concave in  $p_1^k$ , while the remaining  $b_j^k$ 's are convex. The DC structure complicates the problem significantly and, as a consequence,  $L(p_1^k, \lambda_1)$  can have multiple local optima. To find the global optimum, the ISB algorithm performs an exhaustive line search in  $p_1^k$  and picks the point that maximizes  $L(p_1^k, \lambda_1)$ . Alternatively, the optimal  $p_1^k$  can also be found by writing the stationary condition of (2.16), i.e.  $\partial L(p_1^k, \lambda_1) / \partial p_1^k = 0$ . This results in a polynomial of degree  $2N - 1$ . We can find the roots of the polynomial, discard the non-positive ones and calculate the per-tone Lagrangean for the remaining roots and for the border points  $p_n^k = 0$  and  $p_n^k = P_n^{\text{max}}$ . We then pick the point that maximizes the per-tone Lagrangean [97]. Note that ISB does not do approximations to facilitate the line searches. After solving for all variables (i.e. after maximizing  $L(p_1^k, \lambda_1)$  in  $p_1^k$  until  $L(p_N^k, \lambda_N)$

in  $p_N^k$ ) and all tones we obtain an updated  $\mathbf{P}$ . An outer loop should then search for appropriate Lagrange multipliers.

For our proposal, we change the decision variables as follows:

$$\mathbf{p}^k = \eta^k \mathbf{v}^k, \eta^k \geq 0, \|\mathbf{v}^k\|_1 = 1. \quad (2.17)$$

This describes the positive quadrant of an  $N$ -dimensional sphere in taxicab geometry [43]. In (2.17),  $\eta^k$  is the radius and  $\mathbf{v}^k = [v_1^k \ \cdots \ v_N^k] \in \mathbb{R}_+^N$  is a direction vector. As an example, consider  $N = 3$ . Eq. (2.17) is written as

$$\mathbf{p}^k = \eta^k \begin{bmatrix} (1 - \phi_{[1]}^k)(1 - \phi_{[2]}^k) \\ (1 - \phi_{[1]}^k)\phi_{[2]}^k \\ \phi_{[1]}^k \end{bmatrix}, \eta^k \geq 0, \phi_{[1]}^k, \phi_{[2]}^k \in [0, 1]. \quad (2.18)$$

The spherical coordinates in taxicab geometry of a general  $N$ -dimensional vector is provided in Appendix A.1 in (A.4), (A.5) and (A.6). We remark that, as in (2.6), although the vector  $\mathbf{v}^k$  is  $N$ -dimensional, it has only  $N - 1$  free variables, i.e.  $\phi_{[1]}^k, \phi_{[2]}^k, \dots, \phi_{[N-1]}^k$ .

With (2.17) in hands, we re-define  $b_n^k$  (similarly to (2.8), just substitute  $\rho^k$  with  $\eta^k$  and  $d_n^k$  with  $v_n^k$ ). Next, define  $\boldsymbol{\eta} = [\eta^1 \ \cdots \ \eta^K]^T \in \mathbb{R}_+^K$  and  $\boldsymbol{\phi} = [\phi_{[1]} \ \cdots \ \phi_{[N]}] \in \mathbb{R}_+^{N-1 \times K}$ , where  $\phi_{[i]} \in \mathbb{R}_+^K$  is defined similarly to  $\boldsymbol{\eta}$ ,  $i = 1, \dots, N - 1$ . We re-formulate the spectrum coordination problem as

$$\begin{aligned} & \max_{\boldsymbol{\eta}, \boldsymbol{\phi}} \sum_{n \in \mathcal{N}} \sum_{k \in \mathcal{K}} u_n b_n^k \\ & \text{subject to} \quad \sum_{k \in \mathcal{K}} \eta^k \leq \sum_{n \in \mathcal{N}} P_n^{\max} \\ & \quad \quad \quad \sum_{k \in \mathcal{K}} \eta^k v_n^k \leq P_n^{\max}, \quad n \in \mathcal{N} \end{aligned} \quad (2.19)$$

Here we substitute the  $N$  PCs in (2.3) with their equivalent versions in taxicab geometry. Also, we add a constraint to the sum power (the constraint in  $\boldsymbol{\eta}$ ). In total there are  $N + 1$  constraints.

The Lagrangean of (2.19) is given by

$$\begin{aligned} L(\boldsymbol{\eta}, \boldsymbol{\phi}, \bar{\lambda}, \boldsymbol{\lambda}) = & \sum_{n \in \mathcal{N}} \sum_{k \in \mathcal{K}} u_n b_n^k - \bar{\lambda} \left( \sum_{k \in \mathcal{K}} \eta^k - \sum_{n \in \mathcal{N}} P_n^{\max} \right) \\ & - \sum_{n \in \mathcal{N}} \lambda_n \left( \sum_{k \in \mathcal{K}} \eta^k v_n^k - P_n^{\max} \right). \end{aligned} \quad (2.20)$$

Here, there are  $N + 1$  Lagrange multipliers:  $\bar{\lambda}$  for the sum power and, as in (2.4),  $\boldsymbol{\lambda} \in \mathbb{R}_+^N$  for the per-user PCs.

Our strategy is to maximize (2.20) for each of the variables of the problem separately.

The advantage of the taxicab spherical coordinates compared to the Euclidean spherical coordinates is that it is easier to control power for each user with the former than with the latter. Notice that if we change one of the  $\phi_{[i]}^k$  in (2.18), the sum power does not change. This makes it possible to solve first for the radius and then for the angles. In contrast to that, the Euclidean spherical coordinates have some non-linearity to them: by changing one of the angles, the sum power changes.

The advantage of the taxicab spherical coordinates compared to the Cartesian coordinates is that it is easier to find the structure of the problem with them. In the remainder of this section, we show three ways in which we find structure in (2.19). First, similarly to the results in Section 2.3, we show that the problem is concave in the radial dimension. Second, we show that there is some structure to be found in the angle dimensions too. Given one of the angle variables, we provide conditions for the line search to be concave or convex. Third, we show that, since after the solution for  $\boldsymbol{\eta}$  each tone has a sum power constraint, some tones for some angles can be ignored if the sum power constraint is already exhausted.

We detail each of these ways to find structure in the next sections.

### 2.4.1 Solving for the Radius

To solve for the radius  $\boldsymbol{\eta}$  for fixed  $\boldsymbol{\phi}$ ,  $\bar{\lambda}$  and  $\boldsymbol{\lambda}$ , we write

$$\max_{\boldsymbol{\eta}} L(\boldsymbol{\eta}, \boldsymbol{\phi}, \bar{\lambda}, \boldsymbol{\lambda}),$$

which can be decomposed and solved for each tone separately. The per-tone Lagrangean is given by (here we emphasize the dependency with  $\eta^k$  and  $\bar{\lambda}$ )

$$L(\eta^k, \bar{\lambda}) = \sum_{n \in \mathcal{N}} u_n b_n^k - \bar{\lambda} \eta^k - \eta^k \sum_{n \in \mathcal{N}} \lambda_n v_n^k.$$

Here, for every tone concavity holds. The demonstration of this fact is almost identical to Proposition 2.1—in (2.9) and (2.10), we only need to replace all  $d_n^k$  by  $v_n^k$ . Hence, there is no DC structure and we can find the optimal radius with a low complexity line search algorithm.

## 2.4.2 Solving for the Angles

To solve for the angle  $\phi_{[i]}$ , for fixed  $\boldsymbol{\eta}$ ,  $\phi_{[j]}$ ,  $j \neq i$ ,  $\bar{\lambda}$  and  $\boldsymbol{\lambda}$ , we write

$$\max_{\phi_{[i]}} L(\boldsymbol{\eta}, \boldsymbol{\phi}, \bar{\lambda}, \boldsymbol{\lambda}),$$

which can be decomposed and solved for each tone separately. The per-tone Lagrangean is given by (here we emphasize the dependency with  $\phi_{[i]}^k$  and  $\boldsymbol{\lambda}$ )

$$L(\phi_{[i]}^k, \boldsymbol{\lambda}) = \sum_{n \in \mathcal{N}} u_n b_n^k - \sum_{n \in \mathcal{N}} \lambda_n \eta^k v_n^k. \quad (2.21)$$

When we maximize (2.21) in  $\phi_{[i]}^k$ , we notice that *given the right conditions, it is possible to avoid the DC structure*. To see that, first define

$$b_n^k = \log \left( 1 + \frac{a_n^k \phi_{[i]}^k + D_n^k}{c_n^k \phi_{[i]}^k + F_n^k} \right) \quad (2.22)$$

Here we re-write the formula for the data rate with the emphasis on its dependency on  $\phi_{[i]}^k$ . In the numerator of the fraction, we write  $\eta^k v_n^k = a_n^k \phi_{[i]}^k + D_n^k$  and in the denominator, we write  $\sigma_n^k + \sum_{j \neq n} \alpha_{n,j}^k \eta^k v_j^k = c_n^k \phi_{[i]}^k + F_n^k$ . If, for example,  $N = 3$ ,  $n = 1$ , and  $i = 1$ , we have  $a_n^k = -\eta^k(1 - \phi_{[2]}^k)$ ,  $D_n^k = \eta^k(1 - \phi_{[2]}^k)$ ,  $c_n^k = -\eta^k \alpha_{1,2}^k \phi_{[2]}^k + \eta^k \alpha_{1,3}^k$  and  $F_n^k = \sigma_1^k + \eta^k \alpha_{1,2}^k \phi_{[2]}^k$  (see (2.18)). Notice that all of these are real. It is important to notice that  $a_n^k$  and  $c_n^k$  can be positive or negative. A simple look-up table is sufficient for calculating these variables.

Now consider the second derivative of (2.22) in  $\phi_{[i]}^k$ .

$$\frac{\partial^2 b_n^k}{\partial (\phi_{[i]}^k)^2} = u_n (c_n^k D_n^k - a_n^k F_n^k) \frac{(2a_n^k c_n^k + 2(c_n^k)^2) \phi_{[i]}^k + a_n^k F_n^k + 2c_n^k F_n^k + c_n^k D_n^k}{(c_n^k \phi_{[i]}^k + F_n^k)^2 ((a_n^k + c_n^k) \phi_{[i]}^k + F_n^k + D_n^k)^2} \quad (2.23)$$

Here we see that the sign of the second derivative is determined by a simple linear function, i.e.

$$g_n^k(\phi_{[i]}^k) = A_n^k \phi_{[i]}^k + B_n^k \quad (2.24)$$

where

$$A_n^k \triangleq \text{sgn} \{ (c_n^k D_n^k - a_n^k F_n^k) \} (2a_n^k c_n^k + 2(c_n^k)^2)$$

$$B_n^k \triangleq \text{sgn} \{ ((c_n^k D_n^k - a_n^k F_n^k)) \} (a_n^k F_n^k + 2c_n^k F_n^k + c_n^k D_n^k)$$

Here  $\text{sgn}\{\cdot\}$  is the sign function. The variables  $A_n^k$  and  $B_n^k$  can be either positive or negative. Hence, given  $n, k$  and  $i$ , it can be that  $b_n^k$  is concave or convex in  $\phi_{[i]}^k \in [0, 1]$ , depending on the sign of (2.24) in the interval  $[0, 1]$ . This stands in contrast with the case of the Cartesian coordinates and ISB, where, when solving for  $p_1^k$ ,  $b_1^k$  is *always* concave and the  $b_j^k$ 's,  $j \neq 1$ , are *always* convex. With the taxicab spherical coordinates, things are more flexible.

To illustrate this flexibility, consider an example with  $N = 2$ . We identify the variables  $a_n^k, D_n^k, c_n^k$  and  $F_n^k$ .<sup>2</sup> The flexibility lies in the fact that it can be *both* that  $b_1^k$  and  $b_2^k$  are concave in  $\phi^k$ . A sufficient condition for this is

$$g_n^k(0) \leq 0 \quad \forall n \rightarrow B_1^k \leq 0 \quad \text{and} \quad B_2^k \leq 0$$

$$g_n^k(1) \leq 0 \quad \forall n \rightarrow A_1^k + B_1^k \leq 0 \quad \text{and} \quad A_2^k + B_2^k \leq 0$$

Here, we just check the sign of (2.24) in the points 0 and 1. After substituting the appropriate values and some manipulations, we find that, if

$$\alpha_{1,2}^k \leq \frac{\sigma_1^k}{2\sigma_1^k + \eta^k} \quad \text{and} \quad \alpha_{2,1}^k \leq \frac{\sigma_2^k}{2\sigma_2^k + \eta^k} \tag{2.25}$$

then  $b_1^k$  and  $b_2^k$  are concave in  $\phi^k$ . Because the sum of concave function is also concave, (2.21) is concave. If the conditions in (2.25) are satisfied, there is no DC structure.

The conditions in (2.25) add insight and a clear contrast to the case with the Cartesian coordinates. However, they do not exploit all the structure there is. For the  $N$  user case, a stronger sufficient condition for (2.21) to be *concave* in  $\phi_{[i]}^k$  is given by the following proposition.

**Proposition 2.3.** *If*

$$\sum_{n \in \mathcal{N}} \max\left(\frac{\partial^2 u_n b_n^k}{\partial(\phi_{[i]}^k)^2}(0), \frac{\partial^2 u_n b_n^k}{\partial(\phi_{[i]}^k)^2}(1)\right) \leq 0 \tag{2.26}$$

*then the per-tone Lagrangean in (2.21) is concave in  $\phi_{[i]}^k$ .*

In the same vein, a sufficient condition for (2.21) to be *convex* in  $\phi_{[i]}^k$  is given by the following proposition.

**Proposition 2.4.** *If*

$$\sum_{n \in \mathcal{N}} \min\left(\frac{\partial^2 u_n b_n^k}{\partial(\phi_{[i]}^k)^2}(0), \frac{\partial^2 u_n b_n^k}{\partial(\phi_{[i]}^k)^2}(1)\right) \geq 0 \tag{2.27}$$

---

<sup>2</sup>For user 1,  $a_1^k = -\eta^k$ ,  $D_1^k = \eta^k$ ,  $c_1^k = \eta^k \alpha_{1,2}^k$  and  $F_1^k = \sigma_1^k$ . For user 2,  $a_2^k = \eta^k$ ,  $D_2^k = 0$ ,  $c_2^k = -\eta^k \alpha_{2,1}^k$  and  $F_2^k = \eta^k \alpha_{2,1}^k \sigma_2^k$ .

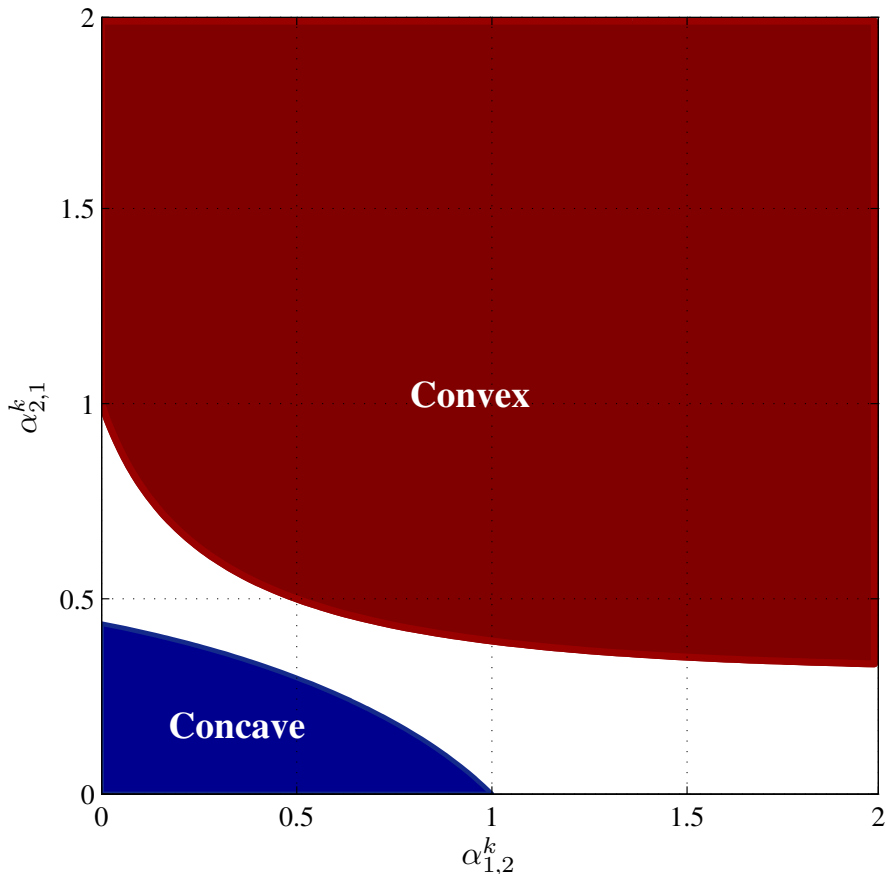


Figure 2.4: Depiction of concave and convex regions of the per-tone Lagrangean for a  $N = 2$  case as a function of the normalized interference channel coefficients. We choose  $u_1 = u_2 = 0.5$ ,  $\eta^k = 1$ ,  $\sigma_1^k = 2$  and  $\sigma_2^k = 1$ .

then the per-tone Lagrangean in (2.21) is convex in  $\phi_{[i]}^k$ .

The proofs of Propositions 2.3 and 2.4 are given in Appendix A.3. Its main steps consist of relaxing the second derivative of (2.21) and simply checking that (2.23) is either a monotonically increasing or a monotonically decreasing function in  $\phi_{[i]}^k$ .

To make these two propositions more palpable, we return to the example with  $N = 2$ . By applying (2.26) and (2.27), we find regions where the maximization of (2.21) is concave and convex. These regions are illustrated in Fig. 2.4 on the

$\alpha_{1,2}^k$ - $\alpha_{2,1}^k$  plane for fixed  $\eta^k$ ,  $\sigma_1^k$ ,  $\sigma_2^k$ ,  $u_1$  and  $u_2$ . For both colored regions, there is no DC structure and the line search can be solved with low complexity. In the unshaded region, neither concavity nor convexity can be established and either a polynomial must be solved or an exhaustive line search has to be performed.

### 2.4.3 Exhausting the Sum Power

After the solution for the radius, each tone has a sum power constraint to be divided among the users. The share that each user gets is determined by solving for the angles. The third way to exploit structure with the taxicab spherical coordinates relies on this fact. This is best conveyed by two examples.

First, it can be that  $\eta^k = 0$ . In this case, there is no power to be distributed among the users. Tones where  $\eta^k = 0$  can be skipped for all angles.

Second, consider  $\eta^k > 0$ . For the  $N = 3$  case, consider that we have solved for  $\boldsymbol{\eta}$  and  $\phi_{[1]}$ . When solving for  $\phi_{[2]}$ , tones where  $\phi_{[1]}^k = 1$  can be skipped. For these tones, the sum power is already exhausted in the  $\phi_{[1]}^k$  direction (see (2.18)).

Hence, when solving for a given  $\phi_{[i]}$  the set of tones that need to be solved for is given by

$$\mathcal{K}_* = \{k | k \in \mathcal{K}, \eta^k > 0 \text{ and } \phi_{[j]}^k \neq 1, j < i\}.$$

### 2.4.4 Algorithm

We are now ready to summarize our second algorithm. A pseudo-code is shown in Algorithm 2.2. We call the algorithm **T**axicab **S**pherical **C**oordinates **S**pectrum **O**ptimization (TaSSO). We remark that, as the ISB, TaSSO does not do approximations to facilitate the line searches.

We first solve for the radius, which corresponds to a concave line search problem. The Lagrange multiplier  $\bar{\lambda}$  can be found with a simple bisection search. Then we solve for the angles. We begin with  $\phi_{[1]}$  and continue until  $\phi_{[N-1]}$ . For a given  $i$ , in lines 8-11 we classify the tones. Here  $\mathcal{K}_*$ ,  $\mathcal{K}_{\text{cnc}}$ ,  $\mathcal{K}_{\text{cvx}}$  and  $\mathcal{K}_{\text{neither}}$  represent, respectively, the set of tones that need to be solved for, the set of tones where (2.26) holds, the set of tones where (2.27) holds, and the set of tones where neither concavity nor convexity can be established. Each set has  $\phi_{[i]}^k$  optimized in a different way:

- If  $k \in \mathcal{K}_{\text{cnc}}$ , then the problem can be easily solved with e.g. the Newton method.
- If  $k \in \mathcal{K}_{\text{cvx}}$ , the optimal is either  $\phi_{[i]}^k = 0$  or  $\phi_{[i]}^k = 1$ .
- If  $k \in \mathcal{K}_{\text{neither}}$ , then an exhaustive line search is necessary. This can be done with

$$\phi_{[i]}^k = \operatorname{argmax}_{\phi_{[i]}^k \in \mathcal{D}} L(\phi_{[i]}^k, \boldsymbol{\lambda}),$$

where  $\mathcal{D}$  contains points in the discretized  $[0, 1]$  segment. Alternatively, we can find the stationary condition of (2.21), i.e.  $\partial L(\phi_{[i]}^k, \boldsymbol{\lambda}) / \partial \phi_{[i]}^k = 0$ . This results in a polynomial of degree  $2N$ . We can find the roots of the polynomial, discard the ones that are not in  $[0, 1]$ , and calculate the per-tone Lagrangean for the remaining roots and for the points  $\phi_{[i]}^k = 0$  and  $\phi_{[i]}^k = 1$ . We then pick the point that maximizes the per-tone Lagrangean. In our implementation, we solve the polynomial.

At the end of the algorithm, we adjust the Lagrange multipliers  $\boldsymbol{\lambda}$  ( $\epsilon$  is a step size). The process repeats until convergence.

## 2.4.5 Computational Complexity and Convergence

The computational complexity of TaSSO is dominated by the exhaustive line searches. It is difficult to estimate how many times these exhaustive line searches take place because it is not known a priori how many tones in the system fall on the concave or convex categories. Complexity is estimated as  $O((2N)^3(N-1)|\mathcal{K}_{\text{neither}}|)$ , where the term  $(2N)^3$  corresponds to the computational complexity of solving a polynomial of degree  $2N$ . In the worst possible case  $\mathcal{K}_{\text{neither}} = \mathcal{K}$ , and computational complexity is given by  $O((2N)^3(N-1)K)$ . As a comparison, the computational complexity of ISB is given by  $O((2N-1)^3NK)$ . In the worst case, TaSSO needs to solve  $K(N-1)$  polynomials of degree  $2N$ . ISB always needs to solve  $KN$  polynomials of degree  $2N-1$ .

We see from experiments that even in the worst case TaSSO is faster than ISB. In practice, however, we see that  $\mathcal{K}_{\text{neither}} = \mathcal{K}$  almost never happens. In the so-called near-far scenarios (see Section 2.5), sometimes the majority of tones fall in the concave case. We observe from experiments with realistic channels that TaSSO is 2-15 times faster than ISB.

Unfortunately, we do not have a proof of convergence of TaSSO. However, the algorithm has been experimented with extensively and has always been observed to converge.

**Algorithm 2.2:** TaSSO

---

```

1  $\lambda = \mathbf{0}_N$ ;
2 repeat
3   repeat
4     Solve for  $\boldsymbol{\eta}$  with Newton method;
5     Adjust  $\bar{\lambda}$ ;
6   until convergence
7   for  $i = 1, \dots, N - 1$  do
8     Calculate  $a_n^k, D_n^k, c_n^k$  and  $F_n^k \forall n, k$ ;
9      $\mathcal{K}_* = \{k | k \in \mathcal{K}, \eta^k > 0 \text{ and } \phi_{[j]}^k \neq 1, j < i\}$ ;
10     $\mathcal{K}_{\text{cnc}} = \{k \in \mathcal{K}_* | \sum_n \max(\frac{\partial^2 u_n b_n^k}{\partial(\phi_{[i]}^k)^2}(0), \frac{\partial^2 u_n b_n^k}{\partial(\phi_{[i]}^k)^2}(1)) \leq 0\}$ ;
11     $\mathcal{K}_{\text{cvx}} = \{k \in \mathcal{K}_* | \sum_n \min(\frac{\partial^2 u_n b_n^k}{\partial(\phi_{[i]}^k)^2}(0), \frac{\partial^2 u_n b_n^k}{\partial(\phi_{[i]}^k)^2}(1)) \geq 0\}$ ;
12     $\mathcal{K}_{\text{neither}} = \mathcal{K}_* - (\mathcal{K}_{\text{cvx}} + \mathcal{K}_{\text{cnc}})$ ;
13    for  $k \in \mathcal{K}_{\text{cnc}}$  do
14      Solve with Newton method;
15    for  $k \in \mathcal{K}_{\text{cvx}}$  do
16      Calculate  $L(0, \boldsymbol{\lambda})$  and  $L(1, \boldsymbol{\lambda})$  in (2.21);
17      if  $L(0, \boldsymbol{\lambda}) > L(1, \boldsymbol{\lambda})$  then  $\phi_{[i]}^k = 0$ , else  $\phi_{[i]}^k = 1$ ;
18    for  $k \in \mathcal{K}_{\text{neither}}$  do
19      Solve line search;
20     $\mathbf{p}^k = \eta^k \mathbf{v}^k, k \in \mathcal{K}$ ;
21     $\lambda_n = \max(\lambda_n + \epsilon(\sum_{k \in \mathcal{K}} p_n^k - P_n^{\text{max}}), 0), n \in \mathcal{N}$ ;
22 until convergence

```

---

## 2.5 Simulation Results

For all simulations in this section, we use  $f_s = 4$  kHz and  $\Delta_f = 4.3125$  kHz. Also, all algorithms are initialized with  $p_n^k = 10^{-6} \forall n, k$ . The criterion for convergence is  $|\text{WRS}(i) - \text{WRS}(i - 1)| \leq N10^{-6}$  for all algorithms, where  $\text{WRS}(i)$  is the resulting WRS from iteration  $i$ .

### 2.5.1 OSB vs. OSB-SC

We simulate OSB and OSB-SC in a typical near-far, downstream ADSL scenario with 2 users. We illustrate the scenario in Fig. 2.5. We consider

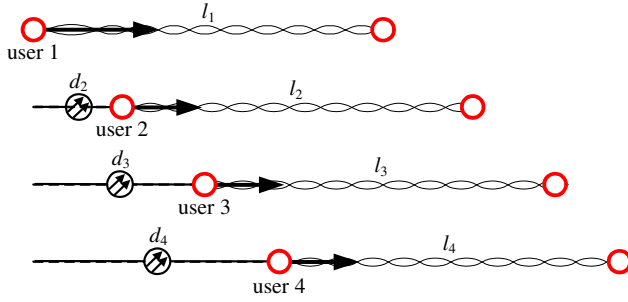


Figure 2.5: ADSL downstream scenario.

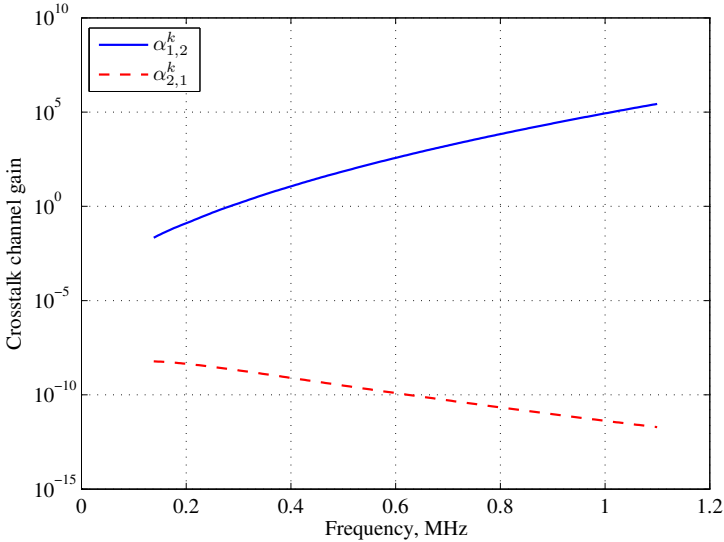


Figure 2.6: Normalized crosstalk channels.

that only the two users on the top of the figure are active. Referring to the figure, we set  $l_1 = 5$  km,  $l_2 = 3$  km and  $d_2 = 4$  km. We use 0.5 mm (24 AWG) cables and noise model ANSI A [71]. We use 20.4 dBm as PC for each user and  $\Gamma = 12.8$  dB. We set  $u_1 = 0.9$  and  $u_2 = 0.1$ . We use  $Q = 301$  lines for OSB-SC and  $Q^2$  points for OSB. We plot the normalized crosstalk channel gains  $\alpha_{n,j}^k$ ,  $n \neq j$  in Fig. 2.6. We see that, for user 1, after 0.3 MHz the crosstalk channel gain is greater than 1, which means that crosstalk from user 2 to user 1 is severe.

We see that OSB-SC is emphatically faster than OSB. While the former

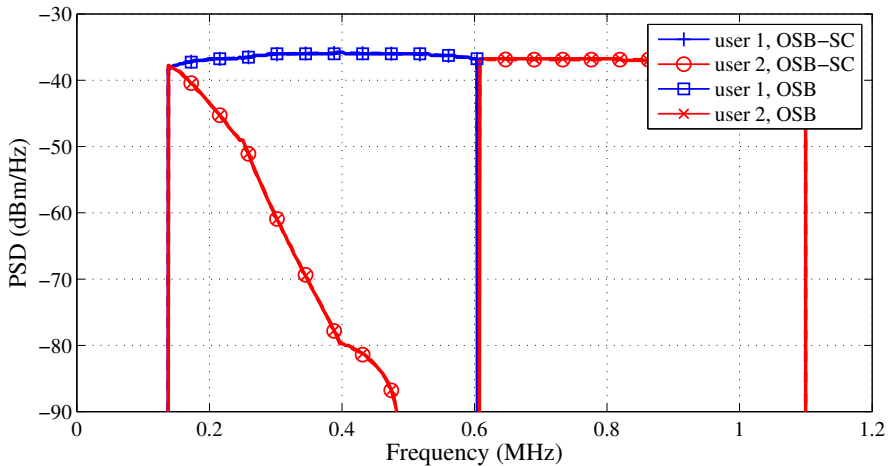


Figure 2.7: Power allocation OSB and OSB-SC. Both algorithms reach basically the same result, but OSB-SC is more precise.

converges in less than 15 seconds, the latter takes approximately 16 minutes. This represents a saving in computational complexity by a factor of 60. In Fig. 2.7, we depict the final power allocation of both algorithms. Seen from far they look the same, but, once zoomed in, we can see that OSB-SC is more precise (see Fig. 2.8 and discussion in Section 2.3.3). The final PSD of OSB is ‘blocky’, whereas that of OSB-SC is much more smooth.

## 2.5.2 Random Downstream ADSL

In this experiment, we simulate a four user random downstream ADSL scenario. All system parameters are the same as in the previous section. Referring to Fig. 2.5, we set  $l_1$  to be a random variable with pdf  $\text{unif}(4, 6)$  km,  $l_2$  to be a random variable with pdf  $\text{unif}(3, 5)$  km,  $l_3$  to be a random variable with pdf  $\text{unif}(2.5, 4.5)$  km, and  $l_4$  to be a random variable with pdf  $\text{unif}(2, 4)$  km. We define  $d_1 = 0$  and  $d_i$ ,  $i = 2, 3, 4$  to be random variables with pdf  $\text{unif}(i - 1, \min_{j < i} d_j + l_j)$ . We define the  $d_i$  sequentially, i.e. first  $d_2$  and continue until  $d_4$ . We create 100 realizations of this scenario, and for each we calculate the solutions of ISB and TaSSO.

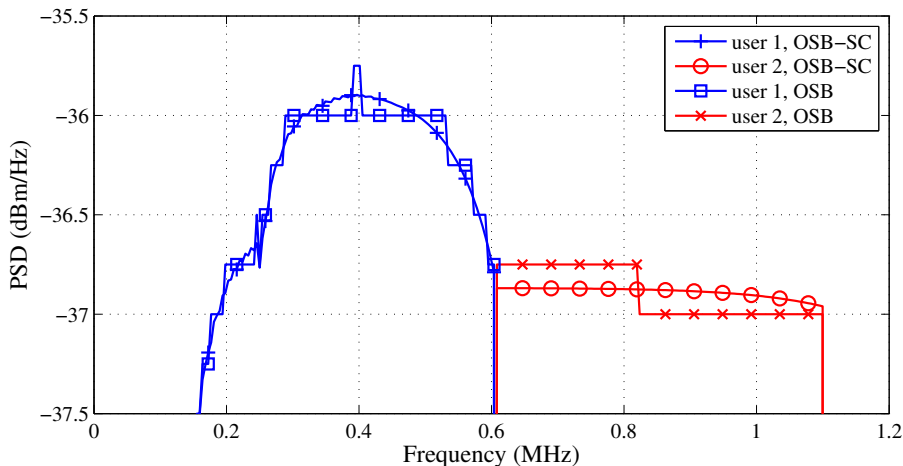


Figure 2.8: Zoomed in region indicated in Fig. 2.7.

	ISB	TaSSO
Convergence time, average (sec)	25.04	6.45
Convergence time, st. deviation	5.71	3.14
no. line searches, average	896	271.76
no. line searches, st. deviation	0	70.15

Table 2.1: Results for the experiment with the random downstream ADSL scenario.

The goal of this experiment is to assess the average behavior of ISB and TaSSO in terms of time complexity. The results are shown in Table 2.1.

On average, TaSSO is almost 4 times faster than ISB. The number of line searches each algorithm needs to solve explains why. For TaSSO, on average 257.25 line searches are solved. For ISB, for every realization  $KN = 224 \times 4 = 896$  line searches are solved. The two algorithms perform equally well in terms of final WRS.

### 2.5.3 Upstream VDSL

We also simulate an upstream VDSL scenario. We use 0.4 mm (AWG 26) cables and an  $\Gamma = 9.45$  dB. Each user has a total power budget of 11.5 dBm. For each line, noise model ETSI A is adopted with a background noise level of  $-140$  dBm/Hz. We use the FDD 998 frequency bandplan over POTS up to 12 MHz.

The scenario is depicted in Fig. 2.9. There are 7 users, with line lengths equal to 1.2, 1.1,  $\dots$ , 0.6 km. We simulate the scenario six times. The first time we consider users 1 and 2 to be active. The second time we consider users 1 to 3 active. We continue until all users are active. For every simulation, we use equal weights for the users. We run ISB and TaSSO and compare their performances.

Both algorithms perform equally well in terms of WRS. The difference is their time complexity, which is depicted in Fig. 2.10. Here we see that TaSSO is 5 to 15 times faster than ISB. For example, with 7 active users, ISB converges in around 24 minutes, while TaSSO does so in 4 and a half minutes.

TaSSO is faster because it uses structure. This is conveyed by Fig. 2.11, where we depict the number of line searches each of the algorithms does in its last iteration (we solve polynomials for both algorithms). With TaSSO, these numbers are from 6 to 2.3 times smaller.

## 2.6 Conclusion

In this chapter, we have proposed two algorithms for the spectrum coordination problem. Both our proposals start with the re-writing of the decision variables in spherical coordinates, i.e. as a function of a radius and angles. The advantage of this change of variables is that we are able to find structure in the problem.

The first algorithm, called OSB-SC, uses standard (Euclidean) spherical coordinates. We exploit the fact that the problem is concave in the radial dimension. An exhaustive search is done for the remaining variables, i.e. the angles. We see from the experiments that OSB-SC can be up to 60 times faster than the previously proposed OSB.

The second algorithm, called TaSSO, uses spherical coordinates in taxicab geometry. This coordinate system makes it easier to solve the problem in a block coordinate descent method, i.e. a sequence of line searches, where we first solve for the radius and subsequently solve for the angles. This algorithm uses structure in three ways. First, the problem is concave in the radial dimension.

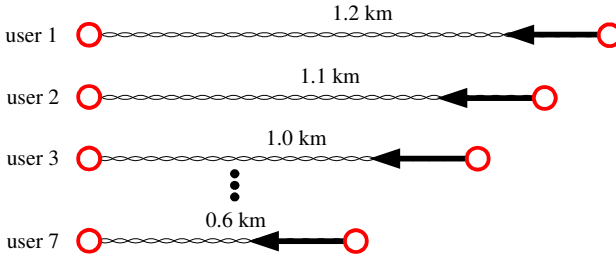


Figure 2.9: Upstream VDSL scenario.

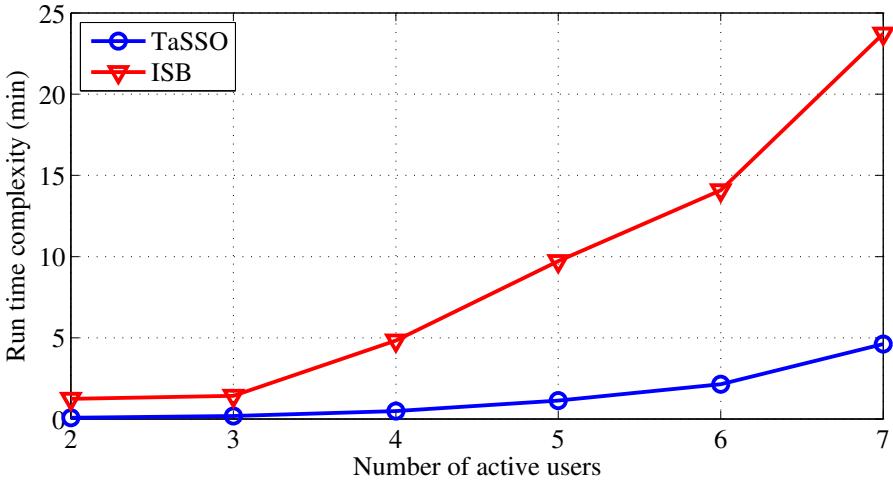


Figure 2.10: Time complexity vs. number of active users for the upstream VDSL scenario.

Second, there is some limited structure to be found in the angle dimensions. We have established sufficient conditions for the line searches to be convex and concave in each of the angle dimensions. And, third, after the solution for the radius there is a sum power constraint for every tone. We see from the experiments that TaSSO can be 2-15 times faster than the previously proposed ISB.

Of these three ways to exploit structure, we believe that the second (i.e. the structure in the angle dimensions) is both the most important and the most surprising. It is the most important because we see from the experiments that it is the one that accounts for the largest savings in computational complexity.

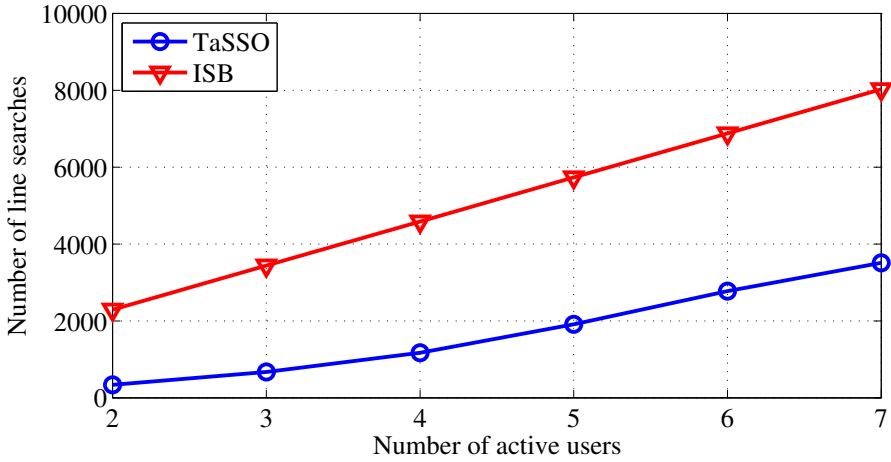


Figure 2.11: Number of line searches (in our case, polynomials to be solved) vs. number of active users for the upstream VDSL scenario.

It is the most surprising because it conveys the message that the spectrum coordination problem has more structure than previously imagined. We should add that we do not exploit all the structure there is. The sufficient conditions for convexity and concavity we propose have the considerable advantage of being easily verified, but they fall short of mapping the ‘real’ concave and convex regions, which are much larger. How to better map these ‘real’ concave and convex regions remains a topic for further research. Perhaps there are also regions of quasi-concavity and quasi-convexity (as defined in [7]).

## **Part II**

# **Combined Signal and Spectrum Coordination**

# Chapter 3

## DMT MIMO IC

### 3.1 Introduction

In a communications system where multiple users have competing utilities, the intelligent allocation of the system resources offers the system designer a chance to significantly improve the network performance. With proper resource allocation, the competing users can be coordinated such that the transmission of each user is designed so as to maximize its own utility while being as little detrimental as possible to the transmission of all others. The system designer can count with a wide range of options so as to perform this coordination, such as the dimensions of power, code, space, frequency, time and waveform.

In Part II of this thesis, we focus on the dimensions of frequency, power and space, i.e. we focus on combined signal and spectrum coordination. More specifically in this chapter, we focus on a DSL scenario we call DMT MIMO IC.

As mentioned in Chapter 1, DSM is classically divided into signal and spectrum coordination techniques. *Spectrum coordination*, the topic of Part I of this thesis, aims to allocate transmit power to the multiple users in the available spectrum so that crosstalk is avoided or minimized. *Signal coordination* involves MIMO processing, either two-sided or single-sided. Although more complex, signal coordination is able to deliver substantial gains in comparison

with spectrum coordination, eliminating most or all crosstalk and sometimes even using crosstalk for its benefit.

Work on signal and spectrum coordination in DSL have progressed steadily and, more often than not, independently. Recently, attention was given to scenarios, in which some of the infrastructure for signal coordination is available, but not all [21, 34, 54]. In this chapter we consider a mixed DSL scenario where each user has a number of transceivers that can be operated jointly, but where signal coordination among all users in the cable binder is not possible.

These mixed scenarios are consistent with the tree topology that is typical of DSL networks. With the tree topology, thick branches start from and arrive at nodes. Within each branch, two-sided signal coordination is theoretically possible. However, whenever some branches terminate on different nodes or when local loop unbundling is regulatory required, signal coordination among all the users is not possible, and so part of the coordination should be done on the spectrum level. Moreover, these mixed scenarios encompass the possible utilization of not only the direct mode of a DSL line, but also its phantom or common modes or split wire transmission [23, 55, 56]. For example, one user with two copper pairs (terminating on the same equipment on both the CPE and the CO side of the network) can have three communication channels, corresponding to two direct modes (one for each DSL line) and the phantom mode. A typical scenario is depicted in Fig. 1.11.

This scenario is generally referred to as MIMO interference channel (MIMO IC). Because of the DMT modulation used in DSL, where tones are coupled through per-user power constraints (PC), we refer to this scenario as the DMT MIMO IC.

In this chapter, we propose two algorithms for weighted rate sum (WRS) maximization for the DMT MIMO IC. The first algorithm builds on the recently suggested equivalence between the WRS maximization problem and the weighted minimum mean squared error (WMMSE) minimization problem [22] for the (single tone) MIMO IC [69, 83, 84]. We show that a simple adjustment on the single tone algorithm is sufficient to adapt it to the multitone case. The resulting multitone algorithm solves the signal and spectrum coordination parts of the problem simultaneously and is guaranteed to reach a stationary point.

The WMMSE minimization approach is surprisingly easy to adapt from the single tone to the multitone problem, but that is not necessarily true for other solutions. That is why, in the second proposed algorithm, we separate the signal and spectrum coordination parts of the problem and solve each of them separately. The advantage here is that many options are possible

for solving these two separate parts. We end up with many independent single tone MIMO ICs (one for each tone). In this way, we can rely on previous work on this topic and select any of the available solutions. For the spectrum coordination part, one of the interesting outcomes of our analysis is a generalization of the distributed spectrum balancing (DSB) [96, 98, 109] power allocation formula for the DMT MIMO IC scenario. Simulation results demonstrate that both algorithms obtain significant gains when compared to pure spectrum coordination algorithms.

This chapter is organized as follows. In Section 3.2, we present the system model and the problem statement. In Section 3.3 we describe the algorithm based on solving the equivalent WMMSE minimization problem and in Section 3.4 we describe the algorithm based on separately solving the signal and spectrum coordination parts. Simulation results are presented in Section 3.5 and final remarks are given in Section 3.6.

## 3.2 Problem Statement

We consider an  $N$  user DSL system with DMT modulation with  $K$   $\Delta_f$ -spaced tones. We denote the set of users by  $\mathcal{N} = \{1, \dots, N\}$  and the set of tones by  $\mathcal{K} = \{1, \dots, K\}$ . We let  $p_n^k$  be the transmit power of user  $n$  on tone  $k$  and we organize these values in the matrix  $\mathbf{P} \in \mathcal{R}^{K \times N}$ . The  $n$ th column of  $\mathbf{P}$ , denoted by  $\mathbf{p}_n = [p_n^1 \ \dots \ p_n^K]^T$ , contains the power allocation of user  $n$  in all tones. The  $k$ th row of  $\mathbf{P}$ ,  $\mathbf{p}^k = [p_1^k \ \dots \ p_N^k] \in \mathbb{R}_+^N$ , represents the power allocation of all users in tone  $k$ . User  $n$  has  $A_n$  transceivers and can adopt two-sided MIMO processing among them. Throughout this chapter, we focus on a linear design for both transmitters and receivers and treat interference as noise. All channel gains are considered perfectly known (not such a tall order in DSL systems). Also, we consider the simplifying assumption of perfect DMT block synchronization between users.<sup>1</sup> Taking that into account, we obtain the received signal for user  $n$  on tone  $k$  as

$$\mathbf{y}_n^k = \mathbf{H}_{n,n}^k \mathbf{T}_n^k \mathbf{x}_n^k + \sum_{j \neq n} \mathbf{H}_{n,j}^k \mathbf{T}_j^k \mathbf{x}_j^k + \mathbf{z}_n^k. \quad (3.1)$$

Here  $\mathbf{y}_n^k, \mathbf{x}_n^k \in \mathbb{C}^{A_n}$  are, respectively, the received and transmitted signal vector for user  $n$  on tone  $k$ ;  $\mathbf{H}_{n,j}^k \in \mathbb{C}^{A_n \times A_j}$ ,  $\mathbf{T}_n^k \in \mathbb{C}^{A_n \times A_n}$  are, respectively, the channel matrix from user  $j$  to user  $n$  on tone  $k$  and the transmit matrix

---

<sup>1</sup>For the case when the DMT blocks of different users are offset in relation to each other, inter carrier interference (ICI) arises. ICI complicates the problem significantly. We deal with this problem in Chapter 5.

for user  $n$  on tone  $k$ . In (3.1), we assume  $\mathbb{E}[\mathbf{x}_n^k(\mathbf{x}_n^k)^H] = \mathbf{I}_{A_n}$ , and hence  $\text{tr}\{\mathbf{T}_n^k(\mathbf{T}_n^k)^H\} = p_n^k$ . Without loss of generality, the noise vector  $\mathbf{z}_n^k$  denotes circularly symmetric zero mean complex Gaussian noise with covariance matrix  $\mathbb{E}[\mathbf{z}_n^k(\mathbf{z}_n^k)^H] = \mathbf{I}_{A_n}$ . The estimated signal vector for user  $n$  on tone  $k$  is given by

$$\hat{\mathbf{x}}_n^k = \mathbf{R}_n^k \mathbf{y}_n^k, \quad (3.2)$$

where  $\mathbf{R}_n^k$  is the receive matrix for user  $n$  on tone  $k$ . We illustrate this situation in Fig. 3.1 for a system with three users and three tones. The receive matrix used in (3.2) is the linear MMSE (LMMSE) matrix. It has been shown that in a MIMO IC scenario the LMMSE receiver provides an optimal linear receiver given a set of linear transmit matrices [22, 69]. For a given set of transmit matrices, we write

$$\mathbf{R}_n^k = (\mathbf{T}_n^k)^H (\mathbf{H}_{n,n}^k)^H (\mathbf{M}_n^k + \mathbf{H}_{n,n}^k \mathbf{T}_n^k (\mathbf{T}_n^k)^H (\mathbf{H}_{n,n}^k)^H)^{-1}, \quad (3.3)$$

where

$$\mathbf{M}_n^k = \sum_{j \neq n} \mathbf{H}_{n,j}^k \mathbf{T}_j^k (\mathbf{T}_j^k)^H (\mathbf{H}_{n,j}^k)^H + \mathbf{I}_{A_n}$$

is the noise plus interference covariance matrix for user  $n$  on tone  $k$ . We remark that, although we do not write it explicitly, this matrix may be normalized by a capacity gap  $\Gamma$ .

With the LMMSE receiver and assuming Gaussian signaling, the achievable data rate for user  $n$  on tone  $k$  is given by

$$b_n^k = \log |(\mathbf{T}_n^k)^H (\mathbf{H}_{n,n}^k)^H (\mathbf{M}_n^k)^{-1} \mathbf{H}_{n,n}^k \mathbf{T}_n^k + \mathbf{I}_{A_n}|. \quad (3.4)$$

We use  $\log(\cdot)$  as the natural logarithm. Users have their total data rate in bits per second defined as  $r_n = f_s / \log(2) \sum_{k \in \mathcal{K}} b_n^k$ , where  $f_s$  is the symbol rate. We remind that in this thesis we ignore the practical constraint of discrete bit loading.

We denote the set of all matrices  $\mathbf{T}_n^k$  as  $\mathcal{T} = \{\mathbf{T}_n^k \mid n \in \mathcal{N}, k \in \mathcal{K}\}$ . The problem we would like to solve is the WRS maximization, which can be written as

$$\begin{aligned} & \max_{\mathcal{T}} \sum_{n \in \mathcal{N}} \sum_{k \in \mathcal{K}} u_n b_n^k \\ & \text{subject to} \sum_{k \in \mathcal{K}} \text{tr}\{\mathbf{T}_n^k (\mathbf{T}_n^k)^H\} \leq P_n^{\max} \quad \forall n \end{aligned} \quad (3.5)$$

Here,  $P_n^{\max}$  is the power budget and  $u_n$  is the weight for user  $n$ .

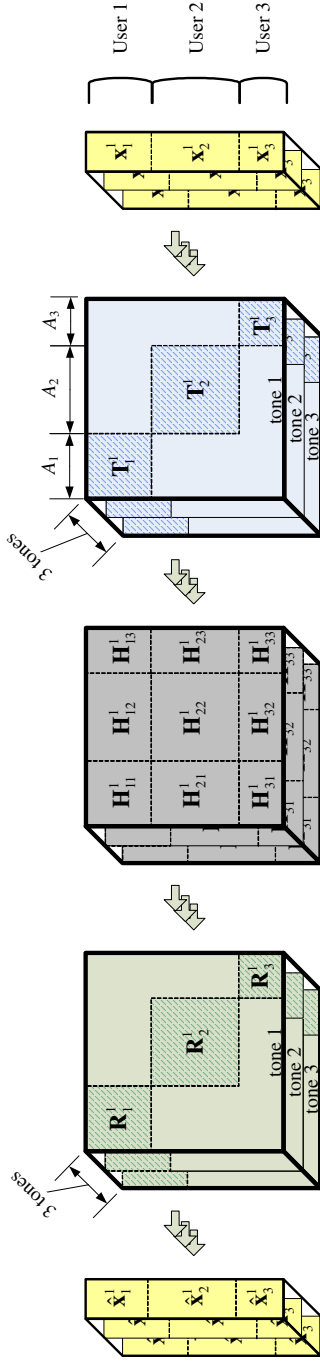


Figure 3.1: Illustration of the DMT MIMO IC for a scenario with 3 users and 3 tones. Each user  $n$  has  $A_n$  transceivers. For simplicity, the zero mean Gaussian noise is not shown.

We remark that, with similar arguments as [53,112], it can be shown that, as the tone spacing  $\Delta_f$  tends to zero, the vector of data rates  $\mathbf{r} = \{r_n\}$ ,  $r_n = \int b_n(f)df$  forms a convex set. That in turn allows us to map the whole border of the rate region (RR) by changing the weights  $u_n$ . Problem (3.5), however, is discretized, with a finite tone spacing. Theoretically, this may imply that some points in the border of the RR cannot be found. However, the tone spacing for DSL impound to be small enough so that, for practical purposes, the WRS approach can characterize the border of the RR almost fully. See e.g. [17].

Note that we use a per-user PC, not a per-transceiver PC. For the sake of appropriately emphasizing the main problem, we also do not use a per-tone PC, i.e. we do not consider a spectral mask. We remark that the design of the receive matrices is the easy part of the problem and that makes these matrices not to be included in the optimization variables in (3.5). We refer to (3.5) as the *DMT MIMO IC WRS maximization problem*.

The optimization in (3.5) is non-concave with respect to  $\mathbf{T}_n^k$  and hence it is not trivial. It comprises  $K$  distinct  $N$ -user MIMO ICs, in which, for all tones, user  $n$  has  $A_n$  transceivers. The challenge in (3.5) is twofold. First, we should design the matrices  $\mathbf{T}_n^k$  for all users and tones so that the resulting signal vectors—the columns of  $\mathbf{T}_n^k$ —are easy to identify in the intended receiver (user  $n$ ) and easy to mitigate in the unintended receivers (users  $j \neq n$ ). The second challenge is about power allocation. Since  $\text{tr}\{\mathbf{T}_n^k(\mathbf{T}_n^k)^H\} = p_n^k$ , we should appropriately choose how much power each tone of each user gets, i.e. we should choose  $\mathbf{P}$ . The design of the matrices  $\mathbf{T}_n^k$  corresponds to the signal coordination part of the problem. The design of  $\mathbf{P}$ , i.e. the power allocation, is the spectrum coordination part. Albeit the spectrum coordination part is not explicitly shown in (3.5), it is crucially important. Note that the per-user PC couples the optimization through the tones, which complicates the problem significantly.

We remark that special cases of (3.5) are well-known in the literature.

- The special case when  $A_n = 1 \forall n$  corresponds to the SISO case, i.e. the pure spectrum coordination problem already discussed in Part I of this thesis. The spectrum coordination problem can also be obtained by restricting the transmit matrices  $\mathbf{T}_n^k$  to be diagonal for all  $n, k$ . Ref. [17] proposes an algorithm with an approximately optimal solution [52], and several other papers have worked on practical and low complexity solutions for an efficient implementation, e.g. [59, 73, 96, 109].
- The special case when  $N = 1$  corresponds to full two-sided signal coordination [47, 89]. For this case, the optimal solution comprises two steps: first, set  $\mathbf{R}_1^k = (\mathbf{U}_1^k)^H$  and  $\mathbf{T}_1^k = 1/\sqrt{A_1}\mathbf{V}_1^k$  for all tones, where  $\mathbf{U}_1^k$

and  $\mathbf{V}_1^k$  are, respectively, the matrices of left and right singular vectors of  $\mathbf{H}_1^k$ , i.e.  $\mathbf{H}_1^k = \mathbf{U}_1^k \text{diag} \{ [\gamma_1^k(1) \ \dots \ \gamma_1^k(A_1)] \} (\mathbf{V}_1^k)^H$ ; and second, consider the noise to channel ratio to be  $1/\gamma_1^k(i)^2$  and allocate power with a waterfilling algorithm.

- For the special case when  $K = 1$ , several solutions are also available, e.g. [9, 32, 42, 69, 81, 83, 84], but they are at best guaranteed to converge to a local optimum.

Although there is some related work in the wireless communication context, to the best of our knowledge the DMT MIMO IC WRS maximization problem in the more general form of (3.5) has not been analyzed in full in the literature. In the wireless context, for example [103, 111] use signal and spectrum coordination algorithms jointly for a multicell broadcast channel problem (in [111] scheduling is also considered), but simplifying assumptions are used. In [111] users are restricted to one data stream. The PCs are also simplified. In [103], users are restricted to have one receive antenna. These limitations clearly do not apply to our scenario. In [4, 24], power is evenly distributed through the sub-carriers. The DSL case, however, is quite different because the channel is highly frequency selective. This makes power allocation across frequency to be a fundamental feature of high performance systems.

### 3.3 Algorithm 1: DMT WMMSE Minimization

#### 3.3.1 WMMSE vs. WRS

A recent paper [22] develops an interesting solution for the design of the transmit matrices for the WRS problem in a MIMO broadcast channel. Instead of directly focusing on the WRS problem, a relation is established to the WMMSE problem, which is simpler [40]. The original WRS problem is then solved through the WMMSE problem. Ref. [22] presents the conditions for the two problems to have the same local optimizers and proposes an iterative algorithm that is efficient and that provides good results.

Following the same idea, [69, 83, 84] extend the algorithm to the MIMO-IC. These three references plus [22] focus on the single tone problem ( $K = 1$ ), i.e. they focus on only one layer in Fig. 3.1.

In this section, we show that the solution for the single tone case is straightforwardly extended to the multitone case. We begin with the definition of the MSE matrix  $\mathbf{E}_n^k$  for user  $n$ , tone  $k$ , after the LMMSE receive filter  $\mathbf{R}_n^k$ ,

i.e.

$$\begin{aligned} \mathbf{E}_n^k &= \mathbb{E} [(\mathbf{R}_n^k \mathbf{y}_n^k - \mathbf{x}_n^k)(\mathbf{R}_n^k \mathbf{y}_n^k - \mathbf{x}_n^k)^H] \\ &= ((\mathbf{M}_n^k)^{-1} \mathbf{H}_{n,n}^k \mathbf{T}_n^k (\mathbf{T}_n^k)^H (\mathbf{H}_{n,n}^k)^H + \mathbf{I}_{A_n})^{-1} \end{aligned} \quad (3.6)$$

As is well known, we can rewrite (3.4) as  $b_n^k = \log(|(\mathbf{E}_n^k)^{-1}|)$ .

The DMT WMMSE minimization problem is then given by

$$\begin{aligned} \mathcal{T}^* &= \arg \max_{\mathcal{T}} \sum_{n \in \mathcal{N}} \sum_{k \in \mathcal{K}} -\text{tr}\{\mathbf{W}_n^k \mathbf{E}_n^k\} \\ &\text{subject to } \sum_{k \in \mathcal{K}} \text{tr}\{(\mathbf{T}_n^k)^H \mathbf{T}_n^k\} \leq P_n^{\max} \quad \forall n. \end{aligned} \quad (3.7)$$

Here  $\mathbf{W}_n^k \in \mathbb{C}^{A_n \times A_n}$  is a weighting matrix that, as we shall see, is the key for the WMMSE and WRS problems to have the same local optimizers. Note that (3.7) is convex in  $\mathbf{T}_n^k$  when  $\mathbf{W}_n^k$  is fixed and vice-versa.

The next step is to identify the local optimizers of the two problems of interest, i.e. (3.5) and (3.7), while keeping in mind that the solution to the latter is easier. We start with (3.5). First, we write the Lagrangian function as

$$L_{\text{wsr}}(\mathcal{T}, \boldsymbol{\lambda}) = \sum_{n \in \mathcal{N}} \sum_{k \in \mathcal{K}} w_n b_n^k - \sum_{n \in \mathcal{N}} \lambda_n \left( \sum_{k \in \mathcal{K}} \text{tr}\{(\mathbf{T}_n^k)^H \mathbf{T}_n^k\} - P_n^{\max} \right). \quad (3.8)$$

According to the well-known Karush-Kuhn-Tucker (KKT) conditions,  $\mathcal{T}$  is a local optimizer of (3.5) if there exists  $\boldsymbol{\lambda} = [\lambda_1 \ \cdots \ \lambda_N]^T \in \mathcal{R}^N$  such that

$$\nabla_{\mathbf{T}_n^k} L_{\text{wsr}}(\mathbf{P}, \mathcal{T}, \boldsymbol{\lambda}) = \mathbf{0} \quad \forall n, k \quad (3.9)$$

$$P_n^{\max} - \sum_{k \in \mathcal{K}} \text{tr}\{(\mathbf{T}_n^k)^H \mathbf{T}_n^k\} \geq 0 \quad \forall n$$

$$\lambda_n (P_n^{\max} - \sum_{k \in \mathcal{K}} \text{tr}\{(\mathbf{T}_n^k)^H \mathbf{T}_n^k\}) = 0 \quad \forall n$$

$$\lambda_n \geq 0 \quad \forall n$$

Eq. (3.9) is known as the stationary condition. Here we define  $\nabla_{\mathbf{A}} f(\mathbf{A}) = \partial f(\mathbf{A}) / \partial \mathbf{A}^*$ . Taking into account that [77]

$$\frac{\partial \log|\mathbf{A}|}{\partial \mathbf{X}_{m,n}^*} = \text{tr}\left\{ \mathbf{A}^{-1} \frac{\partial \mathbf{A}}{\partial \mathbf{X}_{m,n}^*} \right\}, \quad (3.10)$$

$$\frac{\partial \mathbf{A}^{-1}}{\partial \mathbf{X}_{m,n}^*} = -\mathbf{A}^{-1} \frac{\partial \mathbf{A}}{\partial \mathbf{X}_{m,n}^*} \mathbf{A}^{-1}, \quad (3.11)$$

we rewrite (3.9) as

$$\begin{aligned} \nabla_{\mathbf{T}_n^k} L_{\text{wsr}}(\mathcal{T}, \boldsymbol{\lambda}) &= w_n (\mathbf{H}_{n,n}^k)^{\text{H}} (\mathbf{M}_n^k)^{-1} \mathbf{H}_{n,n}^k \mathbf{T}_n^k \mathbf{E}_n^k \\ &- \sum_{j \neq n} w_j (\mathbf{H}_{j,n}^k)^{\text{H}} (\mathbf{M}_j^k)^{-1} \mathbf{H}_{j,j}^k \mathbf{T}_j^k \mathbf{E}_j^k (\mathbf{T}_j^k)^{\text{H}} (\mathbf{H}_{j,j}^k)^{\text{H}} (\mathbf{M}_j^k)^{-1} \mathbf{H}_{j,n}^k \mathbf{T}_n^k - \lambda_n \mathbf{T}_n^k = \mathbf{0} \end{aligned} \quad \forall n, k. \quad (3.12)$$

The derivation of (3.12) here is very similar to that for the single tone MIMO broadcast channel case considered in [22].

Now, we follow a similar procedure for the WMMSE problem in (3.7). The Lagrangian is given by

$$L_{\text{wmmse}}(\mathcal{T}, \boldsymbol{\lambda}) = - \sum_{n \in \mathcal{N}} \sum_{k \in \mathcal{K}} \text{tr}\{\mathbf{W}_n^k \mathbf{E}_n^k\} - \sum_{n \in \mathcal{N}} \lambda_n \left( \sum_k \text{tr}\{(\mathbf{T}_n^k)^{\text{H}} \mathbf{T}_n^k\} - P_n^{\text{max}} \right),$$

and the stationary condition corresponding to (3.8) is written as

$$\begin{aligned} \nabla_{\mathbf{T}_n^k} L_{\text{wmmse}}(\mathcal{T}, \boldsymbol{\lambda}) &= (\mathbf{H}_{n,n}^k)^{\text{H}} (\mathbf{M}_n^k)^{-1} \mathbf{H}_{n,n}^k \mathbf{T}_n^k \mathbf{E}_n^k \mathbf{W}_n^k \mathbf{E}_n^k \\ &- \sum_{j \neq n} (\mathbf{H}_{j,n}^k)^{\text{H}} (\mathbf{M}_j^k)^{-1} \mathbf{H}_{j,j}^k \mathbf{T}_j^k \mathbf{E}_n^k \mathbf{W}_n^k \mathbf{E}_j^k (\mathbf{T}_j^k)^{\text{H}} (\mathbf{H}_{j,j}^k)^{\text{H}} (\mathbf{M}_j^k)^{-1} \mathbf{H}_{j,n}^k \mathbf{T}_n^k - \lambda_n \mathbf{T}_n^k = \mathbf{0} \end{aligned} \quad \forall n, k. \quad (3.13)$$

Again, the derivation of (3.13) here is very similar to that for the single tone MIMO broadcast channel case considered in [22]. By comparing (3.12) and (3.13), we note that by setting

$$\mathbf{W}_n^k = w_n (\mathbf{E}_n^k)^{-1} \quad \forall n, k \quad (3.14)$$

then a local optimizer of (3.5) is also a local optimizer of (3.7). Since the WMMSE is easier to solve, that is the one we focus on. The solution of (3.7) is derived similarly to that for the MIMO broadcast channel case [22, 40], and is given by

$$\mathbf{T}_n^k = \left( \sum_{j \in \mathcal{N}} (\mathbf{H}_{j,n}^k)^{\text{H}} (\mathbf{R}_j^k)^{\text{H}} \mathbf{W}_j^k \mathbf{R}_j^k \mathbf{H}_{j,n}^k + \lambda_n \mathbf{I}_{A_n} \right)^{-1} (\mathbf{H}_{n,n}^k)^{\text{H}} (\mathbf{R}_n^k)^{\text{H}} \mathbf{W}_n^k, \quad (3.15)$$

where  $\mathbf{R}_n^k$  is defined in (3.3)  $\forall n, k$ . Note that  $\mathbf{R}_n^k \forall n, k$  is a function of  $\mathbf{T}_n^k \forall n, k$  and hence (3.15) has to be solved iteratively. Also note that the Lagrange multipliers  $\lambda_n$  should be adjusted so as to satisfy the PCs, i.e. for every user

---

**Algorithm 3.1:** DMT-WMMSE
 

---

```

1 Initialize  $\mathbf{T}_n^k = \mathbf{V}_n^k \forall n, k$ , normalize s.t.  $\sum_k \text{tr}\{(\mathbf{T}_n^k)^H \mathbf{T}_n^k\} = P_n^{\max}$ ;
2 repeat
3   Calculate  $\mathbf{R}_n^k$  with (3.3)  $\forall n, k$ ;
4   Calculate  $\mathbf{W}_n^k$  with (3.14)  $\forall n, k$ ;
5   for  $n = 1, \dots, N$  do
6     repeat
7       Calculate  $\mathbf{T}_n^k$  with (3.15)  $\forall k$ ;
8       if  $\sum_k \text{tr}\{(\mathbf{T}_n^k)^H \mathbf{T}_n^k\} > P_n^{\max}$  then
9         | increase  $\lambda_n$ ;
10        else
11          | decrease  $\lambda_n$ ;
12        until  $\lambda_n |\sum_k \text{tr}\{(\mathbf{T}_n^k)^H \mathbf{T}_n^k\} - P_n^{\max}| < \epsilon$ 
13 until convergence
  
```

---

$\sum_{k \in \mathcal{K}} \text{tr}\{(\mathbf{T}_n^k)^H \mathbf{T}_n^k\} \leq P_n^{\max}$ . A simple bisection search is sufficient for finding the right values.

After solving (3.15) for all tones, we not only have the transmit matrices but also the corresponding power allocation for each user, i.e.  $p_n^k = \text{tr}\{(\mathbf{T}_n^k)^H \mathbf{T}_n^k\}$ . Note that the power allocation is “altruistic” (as opposed to a “selfish” power allocation, e.g. [81, 110]). The allocated power on tone  $k$  of user  $n$  depends on the magnitude of the crosstalk channels from user  $n$  to all its potential victims. So, there is a penalty for user  $n$  to allocate power on tone  $k$  if there exist potential for large interference to the other users.

### 3.3.2 Algorithm

We now describe the first proposed algorithm. Because of the frequency selective characteristic of the calculation of the transmit matrices, we refer to it as DMT WMMSE minimization (DMT-WMMSE). The full procedure is shown as Algorithm 3.1.

The initialization of the  $\mathbf{T}_n^k$  is done in line 1. Here we initialize these matrices with their corresponding matrices of right singular values, i.e.  $\mathbf{T}_n^k = \mathbf{V}_n^k$ . We normalize the result to make sure the PCs are satisfied. This initialization is found to produce consistently good results, but it is not guaranteed to converge to a global optimum.

Like [22], we fix two sets of variables and calculate the other one for all tones and users. We first calculate  $\mathbf{R}_n^k$  with (3.3) for all users and tones in line 3 of Algorithm 3.1, then  $\mathbf{W}_n^k$  with (3.14) for all users and tones in line 4 and then  $\mathbf{T}_n^k$  with (3.15) for all users and tones in line 7. For the transmit matrices, we need to adjust the Lagrange multiplier  $\lambda_n$  so that the power budget is respected. This is done with a simple bisection search. In line 12, the constant  $\epsilon$  is a very small positive number. For the simulations presented later in this paper, they are set to  $10^{-6}$  and  $10^{-10}$ , respectively.

We remark that this algorithm works for any values of  $A_n$ , even when all  $A_n$  are equal to one. In other words, Algorithm 3.1 can also be used for the pure spectrum coordination case. For this special case,  $p_n^k = (T_n^k)^* T_n^k$ , where  $T_n^k$  is now a complex scalar.

The proposed algorithm also works for the cases of  $K = 1$  (single tone) and for  $N = 1$  (single user). For the single user case, the algorithm converges to the optimal solution, which is described in Section 3.2. We see here how the extension of the WMMSE solution is straightforward, and how the algorithms of [69, 83, 84] are special cases of Algorithm 3.1.

### 3.3.3 Convergence and Computational Complexity

Following a similar demonstration of convergence carried out in [22] for the MIMO broadcast channel, we briefly sketch the justification for convergence of the DMT-WMMSE algorithm. Define

$$l(\mathcal{R}, \mathcal{W}, \mathcal{T}) = \sum_{k \in \mathcal{K}} \sum_{n \in \mathcal{N}} w_n \log(|(w_n)^{-1} (\mathbf{W}_n^k)^{-1}|) - \sum_{k \in \mathcal{K}} \sum_{n \in \mathcal{N}} \text{tr}\{\mathbf{W}_n^k \tilde{\mathbf{E}}_n^k\} + K \sum_{n \in \mathcal{N}} w_n A_n, \quad (3.16)$$

where  $\mathcal{R} = \{\mathbf{R}_n^k \mid n \in \mathcal{N}, k \in \mathcal{K}\}$ ,  $\mathcal{W} = \{\mathbf{W}_n^k \mid n \in \mathcal{N}, k \in \mathcal{K}\}$  and  $\tilde{\mathbf{E}}_n^k = \mathbf{E} \left[ (\tilde{\mathbf{R}}_n^k \mathbf{y}_n^k - \mathbf{x}_n^k) (\tilde{\mathbf{R}}_n^k \mathbf{y}_n^k - \mathbf{x}_n^k)^H \right]$ . If  $\tilde{\mathbf{R}}_n^k$  is the LMMSE matrix in (3.3), then  $\tilde{\mathbf{E}}_n^k$  becomes (3.6). Consider the optimization problem in the variables  $\mathcal{R}$ ,  $\mathcal{W}$  and  $\mathcal{T}$  of maximizing (3.16) subject to PCs for every user. The successive optimization of this extended problem in  $\mathcal{R}$ ,  $\mathcal{W}$  and  $\mathcal{T}$  corresponds to lines 3, 4 and 5-12 in Algorithm 3.1, respectively. At the end, it also corresponds to solving (3.5). The iterative procedure leads to a monotonically increasing objective function in (3.16). Also, the objective function of (3.7) is upper bounded due to the PCs. Hence, at the end of the algorithm, the KKT system

of (3.5) is solved. This means we also reach a stationary point of the WRS maximization problem.

The most computationally intensive part of the DMT-WMMSE algorithm is the calculation of the transmit matrices. For each user and each tone, the algorithm has computational complexity of  $O(N A_n^3)$ — $N$  because the sum in (3.15) has  $N$  terms and  $A_n^3$  because of the multiplications and matrix inverse—and hence a total computational complexity of  $O(K N^2 \max_n \{A_n\}^3)$ .

## 3.4 Algorithm 2: WMMSE-GDSB

### 3.4.1 Solving the problem in two parts

First, eq. (3.5) can be rewritten in a slightly different way:

$$\begin{aligned} & \max_{\{\mathbf{P}, \mathcal{T}\}} \sum_{n \in \mathcal{N}} \sum_{k \in \mathcal{K}} u_n b_n^k \\ & \text{subject to } \text{tr}\{\mathbf{T}_n^k (\mathbf{T}_n^k)^H\} = p_n^k \quad \forall k, n \\ & \sum_{k \in \mathcal{K}} p_n^k \leq P_n^{\max} \quad \forall n \end{aligned} \quad (3.17)$$

The optimization problems are equivalent, but (3.17) emphasizes more clearly the signal and spectrum coordination parts of the problem. Note that, by fixing  $\mathbf{P}$  in (3.17), we are left with  $K$  independent  $N$ -user single tone MIMO ICs—thus not coupled across tones anymore. By the same token, by decomposing  $\mathbf{T}_n^k$  as  $\mathbf{T}_n^k = \sqrt{p_n^k} \bar{\mathbf{T}}_n^k$  such that  $\text{tr}\{\bar{\mathbf{T}}_n^k (\bar{\mathbf{T}}_n^k)^H\} = 1$  and fixing  $\bar{\mathbf{T}}_n^k \forall n, k$ , we are left with a pure spectrum coordination problem. The algorithm proposed in this section solves each of those two parts separately and independently.

Consider the Lagrangian of (3.17),

$$\begin{aligned} L(\mathbf{P}, \mathcal{T}, \boldsymbol{\lambda}, \boldsymbol{\mu}) = & \sum_{n \in \mathcal{N}} \sum_{k \in \mathcal{K}} u_n b_n^k - \sum_{n \in \mathcal{N}} \lambda_n \left( \sum_{k \in \mathcal{K}} p_n^k - P_n^{\max} \right) \\ & - \sum_{n \in \mathcal{N}} \sum_{k \in \mathcal{K}} \mu_n^k \left( \text{tr}\{\mathbf{T}_n^k (\mathbf{T}_n^k)^H\} - p_n^k \right). \end{aligned} \quad (3.18)$$

The KKT condition of (3.17) states that, if  $\{\mathbf{P}, \mathcal{T}\}$  is a stationary point of (3.17), there exist  $\boldsymbol{\mu} = [\mu_1^1 \ \dots \ \mu_N^{K}]^T \in \mathcal{R}^{KN}$ , and  $\boldsymbol{\lambda} = [\lambda_1 \ \dots \ \lambda_N]^T \in \mathcal{R}^N$ ,

such that

$$\nabla_{\mathbf{T}_n^k} L(\mathbf{P}, \mathcal{T}, \boldsymbol{\lambda}, \boldsymbol{\mu}) = \mathbf{0} \quad \forall n, k \quad (3.19)$$

$$\nabla_{p_n^k} L(\mathbf{P}, \mathcal{T}, \boldsymbol{\lambda}, \boldsymbol{\mu}) = 0 \quad \forall n, k \quad (3.20)$$

$$\text{tr}\{\mathbf{T}_n^k (\mathbf{T}_n^k)^{\text{H}}\} - p_n^k = 0 \quad \forall n, k$$

$$P_n^{\text{max}} - \sum_{k \in \mathcal{K}} p_n^k \geq 0 \quad \forall n$$

$$\lambda_n (P_n^{\text{max}} - \sum_{k \in \mathcal{K}} p_n^k) = 0 \quad \forall n$$

$$\lambda_n \geq 0 \quad \forall n$$

Eqs. (3.19) and (3.20) are the stationary conditions related respectively to the signal and to the spectrum coordination parts of the problem. Our approach is to solve (3.19) and (3.20) in two steps. First, we fix  $\mathbf{P}$  and  $\boldsymbol{\mu}$  and optimize for  $\mathbf{T}_n^k$  and  $\boldsymbol{\lambda}$  such that  $\text{tr}\{\mathbf{T}_n^k (\mathbf{T}_n^k)^{\text{H}}\} = p_n^k \quad \forall n, k$ . Second, we fix  $\overline{\mathbf{T}}_n^k \quad \forall n, k$  and  $\boldsymbol{\lambda}$ , with  $\text{tr}\{\overline{\mathbf{T}}_n^k (\overline{\mathbf{T}}_n^k)^{\text{H}}\} = 1$ , and optimize  $\mathbf{P}$  and  $\boldsymbol{\mu}$  such that the PCs are satisfied. We apply this process iteratively until convergence.

We now focus on how to solve each of these steps.

### 3.4.2 Solving for $\mathbf{T}_n^k$

When solving for the transmit matrices, we can reduce (3.18) to

$$L(\mathcal{T}, \boldsymbol{\mu}) = \sum_{k \in \mathcal{K}} L(\mathcal{T}^k, \boldsymbol{\mu}^k),$$

where

$$L(\mathcal{T}^k, \boldsymbol{\mu}^k) = \sum_{n \in \mathcal{N}} u_n b_n^k - \sum_{n \in \mathcal{N}} \mu_n^k (\text{tr}\{\mathbf{T}_n^k (\mathbf{T}_n^k)^{\text{H}}\} - p_n^k). \quad (3.21)$$

Here  $\mathcal{T}^k$  denotes the set of transmit matrices for all users and for one given tone  $k$ , i.e.  $\mathcal{T}^k = \{\mathbf{T}_n^k \mid n \in \mathcal{N}\}$  and  $\boldsymbol{\mu}^k = [\mu_1^k \ \cdots \ \mu_N^k]^{\text{T}} \in \mathcal{R}^N$ . As already mentioned, this implies that we have to solve  $K$  independent single tone MIMO IC problems with each user having a power budget of  $p_n^k$ . Previous work has dealt with the single tone MIMO IC problem several times. In the next paragraphs, we discuss (by no means exhaustively) some of the previously proposed solutions.

Recent work has proposed the concept of interference alignment [9]. In this reference it is shown that, when background noise tends to zero and interference is dominant, interference alignment is an optimal strategy. Ref. [32] deals with the case when background noise has to be taken into account, and interference alignment is combined with an SNR maximizing algorithm. Some other direction of research focuses on game theory [81, 110]. These algorithms cast the single tone MIMO IC problem as a non-cooperative game and converge to a Nash equilibrium point. Other references include [42, 69, 83, 84].

However, in this chapter we opt for the WMMSE strategy for the MIMO IC in [69, 83, 84]. This is so for a number of reasons. The WMMSE strategy has reasonable computational complexity and is guaranteed to converge to a stationary point. Convergence to a stationary point does not apply to the game theoretic strategies [81, 110]. The interference alignment strategy approaches optimality when background noise tends to zero, which is not necessarily the case for DSL. Ref. [32] would be more suitable for DSL, but it is also not guaranteed to converge to a stationary point. The algorithm in [42], though also able to reach a stationary point, is more computationally complex than the WMMSE approach.

Although we choose the WMMSE strategy, we emphasize that any other of the cited methods can be applied within our framework. We detail the implementation of the WMMSE approach in Section 3.4.5

### 3.4.3 Solving for P

For the spectrum coordination part of the problem, we can reduce (3.18) to

$$L(\mathbf{P}, \boldsymbol{\lambda}) = \sum_{n \in \mathcal{N}} \lambda_n P_n^{\max} + \sum_{k \in \mathcal{K}} L(\mathbf{p}^k, \boldsymbol{\lambda}),$$

where

$$L(\mathbf{p}^k, \boldsymbol{\lambda}) = \sum_{n \in \mathcal{N}} u_n b_n^k - \sum_{n \in \mathcal{N}} \lambda_n p_n^k. \quad (3.22)$$

Note that here, unlike (3.21), the problem is not decoupled across tones. In this part of the algorithm,  $\bar{\mathbf{T}}_n^k$  is fixed for all  $n, k$ . We remind that we have decomposed  $\mathbf{T}_n^k$  as  $\bar{\mathbf{T}}_n^k \triangleq 1/\sqrt{p_n^k} \mathbf{T}_n^k$  so that  $\text{tr}\{\bar{\mathbf{T}}_n^k (\bar{\mathbf{T}}_n^k)^H\} = 1$ . We can rewrite  $b_n^k$  in (3.22) as

$$b_n^k = \log |p_n^k (\bar{\mathbf{T}}_n^k)^H (\mathbf{H}_{n,n}^k)^H (\mathbf{M}_n^k)^{-1} \mathbf{H}_{n,n}^k \bar{\mathbf{T}}_n^k + \mathbf{I}_{A_n}|,$$

where  $\mathbf{M}_n^k = \sum_{j \neq n} p_j^k \mathbf{H}_{n,j}^k \bar{\mathbf{T}}_j^k (\bar{\mathbf{T}}_j^k)^H (\mathbf{H}_{n,j}^k)^H + \mathbf{I}_{A_n}$

Solving (3.22) is non-concave and thus non trivial. To overcome this, we solve it in a simplified, per-user fashion. Consider (3.22) as a function of the power allocation of one given user, say  $n$ ,

$$\tilde{L}(p_n^k, \lambda_n) = u_n b_n^k + \sum_{j \neq n} u_j \left( b_j^k \Big|_{\bar{\mathbf{p}}^k} + (p_n^k - \bar{p}_n^k) \frac{\partial b_j^k}{\partial p_n^k} \Big|_{\bar{\mathbf{p}}^k} \right) - \lambda_n p_n^k.$$

Here, we approximate  $b_j^k$ ,  $j \neq n$  by the first order Taylor expansion around the point  $\bar{\mathbf{p}}^k$ , which represents the power allocation on tone  $k$  in iteration  $i - 1$ . It can be shown that  $b_n^k$  is a concave function of  $p_n^k$  and that  $b_j^k$  is a convex function of  $p_n^k$  ([7], page 74)—here we again find a difference of convex programming structure, already mentioned in Section 2.4.4. Because of the linearization of the convex part, we avoid the DC programming structure and  $\tilde{L}(p_n^k, \lambda_n)$  becomes concave in  $p_n^k$ .

The next step is to calculate the derivative of  $\tilde{L}(p_n^k, \lambda_n)$  in  $p_n^k$ , set the result to zero and solve for  $p_n^k$ . In order to do that, we take into account that [77]

$$\frac{\partial \log|\mathbf{A}|}{\partial \mathbf{X}_{m,n}^*} = \text{tr} \left\{ \mathbf{A}^{-1} \frac{\partial \mathbf{A}}{\partial \mathbf{X}_{m,n}^*} \right\}, \quad (3.23)$$

$$\frac{\partial \mathbf{A}^{-1}}{\partial \mathbf{X}_{m,n}^*} = -\mathbf{A}^{-1} \frac{\partial \mathbf{A}}{\partial \mathbf{X}_{m,n}^*} \mathbf{A}^{-1}, \quad (3.24)$$

We proceed in two steps. First, using (3.23), we write

$$\frac{\partial b_n^k}{\partial p_n^k} = \text{tr} \left\{ (p_n^k \mathbf{S}_n^k + \mathbf{I}_{A_n})^{-1} \mathbf{S}_n^k \right\}. \quad (3.25)$$

Here, we define  $\mathbf{S}_n^k \triangleq (\bar{\mathbf{T}}_n^k)^H (\mathbf{H}_{n,n}^k)^H (\mathbf{M}_n^k)^{-1} \mathbf{H}_{n,n}^k \bar{\mathbf{T}}_n^k$ . Second, observing (3.23), (3.24) and using the chain rule, we write

$$\begin{aligned} \frac{\partial b_j^k}{\partial p_n^k} \Big|_{\bar{\mathbf{p}}^k} &= \text{tr} \left\{ \mathbf{E}_j^k (\mathbf{T}_j^k)^H (\mathbf{H}_{j,j}^k)^H \frac{\partial (\mathbf{M}_j^k)^{-1}}{\partial p_n^k} \mathbf{H}_{j,j}^k \mathbf{T}_j^k \right\} \\ &= -\text{tr} \left\{ (\bar{\mathbf{T}}_n^k)^H (\mathbf{H}_{j,n}^k)^H (\mathbf{M}_j^k)^{-1} \mathbf{H}_{j,j}^k \mathbf{T}_j^k \mathbf{E}_j^k (\mathbf{T}_j^k)^H (\mathbf{H}_{j,j}^k)^H (\mathbf{M}_j^k)^{-1} \mathbf{H}_{j,n}^k \bar{\mathbf{T}}_n^k \right\}, \end{aligned} \quad (3.26)$$

where  $\mathbf{E}_j^k$  is given by (3.6). Finally, by combining (3.25) and (3.26), we obtain the resulting equation for power allocation:

$$\frac{\partial \tilde{L}(p_n^k, \lambda_n)}{\partial p_n^k} = u_n \text{tr} \left\{ (p_n^k \mathbf{S}_n^k + \mathbf{I}_{A_n})^{-1} \mathbf{S}_n^k \right\} - \tau_n^k - \lambda_n = 0. \quad (3.27)$$

Here, we define

$$\tau_n^k \triangleq - \sum_{j \neq n} u_j \left. \frac{\partial b_j^k}{\partial p_n^k} \right|_{\bar{\mathbf{p}}^k}, \quad (3.28)$$

where the partial derivative is given by (3.26).

For the solution, for every user we should find  $p_n^k$  such that (3.27) holds for every tone. There should also be a search for the Lagrange multiplier  $\lambda_n$  so that the power budget is respected. Although not clear at a first glance, (3.27) is a type of waterfilling formula with frequency selectivity. The frequency selectivity is due to the term  $\tau_n^k$ , which represents how much damage is inflicted to other users if user  $n$  allocates power on tone  $k$ . This variable should be large if there is potential for large interference to other users. We remark that the distributed spectrum balancing (DSB) algorithm has a similar power allocation formula [96, 109], which is a special case of (3.27) for the SISO case. For this case, (3.27) can be rearranged in a closed-form waterfilling formula where  $\tau_n^k$  distorts the waterlevel so that damage to other users is accounted for. Eq. (3.27), however, is more complicated but, as we see next, can be solved efficiently.

The fact that (3.27) is a generalization of the DSB power allocation formula motivates our choice for the name *generalized DSB* (GDSB) for the spectrum coordination part of the algorithm.

### 3.4.4 Solving (3.27)

Let us rewrite (3.27) and define the function  $f(p)$  as

$$f(p) = up^{-1} \text{tr}\{(\mathbf{S} + p^{-1}\mathbf{I})^{-1}\mathbf{S}\} - \nu, \quad (3.29)$$

$\mathbf{S} \in \mathbb{H}^{A \times A}$ , where  $\mathbb{H}^{A \times A}$  represents hermitian matrices of size  $A \times A$ ; and  $\nu \in \mathcal{R}$ ,  $\nu \geq 0$ . For our case  $\mathbf{S}$  is actually not only hermitian, but also positive semi-definite (it is a covariance matrix). However, in order to get some insight, the analysis in this section mostly focuses on the case of  $\mathbf{S}$  being hermitian, except for Corollary 1. For convenience, in this section we ignore the subscripts and superscripts of (3.27). These will be recovered when suitable.

As there is no closed form solution for the roots of (3.27), one particularly straightforward approach is to use a root-finding algorithm, e.g. the Newton method [78]. However, such a method would be very inefficient, given that it should be repeated for all users and all tones of the DSL network. Plus, there is the power budget: for a given user, such a method would have to solve the problem for every tone multiple times until the right Lagrange multiplier  $\lambda_n$  in (3.27) is found and the power budget is respected [in (3.29),  $\nu = \lambda_n + \tau_n^k$ ].

We can find the roots (3.29) efficiently with a different strategy. In the following, we use basic linear algebra concepts to show how to obtain the coefficients  $\boldsymbol{\alpha} = [\alpha_1 \ \dots \ \alpha_{A+1}]^T \in \mathcal{R}^{A+1}$  of a polynomial  $f'(p) = \sum_{i=1}^{A+1} \alpha_i p^{A+1-i}$  whose roots are the same as those of the original (3.29).

We consider the eigenvalue decomposition of  $\mathbf{S}$ ,  $\mathbf{S} = \mathbf{Q}\boldsymbol{\Xi}\mathbf{Q}^H$ . Because  $\mathbf{S}$  is hermitian,  $\mathbf{Q}$  is orthonormal and all eigenvalues  $\xi_i$ ,  $i = 1, \dots, A$  are real. Thus  $\boldsymbol{\Xi} = \text{diag} \{[\xi_1 \ \dots \ \xi_A]\}$  is a real matrix. We rewrite (3.29) as

$$\begin{aligned} f(p) &= up^{-1} \text{tr}\{(\mathbf{Q}\boldsymbol{\Xi}\mathbf{Q}^H + p^{-1}\mathbf{Q}\mathbf{Q}^H)^{-1}\mathbf{Q}\boldsymbol{\Xi}\mathbf{Q}^H\} - \nu \\ &= up^{-1} \text{tr}\{(\boldsymbol{\Xi} + p^{-1}\mathbf{I})^{-1}\boldsymbol{\Xi}\} - \nu \\ &= u \sum_{i=1}^A \frac{\xi_i}{p\xi_i + 1} - \nu. \end{aligned} \quad (3.30)$$

## Analysis

First, we do a brief analysis of  $f(p)$  and its behavior. Clearly, as seen in (3.30), we can write  $f(p) : \mathcal{R} \rightarrow \mathcal{R}$ . Also, it is easy to see that

$$\lim_{p \rightarrow -\infty} f(p) = \lim_{p \rightarrow +\infty} f(p) = -\nu. \quad (3.31)$$

**Proposition 3.1.** *If,  $\nu > 0$ , the number of roots to  $f(p)$  is equal to the number of distinct non-zero eigenvalues of  $\mathbf{S}$ .*

**Proof.** *To prove this statement, we need two things. First, we focus on the behavior of  $f(p)$  when  $p \rightarrow -1/\xi_i$ . Second, we check the derivative of  $f(p)$*

*We assume that  $\mathbf{S}$  has  $D$  distinct non-zero eigenvalues. Note that eigenvalues equal to zero do not contribute to  $f(p)$ . When  $p = -1/\xi_i$ , then  $p\xi_i + 1 = 0$  and (3.30) is undefined. Consider  $\lim_{p \rightarrow \{-1/\xi_i\}^-} f(p)$  and  $\lim_{p \rightarrow \{-1/\xi_i\}^+} f(p)$ ,  $i = 1, \dots, D$ . Here  $p \rightarrow \{P\}^-$  and  $p \rightarrow \{P\}^+$  denote  $p$  approaching  $P$  from the left and from the right, respectively. It is clear that these two limits will be either  $\infty$  or  $-\infty$ . At this point we cannot guarantee, however, whether they are both equal or whether they differ in sign.*

*Calculating the derivative of  $f(p)$ , we obtain*

$$\frac{\partial f(p)}{\partial p} = -u \sum_{i=1}^A \frac{(\xi_i)^2}{(p\xi_i + 1)^2}. \quad (3.32)$$

*Define  $\mathcal{P} = \{p \in \mathcal{R} \mid p \neq -1/\xi_i, i = 1, \dots, D\}$ . Then, (3.32) implies that in  $\mathcal{P}$  the derivative  $\partial f(p)/\partial p$  is negative and so  $f(p)$  is strictly decreasing. That leads*

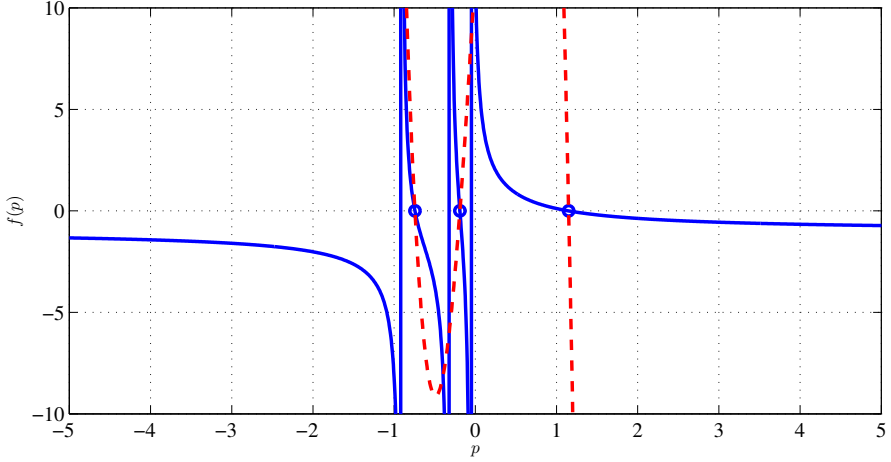


Figure 3.2: Example of the behavior of the function  $f(p) = \text{utr}\{(p\mathbf{S}+\mathbf{I})^{-1}\mathbf{S}\} - \nu$  for a randomly generated, hermitian and positive semi-definite  $\mathbf{S}$  and  $\nu = 0.75$ . The solid line represents  $f(p)$  and the dotted line represents the polynomial  $f'(p)$ . Their roots are the same. When  $\mathbf{S}$  is positive semi-definite, at most one root is non-negative.

us to conclude that

$$\lim_{p \rightarrow [-1/\epsilon_i]^-} f(p) = -\infty \quad (3.33)$$

$$\lim_{p \rightarrow [-1/\epsilon_i]^+} f(p) = \infty \quad (3.34)$$

For  $p \in \mathcal{P}$ ,  $f(p)$  is continuous. The continuity and the strictly decreasing behavior of  $f(p)$  in  $\mathcal{P}$  plus (3.31), (3.33) and (3.34) lead us to complete the proof.  $\square$

As (3.30) has  $D$  distinct solutions, an additional pertinent question is how to handle these different solutions. For example, of the  $D$  roots of  $f(p)$ , which one should be picked? We remind that these roots should be the power allocation  $p_n^k$  for a given user and tone in (3.17). For a given user with  $K$  tones, if each tone has  $D$  solutions, is it necessary to combine these  $KD$  solutions? Would all combinations be equivalent? Fortunately, because of the following corollary we need not worry about this issue.

*Corollary 3.1.* If  $\nu > 0$  and  $\mathbf{S}$  is positive semi-definite, there can be at most one non-negative root to  $f(p)$ .

**Proof.** If  $\mathbf{S}$  is positive semi-definite, then  $\xi_i \geq 0$ ,  $i = 1, \dots, D$ . That implies that  $f(p)$  approaches infinity only for  $p < 0$ . Order the values of  $p$  for which  $f(p)$  approaches infinity in ascending order as  $\{-1/\xi_1, -1/\xi_2, \dots, -1/\xi_D\}$ . There are  $D$  roots to  $f(p)$ . Because of (3.31) and the strictly decreasing behavior of  $f(p)$ , there is one root between  $-1/\xi_i$  and  $-1/\xi_{i+1}$ ,  $i = 1, \dots, D-1$  and one root between  $-1/\xi_D$  and  $+\infty$ . This means that, for  $p \geq 0$ ,  $f(p)$  crosses zero at most once.  $\square$

As already mentioned, for our problem  $\mathbf{S}$  is a covariance matrix, so it is always positive semi-definite. For the solution of the spectrum coordination problem, what happens in practice is that either only one root of  $f(p)$  is positive or all roots are negative. Since a negative  $p_n^k$  has no physical meaning, for the former case we need to discard the negative roots of  $f(p)$ . For the latter case, the optimal solution is  $p_n^k = 0$  and user  $n$  allocates no power on tone  $k$ . Thus Corollary 1 guarantees there will always be only one feasible solution.

In Fig. 3.2, the solid line illustrates the behavior of  $f(p)$  for a hermitian, positive semi-definite and randomly generated  $\mathbf{S} \in \mathbb{H}^{3 \times 3}$  and  $\nu = 0.75$ . Note that there is only one non-negative root.

### Eq. (3.27) in Polynomial Form

Clearly, (3.30) can be written as a polynomial and thus be solved efficiently. In this subsection, we consider some examples. First, consider  $\mathbf{S} \in \mathbb{H}^{3 \times 3}$ . Set  $f(p) = 0$ . Re-arranging, we obtain

$$f'(p) = u \sum_{i=1}^3 \xi_i \sum_{\substack{j=1 \\ j \neq i}}^3 (p\xi_i + 1) - \nu \prod_{i=1}^3 (p\xi_i + 1) = 0.$$

Re-arranging again, we finally get  $f'(p_n^k)$  to be (here we re-introduce the subscripts and superscripts)

$$\begin{aligned} & (p_n^k)^3 (-\nu_n^k |\mathbf{S}_n^k|) + (p_n^k)^2 (3u_n |\mathbf{S}_n^k| - \nu_n^k (\xi_1 \xi_2 + \xi_1 \xi_3 + \xi_2 \xi_3)) \\ & + p_n^k \left( u_n \left( \sum_{i=1}^3 \xi_i \sum_{\substack{j=1 \\ j \neq i}}^3 \xi_j \right) - \nu_n^k \text{tr}\{\mathbf{S}_n^k\} \right) + (u_n \text{tr}\{\mathbf{S}_n^k\} - \nu_n^k) = 0. \end{aligned} \quad (3.35)$$

We remind that  $\nu_n^k = \tau_n^k + \lambda_n$ . Eq. (3.35) is shown in the dotted line in Fig. 3.2 for the same hermitian, positive semi-definite and randomly generated  $\mathbf{S}$  and  $\nu = 0.75$ . Note that the roots of the original  $f(p)$  and of  $f'(p)$  are the same.

As another example, if  $\mathbf{S} \in \mathbb{H}^{2 \times 2}$ , then  $f'(p)$  is written as

$$(p_n^k)^2(-\nu_n^k |\mathbf{S}_n^k|) + p_n^k(2u_n |\mathbf{S}_n^k| - \nu_n^k \text{tr}\{\mathbf{S}_n^k\}) + (u_n \text{tr}\{\mathbf{S}_n^k\} - \nu_n^k) = 0. \quad (3.36)$$

If  $S_n^k$  is a scalar then we are back at the SISO case, which is solved in [96, 109].

Solving this polynomial is much easier and computationally cheaper than, for example, the root-finding algorithm mentioned in Section 3.4.4. For example, for polynomials of degrees 2, 3 and 4 there are closed-form solutions to the roots. For polynomials of larger degree, finding the roots has computational complexity  $O(A^2)$ . However, we can do better than that. Because  $\mathbf{S}$  in our problem is positive semi-definite, we are only interested in the largest (rightmost) root of  $f(p)$  (see Corollary 1). We can thus use the *power method* ([31], Sec. 7.3.1). The power method obtains the largest eigenvalue in terms of absolute value of a given matrix. Consider the *companion matrix* formed with the coefficients of, say, (3.35).

$$\begin{bmatrix} 0 & 0 & -\alpha_4/\alpha_1 \\ 1 & 0 & -\alpha_2/\alpha_1 \\ 0 & 1 & -\alpha_2/\alpha_1 \end{bmatrix}$$

Here  $\alpha_1 = -\nu_n^k |\mathbf{S}_n^k|$ ,  $\alpha_2 = 3u_n |\mathbf{S}_n^k| - \nu(\xi_1 \xi_2 + \xi_1 \xi_3 + \xi_2 \xi_3)$ , etc.<sup>2</sup> It is well known that the eigenvalues of the companion matrix correspond to the roots of the polynomial  $f'(p) = \sum_{i=1}^{A+1} \alpha_i p^{A+1-i}$ . Hence, we only need to apply the power method and find the largest eigenvalue of the companion matrix. We can avoid obtaining a large negative eigenvalue with a simple procedure, which entails running the power method at most twice. First, run the power method. If a positive eigenvalue is found, then the procedure is successful and can finish. If a negative eigenvalue is found, then run the power method for a second time with a shift in  $f'(p)$  to the right. The shift is denoted by  $\delta \in \mathcal{R}$ ,  $\delta > 0$ . The polynomial in (3.35) becomes

$$\begin{aligned} & (p_n^k - \delta)^3(-\nu_n^k |\mathbf{S}_n^k|) + (p_n^k - \delta)^2(3u_n |\mathbf{S}_n^k| - \nu(\xi_1 \xi_2 + \xi_1 \xi_3 + \xi_2 \xi_3)) \\ & + (p_n^k - \delta) \left( u_n \left( \sum_{i=1}^A \xi_i \sum_{\substack{j=1 \\ j \neq i}}^A \xi_j \right) \nu_n^k \text{tr}\{\mathbf{S}_n^k\} \right) + (u_n \text{tr}\{\mathbf{S}_n^k\} - \nu_n^k) = 0. \end{aligned}$$

The shift should be equal to the absolute value of the negative number that is the result of the first run of the power method. The power method has computational complexity of  $O(A)$ .

---

<sup>2</sup>Thanks to Prof. Raf Vandebril, from the Department of Computer Science, KU Leuven, Belgium, for the helpful discussions concerning companion matrices and the power method.

**Algorithm 3.2:** WMMSE-Generalized DSB

---

```

1 Initialize  $\mathbf{T}_n^k = \mathbf{V}_n^k \forall n, k$ , normalize s.t.  $\text{tr}\{\mathbf{T}_n^k(\mathbf{T}_n^k)^H\} = P_n^{\max}$ ;
2 Initialize  $\mathbf{P} = \mathbf{0}_{K \times N}$ ;
3 repeat
4   Calculate  $\tau_n^k$  with (3.28)  $\forall n, k$ ;
5   Calculate  $\mathbf{S}_n^k \triangleq (\bar{\mathbf{T}}_n^k)^H (\mathbf{H}_{n,n}^k)^H (\mathbf{M}_n^k)^{-1} \mathbf{H}_{n,n}^k \bar{\mathbf{T}}_n^k \forall n, k$ ;
6   for  $n = 1, \dots, N$  do
7     repeat
8        $\nu_n^k = \tau_n^k + \lambda_n$ ;
9        $p_n^k = \max(\mathcal{P}, 0)$ ,  $\mathcal{P} = \{p | u_n \sum_{i=1}^{A_n} \xi_i \sum_{j=1, j \neq i}^{A_n} -\nu_n^k \prod_{i=1}^{A_n} (p\xi_i + 1) = 0\}$ 
10       $\forall k$ ;
11      if  $\sum_k p_n^k > P_n^{\max}$  then
12        increase  $\lambda_n$ ;
13      else
14        decrease  $\lambda_n$ ;
15    until  $\lambda_n |\sum_k p_n^k - P_n^{\max}| < \epsilon$ 
16   Calculate  $\mathbf{R}_n^k$  with (3.3)  $\forall n, k$ ;
17   Calculate  $\mathbf{W}_n^k$  with (3.14)  $\forall n, k$ ;
18   for  $n = 1, \dots, N$  do
19     for  $k = 1, \dots, K$  do
20       repeat
21         Calculate  $\mathbf{T}_n^k$  with (3.15);
22         if  $\text{tr}\{\mathbf{T}_n^k(\mathbf{T}_n^k)^H\} > p_n^k$  then
23           increase  $\mu_n^k$ ;
24         else
25           decrease  $\mu_n^k$ ;
26       until  $|\text{tr}\{\mathbf{T}_n^k(\mathbf{T}_n^k)^H\} - p_n^k| < \epsilon$ 
27 until convergence

```

---

### 3.4.5 Algorithm

We now proceed to writing an algorithm to solve (3.17). Since our method of choice for the signal coordination part is the WMMSE algorithm and our choice for the spectrum coordination part is the generalized DSB method (GDSB), we refer to the combination of the two as WMMSE-GDSB.

An algorithm description is provided in Algorithm 3.2. We initialize the algorithm with  $\mathbf{T}_n^k$  equal to the right singular vector matrices in line 1. Also,

we initialize the power allocation in line 2. In lines 4-14, we solve the spectrum coordination part and in lines 15-25 we solve the signal coordination part. We remark that it is not necessary to solve the spectrum coordination part first and the signal coordination part second. Inverting that order would work just as well. We briefly detail the two parts in the next paragraphs.

In lines 4 and 5,  $\mathbf{S}_n^k$  and  $\tau_n^k$  are calculated for every user and tone. Since these are calculated outside the ‘for’ loop in lines 6-14, power allocation is done in parallel and the calculation of  $\tau_n^k$  takes into account the power allocation of the previous iteration. In line 9, for every user separately  $p_n^k$  is found by solving a polynomial— $\xi_i$  is the  $i$ th eigenvalue of  $\mathbf{S}_n^k$ . Here we can either find all roots and keep the largest root or use the power method. Note that we should find an appropriate Lagrange multiplier so that the power budget is respected. We do this with a simple bisection search.

For the signal coordination part, the procedure is very similar to the one described in Algorithm 3.1. The variables  $\mathbf{R}_n^k$ ,  $\mathbf{W}_n^k$  and  $\mathbf{T}_n^k$  should be calculated. As before, we fix two variables and solve for the third one. One difference between the signal coordination part in Algorithm 3.1 and in Algorithm 3.2 is that for the latter we should solve an equality constrained problem for every tone separately. That implies that the Lagrange multipliers, denoted as  $\mu_n^k$  in Algorithm 3.2, can be negative. The loop in lines 19-25 will converge when the total power allocated for the matrix  $\mathbf{T}_n^k$  is sufficiently close to  $p_n^k$ , calculated in the spectrum coordination part of the algorithm.

### 3.4.6 Convergence and Complexity

First, we analyze the convergence of the spectrum coordination part of the algorithm under fixed  $\overline{\mathbf{T}}_n^k \forall n, k$  when  $\mathbf{T}_n^k \in \mathbb{C}^{2 \times 2}$  and with a high SNR approximation.

**Proposition 3.2.** *Consider  $\overline{\mathbf{T}}_n^k$ ,  $u_n$  and  $\tau_n^k$  fixed  $\forall n, k$ , and  $A_n = 2 \forall n$ . Define  $\overline{\mathbf{H}}_{n,j}^k = \mathbf{H}_{n,j}^k \overline{\mathbf{T}}_j^k (\overline{\mathbf{T}}_j^k)^H (\mathbf{H}_{n,j}^k)^H$ . Define  $\mathbf{S}_n^k = \begin{bmatrix} a & b^* \\ b & a \end{bmatrix}$ . Considering a high SNR approximation of the form*

$$\frac{|b|^2}{(a^2 - |b|^2)^2} \approx 0,$$

if

$$(N-1) \max_{\substack{j,n,k \\ j \neq n}} \left\{ \frac{\text{tr} \left\{ \text{adj} \left\{ \overline{\mathbf{H}}_{n,j}^k \right\} \overline{\mathbf{H}}_{n,n}^k \right\}}{2 |\overline{\mathbf{H}}_{n,n}^k|} \right\} < 1,$$

where  $\text{adj}\{\cdot\}$  stands for the matrix adjugate operator, then the spectrum coordination part of Algorithm 3.2 converges to a unique fixed point.

The details of the proof are left to Appendix B.1. It basically consists in showing that the sequence of iterations is a contraction mapping in the power updates if users operate with high SNR and if the crosstalk channels are relatively weak compared to the direct channels. We emphasize that Proposition 3.2 deals only with the spectrum coordination algorithm, i.e. the GDSB algorithm—the pseudo-code of the GDSB is the same as that in Algorithm 3.2 excluding lines 15-25. Although Proposition 3.2 deals only with the  $2 \times 2$  case under a high SNR assumption, we observe convergence experimentally for a broad range of scenarios.

We make a small digression to remark that Proposition 3.2 is a generalization of the convergence result in [15]. In this reference, the SISO spectrum balancing problem is considered, whereas our result focuses on a MIMO spectrum balancing—both [15] and Proposition 3.2 assume a high SNR regime. The power allocation formula in [15] is the equivalent of (3.27) for the SISO case. To show that the result in [15] is a special case of ours, consider  $\mathbf{H}_{n,n}^k = d_{n,n}^k \mathbf{I}_2 \forall n, k$ . Also consider  $\mathbf{H}_{n,j}^k = h_{n,j}^k \mathbf{I}_2 \forall n, j, k, n \neq j$ . Because of the diagonal structure of  $\mathbf{H}_{n,n}^k$ , the optimal  $\bar{\mathbf{T}}_n^k$  equals the identity matrix times  $1/\sqrt{2}$ . Since the optimal transmit matrix is diagonal, this corresponds to a pure spectrum coordination case (see Section 3.1). The condition in Proposition 3.2 is rewritten as

$$(N-1) \max_{\substack{j,n,k \\ j \neq n}} \left\{ \frac{\text{tr}\{|h_{n,j}^k|^2 \mathbf{I}_2 |d_{n,n}^k|^2 \mathbf{I}_2\}}{2|d_{n,n}^k|^4} \right\} = (N-1) \max_{\substack{j,n,k \\ j \neq n}} \frac{|h_{n,j}^k|^2}{|d_{n,n}^k|^2} < 1,$$

which is exactly the result of [15].

Focusing back on Algorithm 3.2, we know that signal coordination part (the WMMSE algorithm) converges. By applying the signal and spectrum coordination parts in sequence and independently, we have consistently observed from the simulations a monotonically increasing objective function. Some results will be given in Section 3.5. Also, these results also show that after convergence the WMMSE-GDSB algorithm, just like the DMT-WMMSE, reaches a stationary point. We will see, however, that the WMMSE-GDSB needs a significant smaller number of iterations to converge.

The computational complexity of the signal coordination part is estimated as  $O(KN^2 \max_n \{A_n\}^3)$ . The computational complexity of the spectrum coordination part is also estimated as  $O(KN^2 \max_n \{A_n\}^3)$ .

## 3.5 Simulation Results

In this section, we present some results for the two proposed algorithms. Two scenarios are considered: an ADSL downstream scenario and a VDSL upstream scenario. For all simulations, the values for the inter-channel spacing  $\Delta_f$  and the symbol rate  $f_s$  are set to 4.3125 kHz and 4 kHz, respectively.

### 3.5.1 Downstream ADSL

We simulate a system with cables of 0.5 mm (AWG 24) and an SNR gap of 12.8 dB. We consider the near-far downstream ADSL scenario depicted in Fig. 5.5, where two users, each with 2 transceivers (2 direct modes), share the system. Each user has a total power budget of 23.4 dBm. For each line, noise model ANSI A is adopted.

The near-far scenario is one of the main testing grounds for DSM algorithms and it encompasses a good deal of the complexity of the problem. User 1, connected to a central office (CO), shares a cable binder with a far user connected to a remote terminal (RT). Crosstalk from user 2 into user 1 can be prohibitively high, to the point where transmission for user 1 may be seriously compromised. A good solution is one in which user 2 protects user 1 from excessive crosstalk so that both users socially share the system's resources. Referring to Fig. 5.5, we set  $l_1 = 4$  km and  $l_2 = 3$  km and  $d_2 = 3$  km.

We simulate four different algorithms for this scenario, namely the DMT-WMMSE, the WMMSE-GDSB, the GDSB and the SISO DSB. The first two are the algorithms presented in Sections 3.3 and 3.4. As already mentioned, the GDSB corresponds to the spectrum coordination part in WMMSE-GDSB. This algorithm fixes the transmit matrices to the right singular vectors matrix of the direct channel matrix for all users and iterates only the power allocation formula until convergence. The SISO DSB algorithm is the solution of [96, 109]. It is a pure spectrum coordination algorithm where  $A_n = 1 \forall n$ . For SISO DSB, the number of users in the network is 4.

In Fig. 3.4 we depict the four corresponding RRs. We see that the gains obtained with the combined signal and spectrum coordination for this scenario are quite significant. We also see that the DMT-WMMSE and the WMMSE-GDSB have very similar rate performance, while, not surprisingly, the GDSB is worse. The latter does not profit from signal coordination, which is the reason for its weaker performance. Referring to Fig. 3.4, when fixing a data rate of 7 Mb/s for user 1, the SISO DSB can provide approximately 9.3 Mb/s for user 2. For the GDSB, we achieve approximately 12.2 Mb/s for user 2. For both

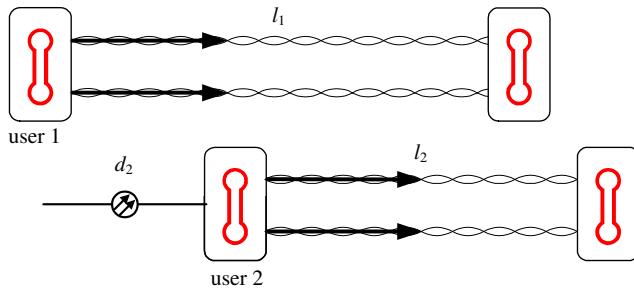


Figure 3.3: Near-far downstream ADSL scenario.

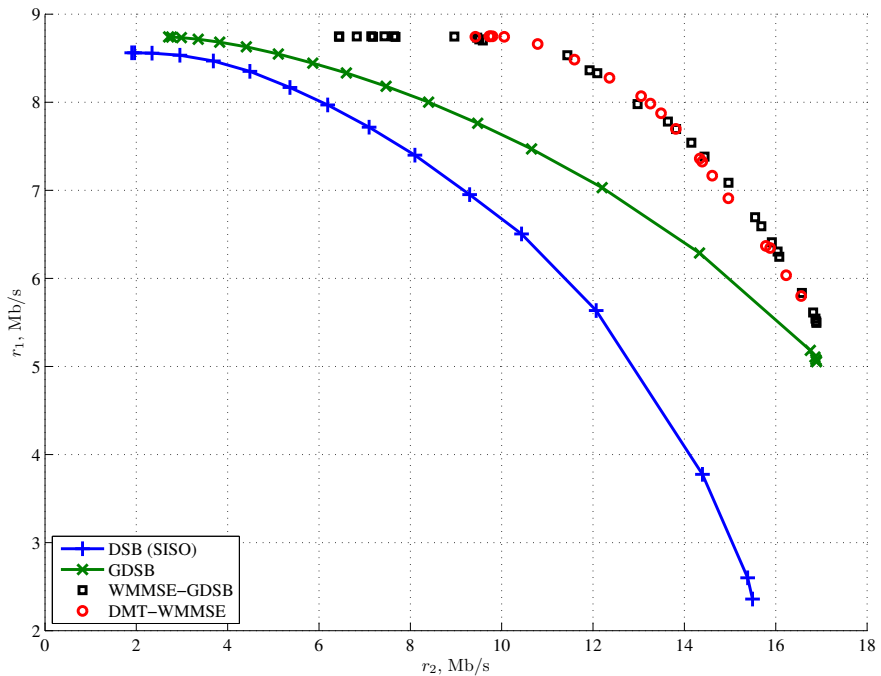


Figure 3.4: RR for the downstream ADSL scenario for four different algorithms: DSB (SISO), GDSB, WMMSE-GDSB and DMT-WMMSE.

DMT-WMMSE and WMMSE-GDSB, we achieve about 15 Mb/s for user 2. Comparing these last two to the SISO DSB, the gain is approximately 80 %.

The power allocations for the GDSB and the WMMSE-GDSB are shown in Figs. 3.5 and 3.6. The two figures have user 1 with a data rate of 7 Mb/s. The

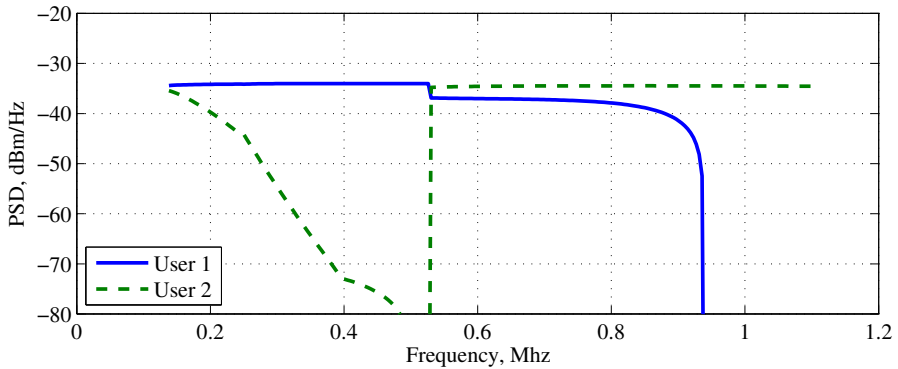


Figure 3.5: Power allocation obtained with GDSB. Data rates are approximately  $r_1 = 7$  Mb/s and  $r_2 = 12.2$  Mb/s.

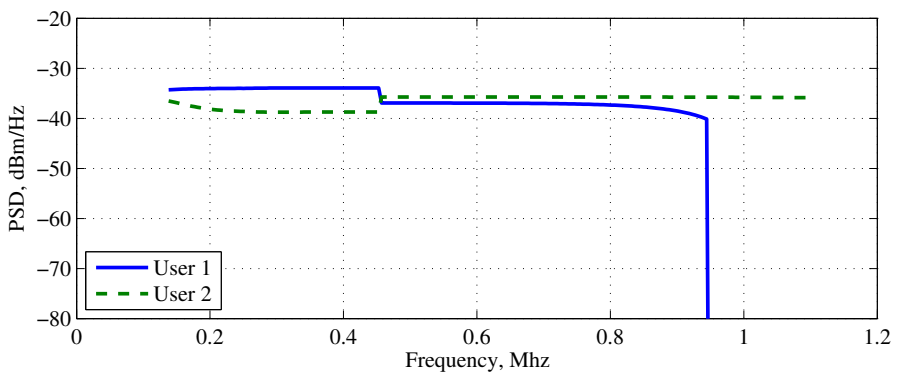


Figure 3.6: Power allocation obtained with WMMSE-GDSB. Data rates are approximately  $r_1 = 7$  Mb/s and  $r_2 = 15$  Mb/s.

difference between the two algorithms is the signal coordination part, and this reflects on the final power allocation. For GDSB there is no signal coordination, so excessive crosstalk to user 1 should be avoided by significant power reduction by user 2 in lower frequencies. WMMSE-GDSB can coordinate users on both the signal and spectrum levels. The signal coordination part can cancel some of the crosstalk. However, some of it may still remain, and hence should be avoided with spectrum coordination. This is reflected in the final power allocation. On lower frequencies, a lot of the crosstalk can be canceled, so the power reduction for user 2 on lower frequencies is significantly smaller.

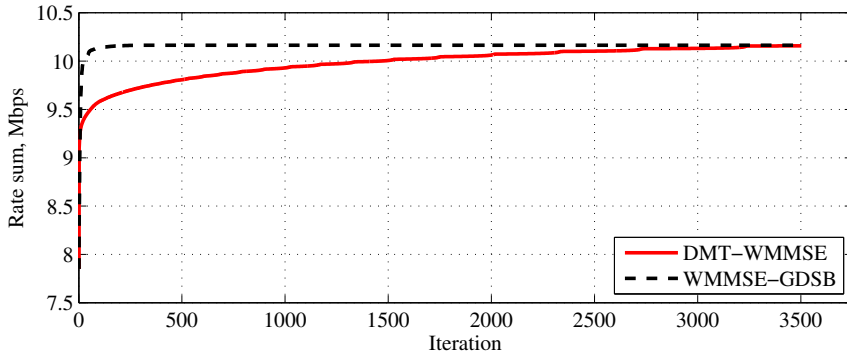


Figure 3.7: Convergence speed for the scenario in Fig. 5.5 for the DMT-WMMSE and the WMMSE-GDSB.

Finally, convergence of the two algorithms proposed in this chapter is depicted in Fig. 3.7. If the data rate performance of the two algorithms is very similar, in terms of convergence there is a big difference. In the example of the figure, the WMMSE-GDSB attains convergence in less than 200 iterations, while the DMT-WMMSE needs more than 3000 iterations. This observation holds true for a large range of scenarios.

The time complexity of one iteration of the DMT-WMMSE (one run of the “repeat” loop in Algorithm 3.1) takes less time than one iteration of the WMMSE-GDSB (one run of the “repeat” loop in Algorithm 3.2). To give a practical example, in our implementation for the scenario in Fig. 3 one iteration of the DMT-WMMSE takes on average 0.3 seconds and one iteration of the WMMSE-GDSB takes on average 0.9 seconds. However, the fact that the latter needs much less iterations to converge more than makes up for this. Plus, in a changing environment, such faster convergence is of great importance. Applied either to wireless or DSL, a good algorithm should be able to quickly respond to a changing network. In DSL, users turn on and off, in wireless the channel changes constantly.

### 3.5.2 Upstream VDSL

In the second experiment, we simulate a VDSL upstream scenario. Cables of 0.4 mm (AWG 26) are used and an SNR gap of 9.45 dB is considered. Each

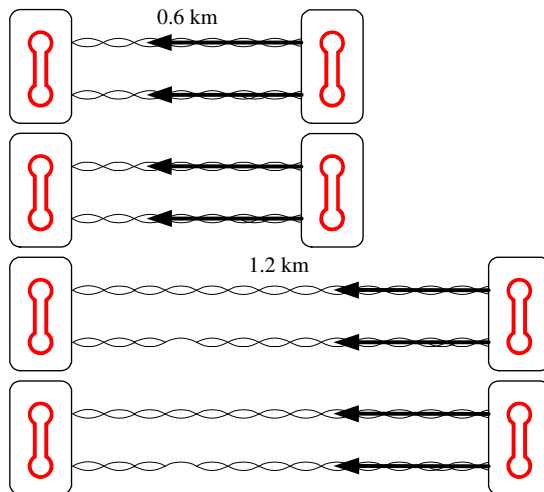


Figure 3.8: Near-far upstream VDSL scenario.

user has a total power budget of 14.5 dBm. For each line, noise model ETSI A is adopted with a background noise level of  $-140$  dBm/Hz. We use the FDD 998 frequency bandplan over POTS up to 12 MHz. The scenario has 4 users, two with long lines and two with short lines, each with two transceivers (two direct modes), as depicted in Fig. 3.8. The long lines are 1.2 km and the short lines are 0.6 km. For this scenario, the users with the short lines have to avoid excessive crosstalk to the users with the long lines.

We depict the RRs of the SISO DSB, the GDSB and the WMMSE-GDSB in Fig. 3.9. We again conclude that the gains of adding signal coordination are very significant.

### 3.6 Conclusion

Signal coordination and spectrum coordination have become crucial for mitigating the effects of multi-user interference in DSL networks. In this chapter, we have combined the two strategies for the DMT MIMO IC, a scenario where only some of the infrastructure for full two-sided signal coordination is available. We have presented two distinct algorithms, the DMT-WMMSE and the WMMSE-GDSB. By means of numerical experiments, we have demonstrated that the addition of per-user MIMO signal coordination

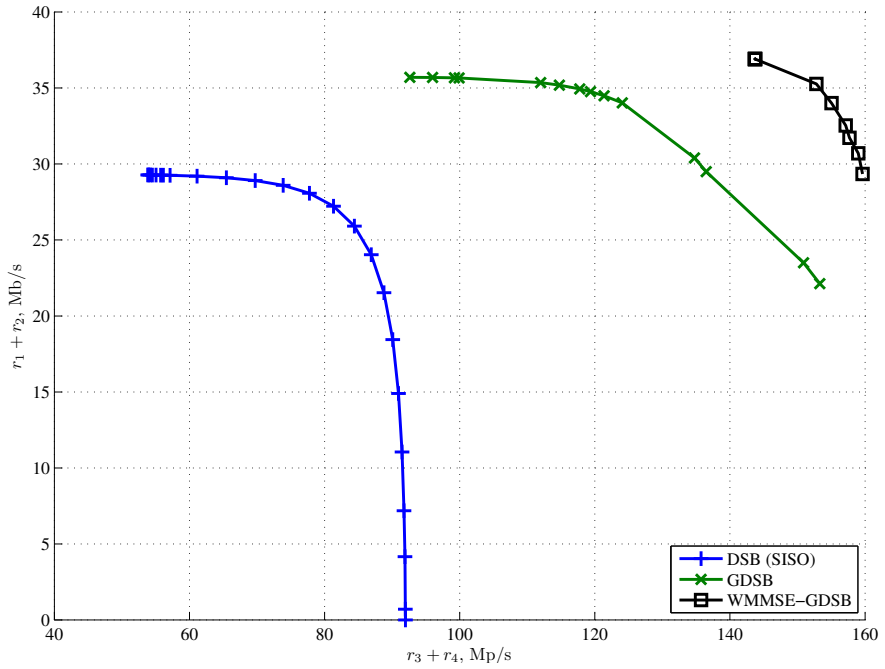


Figure 3.9: RR for the upstream VDSL scenario for DSB (SISO) and WMMSE-GDSB.

can have a significant impact on the achievable rates when compared to multi-user spectrum coordination only.

## Chapter 4

# DMT MIMO IC with Per-Transceiver Power Constraints

### 4.1 Introduction

In Chapter 3, the DMT MIMO IC scenario is suggested as a bridge between spectrum and signal coordination DSM. In such a scenario, a user is characterized by having multiple transceivers, to which it can apply two-sided MIMO processing—this is for instance the case in networks using common mode, phantom mode or split wire transmission [23,56]. There are several such users sharing the channel, each with a distinct set of transceivers. Coordination among them should be done both on the signal and on the spectrum levels. More specifically, the goal of the problem is to come up with transmit matrices for all users and tones. These transmit matrices should be set so as to make it easy to detect the desired signal and easy to cancel the undesired ones (signal coordination). The cancelation of undesired signals is not perfect, and hence some interference will remain. To decrease this remaining interference, an appropriate amount of power should be used for every user and tone (spectrum coordination). Every user is also subject to a power constraint (PC), and that complicates the problem significantly.

In Chapter 3, two distinct algorithms are proposed for the DMT MIMO IC. Both of them provide noteworthy gains in comparison to, for example, a situation where only spectrum coordination is available. However, these two algorithms consider *per-user* PCs, i.e. the sum of the transmit power of all transmitters is limited. This might not be very realistic in practice. To understand why, consider a situation where one user has three transceivers at its disposal—for example, corresponding to two direct modes and one common mode. Each transceiver is associated with a line driver. Each line driver has a PC of, say, 100 mW. For the per-user PC case, the constraint is satisfied if the sum of the power consumption of the three line drivers is 300 mW. However, it can be that the individual line drivers use, say, 80, 100 and 120 mW respectively, which constitutes a violation of the PC of the third line driver. In this chapter, we consider *per-transceiver* (i.e. per-line driver) PCs. A similar problem occurs in wireless communications. For this situation, we refer to *per-antenna* PCs.

The optimization problem with per-transceiver PCs is more difficult than the one with per-user PCs as in Chapter 3. There are more variables and more constraints to be satisfied. In this chapter, we adapt the two algorithms proposed in Chapter 3 to the current situation. First, we derive a new version of the DMT-WMMSE algorithm. This algorithm solves the signal and spectrum coordination parts of the problem simultaneously. The difference with the algorithm with per-user PCs proposed in Chapter 3 is that several Lagrange multipliers have to be found simultaneously. Second, we derive an adaptation of the WMMSE-GDSB algorithm. This algorithm separates the signal and spectrum coordination parts of the problem and solves them sequentially and iteratively. For the spectrum coordination part, we observe that a simple extension of the algorithm presented in Chapter 3 fails to produce a functioning algorithm. We propose to optimize the power allocation of all the transceivers of user  $n$  on tone  $k$  by first doing a change of variables. Consider the vector  $\mathbf{p}_n^k = [p_{n,(1)}^k \ \dots \ p_{n,(A_n)}^k] \in \mathbb{R}_+^{A_n}$ , denoting the power allocation for user  $n$  on tone  $k$  for all transceivers. The  $i$ th variable,  $p_{n,(i)}^k$ , represents the power allocation for the  $i$ th transceiver of a total of  $A_n$  transceivers. Similarly to Chapter 2, we re-write this vector in spherical coordinates, i.e. as a function of a radius and a direction vector. We observe that for the radial dimension the problem can be made concave after approximations. It thus becomes easy to solve. To solve for the remaining dimensions more efficiently, we restrict the direction vector to have a fixed  $\ell_1$  norm. Again, a similar change of variables is used in Chapter 2. The resulting coordinate system can be interpreted as spherical coordinates in taxicab geometry [43]. This coordinate system allows us to solve for each dimension of the direction vector iteratively and sequentially. Simulation results show good performance with the two proposed algorithms. The WMMSE-GDSB has an advantage in that it is seen to converge much faster than the DMT-WMMSE.

This chapter is organized as follows. Section 4.2 describes the DMT MIMO IC problem with per-transceiver PCs mathematically. In Section 4.3 we describe the DMT-WMMSE and in Section 4.4 we describe the WMMSE-GDSB. Some simulation results are presented in Section 4.5 and we conclude with Section 4.6.

## 4.2 Problem Statement

We consider a DSL network with  $N$  independent users, with user  $n$  having  $A_n$  transceivers. We also consider discrete multitone (DMT) modulation with  $K$   $\Delta_f$ -spaced tones. We denote the set of users by  $\mathcal{N} = \{1, \dots, N\}$ , the set of transceivers for user  $n$  as  $\mathcal{A}_n = \{1, \dots, A_n\}$  and the set of tones by  $\mathcal{K} = \{1, \dots, K\}$ . The total number of transceivers in the system is given by  $A = \sum_{n \in \mathcal{N}} A_n$ . We let  $p_{n,(i)}^k$  be the transmit power of transceiver  $i$  of user  $n$  on tone  $k$  and we organize these values in the matrix  $\mathbf{P} \in \mathbb{R}_+^{K \times A}$ . A column of  $\mathbf{P}$ , denoted by  $\mathbf{p}_{n,(i)} = [p_{n,(i)}^1 \ \dots \ p_{n,(i)}^K]^T \in \mathbb{R}_+^K$ , contains the power allocation of transceiver  $i$  of user  $n$  in all tones. We similarly define the matrix that contains the power allocation of all transceivers of user  $n$  in all tones as  $\mathbf{P}_n \in \mathbb{R}_+^{K \times A_n}$ ,  $\mathbf{P}_n = [\mathbf{p}_{n,(1)} \ \dots \ \mathbf{p}_{n,(A_n)}]$  and the vector with the power allocation of all transceivers of user  $n$  in tone  $k$  as  $\mathbf{p}_n^k \in \mathbb{R}_+^{A_n}$  (the  $k$ th row of  $\mathbf{P}_n$ ). We remind that, throughout this thesis, we focus on a linear design for both transmit and receive matrices and treat interference as noise. All channel gains are considered perfectly known (not such a tall order in DSL systems). Also, we consider the simplifying assumption of perfect DMT block synchronization between users.<sup>1</sup> Taking that into account, we obtain the received signal vector for user  $n$  on tone  $k$  as

$$\mathbf{y}_n^k = \mathbf{H}_{n,n}^k \mathbf{T}_n^k \mathbf{x}_n^k + \sum_{j \neq n} \mathbf{H}_{n,j}^k \mathbf{T}_j^k \mathbf{x}_j^k + \mathbf{z}_n^k. \quad (4.1)$$

Here  $\mathbf{x}_n^k = [x_{n,(1)}^k \ \dots \ x_{n,(A_n)}^k]^T \in \mathbb{C}^{A_n}$  is the transmit signal vector for user  $n$  on tone  $k$ ;  $\mathbf{y}_n^k \in \mathbb{C}^{A_n}$  is the received signal vector for user  $n$  on tone  $k$ ; and  $\mathbf{H}_{n,j}^k \in \mathbb{C}^{A_n \times A_j}$ ,  $\mathbf{T}_n^k \in \mathbb{C}^{A_n \times A_n}$  are, respectively, the channel matrix from the transmitter of user  $j$  to the receiver of user  $n$  on tone  $k$  and the transmit matrix for user  $n$  on tone  $k$ . In (4.1), we assume  $\mathbb{E}[\mathbf{x}_n^k (\mathbf{x}_n^k)^H] = \mathbf{I}_{A_n} \forall n$ , and hence  $\mathbf{e}_i^T \mathbf{T}_n^k (\mathbf{T}_n^k)^H \mathbf{e}_i = p_{n,(i)}^k$ , where  $\mathbf{e}_i$  is a vector with 1 in the  $i$ th position and 0 elsewhere. The noise vector  $\mathbf{z}_n^k \in \mathbb{C}^{A_n}$  denotes circularly symmetric zero

<sup>1</sup>For the case when the DMT blocks of different users are offset in relation to each other, inter carrier interference (ICI) arises. ICI complicates the problem significantly. See e.g. [15]

mean complex Gaussian noise. Without loss of generality,  $\mathbf{z}_n^k$  is assumed to be spatially white with covariance matrix  $\mathbb{E}[\mathbf{z}_n^k(\mathbf{z}_n^k)^H] = \mathbf{I}_{A_n}$ . The estimated signal vector for user  $n$  on tone  $k$  is given by

$$\hat{\mathbf{x}}_n^k = \mathbf{R}_n^k \mathbf{y}_n^k, \quad (4.2)$$

where  $\mathbf{R}_n^k \in \mathbb{C}^{A_n \times A_n}$  is the receive matrix for user  $n$  on tone  $k$ . The receive matrix used in (4.2) is the linear MMSE (LMMSE) matrix. For a MIMO IC scenario the LMMSE receiver provides an optimal linear receiver given a set of linear transmit matrices [22]. For a given set of transmit matrices, we have

$$\mathbf{R}_n^k = (\mathbf{T}_n^k)^H (\mathbf{H}_{n,n}^k)^H (\mathbf{M}_n^k + \mathbf{H}_{n,n}^k \mathbf{T}_n^k (\mathbf{T}_n^k)^H (\mathbf{H}_{n,n}^k)^H)^{-1}, \quad (4.3)$$

where

$$\mathbf{M}_n^k = \sum_{j \neq n} \mathbf{H}_{n,j}^k \mathbf{T}_j^k (\mathbf{T}_j^k)^H (\mathbf{H}_{n,j}^k)^H + \mathbf{I}_{A_n} \quad (4.4)$$

is the noise plus interference covariance matrix for user  $n$  on tone  $k$ . We remark that, although we do not write it explicitly, this matrix may be normalized by a SNR gap  $\Gamma$ .

With the LMMSE receiver and assuming Gaussian signaling, the achievable data rate for user  $n$  on tone  $k$  is given by

$$b_n^k = \log |(\mathbf{T}_n^k)^H (\mathbf{H}_{n,n}^k)^H (\mathbf{M}_n^k)^{-1} \mathbf{H}_{n,n}^k \mathbf{T}_n^k + \mathbf{I}_{A_n}|. \quad (4.5)$$

Here  $\log(\cdot)$  denotes the natural logarithm. The total data rate of user  $n$  in bits per second is given by  $r_n = f_s / \log(2) \sum_{k \in \mathcal{K}} b_n^k$ , where  $f_s$  is the symbol rate. We remind that in this thesis we ignore the practical constraint of discrete bit loading.

We denote the set of all transmit matrices  $\mathbf{T}_n^k$  as  $\mathcal{T} = \{\mathbf{T}_n^k \mid n \in \mathcal{N}, k \in \mathcal{K}\}$ . The problem we want to solve is the weighted rate sum (WRS) maximization with per-transceiver PCs, which can be written as

$$\begin{aligned} & \max_{\mathcal{T}} \sum_{n \in \mathcal{N}} \sum_{k \in \mathcal{K}} u_n b_n^k \\ & \text{subject to} \quad \sum_{k \in \mathcal{K}} \mathbf{e}_i^T \mathbf{T}_n^k (\mathbf{T}_n^k)^H \mathbf{e}_i \leq P_n^{\max} \quad \forall n, i \end{aligned} \quad (4.6)$$

Here,  $P_n^{\max}$  is the PC for transceiver  $i$  of user  $n$  (for simplicity, we assume that all transceivers of a user have the same PC) and  $u_n$  is the weight assigned to user  $n$ . This problem can be written in an equivalent form, where the signal and spectrum coordination parts are more easily distinguished.

$$\begin{aligned} & \max_{\mathcal{T}, \mathbf{P}} \sum_{n \in \mathcal{N}} \sum_{k \in \mathcal{K}} u_n b_n^k \\ & \text{subject to } \mathbf{e}_i^T \mathbf{T}_n^k (\mathbf{T}_n^k)^H \mathbf{e}_i = p_{n,(i)}^k \quad \forall n, i, k \\ & \sum_{k \in \mathcal{K}} p_{n,(i)}^k \leq P_n^{\max} \quad \forall n, i \end{aligned} \quad (4.7)$$

Note that here, by fixing  $\mathbf{P}$ , we are left with  $K$  independent MIMO IC's—and thus a signal coordination problem. By decomposing  $\mathbf{T}_n^k$  as  $\mathbf{T}_n^k = \text{diag} \left\{ \left[ \sqrt{p_{n,(1)}^k} \quad \cdots \quad \sqrt{p_{n,(A_n)}^k} \right] \right\} \bar{\mathbf{T}}_n^k$ , where  $\mathbf{e}_i^T \bar{\mathbf{T}}_n^k (\bar{\mathbf{T}}_n^k)^H \mathbf{e}_i = 1 \quad \forall n, i, k$ , and fixing  $\bar{\mathbf{T}}_n^k \quad \forall n, k$ , the problem is described as finding power allocation for every user, tone and transceiver. Hence, it is a spectrum coordination problem.

We call (4.6) and (4.7) the *DMT MIMO IC WRS maximization problem with per-transceiver PCs*.

The single tone MIMO IC (i.e. when  $K = 1$ ), either with per-user or per-transceiver PCs, has been the subject of intensive research [9, 32, 37, 42, 83, 86]. Its multitone version, however, has hitherto received much less attention. There is some related work in the wireless communications literature. In [103, 111], sequential beamforming and multitone power allocation are considered, but with simplifying assumptions. In [111], users are restricted to one data stream and in [103] they are restricted to one receive antenna. In [24] the multitone aspect is pretty much passed by because the authors have assumed that power should be equally divided among the tones. Some of the recent work on the single tone MIMO IC can be easily adapted to the multitone situation by just stacking matrices into a block diagonal structure—the first block corresponding to tone 1, the second to tone 2, etc, see, e.g. [62, 83]. However that does not seem to be the case for all single tone solutions. It is difficult to see, for example, how interference alignment algorithms [9, 32] can be easily adapted to the multitone case. Interference alignment algorithms have no apparent way to perform the power allocation throughout the tones.

It remains a fact that high performance multitone systems benefit considerably by dynamic power allocation through the tones. This is specially true for the DSL case, where the channel is known to be highly frequency selective and the so-called near-far effects are abundant.

In Chapter 3 two algorithms are proposed. Both consider the DMT MIMO IC WRS maximization problem with per-user PCs. In the next two sections, we adapt these algorithms to the problem at hand.

### 4.3 DMT-WMMSE with Per-Transceiver Power Constraints

In [22], the broadcast channel WRS maximization problem is solved through the simpler weighted MMSE (WMMSE) minimization problem. The resulting algorithm is found to provide good performance with reasonable computational complexity. Several works have adapted the main idea of [22] to the MIMO IC WRS maximization problem [83, 84] and in Chapter 3 we have adapted it to the DMT MIMO IC. These works have only treated the per-user PC case. In this section, we show that the same idea can be easily adapted for the per-transceiver PC case.

Since similar derivations have been presented in [83, 84] and in Chapter 3, here we briefly sketch the derivation of the algorithm for the per-transceiver PC case.

We first define the MSE matrix for user  $n$  on tone  $k$  as

$$\begin{aligned} \mathbf{E}_n^k &= \mathbb{E} [(\mathbf{R}_n^k \mathbf{y}_n^k - \mathbf{x}_n^k)(\mathbf{R}_n^k \mathbf{y}_n^k - \mathbf{x}_n^k)^H] \\ &= \left( (\mathbf{T}_n^k)^H (\mathbf{H}_{n,n}^k)^H (\mathbf{M}_n^k)^{-1} \mathbf{H}_{n,n}^k \mathbf{T}_n^k + \mathbf{I}_{A_n} \right)^{-1} \end{aligned} \quad (4.8)$$

and the DMT WMMSE minimization problem as

$$\begin{aligned} \max_{\mathcal{T}} \quad & \sum_{n \in \mathcal{N}} \sum_{k \in \mathcal{K}} -\text{tr} \{ \mathbf{W}_n^k \mathbf{E}_n^k \} \\ \text{subject to} \quad & \sum_{k \in \mathcal{K}} \mathbf{e}_i^T \mathbf{T}_n^k (\mathbf{T}_n^k)^H \mathbf{e}_i \leq P_n^{\max} \quad \forall n, i \end{aligned} \quad (4.9)$$

Here,  $\mathbf{W}_n^k \in \mathbb{C}^{A_n \times A_n}$  is a weighting matrix. Next, we write the Lagrangean of (4.6) and (4.9), find the stationary conditions by calculating the gradient in  $\mathbf{T}_n^k$  and compare the two. Just like in [83, 84] and Chapter 3, it is observed that if the weighting matrix is set as

$$\mathbf{W}_n^k = u_n(\mathbf{E}_n^k)^{-1} \quad \forall n, k \quad (4.10)$$

then a  $\mathcal{T}$  that is a stationary point of (4.9) is also a stationary point of (4.6). This is why we can solve the WRS maximization problem through the simpler WMMSE minimization problem. To solve the latter, we write

$$\begin{aligned} & \max_{\mathcal{T}} \sum_{n \in \mathcal{N}} \sum_{k \in \mathcal{K}} -\mathbb{E} \left[ (\mathbf{R}_n^k \mathbf{y}_n^k - \mathbf{x}_n^k)^H \mathbf{W}_n^k (\mathbf{R}_n^k \mathbf{y}_n^k - \mathbf{x}_n^k) \right] \\ & \text{subject to} \quad \sum_{k \in \mathcal{K}} \mathbf{e}_i^T \mathbf{T}_n^k (\mathbf{T}_n^k)^H \mathbf{e}_i \leq P_n^{\max} \quad \forall n, i \end{aligned}$$

The solution is given by

$$\mathbf{T}_n^k = \left( \sum_{j \in \mathcal{N}} (\mathbf{H}_{j,n}^k)^H (\mathbf{R}_j^k)^H \mathbf{W}_j^k \mathbf{R}_j^k \mathbf{H}_{j,n}^k + \text{diag} \{ \boldsymbol{\lambda}_n \} \right)^{-1} (\mathbf{H}_{n,n}^k)^H (\mathbf{R}_n^k)^H \mathbf{W}_n^k \quad (4.11)$$

where  $\boldsymbol{\lambda}_n = [\lambda_{n,(1)} \cdots \lambda_{n,(A_n)}]^T \in \mathbb{R}_+^{A_n}$  and  $\lambda_{n,(i)}$  is the Lagrange multiplier associated to the  $i$ th transceiver of user  $n$ . Comparing (4.11) to (3.15), we notice that the difference is that in (4.11) there are multiple Lagrange multipliers in a diagonal matrix instead of a single Lagrange multiplier times an identity matrix.

We can write a similar algorithm to the one in Chapter 3, except that our version includes the search for the Lagrange multiplier vector  $\boldsymbol{\lambda}_n$  instead of a scalar Lagrange multiplier. So, as in Chapter 3, we first calculate  $\mathbf{R}_n^k$  with (4.3)  $\forall n, k$ , then  $\mathbf{W}_n^k$  with (4.10)  $\forall n, k$  and then  $\mathbf{T}_n^k$  with (4.11)  $\forall n, k$ . A complete algorithm description is provided in Algorithm 4.1. The calculation of  $\mathbf{T}_n^k$  for user  $n$  should be done inside a loop, wherein (4.11) is calculated for all tones and the vector  $\boldsymbol{\lambda}_n$  is adjusted. This adjustment can be done by a sub-gradient method, as shown in line 8 in Algorithm 4.1—here  $\epsilon$  is a predefined step size.

The demonstrations of convergence and of the fact that the DMT-WMMSE algorithm reaches a stationary point provided in [22, 62, 83] are also valid for the current case. The computational complexity of the DMT-WMMSE with per-transceiver PCs is  $O(KN^2 \max_n((A_n)^3 \exp(A_n)))$ . The term with  $(A_n)^3$  is due to the matrix multiplications and inversions. The term  $\exp(A_n)$  is due to the multidimensional search for an appropriate  $\boldsymbol{\lambda}_n$ .

---

**Algorithm 4.1:** DMT-WMMSE with per-transceiver PCs
 

---

```

1 Initialize  $\mathbf{T}_n^k \forall n, k$ ;
2 repeat
3   Calculate  $\mathbf{R}_n^k$  with (4.3)  $\forall n, k$ ;
4   Calculate  $\mathbf{W}_n^k$  with (4.10)  $\forall n, k$ ;
5   for  $n = 1, \dots, N$  do
6     repeat
7       Calculate  $\mathbf{T}_n^k$  with (4.11)  $\forall k$ ;
8        $\lambda_{n,(i)} = \max(\lambda_{n,(i)} + \epsilon(\sum_{k \in \mathcal{K}} \mathbf{e}_i^T \mathbf{T}_n^k (\mathbf{T}_n^k)^H \mathbf{e}_i - P_n^{\max}), 0) \forall i$ ;
9     until convergence ;
10 until convergence ;
    
```

---

## 4.4 WMMSE-GDSB with Per-Transceiver Power Constraints

For this part of the chapter, we start from (4.7). This version of the problem emphasizes more clearly its distinct signal and spectrum coordination parts. The goal in this section is to solve these two parts sequentially and iteratively.

For the signal coordination part, each tone, transceiver and user has a fixed PC and so each tone can be solved separately. Here we opt for the WMMSE algorithm of Section 4.3. We detail the implementation later in the chapter when we talk about algorithm design. For the remainder of this section, we focus on how to solve the spectrum coordination part.

We solve the spectrum coordination part in an iterative, per-user fashion. For example, for a two user case, we first fix  $\mathbf{P}_2$  and solve for  $\mathbf{P}_1$ , then we fix  $\mathbf{P}_1$  and solve for  $\mathbf{P}_2$ . The optimization problem for a given user  $n$  is given by

$$\begin{aligned}
 & \max_{\mathbf{P}_n} \sum_{j \in \mathcal{N}} \sum_{k \in \mathcal{K}} u_j b_j^k \\
 & \text{subject to} \quad \sum_{k \in \mathcal{K}} p_{n,(i)}^k \leq P_n^{\max}, \quad i \in \mathcal{A}_n
 \end{aligned} \tag{4.12}$$

Here, similarly to (4.4) and (4.5), we write

$$b_n^k = \log | (\overline{\mathbf{T}}_n^k)^H \mathbf{G}_n^k (\mathbf{H}_{n,n}^k)^H (\mathbf{M}_n^k)^{-1} \mathbf{H}_{n,n}^k \mathbf{G}_n^k \overline{\mathbf{T}}_n^k + \mathbf{I}_{A_n} |, \quad (4.13)$$

$$\mathbf{M}_n^k = \sum_{j \neq n} \mathbf{H}_{n,j}^k \mathbf{G}_j^k \overline{\mathbf{T}}_j^k (\overline{\mathbf{T}}_j^k)^H \mathbf{G}_j^k (\mathbf{H}_{n,j}^k)^H + \mathbf{I}_{A_n}.$$

Here  $\mathbf{G}_n^k \triangleq \text{diag} \left\{ \left[ \sqrt{p_{n,(1)}^k} \quad \cdots \quad \sqrt{p_{n,(A_n)}^k} \right] \right\}$ . Notice that  $\mathbf{G}_n^k = (\mathbf{G}_n^k)^H$ .

Consider the Lagrangean of (4.12),

$$L(\mathbf{P}_n, \boldsymbol{\lambda}_n) = \sum_{j \in \mathcal{N}} \sum_{k \in \mathcal{K}} u_j b_j^k - \sum_{i \in \mathcal{A}_n} \lambda_{n,(i)} \left( \sum_{k \in \mathcal{K}} p_{n,(i)}^k - P_n^{\max} \right). \quad (4.14)$$

Here,  $\lambda_{n,(i)}$  is the Lagrange multiplier associated with transceiver  $i$  of user  $n$ .

We also define  $\boldsymbol{\lambda}_n = [\lambda_{n,(1)} \quad \cdots \quad \lambda_{n,(A_n)}]^T \in \mathbb{R}_+^{A_n}$ . Notice that (4.14) can be decomposed through the tones, i.e. by defining

$$L(\mathbf{p}_n^k, \boldsymbol{\lambda}_n) = \sum_{j \in \mathcal{N}} u_j b_j^k - \sum_{i \in \mathcal{A}_n} \lambda_{n,(i)} p_{n,(i)}^k \quad (4.15)$$

and rewriting (4.14) as  $L(\mathbf{P}_n, \boldsymbol{\lambda}_n) = \sum_{k \in \mathcal{K}} L(\mathbf{p}_n^k, \boldsymbol{\lambda}_n) + \sum_{i \in \mathcal{A}_n} \lambda_{n,(i)} P_n^{\max}$ . By separately solving

$$\max_{\mathbf{p}_n^k} L(\mathbf{p}_n^k, \boldsymbol{\lambda}_n) \quad (4.16)$$

for each  $k$  we also maximize  $L(\mathbf{P}_n, \boldsymbol{\lambda}_n)$  in (4.14). In the rest of this section we will focus on how to solve (4.16) quickly and accurately for fixed Lagrange multipliers. It is not difficult to see that (4.16) is neither concave nor convex in  $\mathbf{p}_n^k$ , which makes the optimization challenging.

In the next sub-sections we describe four approaches to solve (4.16).

First, in Section 4.4.1 we try to straightforwardly adapt the algorithm described in Chapter 3 to the per-transceiver PC case. The idea here is to linearize the non-concave part of  $L(\mathbf{p}_n^k, \boldsymbol{\lambda}_n)$ , which allows for a simple solution. We come to the conclusion that such an approach ultimately fails to produce a functioning algorithm.

In Section 4.4.2 we use an exhaustive search for  $\mathbf{p}_n^k$ . We observe that, although this can provide good results, computational complexity grows exponentially with  $A_n$ , which becomes prohibitive for large  $A_n$ .

In Section 4.4.3, we propose an approach that saves a little on computational complexity. We begin by doing a change of variables: we replace the Cartesian vector of powers  $\mathbf{p}_n^k$  by a spherical coordinates equivalent. We re-write  $\mathbf{p}_n^k$  as  $\rho_n^k \mathbf{d}_n^k$ , where  $\rho_n^k$  is the radius and  $\|\mathbf{d}_n^k\|_2 = 1$  is a direction vector. The important observation is that for the radial dimension the problem can be made concave after approximations. An exhaustive search is still necessary for the other variables, but now only in  $A_n - 1$  dimensions. Hence, computational complexity grows exponentially with  $A_n - 1$ . This still becomes prohibitive for large  $A_n$ .

Finally, in Section 4.4.4 we explain the approach that forms the core of our proposal. We use yet another change of variables. We replace the original Cartesian vector with coordinates of the type  $\eta_n^k \mathbf{v}_n^k$ , with  $\|\mathbf{v}_n^k\|_1 = 1$ . This coordinate system can be interpreted as spherical coordinates in taxicab geometry [43]. With this new formulation, it is possible to more easily decouple the optimization through the variables. The strategy is to solve for each variable independently and sequentially while keeping the others fixed, i.e. a sequence of line searches. The advantage is that computational complexity grows linearly with  $A_n$ .

#### 4.4.1 The Limitations of the Traditional Approach

In Chapter 3, the GDSB algorithm is proposed to iteratively solve the spectrum coordination problem with per-user PCs. In such a case,  $\mathbf{T}_n^k$  is decomposed as  $\mathbf{T}_n^k = \sqrt{p_n^k} \overline{\mathbf{T}}_n^k$ , with  $\text{tr}\{\overline{\mathbf{T}}_n^k (\overline{\mathbf{T}}_n^k)^H\} = 1$ , and the variable is  $p_n^k$ . In Chapter 3, when solving for user  $n$  the Lagrangean is formulated (similar to (4.15)) and an approximated Lagrangean function is maximized (as in (4.16)). For the approximation, the problem is divided in concave and non-concave parts. The latter is given by  $\sum_{j \neq n} b_j^k$ . By approximating the non-concave part by its first order Taylor expansion, a concave function is found, which is then solved straightforwardly. Lagrange multipliers have to be adjusted so that the PC is respected. By solving the approximated Lagrangean iteratively, at convergence a local optimum of the problem is found.

In this section, we try to apply the same procedure to the per-transceiver PC case but conclude that it does not work. We depart from the per-tone problem in (4.15) and re-write it as

$$L(\mathbf{P}_n^k, \boldsymbol{\lambda}_n) = u_n b_n^k + \sum_{j \neq n} u_j b_j^k - \sum_{i \in \mathcal{A}_n} \lambda_{n,(i)} p_{n,(i)}^k. \quad (4.17)$$

As in Chapter 3, we notice that the first and last terms of this equation are increasing with  $\mathbf{p}_n^k$ . The term with the summation in  $j$  is decreasing with  $\mathbf{p}_n^k$ . We linearize the part with the sum in  $j$  by approximating it by its first order Taylor expansion. So, consider

$$b_j^k \approx b_j^k \Big|_{\bar{\mathbf{p}}_n^k} + (p_{n,(i)}^k - \bar{p}_{n,(i)}^k) \frac{\partial b_j^k}{\partial p_{n,(i)}^k} \Big|_{\bar{\mathbf{p}}_n^k} \quad (4.18)$$

Here  $\bar{\mathbf{p}}_n^k$  denotes the power allocation for user  $n$  on tone  $k$  on the previous iteration. To maximize (4.17) in  $p_{n,(i)}^k$ , we plug (4.18) in (4.17), take the derivative in  $p_{n,(i)}^k$  and set it to zero. The derivative of the part that is increasing with  $\mathbf{p}_n^k$  is given by

$$\frac{u_n \partial (b_n^k - \lambda_{n,(i)} p_{n,(i)}^k)}{\partial p_{n,(i)}^k} = -\lambda_{n,(i)} + u_n \text{tr} \{ \mathbf{E}_n^k (\bar{\mathbf{T}}_n^k)^H \text{diag} \left\{ [\cdots \ 0 \ 1/\sqrt{p_{n,(i)}^k} \ 0 \ \cdots] \right\} (\mathbf{H}_{n,n}^k)^H (\mathbf{M}_n^k)^{-1} \mathbf{H}_{n,n}^k \mathbf{G}_n^k \bar{\mathbf{T}}_n^k \},$$

where  $\mathbf{E}_n^k$  is given by (4.8).

$$\sum_{j \neq n} \frac{\partial u_j b_j^k}{\partial p_{n,(i)}^k} = \sum_{j \neq n} -u_j \text{tr} \left\{ (\bar{\mathbf{T}}_n^k)^H \mathbf{G}_n^k (\mathbf{H}_{j,n}^k)^H (\mathbf{M}_n^k)^{-1} \mathbf{H}_{j,j}^k \mathbf{T}_j^k \mathbf{E}_j^k \right. \\ \left. (\bar{\mathbf{T}}_j^k)^H (\mathbf{H}_{j,j}^k)^H (\mathbf{M}_n^k)^{-1} \mathbf{H}_{j,n}^k \times \text{diag} \left\{ [\cdots \ 0 \ 1/\sqrt{p_{n,(i)}^k} \ 0 \ \cdots] \right\} \bar{\mathbf{T}}_n^k \right\}. \quad (4.19)$$

The problem with this approach is that for the per-transceiver PC case the first order Taylor expansion of  $b_j^k$  (see (4.18) and (4.19)) is a very poor characterization of its behavior. This is so because  $b_j^k$  is not a convex, monotonically decreasing function of  $\mathbf{p}_n^k$ ,  $\mathbf{p}_n^k \geq 0$ . See Fig. 4.1 for an illustration. In the figure, we calculate  $b_j^k$  with (4.13) for different values of power for an interfering user  $n$  that has two transceivers, i.e we calculate  $b_j^k$  as a function of  $p_{n,(1)}^k$  and  $p_{n,(2)}^k$ . All matrices involved are randomly chosen and of size two by two. In this figure, the thick line marks the behavior of  $b_j^k$  as we fix  $p_{n,(1)}^k = 1.5$ . This curve is shown more clearly in Fig. 4.2 along with its first order Taylor expansion around  $p_{n,(2)}^k = 0.25$ .

The Taylor expansion influences the power allocation for the transceiver  $i$  of user  $n$  by including a price for interference it causes [96, 109]. For the particular point shown in the figure, the Taylor expansion actually represents an incentive. User  $n$  has an incentive to increase  $p_{n,(2)}^k$ , as if  $b_j^k$  would increase indefinitely with more interference. Accordingly, note that in (4.19) the argument of the trace is a matrix with no special properties—it is not necessarily hermitian or positive definite. The result of the trace operation can be a positive or a negative or even a complex number.

If the algorithm finds itself in such a point, i.e. when for a particular tone the prices for loading power become incentives, a very large amount of power is used in this tone. Because of the common PC, all other tones have to decrease power greatly, even if they have favorable channel conditions. Data rate for user  $n$  most likely drops. The algorithm does not work.

This is in contrast with the case of the algorithms proposed in [96, 109] and in Chapter 3 that deal with the per-user PC. In these references,  $b_j^k$  is a convex and monotonically decreasing function of  $p_n^k$ , which means that  $\partial u_j b_j^k / \partial p_n^k$  is always real and non-positive, i.e. a true price rather than an incentive. Similar convex approximations proposed to the per-user PC case, e.g. [73] also do not work for the per-transceiver PC case for the same reason.

#### 4.4.2 Exhaustive Search in $\mathbf{p}_n^k$

One straightforward way of solving (4.16) is with an exhaustive grid search in  $\mathbf{p}_n^k$ . This is actually the most direct way to solve (4.16). The problem is that the grid increases exponentially with the number of transceivers  $A_n$ , as does the number of functions evaluations.

For a small number of transceivers, e.g.  $A_n$  equals 2 or 3, it is actually possible to perform the exhaustive search. However, such a search is embedded in an algorithm that also adjusts transmit matrices. Each time the transmit matrices are updated, the power allocation needs to be updated as well and the algorithm continues sequentially. This means that, if we choose the exhaustive search to solve the spectrum coordination part, we would have to repeat it tens, maybe hundreds of times. This makes this option not effective at all.

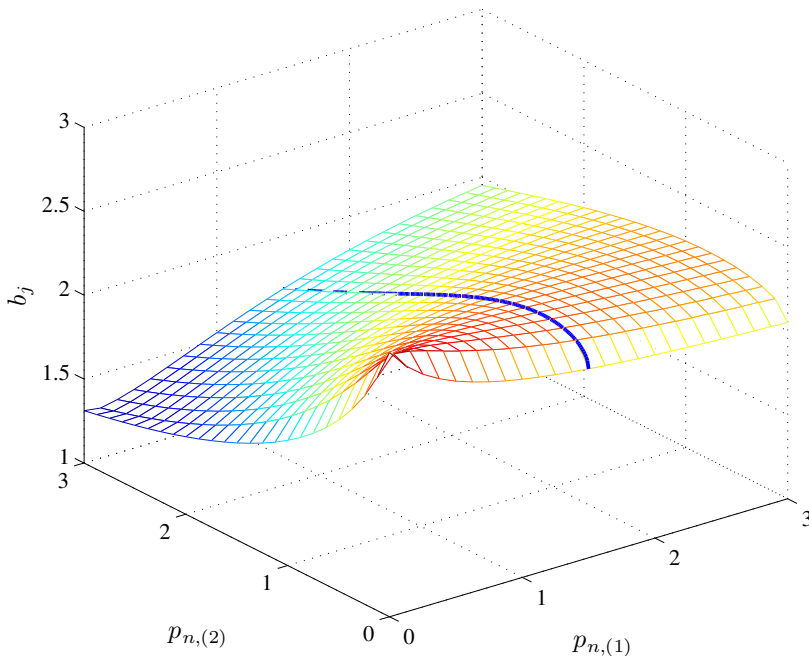


Figure 4.1: Illustration of  $b_j$  as a function of interfering powers  $p_{n,(1)}$  and  $p_{n,(2)}$  (we suppress the superscript  $k$  for simplicity). All matrices involved, including direct channel, crosstalk channel and transmit matrices, are randomly chosen. The thick line illustrates the behavior of the function for fixed  $p_{n,(1)}$ .

#### 4.4.3 Changing $\mathbf{p}_n^k$ to Spherical Coordinates—Exhaustive Search for the Direction Vector

We can save on computational complexity by changing our search slightly. Consider  $\mathbf{p}_n^k$  in spherical coordinates.

$$\mathbf{p}_n^k = \rho_n^k \mathbf{d}_n^k, \quad \rho_n^k \geq 0, \quad \|\mathbf{d}_n^k\|_2 = 1 \quad (4.20)$$

Here  $\rho_n^k$  is the radius, i.e.  $\rho_n^k = \|\mathbf{p}_n^k\|_2$ , and  $\mathbf{d}_n^k = [d_{n,[1]}^k \ \cdots \ d_{n,[A_n]}^k]^\top \in \mathbb{R}_+^{A_n}$ , i.e.  $d_{n,[i]}^k \geq 0$ ,  $i \in \mathcal{A}_n$ , is a direction. Here we make two remarks. First notice that while in the Cartesian vector  $\mathbf{p}_n^k$  each element is associated with a transceiver (e.g.  $p_{n,(1)}^k$  for transceiver 1), this is not true for the spherical

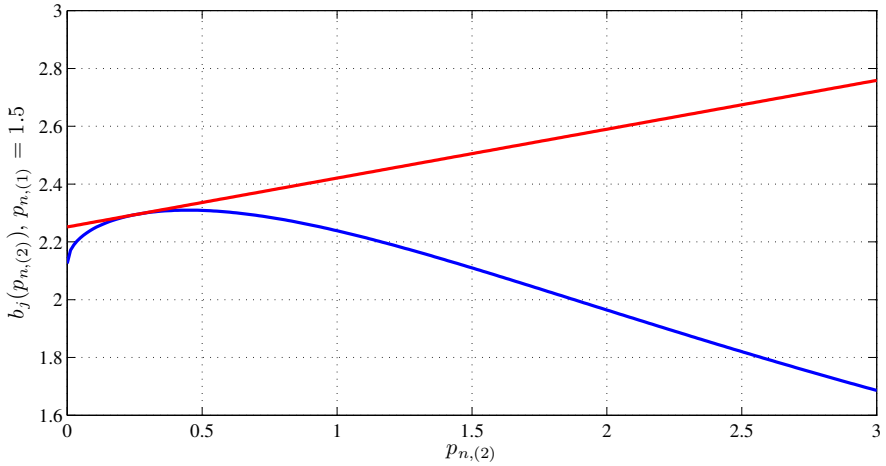


Figure 4.2: Detail of  $b_j$  as a function of  $p_{n,(2)}$  for fixed  $p_{n,(1)} = 1.5$  (we suppress the superscripts  $k$  for simplicity). A first order Taylor expansion around point  $p_{n,(2)} = 0.25$  shows that such approximation is a poor characterization of the behavior of the original function.

coordinates vector. If, for example, we change the value of  $\rho_n^k$ , all transceivers' powers change. This is why  $\rho_n^k$  has only one subscript and why we add brackets to the subscripts in  $d_{n,[i]}^k$ . In  $d_{n,[i]}^k$ , the bracketed subscripts now represent directions, not transceivers. Second, notice that, although the vector  $\mathbf{d}_n^k$  is of size  $A_n$ , it contains only  $A_n - 1$  free variables that we denote as the angles  $\theta_{n,[1]}^k, \dots, \theta_{n,[A_n-1]}^k$ . For example, for a case with three transceivers, we have

$$\mathbf{p}_n^k = \rho_n^k \begin{bmatrix} \cos \theta_{n,[1]}^k & \cos \theta_{n,[2]}^k \\ \cos \theta_{n,[1]}^k & \sin \theta_{n,[2]}^k \\ \sin \theta_{n,[1]}^k & \end{bmatrix}, \quad \rho_n^k \geq 0, \quad \theta_{n,[1]}^k, \theta_{n,[2]}^k \in [0, \frac{\pi}{2}].$$

In Appendix C.1, we write the spherical coordinates vector for the general  $A_n$  transceiver case. See Eqs. (C.1), (C.2) and (C.3). In this section, we use the vector  $\boldsymbol{\theta}_n^k = [\theta_{n,[1]}^k \ \dots \ \theta_{n,[A_n-1]}^k]^T \in \mathbb{R}_+^{A_n-1}$  to represent the angles for user  $n$  and tone  $k$ . Notice that  $\boldsymbol{\theta}_n^k$  and  $\mathbf{d}_n^k$  are related in a simple way.

We now define  $\mathbf{D}_n^k \triangleq \text{diag} \left\{ \left[ \sqrt{d_{n,[1]}^k} \ \dots \ \sqrt{d_{n,[A_n]}^k} \right] \right\} \in \mathbb{R}_+^{A_n \times A_n}$ . Notice that  $\mathbf{D}_n^k = (\mathbf{D}_n^k)^H$ . Next we decompose  $\mathbf{T}_n^k$  as  $\mathbf{T}_n^k = \sqrt{\rho_n^k} \mathbf{D}_n^k \overline{\mathbf{T}}_n^k$ . Here again

$\mathbf{e}_i^T \bar{\mathbf{T}}_n^k (\bar{\mathbf{T}}_n^k)^H \mathbf{e}_i = 1 \forall i$ . We re-write (4.5) and (4.4) as

$$b_n^k = \log \left| \rho_n^k (\bar{\mathbf{T}}_n^k)^H \mathbf{D}_n^k (\mathbf{H}_{n,n}^k)^H (\mathbf{M}_n^k)^{-1} \mathbf{H}_{n,n}^k \mathbf{D}_n^k \bar{\mathbf{T}}_n^k + \mathbf{I}_{A_n} \right| \quad (4.21)$$

$$\mathbf{M}_n^k = \sum_{j \neq n} \rho_j^k \mathbf{H}_{n,j}^k \mathbf{D}_j^k \bar{\mathbf{T}}_j^k (\bar{\mathbf{T}}_j^k)^H \mathbf{D}_j^k (\mathbf{H}_{n,j}^k)^H + \mathbf{I}_{A_n} \quad (4.22)$$

Now we write the equivalent of (4.15) as

$$L(\rho_n^k, \boldsymbol{\theta}_n^k, \boldsymbol{\lambda}_n) = u_n b_n^k + \sum_{j \neq n} u_j b_j^k - \sum_{i \in \mathcal{A}_n} \lambda_{n,(i)} \rho_n^k d_{n,[i]}^k. \quad (4.23)$$

The maximization of (4.23) in  $\rho_n^k$  and  $\boldsymbol{\theta}_n^k$  has one fundamental advantage: when maximizing for  $\rho_n^k$  while keeping  $\boldsymbol{\theta}_n^k$  fixed, the first order Taylor expansion of the non-concave part of (4.23) (i.e.  $\sum_{j \neq n} u_j b_j^k$ ) provides a good enough approximation of the behavior of the  $b_j^k$ 's. That is because, for each fixed direction  $\boldsymbol{\theta}_n^k$ ,  $b_j^k$  is a convex, monotonically decreasing function of  $\rho_n^k$ ,  $\rho_n^k \geq 0$ . Additionally,  $b_n^k$  is a concave function of  $\rho_n^k$  ([7], pg. 74). After the approximations, the stationary condition of (4.23) in  $\rho_n^k$  for fixed  $\boldsymbol{\theta}_n^k$  is given by

$$\frac{\partial L(\rho_n^k, \boldsymbol{\theta}_n^k, \boldsymbol{\lambda}_n)}{\partial \rho_n^k} = u_n \text{tr} \left\{ (\rho_n^k \mathbf{S}_n^k(\mathbf{D}_n^k) + \mathbf{I}_{A_n})^{-1} \mathbf{S}_n^k(\mathbf{D}_n^k) \right\} - \tau_n^k(\mathbf{D}_n^k) - \boldsymbol{\lambda}_n^T \mathbf{d}_n^k = 0. \quad (4.24)$$

Here

$$\mathbf{S}_n^k(\mathbf{D}_n^k) = (\bar{\mathbf{T}}_n^k)^H \mathbf{D}_n^k (\mathbf{H}_{n,n}^k)^H (\mathbf{M}_n^k)^{-1} \mathbf{H}_{n,n}^k \mathbf{D}_n^k \bar{\mathbf{T}}_n^k. \quad (4.25)$$

The variable  $\tau_n^k(\mathbf{D}_n^k)$  is obtained after the linearization with the Taylor expansion and is given by

$$\tau_n^k(\mathbf{D}_n^k) \triangleq - \sum_{j \neq n} u_j \frac{\partial b_j^k}{\partial \rho_n^k} = \sum_{j \neq n} u_j \text{tr} \left\{ (\bar{\mathbf{T}}_n^k)^H \mathbf{D}_n^k (\mathbf{H}_{j,n}^k)^H (\mathbf{M}_j^k)^{-1} \mathbf{H}_{j,j}^k \mathbf{T}_j^k \mathbf{E}_j^k (\mathbf{T}_j^k)^H (\mathbf{H}_{j,j}^k)^H (\mathbf{M}_j^k)^{-1} \mathbf{H}_{j,n}^k \mathbf{D}_n^k \bar{\mathbf{T}}_n^k \right\}. \quad (4.26)$$

Here  $\mathbf{E}_n^k$  is given by (4.8). Note that, in contrast to (4.19), the argument of the trace operator is now a hermitian positive semidefinite matrix. Its trace will always be non-negative and, as a consequence,  $-\tau_n^k(\mathbf{d}_n^k)$  acts as a price for the radius of user  $n$ . For each fixed  $\boldsymbol{\theta}_n^k$ , we obtain an easy, concave problem after the linearization of the non-concave parts.

Eq. (4.24) can be solved by finding the roots of a polynomial of degree  $A_n$ . It can be shown that there is at most one non-negative root (see Chapter 3), which implies that the only root of interest is the rightmost one. The problem in  $\rho_n^k$  is in essence the problem with the per-user PCs in Chapter 3.

If solving for  $\rho_n^k$  is easy, the same cannot be said for the angles  $\boldsymbol{\theta}_n^k$ . The  $\theta_{n,[i]}^k$ 's are coupled among themselves and with  $\rho_n^k$ . The way to solve the full problem is to do an exhaustive search in the angle vector  $\boldsymbol{\theta}_n^k$ . The advantage is that, since there are  $A_n - 1$  angles, the exhaustive search is done in a grid with one dimension less in comparison to the Cartesian exhaustive search of Section 4.4.2. For each fixed  $\boldsymbol{\theta}_n^k$ , solving for  $\rho_n^k$  is easy. We can then develop an algorithm where all possible directions are searched for exhaustively, for example by sampling  $[0, \pi/2]$  with  $Q$  points and building a  $(A_n - 1)$ -dimensional grid with such points. For a given point in the grid, we have values for  $\theta_{n,[i]}^k$ ,  $i = 1, \dots, A_n - 1$  (and  $\mathbf{d}_n^k$ ) and solve for  $\rho_n^k$ . Lagrange multipliers have to be searched for in an outer loop so that the PCs are respected. We have tested such algorithm and it works well. However, it only works for small  $A_n$ . The grid search grows exponentially with  $A_n - 1$ , which quickly becomes unfeasible. The fact of the matter is that such an algorithm is still very limited. The shortcomings of the Cartesian vector exhaustive search described in Section 4.4.2 are but slightly mitigated.

#### 4.4.4 Changing $\mathbf{p}_n^k$ to Spherical Coordinates in Taxicab Geometry—Iterative Search for the Direction Vector

Consider that the vector  $\mathbf{p}_n^k$  is re-written as

$$\mathbf{p}_n^k = \eta_n^k \mathbf{v}_n^k, \quad \eta_n^k \geq 0, \quad \|\mathbf{v}_n^k\|_1 = 1 \quad (4.27)$$

where, just as before,  $\mathbf{v}_n^k = [v_{n,[1]}^k \ \cdots \ v_{n,[A_n]}^k]^\top \in \mathbb{R}_+^{A_n}$ , i.e.  $v_{n,[i]}^k \geq 0, i \in \mathcal{A}_n$ , points to a direction and  $\eta_n^k$  is the radius. Because of the  $\ell_1$  norm constraint in  $\mathbf{v}_n^k$ ,  $\eta_n^k \mathbf{v}_n^k$  describes a sphere of radius  $\eta_n^k$  in taxicab geometry [43], which we already used in Chapter 2. Hence we refer to this system of coordinates as spherical coordinates in taxicab geometry. As is the case in Section 4.4.3, the vector  $\mathbf{v}_n^k$  is of size  $A_n$  but contains only  $A_n - 1$  free variables that we denote as

the angles  $\phi_{n,[1]}^k, \dots, \phi_{n,[A_n-1]}^k$ . For example, for a case with three transceivers, we write (4.27) as

$$\mathbf{p}_n^k = \eta_n^k \mathbf{v}_n^k = \eta_n^k \begin{bmatrix} (1 - \phi_{n,[1]}^k)(1 - \phi_{n,[2]}^k) \\ (1 - \phi_{n,[1]}^k)\phi_{n,[2]}^k \\ \phi_{n,[1]}^k \end{bmatrix}, \eta_n^k \geq 0, \phi_{n,[1]}^k, \phi_{n,[2]}^k \in [0, 1] \quad (4.28)$$

In Appendix C.1, we write the taxicab spherical coordinates vector for the general  $A_n$  transceiver case. See Eqs. (C.4), (C.5) and (C.6). In this section, we use the vector  $\boldsymbol{\phi}_n^k = [\phi_{n,[1]}^k \ \dots \ \phi_{n,[A_n-1]}^k]^\top \in \mathbb{R}_+^{A_n-1}$  to represent the angles for user  $n$  and tone  $k$ . Notice that  $\boldsymbol{\phi}_n^k$  and  $\mathbf{v}_n^k$  are related in a simple way.

In Section 4.4.3, we remarked that the spherical coordinates (in Euclidean geometry) representation of  $\mathbf{p}_n^k$  is a bit unusual in the sense that the variables are not directly related to users' powers. This still applies to the spherical coordinates in taxicab geometry. However, for the latter it is easier to control the share of power that is allocated to each transceiver and to thus optimize the variables separately. Because of the fixed  $\ell_1$  norm, the per-user power does not depend on the angles, i.e.

$$\sum_{k \in \mathcal{K}} \sum_{i \in \mathcal{A}_n} \eta_n^k v_{n,[i]}^k = \sum_{k \in \mathcal{K}} \eta_n^k \|\mathbf{v}_n^k\|_1 = \sum_{k \in \mathcal{K}} \eta_n^k.$$

This is clearly not true for the (Euclidean) spherical coordinates (see Section 4.4.3). The Euclidean spherical coordinates have some non-linearity to them: by changing one of the angles, the sum power changes. What we do next is to solve for the radius  $\eta_n^k$  with a per-user PC and then solve for each  $\phi_{n,[i]}^k$  separately with line searches. By adjusting prices for the angles in the form of Lagrange multipliers, we can satisfy all per-transceiver PCs.

First we define some variables. Define  $\mathbf{V}_n^k \triangleq \text{diag} \left\{ \left[ \sqrt{v_{n,[1]}^k} \ \dots \ \sqrt{v_{n,[A_n]}^k} \right] \right\} \in \mathbb{R}_+^{A_n \times A_n}$ . Next we decompose  $\mathbf{T}_n^k$  as  $\mathbf{T}_n^k = \sqrt{\eta_n^k} \mathbf{V}_n^k \bar{\mathbf{T}}_n^k$ . Here again  $\mathbf{e}_i^\top \bar{\mathbf{T}}_n^k (\bar{\mathbf{T}}_n^k)^\text{H} \mathbf{e}_i = 1 \ \forall i$ . We then define very similar equations to (4.21) and (4.22), with the difference that we substitute  $\rho_n^k$  by  $\eta_n^k$  and  $\mathbf{D}_n^k$  by  $\mathbf{V}_n^k$ .

The next step is writing the per-tone Lagrangean as a function of  $\eta_n^k$  and  $\boldsymbol{\phi}_n^k$ . Before that, we add a constraint to the problem. Besides the  $A_n$  per-transceiver PCs of the form  $\sum_{k \in \mathcal{K}} p_{n,(i)}^k \leq P_n^{\max}$ ,  $i = 1, \dots, A_n$  we add a constraint on the sum power as follows

$$\sum_{k \in \mathcal{K}} \eta_n^k \leq A_n P_n^{\max} \quad (4.29)$$

With (4.29) and the per-transceiver constraints in hands, we re-write the equivalent of (4.15) as

$$L(\eta_n^k, \phi_n^k, \bar{\lambda}_n, \boldsymbol{\lambda}_n) = \sum_{n \in \mathcal{N}} u_n b_n^k - \bar{\lambda}_n \eta_n^k - \sum_{i \in \mathcal{A}_n} \lambda_{n,(i)} \eta_n^k v_{n,[i]}^k. \quad (4.30)$$

Here we define  $\bar{\lambda}_n \in \mathbb{R}_+$  and  $\boldsymbol{\lambda}_n = [\lambda_{n,(1)} \ \cdots \ \lambda_{n,(A_n)}]^\top \in \mathbb{R}_+^{A_n}$ .

Our strategy is to maximize (4.30) for each of the variables of the problem separately. First we solve for the radius and then for each of the angles.

To solve for the radius  $\eta_n^k$  for fixed  $\phi_n^k$ ,  $\bar{\lambda}_n$  and  $\boldsymbol{\lambda}_n$ , we write

$$\max_{\eta_n^k} L(\eta_n^k, \phi_n^k, \bar{\lambda}_n, \boldsymbol{\lambda}_n),$$

Here, after approximating its convex part (the  $b_j^k$ 's) by the first order Taylor expansion, the stationary condition of this problem is given by

$$\begin{aligned} \frac{\partial L(\eta_n^k, \phi_n^k, \bar{\lambda}_n, \boldsymbol{\lambda}_n)}{\partial \eta_n^k} &= u_n \text{tr} \left\{ (\eta_n^k \mathbf{S}_n^k(\mathbf{V}_n^k) + \mathbf{I}_{A_n})^{-1} \mathbf{S}_n^k(\mathbf{V}_n^k) \right\} - \tau_n^k(\mathbf{V}_n^k) - \bar{\lambda}_n \\ &\quad - \sum_{i \in \mathcal{A}_n} \lambda_{n,(i)} v_{n,[i]}^k = 0, \end{aligned} \quad (4.31)$$

where  $\mathbf{S}_n^k(\mathbf{V}_n^k)$  is given by (4.25) and  $\tau_n^k(\mathbf{V}_n^k)$  is given by (4.26). This problem is the same as that already solved in Chapter 3 and in Section 4.4.3.

Next, we solve for  $\phi_{n,[i]}^k$  sequentially. To solve for the angle  $\phi_{n,[i]}^k$  for fixed  $\eta_n^k$ ,  $\phi_{n,[l]}^k$ ,  $l \neq i$ ,  $\bar{\lambda}_n$  and  $\boldsymbol{\lambda}_n$ , we write

$$\max_{\phi_{n,[i]}^k} L(\eta_n^k, \phi_n^k, \bar{\lambda}_n, \boldsymbol{\lambda}_n), \quad (4.32)$$

It is not easy to solve (4.32), even if we do some approximations. We solve (4.32) with an exhaustive search. Our strategy starts by sampling the  $[0, 1]$  axis uniformly with  $Q$  points. Denote the set of these points as  $\mathcal{Q} = \{\phi^{\{q\}} | q = 1, \dots, Q\}$ . We then calculate  $L(\eta_n^k, \phi_n^k, \bar{\lambda}_n, \boldsymbol{\lambda}_n)$  for each  $\phi^{\{q\}} \in \mathcal{Q}$  by substituting  $\phi_{n,[i]}^k$  by  $\phi^{\{q\}}$ . Finally, we pick the  $\phi^{\{q\}}$  that maximizes  $L(\eta_n^k, \phi_n^k, \bar{\lambda}_n, \boldsymbol{\lambda}_n)$ . Note here that  $\mathcal{Q}$  does not grow exponentially with the number of transceivers.

**Algorithm 4.2:** WMMSE-GDSB with per-transceiver PCs

---

```

1 Initialize  $\mathbf{T}_n^k$ ,  $\boldsymbol{\lambda}_n$  and  $\bar{\lambda}_n \forall n, k$ ;
2  $\mathcal{Q} \leftarrow$  discretized  $\phi$ -space with  $\phi \in [0, 1]$ ;
3 repeat
4   Calculate  $\tau_n^k(\mathbf{V}_n^k)$  with (4.26) and  $\mathbf{S}_n^k(\mathbf{V}_n^k)$ ,  $n \in \mathcal{N}$ ,  $k \in \mathcal{K}$ ;
5   for  $n = 1, \dots, N$  do
6     repeat
7       Find  $\eta_n^k$  with (4.31),  $k \in \mathcal{K}$ ;
8       Adjust  $\bar{\lambda}_n$  (with bisection);
9     until convergence;
10    for  $i = 1, \dots, A_n - 1$  do
11       $\mathcal{K}_* = \{k | k \in \mathcal{K}, \eta_n^k > 0 \text{ and } \phi_{n,[l]}^k \neq 1, l < i\}$ ;
12      Calculate  $L(\eta_n^k, \phi_n^k, \bar{\lambda}_n, \boldsymbol{\lambda}_n)$  with  $\phi_{n,[i]}^k = \phi^{\{q\}}$ ,  $k \in \mathcal{K}_*$ ,  $q \in \mathcal{Q}$ ;
13       $\phi_{n,[i]}^k = \operatorname{argmax}_{\phi^{\{q\}} \in \mathcal{Q}} L(\eta_n^k, \phi_n^k, \bar{\lambda}_n, \boldsymbol{\lambda}_n)$ ,  $k \in \mathcal{K}_*$ ;
14     $\mathbf{p}_n^k = \eta_n^k \mathbf{v}_n^k$ ,  $n \in \mathcal{N}$ ,  $k \in \mathcal{K}$ ;
15    Calculate  $\mathbf{R}_n^k$  with (4.3),  $n \in \mathcal{N}$ ,  $k \in \mathcal{K}$ ;
16    Calculate  $\mathbf{W}_n^k$  with (4.10),  $n \in \mathcal{N}$ ,  $k \in \mathcal{K}$ ;
17    for  $n = 1, \dots, N$  do
18      for  $k = 1, \dots, K$  do
19        repeat
20          Calculate  $\mathbf{T}_n^k$  with (4.11);
21           $\mu_{n,(i)}^k = \mu_{n,(i)}^k + \epsilon (\mathbf{e}_i^T \mathbf{T}_n^k (\mathbf{T}_n^k)^H \mathbf{e}_i - p_{n,(i)}^k) \forall i$ ;
22        until convergence;
23       $\lambda_{n,(i)} = \max(\lambda_{n,(i)} + \epsilon (\sum_{k \in \mathcal{K}} p_{n,(i)}^k - P_n^{\max}), 0) \forall n, i$ ;
24 until convergence;

```

---

**Algorithm**

We are now ready to write an algorithm. The pseudo-code of the proposed method is shown in Algorithm 4.2. In line 2, we sample the  $\phi$ -space,  $\phi \in [0, 1]$ . The set of points is represented as  $\mathcal{Q}$ . We refer to an element of  $\mathcal{Q}$  as  $\phi^{\{q\}}$ .

Lines 4 to 13 contain the steps for the optimization of the radius and angles. In Lines 6 to 9 we solve for the radius  $\eta_n^k$ —the Lagrange multiplier  $\bar{\lambda}_n$  is found with a bisection search. After, the solution for all tones, we obtain  $\boldsymbol{\eta}_n = [\eta_n^k \dots \eta_n^K]^T \in \mathbb{R}_+^K$ , with  $\sum_{k \in \mathcal{K}} \eta_n^k \leq A_n P_n^{\max}$ .

In lines 11-13 we solve for the  $\phi_{n,[i]} = [\phi_{n,(i)}^k \dots \phi_{n,(i)}^K]^T \in \mathbb{R}_+^K$ , one at

a time and for fixed  $\boldsymbol{\eta}_n$ ,  $\boldsymbol{\lambda}_n$  and  $\boldsymbol{\phi}_{n,[l]}$ ,  $l \neq i$ . One interesting point is that, for some tones, the maximization for  $\phi_{n,[i]}^k$  can be skipped. That is so because, after the solution for the radius, each tone has a sum power constraint to be divided among the transceivers. The share that each transceiver gets is determined by solving for the angles. We can save on computational complexity by exploiting this fact. This is best conveyed by two examples.

First, it can be that  $\eta_n^k = 0$ . In this case, there is no power to be distributed among the users. Tones where  $\eta_n^k = 0$  can be skipped for all angles.

Second, consider  $\eta_n^k > 0$ . For the  $N = 3$  example, consider that we have solved for  $\boldsymbol{\eta}_n$  and  $\boldsymbol{\phi}_{n,[1]}$ . When solving for  $\boldsymbol{\phi}_{n,[2]}$ , tones where  $\phi_{n,[1]}^k = 1$  can be skipped. For these tones, the sum power is already exhausted in the  $\phi_{n,[1]}^k$  direction (see (4.28)).

Hence, when solving for a given  $\boldsymbol{\phi}_{n,[i]}$  the set of tones that need to be solved for is given by

$$\mathcal{K}_* = \{k | k \in \mathcal{K}, \eta_n^k > 0 \text{ and } \phi_{n,[l]}^k \neq 1, l < i\},$$

which we call the set of active tones. This is calculated in line 11 of the algorithm.

For the maximization in  $\phi_{n,[i]}^k$ , we calculate (4.30) for all tones in this set and all values of  $\phi^{\{q\}} \in \mathcal{Q}$ . Here, the per-tone data rates are calculated as a function of  $\eta_n^k$  (calculated in the previous step) and  $\phi_{n,[i]}^k = \phi^{\{q\}}$ . Accordingly, we calculate (4.30) with (we remind that  $\mathbf{V}_n^k = \text{diag} \left\{ \left[ \sqrt{v_{n,[1]}^k} \cdots \sqrt{v_{n,[A_n]}^k} \right] \right\}$ )

$$b_n^k = \log \left| \eta_n^k (\overline{\mathbf{T}}_n^k)^H \mathbf{V}_n^k (\mathbf{H}_{n,n}^k)^H (\mathbf{M}_n^k)^{-1} \mathbf{H}_{n,n}^k \mathbf{V}_n^k \overline{\mathbf{T}}_n^k + \mathbf{I}_{A_n} \right|,$$

where  $\mathbf{M}_n^k$  is given by (4.4), and, for  $j \neq n$ ,

$$b_j^k = \log \left| (\mathbf{T}_j^k)^H (\mathbf{H}_{j,j}^k)^H (\mathbf{M}_j^k)^{-1} \mathbf{H}_{j,j}^k \mathbf{T}_j^k + \mathbf{I}_{A_j} \right|$$

$$\mathbf{M}_j^k = \sum_{\substack{m \neq j \\ m \neq n}} \mathbf{H}_{j,m}^k \mathbf{T}_m^k (\mathbf{T}_m^k)^H (\mathbf{H}_{j,m}^k)^H + \eta_m^k \mathbf{H}_{j,n}^k \mathbf{V}_n^k \overline{\mathbf{T}}_n^k (\overline{\mathbf{T}}_n^k)^H \mathbf{V}_n^k (\mathbf{H}_{j,n}^k)^H + \mathbf{I}_{A_j}.$$

After power allocation, in line 14 we transform back to Cartesian coordinates and we continue with the signal coordination in lines 15-22. As in Chapter 3, we first calculate  $\mathbf{R}_n^k$  and then  $\mathbf{W}_n^k$  for all users and tones. In the loop on

lines 19-22 we calculate  $\mathbf{T}_n^k$  and search for adequate Lagrange multipliers (here denoted by  $\boldsymbol{\mu}_n^k = [\mu_{n,(i)}^k \ \dots \ \mu_{n,(A_n)}^k] \in \mathbb{R}^{A_n}$ ).

At the end of the first iteration, the PCs are most likely not satisfied. If at least one transceiver violates its PC, we have to adjust its Lagrange multiplier. This is done in lines 23. Here  $\epsilon$  is a predefined step size.

We repeat the whole process until convergence.

### Computational Complexity

The computational complexity of the WWMSE-GDSB with per-transceiver PCs is estimated as follows. For the solution for  $\boldsymbol{\eta}_n$  for one user  $n$ , the algorithm calculates  $\tau_n^k(\mathbf{E}_n^k)$ , which implies a complexity of the order of  $KN(A_n)^3$ . For the solution for one of the  $\phi_{n,[i]}$ , say  $i = 1$ , for user  $n$ , the complexity is proportional to  $KNQ(A_n)^3$  (the term  $(A_n)^3$  is due to the matrix multiplications and inversions). This should be repeated for all  $i$ , which implies a complexity proportional to  $KNQ(A_n)^3(A_n - 1)$ . The whole process should repeat for all users, so the computational complexity of the spectrum coordination part of Algorithm 4.1 (i.e. lines 4-13) is  $O(KN^2 \max((A_n)^3) + KN^2Q \max_n((A_n)^3(A_n - 1)))$ .

Computational complexity of the signal coordination part is estimated as  $O(KN^2 \max((A_n)^3 \exp(A_n)))$ .

### 4.4.5 Convergence

It is very difficult to show convergence of the whole procedure, but some partial results provide some guarantee. For example, with the same line of thinking as in Proposition 3.2, we can show that the update for the radius  $\eta_n^k$  converges to a unique fixed point if we consider  $\phi_{n,[i]}^k$  and  $\overline{\mathbf{T}}_n^k$  fixed for  $i \in \mathcal{A}_n$ ,  $n \in \mathcal{N}$ ,  $k \in \mathcal{K}$ ,  $A_n = 2 \forall n$ , a high SNR approximation and if

$$(N - 1) \max_{\substack{j,n,k \\ j \neq k}} \left( \frac{\text{tr}\{\text{adj}\{\overline{\mathbf{H}}_{j,n}^k\} \overline{\mathbf{H}}_{n,n}^k\}}{2|\overline{\mathbf{H}}_{n,n}^k|} \right) \leq 1.$$

Here  $\overline{\mathbf{H}}_{n,j}^k = \mathbf{H}_{n,j}^k \mathbf{E}_j^k \overline{\mathbf{T}}_j^k (\overline{\mathbf{T}}_j^k)^H \mathbf{E}_j^k (\mathbf{H}_{n,j}^k)^H$  and  $\text{adj}\{\cdot\}$  represents the matrix adjugate operator..

The following proposition treats the convergence of the  $\phi_{n,[i]}^k$ 's.

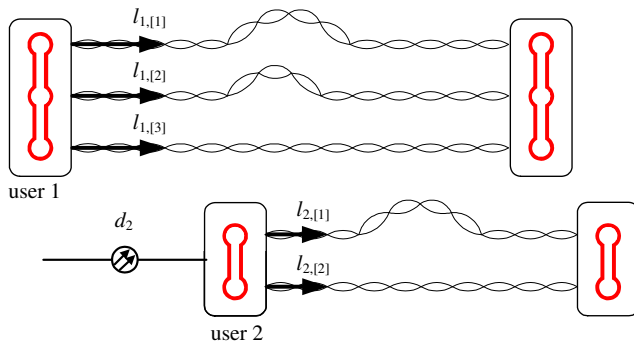


Figure 4.3: Near-far downstream ADSL scenario.

**Proposition 4.1.** *Consider a two user case where  $\eta_n^k$ ,  $\overline{\mathbf{T}}_n^k$  are fixed  $\forall k$  and  $A_n = 2 \forall n$ . The update for the angles  $\phi_1$  and  $\phi_2$  converges to a critical point in a finite number of steps.*

We leave the proof of this proposition to Appendix C.2.

The signal coordination part is guaranteed to converge if  $\mathbf{P}$  is fixed. See, e.g. [22, 83].

To summarize our results about convergence: For a two user case where each user has two transceivers, consider the three variables of the problem as  $\overline{\mathbf{T}}_n^k$ ,  $\eta_n^k$  and  $\phi_n^k$ . We have partial convergence results showing the convergence of each one when the other two are held fixed. For the general case, we always observe that the whole procedure converges—some results are shown in the next section. We performed hundreds of experiments, and this was always the case.

## 4.5 Simulation Results

In this section, we present some results for the two proposed algorithms. Two scenarios are considered: an ADSL downstream scenario and a VDSL upstream scenario. For all simulations, the values for the inter-channel spacing  $\Delta_f$  and the symbol rate  $f_s$  are set to 4.3125 kHz and 4 kHz, respectively.

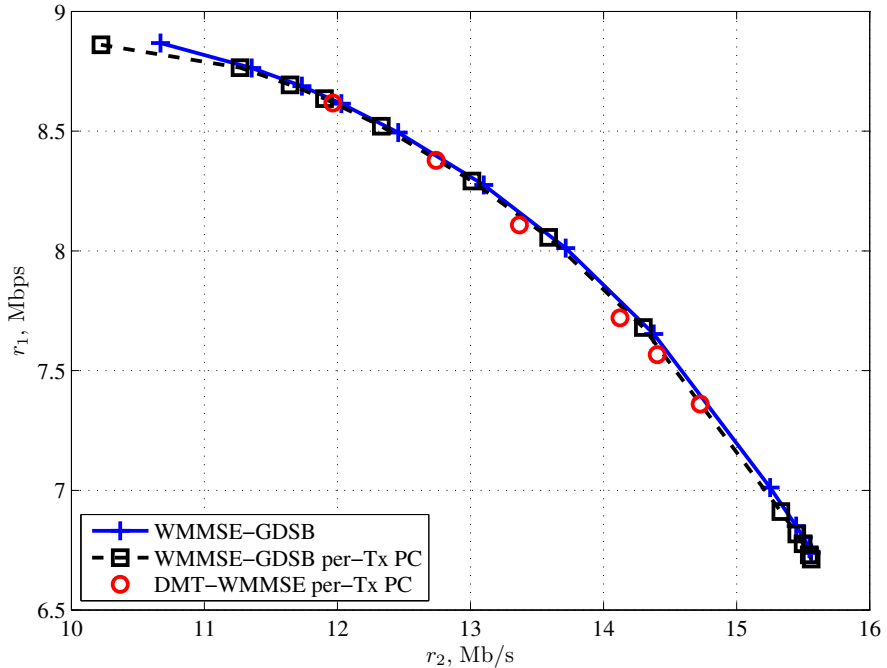


Figure 4.4: Rate region for the near-far ADSL scenario. We set  $\mathbf{l}_1 = [4.8 \ 4.5 \ 4.2]$  km,  $\mathbf{l}_2 = [3.3 \ 3]$  km and  $d_2 = 3$  km

### 4.5.1 Downstream ADSL

We simulate a system with cables of 0.5 mm (AWG 24) and an SNR gap of 12.8 dB. We consider the near-far downstream ADSL scenario depicted in Fig. 4.3, with two users, one with three and one with two transceivers (all direct modes). A good solution is one in which user 2 spares user 1 from excessive interference. To dramatize the effect of the per-transceiver PCs, we consider the case where some lines have a ‘detour’, i.e. they start and end on the same node but their line lengths are not the same. This effect may represent practical unevenness between the pairs due to different patching applied to the different pairs, and due to differences in the quality and integrity of the pairs and connectors. Referring to Fig. 4.3, we define  $\mathbf{l}_n = [l_{n,[1]} \ \cdots \ l_{n,[A_n]}]$  and set  $\mathbf{l}_1 = [4.8 \ 4.5 \ 4.2]$  km and  $\mathbf{l}_2 = [3.3 \ 3]$  km. We also use  $d_2 = 3$  km. Each transceiver has a PC of 20.4 dBm (equal to 109.64 mW). For each line, noise model ANSI A is adopted.

In Fig. 4.4 we depict the rate regions of the WMMSE-GDSB with per-user

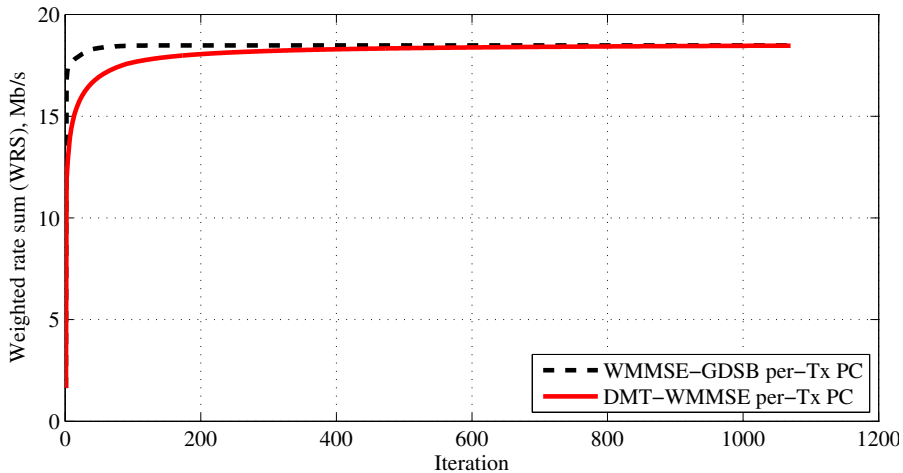


Figure 4.5: Convergence speed for the WMMSE-GDSB per-Tx PC and the DMT-WMMSE per-Tx PC.

PCs (i.e. the algorithm in Chapter 3), the DMT-WMMSE with per-transceiver PCs (i.e. Algorithm 4.1 in this chapter) and the WMMSE-GDSB with per-transceiver PCs (i.e. Algorithm 4.2 in this chapter). Not surprisingly, the algorithm with the per-user constraints does better through all the rate region. The algorithms with per-transceiver PCs are more limited in their solution space, and this has an impact on the performance. However, as we mentioned in Section 4.1, the per-transceiver PCs are in many situations more realistic.

Both algorithms that consider the per-transceiver PCs perform equally well. When they exist, the small differences in performance are due to a badly chosen starting point. However, in terms of convergence speed the advantage is clearly with the WMMSE-GDSB (a fact that was already mentioned in Chapter 3). In Fig. 4.5 we illustrate the weighted rate sum (WRS) after each iteration of both algorithms. As we can see, the DMT-WMMSE converges much slower. It needs approximately 800 iterations to converge, while the WMMSE-GDSB needs less than 70. Because of its faster convergence, we observe that, although more complex, the WMMSE-GDSB takes most of the time less time to finish in comparison to the DMT-WMMSE. One iteration of the former takes approximately 10 seconds (we use  $Q = 100$ ) while one iteration of the latter takes approximately 1 seconds. The faster convergence of the WMMSE-GDSB also means advantages in terms of how fast the algorithm

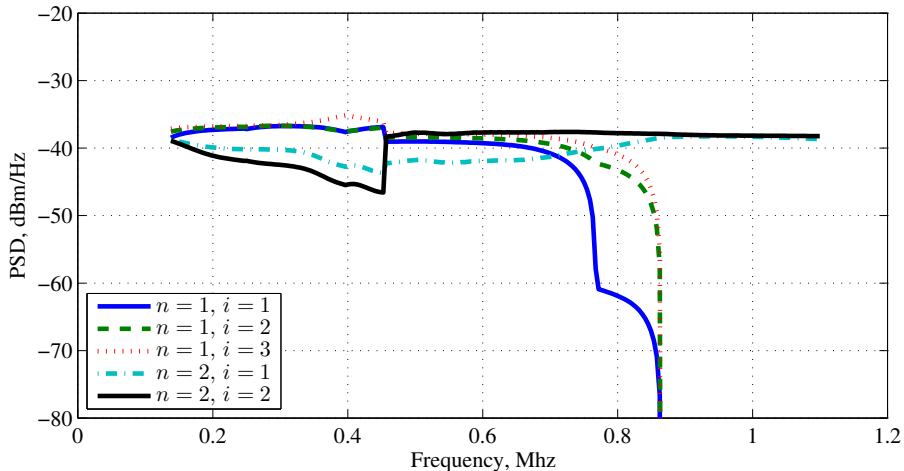


Figure 4.6: PSD's for the WMMSE-GDSB with per-user PCs.

can respond to changing channel conditions, specially if the algorithms are implemented in a distributed way with message exchanges.

In Fig. 4.6 and 4.7 we illustrate the final power allocation of the WMMSE-GDSB with per-user PCs and with per-transceiver PCs. We observe that, for user 1, the former allocates excessive power on the third transceiver—it is the one connected to the shortest line. The first transceiver, with the longest line, receives little power. This makes the transceivers uneven. For the result in the figure, we obtain a total power of approximately 98.15, 110.79 and 119.98 mW, respectively, for the transceivers of user 1. That constitutes a breach of the PCs for second and third transceivers. For user 2, these numbers are 104.62 and 114.67 mW, which violates the PC of the second transceiver. The achieved data rates are approximately  $r_1 = 8.0$  Mb/s and  $r_2 = 13.74$  Mb/s. For the situation in Fig. 4.7, all transceivers of both users satisfy the PC. The achieved data rates for the WMMSE-GDSB per-Tx PC are approximately  $r_1 = 8$  Mb/s and  $r_2 = 13.69$  Mb/s.

## 4.5.2 Upstream VDSL

We also simulate a VDSL upstream scenario. Cables of 0.4 mm (AWG 26) are used and an SNR gap of 9.45 dB is considered. Each transceiver has a PC of 11.5 dBm. For each line, noise model ETSI A is adopted with a background

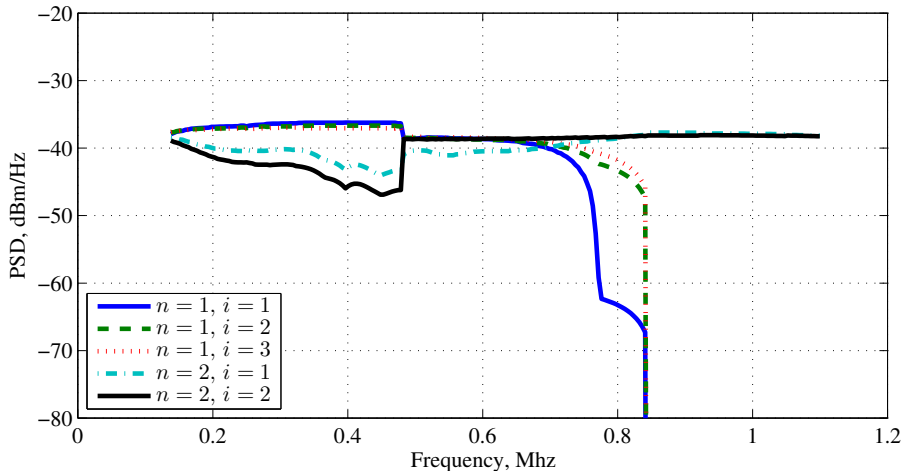


Figure 4.7: PSD's for the WMMSE-GDSB per-Tx PC.

noise level of  $-140$  dBm/Hz. We use the FDD 998 frequency bandplan over POTS up to 12 MHz.

We consider three users, the first two with 3 transceivers and the third with two. In this experiment, we want to assess the effect of the ‘detours’ in the solutions for both the per-user and the per-transceiver PC cases. We define, just as for the ADSL scenario,  $\mathbf{I}_1 = [1.2 + \beta \ 1.2 \ 1.2 - \beta]$  km,  $\mathbf{I}_2 = [0.8 + \beta \ 0.8 \ 0.8 - \beta]$  km and  $\mathbf{I}_3 = [0.6 + \beta \ 0.6 - \beta]$ , where  $\beta \geq 0$  introduces some imbalance between the DSL lines. We simulate the system for 4 distinct values of  $\beta$ , ranging from 0 to 75 m, and calculate the solutions of the WMMSE-GDSB with per-user PCs (i.e. the algorithm in Chapter 3) and with per-transceiver PCs (i.e. the algorithm discussed in Section 4.4 in this chapter). We depict the respective WRS as a function of  $\beta$  in Fig. 4.8.

For perfectly even lines (i.e.  $\beta = 0$ ), both algorithms return the same result. As  $\beta$  increases, so does the disparity between the lines. The algorithm with per-user PCs is able to allocate more power on the shorter lines, thus increasing its WRS, while the algorithm with the per-transceiver PCs cannot exploit this effect.

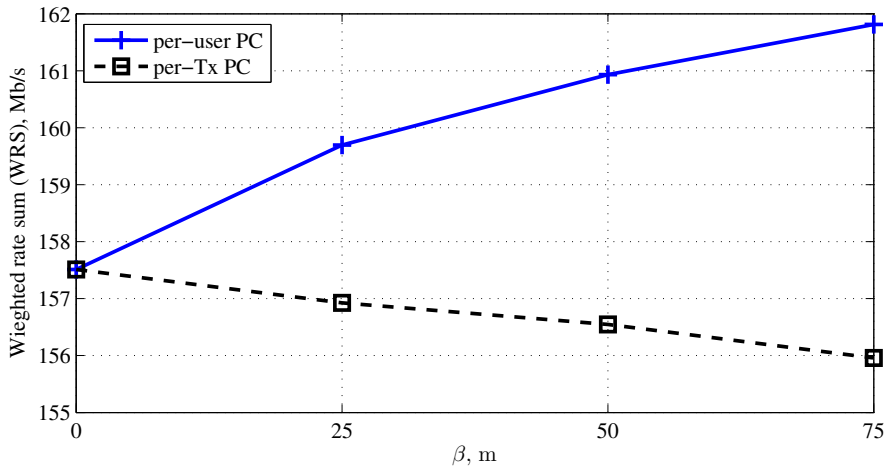


Figure 4.8: Results for the WMMSE-GDSB with per-user and per-transceiver PCs as a function of  $\beta$ .

## 4.6 Conclusion

In this chapter, we have focused on the DMT MIMO IC WRS maximization problem with per-transceiver PCs. Two solutions are proposed. The first builds on the recent work showing the relation between the WRS maximization problem and the MMSE minimization problem. The algorithm, called DMT-WMMSE with per-transceiver PCs, solves the signal and spectrum coordination parts of the problem simultaneously. The second proposal, called WMMSE-GDSB with per-transceiver PCs, separates these two parts. For the spectrum coordination part, we observe that the problem can be solved more efficiently with a change of variables. By using spherical coordinates in taxicab geometry (i.e. in the form of  $\eta_n^k \mathbf{v}_n^k$ , with  $\|\mathbf{v}_n^k\|_1 = 1$ ), we obtain for the radius  $\eta_n^k$  a concave problem. For the angles, it is shown that they can be solved independently.

Both algorithms achieve good results. As in Chapter 3, it is observed that the WMMSE-GDSB with per transceiver PCs converges much faster.

# Chapter 5

## General Framework

### 5.1 Introduction

Given a DSL network, depending on the kind of coordination on the transmitter and on the receiver sides, e.g. receiver-only, transmitter-only, etc., a BC, a MAC, an IC or a combination of them can be used as a model. Several papers have focused on the design of the transmission and reception strategies for such scenarios, e.g. [13, 14, 26, 27, 29, 39, 44, 45, 47, 48]. However, it is observed that these references base their designs on strong assumptions about the network infrastructure. We give four examples of these assumptions.

- First, most previous work considers a synchronous transmission case, i.e. the situation when all users' discrete multitone (DMT) blocks are aligned (i.e. time synchronized) at the receivers. This is not necessarily the case. Users who are in different physical locations or who belong to different service providers are difficult to synchronize. The result of asynchronous DMT transmission is inter-carrier interference (ICI) [15, 18, 66, 74], which complicates the problem significantly.
- Some previous references [13, 14, 29, 48] assume that in DSL coordination is only possible on the central office (CO) side of the network.<sup>1</sup> In

---

<sup>1</sup>By 'coordination on the CO side of the network' we mean that coordination can be done in the CO itself, in a fiber-fed cabinet in the street, a distribution point or in the basement of a large building.

other words, there is either a BC scenario for downstream transmission or a MAC scenario for upstream transmission. We believe this is too restrictive. E.g. it can be that a number of DSL lines arrive at the same box on the CPE if the connection serves a large residential building. This allows for some limited coordination on the CPE side as well. Plus, if two copper pairs that arrive on the CPE use PM transmission, then there is a three transceiver system that can be coordinated on the CPE side.

- Another assumption is that every user uses only one line (or one transceiver). This is not always the case. There are places where it is not uncommon that there are two DSL lines connected to a user. In some places, quads are popular. A quad is a group of four copper wires twisted together that serve a single customer. In these case, pair bonding, CM, PM or SW transmission can then be used.
- A final common assumption is that DSL channels have the so-called property of column-wise or row-wise diagonal dominance [13, 14, 48]. However, this only holds true for the case when sources of noise other than crosstalk are spatially white.

We believe there is a much richer range of interesting scenarios than what hitherto has been considered. Telephone networks have evolved differently through the decades in different parts of the world, giving rise to complex networks that have each their characteristics (e.g. in Europe quads are widespread, in North America they are not). Many of these networks would probably not fit on the scenarios considered previously in the literature. Modern DSL networks are likely better represented by an abundant set of different hybrid scenarios, where users can have multiple transceivers and elements of IC, MAC and BC are present. In this chapter we consider a general framework that encompasses all these hybrid situations as special cases, including the previously studied scenarios in this thesis. Our only assumption about the DSL network is that it is organized in a tree topology [70, 87].

To the best of our knowledge, no work up to now has developed a general framework and a corresponding algorithm that apply to this general scenario. This is the goal of this chapter. We develop a general system framework that includes MAC, BC and IC and any combination of them as a special case (we consider only linear transmission schemes). We propose an algorithm similar to the one in Chapter 3 that works for all cases, including any number of users, any number of transceivers, any number of tones, any kind of coordination on both the transmitter and on the receiver sides, and synchronous or asynchronous transmission. Through numerical simulations, the algorithm is seen to perform very well and it is seen to be polynomial time solvable.

We organize this chapter as follows. Section 5.2 presents the system model, the notation, the problem of interest and previous solutions. In Section 5.3 we derive and present our proposed approach. Section 5.4 contains some simulation results and Section 5.5 presents final remarks.

## 5.2 System Model and Problem Statement

### 5.2.1 System Model and Notation—Synchronous Case

This is the only section in this chapter where we specifically treat the *synchronous* transmission situation. That is so because the aim of this section is to present the notation we use and to see the effects of adding coordination on the transmitter and receiver sides of the network. To consider the asynchronous situation here would be too cumbersome. All conclusions from this section are readily extendable to the more general asynchronous case.

We consider an  $N$  user DSL system with DMT modulation with  $K$   $\Delta_f$ -spaced tones. We consider a system where upstream and downstream transmission are separated (with, e.g. time or frequency division duplexing), hence the crosstalk we consider is far end crosstalk (FEXT).<sup>2</sup> We denote the set of users by  $\mathcal{N} = \{1, \dots, N\}$  and the set of tones by  $\mathcal{K} = \{1, \dots, K\}$ . We let  $p_n^k$  be the transmit power of user  $n$  on tone  $k$  and we organize these values in the matrix  $\mathbf{P} \in \mathbb{R}_+^{K \times N}$ . The  $n$ th column of  $\mathbf{P}$ , denoted by  $\mathbf{p}_n = [p_n^1 \ \dots \ p_n^K]^T \in \mathbb{R}_+^K$ , contains the power allocation of user  $n$  in all tones. The  $k$ th row of  $\mathbf{P}$ ,  $\mathbf{p}^k = [p_1^k \ \dots \ p_N^k] \in \mathbb{R}_+^N$ , represents the power allocation of all users in tone  $k$ . User  $n$  has  $A_n$  transceivers.

Every user belongs to a group both on the transmitter side and on the receiver side. Inside a group, users can apply coordinated MIMO processing. We define each group as a set. For the grouping on the transmitter side, we define  $\mathcal{G}_i^{\text{tx}}$ ,  $i = 1, \dots, I \leq N$ . For the grouping on the receiver side, we similarly define  $\mathcal{G}_q^{\text{rx}}$ ,  $q = 1, \dots, Q \leq N$ . Here  $I$  and  $Q$  denote the number of groups on the transmitter and on the receiver sides, respectively. A user can only be in a single group both on the transmitter and on the receiver side, i.e. if  $n \in \mathcal{G}_i^{\text{tx}}$  then  $n \notin \mathcal{G}_q^{\text{tx}}$ ,  $q \neq i$  and if  $n \in \mathcal{G}_q^{\text{rx}}$  then  $n \notin \mathcal{G}_i^{\text{rx}}$ ,  $q \neq i$ . We also define the number of transceivers per group on the transmitter and on the receiver sides

---

<sup>2</sup>The system model can be straightforwardly generalized to a situation where upstream and downstream transmission are jointly optimized, eventually taking near end crosstalk (NEXT) into account.

respectively as

$$A_{\mathcal{G}_i^{\text{tx}}} = \sum_{n \in \mathcal{G}_i^{\text{tx}}} A_n \quad (5.1)$$

$$A_{\mathcal{G}_q^{\text{rx}}} = \sum_{n \in \mathcal{G}_q^{\text{rx}}} A_n \quad (5.2)$$

As already mentioned, throughout this chapter we focus on a linear design for both transmitters and receivers and treat interference as noise. All channel gains are considered perfectly known. Taking this into account, we obtain the received signal vector for group  $\mathcal{G}_q^{\text{rx}}$  on tone  $k$  as

$$\mathbf{y}_{\mathcal{G}_q^{\text{rx}}}^k = \widetilde{\mathbf{H}}_{n,n}^k \mathbf{T}_n^k \mathbf{x}_n^k + \sum_{\substack{j \in \mathcal{N} \\ j \neq n}} \widetilde{\mathbf{H}}_{n,j}^k \mathbf{T}_j^k \mathbf{x}_j^k + \mathbf{z}_{\mathcal{G}_q^{\text{rx}}}^k, \quad n \in \mathcal{G}_q^{\text{rx}}. \quad (5.3)$$

Here  $\mathbf{y}_{\mathcal{G}_q^{\text{rx}}}^k \in \mathbb{C}^{A_{\mathcal{G}_q^{\text{rx}}}}$  is the received signal vector for group  $\mathcal{G}_q^{\text{rx}}$  on tone  $k$ ;  $\mathbf{x}_n^k \in \mathbb{C}^{A_n}$  is the transmitted signal vector for user  $n$  on tone  $k$ ;  $\mathbf{T}_n^k \in \mathbb{C}^{A_{\mathcal{G}_i^{\text{tx}}} \times A_n}$ , where  $n \in \mathcal{G}_i^{\text{tx}}$ , is the transmit matrix for user  $n$  on tone  $k$ ; and  $\widetilde{\mathbf{H}}_{n,j}^k \in \mathbb{C}^{A_{\mathcal{G}_q^{\text{rx}}} \times A_{\mathcal{G}_i^{\text{tx}}}}$ , where  $q$  and  $i$  are such that  $n \in \mathcal{G}_q^{\text{rx}}$  and  $j \in \mathcal{G}_i^{\text{tx}}$ , is the channel matrix on tone  $k$  between the group to which user  $j$  belongs on the transmitter side to the group to which user  $n$  belongs on the receiver side. Still in (5.3), the vector  $\mathbf{z}_{\mathcal{G}_q^{\text{rx}}}^k \in \mathbb{C}^{A_{\mathcal{G}_q^{\text{rx}}}}$  represents circularly symmetric zero mean complex Gaussian noise.

In (5.3), we assume that user  $n$  has  $A_n$  parallel data streams, but some of these streams can have rate of zero. We also assume  $\mathbb{E}[\mathbf{x}_n^k (\mathbf{x}_n^k)^{\text{H}}] = \mathbf{I}_{A_n}$ . Still in (5.3), the noise vector  $\mathbf{z}_{\mathcal{G}_q^{\text{rx}}}^k$  is assumed to be spatially white with covariance matrix  $\mathbb{E}[\mathbf{z}_{\mathcal{G}_q^{\text{rx}}}^k (\mathbf{z}_{\mathcal{G}_q^{\text{rx}}}^k)^{\text{H}}] = \mathbf{I}_{A_{\mathcal{G}_q^{\text{rx}}}}$ ,  $q = 1 \dots, Q$ . The estimated signal vector for user  $n$  on tone  $k$  is given by

$$\mathbf{x}_n^k = \mathbf{R}_n^k \mathbf{y}_{\mathcal{G}_q^{\text{rx}}}^k, \quad n \in \mathcal{G}_q^{\text{rx}}. \quad (5.4)$$

Here  $\mathbf{R}_n^k \in \mathbb{C}^{A_n \times A_{\mathcal{G}_q^{\text{rx}}}}$ , where  $n \in \mathcal{G}_q^{\text{rx}}$ , is the receive matrix for user  $n$  on tone  $k$ .

We now show that  $\widetilde{\mathbf{H}}_{n,j}^k$  depends on the type of coordination on both sides of the channel and that it can be viewed as a concatenation of matrices relating to the MIMO IC, that we define as  $\mathbf{H}_{n,j}^k \in \mathbb{C}^{A_n \times A_j}$ . This is best conveyed by three examples.

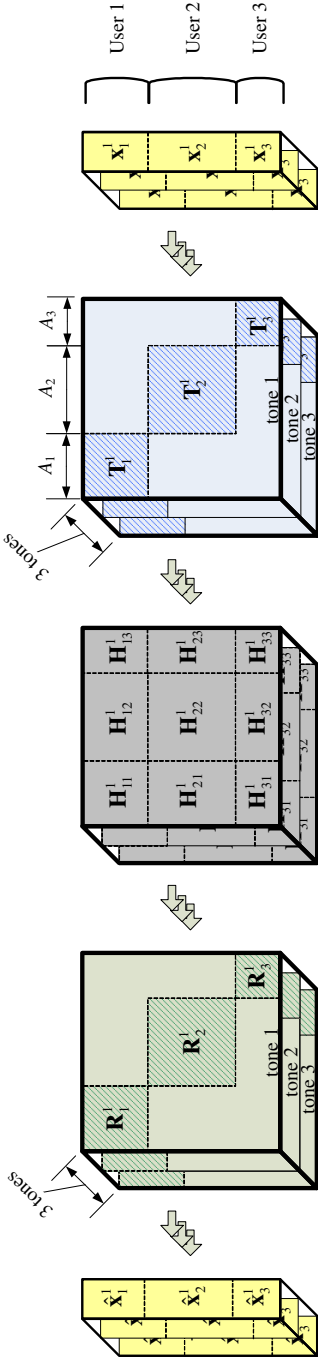


Figure 5.1: Illustration of a MIMO IC. For this case, there is only one user on every group in both the transmitter and on the receiver sides. Here, we have  $Q = I = N = 3$  and  $\mathcal{G}_n^{\text{tx}} = \mathcal{G}_n^{\text{rx}} = \{n\}$ ,  $n = 1, \dots, 3$ .

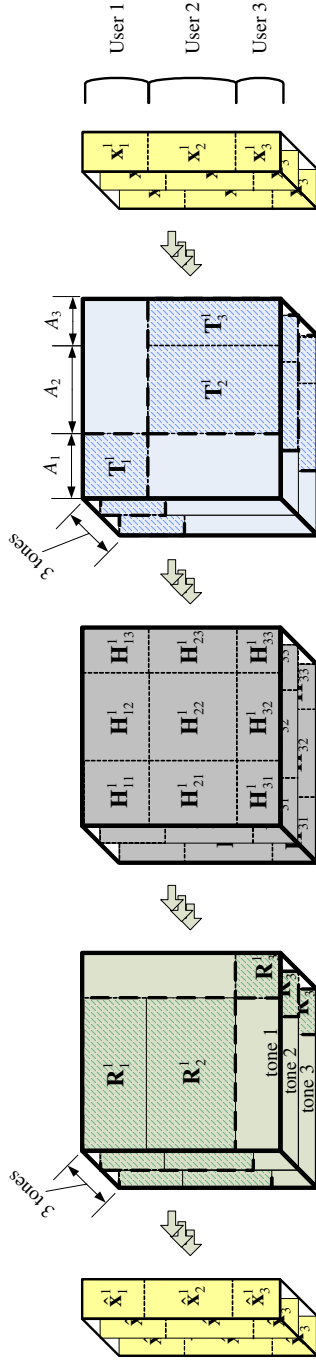


Figure 5.2: Illustration of a hybrid MAC, BC and IC. For this case, we have on the transmitter side  $\mathcal{G}_1^{\text{tx}} = \{1\}$  and  $\mathcal{G}_2^{\text{tx}} = \{2, 3\}$ ; and on the receiver side  $\mathcal{G}_1^{\text{rx}} = \{1, 2\}$  and  $\mathcal{G}_2^{\text{rx}} = \{3\}$ .

The **first example** is depicted in Fig. 5.1. This is a system with three users and three tones. This is a pure MIMO IC, i.e. every group contains a single user. This is the situation where there is a minimum amount of coordination. We have  $Q = I = N = 3$  and  $\mathcal{G}_n^{\text{tx}} = \mathcal{G}_n^{\text{rx}} = \{n\}$ ,  $n \in \mathcal{N}$ . In this case, for all tones we have  $\tilde{\mathbf{H}}_{n,j}^k = \mathbf{H}_{n,j}^k$ ,  $n, j \in \mathcal{N}$ ;  $A_{\mathcal{G}_n^{\text{tx}}} = A_{\mathcal{G}_n^{\text{rx}}} = A_n$ ,  $n \in \mathcal{N}$ ; and  $\mathbf{T}_n^k, \mathbf{R}_n^k \in \mathbb{C}^{A_n \times A_n}$ .

The **second example** is depicted in Fig. 5.2. This is a system with three users, with, say  $A_1 = 2$ ,  $A_2 = 3$  and  $A_3 = 1$ , and three tones. There are two groups on both transmitter and receiver side, i.e.  $Q = I = 2$ . We have  $\mathcal{G}_1^{\text{tx}} = \{1\}$  and  $\mathcal{G}_2^{\text{tx}} = \{2, 3\}$ ; and on the receiver side  $\mathcal{G}_1^{\text{rx}} = \{1, 2\}$  and  $\mathcal{G}_2^{\text{rx}} = \{3\}$ . Using (5.1) and (5.2), we obtain  $A_{\mathcal{G}_1^{\text{tx}}} = 2$ ,  $A_{\mathcal{G}_2^{\text{tx}}} = 4$ ,  $A_{\mathcal{G}_1^{\text{rx}}} = 5$  and  $A_{\mathcal{G}_2^{\text{rx}}} = 1$ . As a consequence, for all tones we have  $\mathbf{T}_1^k \in \mathbb{C}^{2 \times 2}$ ,  $\mathbf{T}_2^k \in \mathbb{C}^{4 \times 3}$ , etc. Notice that this system does not fit exactly neither the MAC, nor the BC, nor the IC case. This is a scenario with elements of BC, MAC and IC.

To calculate the equivalent channel matrices, we take into account the matrices  $\mathbf{H}_{n,j}^k \in \mathbb{C}^{A_n \times A_j}$ ,  $n, j \in \mathcal{N}$  and  $k \in \mathcal{K}$ . As mentioned in the previous paragraph, these would be the channel matrices for the case of a pure MIMO IC. The received signal for, say, group 1 is given by

$$\mathbf{y}_{\mathcal{G}_1^{\text{rx}}}^k = \begin{bmatrix} \mathbf{H}_{1,1}^k \\ \mathbf{H}_{2,1}^k \end{bmatrix} \mathbf{T}_1^k \mathbf{x}_1^k + \begin{bmatrix} \mathbf{H}_{1,2}^k & \mathbf{H}_{1,3}^k \\ \mathbf{H}_{2,2}^k & \mathbf{H}_{2,3}^k \end{bmatrix} \mathbf{T}_2^k \mathbf{x}_2^k + \begin{bmatrix} \mathbf{H}_{1,2}^k & \mathbf{H}_{1,3}^k \\ \mathbf{H}_{2,2}^k & \mathbf{H}_{2,3}^k \end{bmatrix} \mathbf{T}_3^k \mathbf{x}_3^k + \begin{bmatrix} \mathbf{z}_1^k \\ \mathbf{z}_2^k \end{bmatrix}.$$

The estimated signal for, say, user 2 is given by applying (5.4), i.e.

$$\hat{\mathbf{x}}_2^k = \mathbf{R}_2^k \underbrace{\begin{bmatrix} \mathbf{H}_{1,1}^k \\ \mathbf{H}_{2,1}^k \end{bmatrix}}_{\triangleq \tilde{\mathbf{H}}_{2,1}^k} \mathbf{T}_1^k \mathbf{x}_1^k + \mathbf{R}_2^k \underbrace{\begin{bmatrix} \mathbf{H}_{1,2}^k & \mathbf{H}_{1,3}^k \\ \mathbf{H}_{2,2}^k & \mathbf{H}_{2,3}^k \end{bmatrix}}_{\triangleq \tilde{\mathbf{H}}_{2,2}^k} \mathbf{T}_2^k \mathbf{x}_2^k + \mathbf{R}_2^k \underbrace{\begin{bmatrix} \mathbf{H}_{1,2}^k & \mathbf{H}_{1,3}^k \\ \mathbf{H}_{2,2}^k & \mathbf{H}_{2,3}^k \end{bmatrix}}_{\triangleq \tilde{\mathbf{H}}_{2,3}^k} \mathbf{T}_3^k \mathbf{x}_3^k + \mathbf{R}_2^k \underbrace{\begin{bmatrix} \mathbf{z}_1^k \\ \mathbf{z}_2^k \end{bmatrix}}_{\triangleq \mathbf{z}_{\mathcal{G}_1^{\text{rx}}}^k}.$$

Hence we define the  $\tilde{\mathbf{H}}_{n,j}^k$ ,  $n, j \in \mathcal{N}$  as the channel matrix that comes between  $\mathbf{R}_n^k$  and  $\mathbf{T}_j^k$ . It is a concatenation of the matrices  $\mathbf{H}_{n,j}^k$ . The concatenation depends on the grouping on both the receiver and transmitter sides.

The **third example** is that of a three user MIMO BC. This system is represented by  $\mathcal{G}^{\text{tx}} = \{1, 2, 3\}$ , i.e.  $I = 1$ , and  $\mathcal{G}_n^{\text{rx}} = \{n\}$ ,  $n \in \mathcal{N}$ , i.e.  $Q = 3$ . If

$A_n = 2 \forall n$ , then  $A_{\mathcal{G}^{\text{tx}}} = 6$  and  $A_{\mathcal{G}_q^{\text{rx}}} = 2$ ,  $s = 1, 2, 3$ . For this case, we have

$$\tilde{\mathbf{H}}_{1,n}^k = [\mathbf{H}_{1,1}^k \quad \mathbf{H}_{1,2}^k \quad \mathbf{H}_{1,3}^k], \quad n \in \mathcal{N}$$

$$\tilde{\mathbf{H}}_{2,n}^k = [\mathbf{H}_{2,1}^k \quad \mathbf{H}_{2,2}^k \quad \mathbf{H}_{2,3}^k], \quad n \in \mathcal{N}$$

$$\tilde{\mathbf{H}}_{3,n}^k = [\mathbf{H}_{3,1}^k \quad \mathbf{H}_{3,2}^k \quad \mathbf{H}_{3,3}^k], \quad n \in \mathcal{N}$$

Because of the structure with groups and because the  $\tilde{\mathbf{H}}_{n,j}^k$  are defined as functions of the  $\mathbf{H}_{n,j}^k$ , the proposed system model includes any kind of transmitter and receiver coordination. On one extreme, we have a MIMO IC, as explained in the first example. On the other extreme, there is only one group both on the transmitter and on the receiver side, i.e.  $\mathcal{G}^{\text{tx}} = \mathcal{G}^{\text{rx}} = \{1, \dots, N\}$ . This is the case with full two-sided coordination. It is often called a MIMO point-to-point system. With our formulation, every case between (and including) these two extremes is possible.

As a rule of thumb, we remark that coordination on the transmitter side makes  $\tilde{\mathbf{H}}_{n,j}^k$  ‘wider’ (more columns) than  $\mathbf{H}_{n,j}^k$ , and that coordination on the receiver side makes  $\tilde{\mathbf{H}}_{n,j}^k$  ‘taller’ (more rows) than  $\mathbf{H}_{n,j}^k$ .

## 5.2.2 System Model and Notation—Asynchronous Case

An asynchronous transmission scenario occurs when the DMT blocks of the different users are not aligned in time. We demonstrate this with the example of Fig. 5.3, where two users (denoted  $n$  and  $j$ ), each with two transceivers, interfere with each other. Their respective DMT blocks are offset by  $\beta_{n,j}$ ,  $0 \leq \beta_{n,j} \leq 1$ , as shown in the figure. Such a situation gives rise to ICI, which complicates the problem significantly. With ICI, transmission on a given tone  $k$  of an interferer influences not only the corresponding tone  $k$  of a victim, but all neighboring tones as well.

The bulk of the system model described in Section 5.2 continues to be valid for the asynchronous case, including the definition of groups on the transmitter and receiver sides and the fact that more coordination makes the channel matrices increase in size. We assume that all the transceivers inside a group either on the transmitter or on the receiver sides are synchronized. The received signal vector for group  $\mathcal{G}_q^{\text{rx}}$  on tone  $k$  is given by

$$\mathbf{y}_{\mathcal{G}_q^{\text{rx}}}^k = \tilde{\mathbf{H}}_{n,n}^k \mathbf{T}_n^k \mathbf{x}_n^k + \sum_{\substack{j \in \mathcal{N} \\ j \neq n}} \sum_{s \in \mathcal{K}} \mathbf{A}_{n,j}^{k,s} \mathbf{T}_j^s \mathbf{x}_j^s + \mathbf{B}_{n,j}^{k,s} \mathbf{T}_j^s \bar{\mathbf{x}}_j^s + \mathbf{z}_{\mathcal{G}_q^{\text{rx}}}^k, \quad n \in \mathcal{G}_q^{\text{rx}}. \quad (5.5)$$

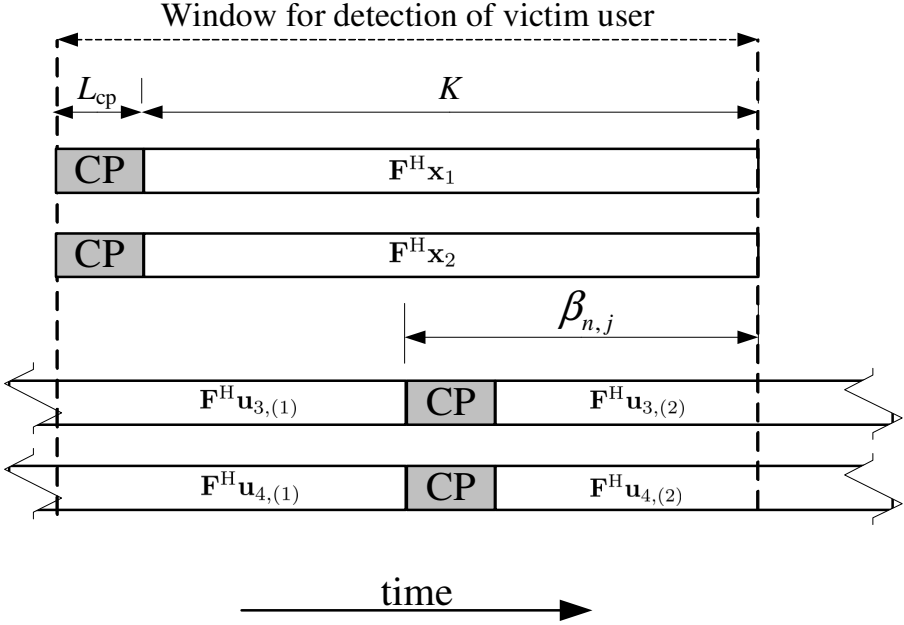


Figure 5.3: Model for asynchronous transmission. In this example, two users, each with two transceivers, interfere with one another. Here the victim user, denoted  $n$ , has a DMT block for its  $i$ th transceiver given by  $\mathbf{x}_i$ , while the DMT block of the interfering user, denoted  $j$ , is denoted by  $\mathbf{u}_i$ . Symbols from two time instants of the interfering user affect the victim. These instants are denoted by the subscripts (1) and (2). The offset on reception is given by  $\beta_{n,j}$ , as defined in the figure..

Here  $\mathbf{x}_j^s, \bar{\mathbf{x}}_j^s$  are the DMT symbols of user  $j$  on tone  $s$  that interfere with the reception of the DMT symbol of user  $n$  on tone  $k$ . Symbol  $\bar{\mathbf{x}}_j^s$  comes before (in time) the reception of user  $n$  and symbol  $\mathbf{x}_j^s$  comes after. The matrices  $\mathbf{A}_{n,j}^{k,s}, \mathbf{B}_{n,j}^{k,s} \in \mathbb{C}^{A_{\mathcal{G}_q^{\text{rx}}} \times A_{\mathcal{G}_i^{\text{tx}}}}$ , where  $q$  and  $i$  are such that  $n \in \mathcal{G}_q^{\text{rx}}$  and  $j \in \mathcal{G}_i^{\text{tx}}$ , account for the ICI. They represent the channel matrices from user  $j$  to user  $n$ ,  $j \neq n$ , and from tone  $s$  to tone  $k$ . If  $\beta_{n,j} = 0$  or  $\beta_{n,j} = 1$ , then users  $n$  and  $j$  are synchronized and there is no ICI. Hence the model in (5.5) is a generalization of the one in (5.3). If  $\beta_{n,j} = 1$ , then  $\mathbf{A}_{n,j}^{k,k} = \tilde{\mathbf{H}}_{n,j}^k$ ,  $\mathbf{A}_{n,j}^{k,s} = \mathbf{0}$  for  $k \neq s$  and  $\mathbf{B}_{n,j}^{k,s} = \mathbf{0}$  for all  $s, k$ . If  $\beta_{n,j} = 0$ , then  $\mathbf{B}_{n,j}^{k,k} = \tilde{\mathbf{H}}_{n,j}^k$ ,  $\mathbf{B}_{n,j}^{k,s} = \mathbf{0}$  for  $k \neq s$  and  $\mathbf{A}_{n,j}^{k,s} = \mathbf{0}$  for all  $s, k$ . If users  $n$  and  $j$  belong to the same group in either the receiver or the transmitters sides, then we set  $\beta_{n,j} = 0$ .

The accurate calculation of the ICI matrices is a fundamental part of the problem. Inaccurate characterizations lead to inaccurate parameters for the optimization problem, which in turn influences the resource allocation and performance. This characterization was attempted only for the single input, single output (SISO) IC case in [18, 74, 75]. For the general, MIMO case we detail how to accurately calculate the ICI matrices  $\mathbf{A}_{n,j}^{k,s}$  and  $\mathbf{B}_{n,j}^{k,s}$  as a function of a fixed offset  $\beta_{n,j}$  in Appendix D.1.

In order to show the ICI, we briefly focus on the SISO IC case with two users, where (5.5) is re-written for, say, user 1, as

$$y_1^k = h_{1,1}^k x_1^k + \sum_{s \in \mathcal{K}} A_{1,2}^{k,s} x_2^s + B_{1,2}^{k,s} \bar{x}_2^s + z_1^k$$

Considering  $\mathbb{E}[(x_n^k)^* x_n^k] = \mathbb{E}[(\bar{x}_n^k)^* \bar{x}_n^k] = p_n^k \forall n$ , the SNR for user 1 on tone  $k$  is given by  $p_1^k |h_{1,1}^k|^2 (\sigma_1^k + \sum_{s \in \mathcal{K}} \alpha_{1,2}^{k,s} P_2^s)^{-1}$ , where we define  $\alpha_{1,2}^{k,s} = (A_{1,2}^{k,s})^2 + (B_{1,2}^{k,s})^2$ —in contrast to the MIMO case, for the SISO IC case the ICI from tone  $s$  to tone  $k$  can be characterized with a single scalar. We plot these scalars for an ADSL network with an interfering and a victim user with different offsets in Fig. 5.4. The crosstalk channel is chosen with impulse response equal to  $\mathbf{g}_{1,2} = [1 \ 0 \ 0 \ \dots \ 0]^T \in \mathbb{C}^L$  (see Appendix D to see how this influences the ICI coefficients). In the figure, we see how the ICI spreads power through frequency as  $\beta_{1,2}$  increases. We also show the ICI coefficients calculated in [18], which are calculated considering a worst case situation and are too pessimistic.

Just as in (5.4), the received signal vector in (5.5) is processed by the receive matrix  $\mathbf{R}_n^k$  for every user and tone. In this chapter, we use the linear MMSE (LMMSE) receiver, which is given by

$$\mathbf{R}_n^k = (\mathbf{T}_n^k)^H (\tilde{\mathbf{H}}_{n,n}^k)^H \left( \mathbf{M}_n^k + \tilde{\mathbf{H}}_{n,n}^k \mathbf{T}_n^k (\mathbf{T}_n^k)^H (\tilde{\mathbf{H}}_{n,n}^k)^H \right)^{-1}, \quad (5.6)$$

where, considering  $\mathbb{E}[\mathbf{x}_n^s (\mathbf{x}_n^s)^H] = \mathbb{E}[\bar{\mathbf{x}}_n^s (\bar{\mathbf{x}}_n^s)^H] = \mathbf{I}_{A_n} \forall n$ , the noise covariance matrix  $\mathbf{M}_n^k$  is given by

$$\mathbf{M}_n^k = \sum_{\substack{j \in \mathcal{N} \\ j \neq n}} \sum_{s \in \mathcal{K}} \mathbf{A}_{n,j}^{k,s} \mathbf{T}_j^s (\mathbf{T}_j^s)^H (\mathbf{A}_{n,j}^{k,s})^H + \mathbf{B}_{n,j}^{k,s} \mathbf{T}_j^s (\mathbf{T}_j^s)^H (\mathbf{B}_{n,j}^{k,s})^H + \mathbf{I}_{A_{G_{rx}^k}}.$$

Although we do not write it explicitly, this matrix can be normalized by a SNR gap  $\Gamma$ . It is well known that the LMMSE receiver is optimal given a set of fixed transmit matrices  $\mathbf{T}_n^k$ .

The optimization problem we consider is the maximization of the weighted rate sum (WRS) of the participating users in the network subject to per-user

Table 5.1: Comparison of previous solutions

Solution [reference] <sup>†</sup>	Description	Restrictions <sup>‡</sup>
IWF, OSB, SC/ALP, DSB, 2SB, MIW, NDW-DSM [17, 59, 73, 96, 105, 109, 110]	solutions to SISO spectrum management	$A_n = 1 \forall n$ , IC, synchronous
ZF-GDFE [29]	ZF, (non-linear) GDFE and waterfilling	$A_n = 1 \forall n$ , BC or MAC, synchronous
ZF [13, 14]	linear ZF plus waterfilling	$A_n = 1 \forall n$ ; BC or MAC, diagonally dominant channel matrix, synchronous
Low complexity linear ZF [48]	linear ZF, lower complexity version	$A_n = 1 \forall n$ , BC or MAC, diagonally dominant channel matrix, synchronous
MAC-OSB [101]	MMSE-GDFE plus OSB	MAC, $A_n = 1 \forall n$ , synchronous
SVD [44, 47]	SVD applied to channel matrix	MIMO point-to-point, synchronous
Vectoring with common mode [39]	SVD applied to channel matrix of each user, inter-user interference with GDFE	IC, synchronous
IC-MAC OSB/ IC-BC OSB [26, 27]	MMSE-GDFE plus OSB	Partial MAC ( $I = N$ , $Q < N$ , with $G_n^{rx} = \{n\}$ , $n \in \mathcal{N}$ and $Q$ groups on receiver) or partial BC ( $I < N$ , $Q = N$ , with $G_n^{rx} = \{n\}$ , $n \in \mathcal{N}$ and $I$ groups on transmitter), $A_n = 1 \forall n$ , synchronous
WMNSE-GDSB [62]	WMNSE solution for signal coordination plus generalized DSB for power allocation	IC, synchronous
MIW, ASB-A1, ASB-A2, GPS/GPA [15, 18, 109] <sub>1</sub>	solutions to SISO spectrum management, asynchronous case	$A_n = 1 \forall n$ , IC

<sup>†</sup> A list of the acronyms is given as follows: optimal spectrum balancing (OSB), single input, single output (SISO), generalized decision feedback equalization (GDFE), zero forcing (ZF), minimum mean squared error (MMSE), weighted MMSE (WMNSE) and singular value decomposition (SVD).

<sup>‡</sup> In the notation of this paper, a BC is characterized by  $I = 1$ ,  $Q = N$ ,  $G_1^{rx} = \{1, \dots, N\}$  and  $G_n^{rx} = \{n\}$ ,  $n \in \mathcal{N}$ ; a MAC is characterized by  $I = N$ ,  $Q = 1$ ,  $G_n^{rx} = \{n\}$ ,  $n \in \mathcal{N}$  and  $G_1^{rx} = \{1, \dots, N\}$ ; and an IC is characterized by  $I = Q = N$  and  $G_n^{rx} = \{n\}$ ,  $n \in \mathcal{N}$ .

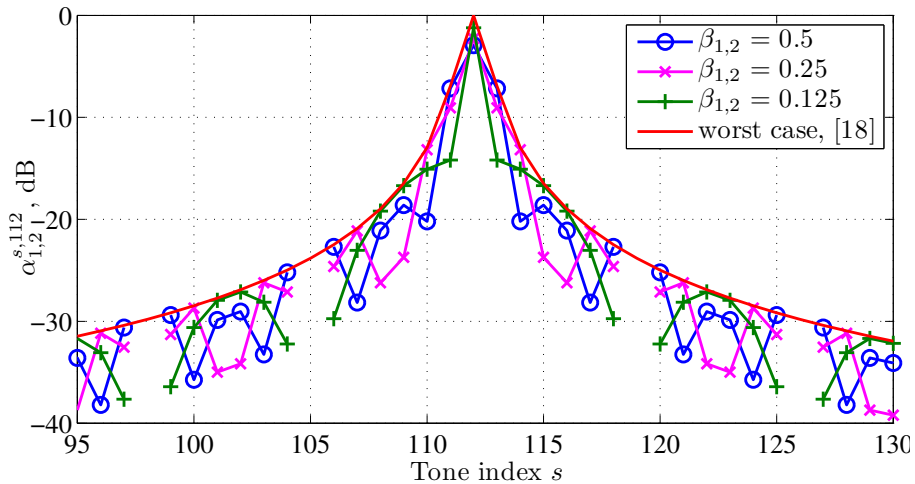


Figure 5.4: ICI coefficient  $\alpha_{1,2}^{s,112}$  for the SISO IC calculated for different values of  $\beta_{1,2}$  as in the Appendix D.1. We use an ADSL system ( $K = 224$ ) and a frequency flat crosstalk channel. We show only the 35 largest coefficient around tone 112. We also show the worst case coefficients of [18].

power constraints (PC). Consider  $\mathcal{T} = \{\mathbf{T}_n^k | n \in \mathcal{N}, k \in \mathcal{K}\}$ . The optimization problem is then given as

$$\begin{aligned} \max_{\mathcal{T}, \mathbf{P}} \quad & \sum_{n \in \mathcal{N}} \sum_{k \in \mathcal{K}} u_n b_n^k \\ \text{subject to} \quad & \text{tr}\{\mathbf{T}_n^k (\mathbf{T}_n^k)^H\} = p_n^k, \quad k \in \mathcal{K}, \quad n \in \mathcal{N} \\ & \sum_{k \in \mathcal{K}} p_n^k \leq P_n^{\max}, \quad n \in \mathcal{N} \end{aligned} \quad (5.7)$$

Here, with (5.6) and (5.2.2) in hands and assuming Gaussian signaling, we write the data rate for user  $n$  and tone  $k$  as

$$b_n^k = \log |\mathbf{I}_{A_n} + (\mathbf{T}_n^k)^H (\tilde{\mathbf{H}}_{n,n}^k)^H (\mathbf{M}_n^k)^{-1} \tilde{\mathbf{H}}_{n,n}^k \mathbf{T}_n^k|.$$

Here  $\log(\cdot)$  denotes the natural logarithm. The total data rate of user  $n$  in bits per second is given by  $r_n = f_s / \log(2) \sum_{k \in \mathcal{K}} b_n^k$ , where  $f_s$  is the symbol rate. We remind that in this thesis we ignore the practical constraint of discrete bit loading.

Still in (5.7), the variables  $u_n$  are weights or priorities given to each user and  $P_n^{\max}$  is the PC for user  $n$ . In Chapter 4 a similar problem is treated with per-transceiver PCs, whereas here a per-user PC is considered. The situation with the per-transceiver PCs adds complexity to the problem, and for simplicity is not considered in this chapter.

The optimization problem in (5.7) is NP-hard [53], which makes it very challenging. The challenge is twofold. On the one hand, the transmit matrices, i.e.  $\mathcal{T}$ , should be designed so that the desired signal is easy to identify and the undesired signals are easy to cancel. On the other hand, power should be carefully allocated for every user and tone depending on the signal to noise ratio. These two challenges have a strong interplay with each other. The choice of  $\mathcal{T}$  determines the spatial separation or spatial multiplexing that is characteristic of MIMO systems. How this separation occurs depends on the kind of coordination present on both sides of the network. Notice that more transmitter and receiver coordination makes the channel matrices ‘wider’ or ‘taller’, which means that there are more dimensions in which this separation can take place. For a (synchronous) MIMO point-to-point system, perfect spatial separation is possible. In this particular case, the singular value decomposition (SVD) of the channel matrix separates the channel in independent eigenmodes, one for each data stream (e.g. [72, 89]). For anything with less coordination, there will be some residual interference that every user has to withstand. Users should avoid excessive residual interference to each other by choosing a smart power allocation through frequency, i.e. by choosing  $\mathbf{P}$ .

Table 5.1 reviews previous solutions to this problem. We give preference to papers dealing with DSL. As we already mentioned, all previous work focuses on special assumptions on the network infrastructure. The majority focuses solely on the synchronous case. As we briefly describe the previous solutions in Table 5.1, we always use the framework just discussed.

We now briefly describe the solutions with more detail.

In [44, 47], a MIMO point-to-point scenario is considered and the classical SVD-based solution is used.

If  $A_n = 1 \forall n$  and there is no signal coordination on both sides of the network (an IC), then (5.7) is equivalent to a spectrum coordination problem. This is a single-input, single-output system that has been well studied in the literature, e.g. [17, 59, 73, 96, 110].

Several works consider that all users have  $A_n = 1$  and that there is only coordination on the service provider side. This gives rise to a BC on the downstream and a MAC on the upstream. In [29], a QR decomposition

of the channel matrix is used with subsequent generalized decision feedback equalization (GDFE). In [13] and [14], a linear zero forcing (ZF) receive or transmit matrix is shown to be near-optimal in the case when the channel matrix is diagonally dominant. Ref. [48] proposes a ZF with lower computational complexity. Ref. [45] considers the BC scenario with nonlinear processing. Ref. [101] deals with a MAC with  $A_n = 1$  for all users with any channel matrix structure (i.e. not necessarily diagonal dominant matrices).

In [26,27,39], a hybrid BC-IC or MAC-IC is considered. In [39], each user can use both its direct and common mode on the CPE side and coordination is possible among them, i.e.  $A_n = 2 \forall n$ . There is full coordination on the receiver side. A SVD decomposition is used for each user and inter-user crosstalk is mitigated with nonlinear processing. Refs. [26, 27] consider either a partial MAC or a partial BC with  $A_n = 1 \forall n$ . There are groupings of users on the CO side of the network, but on the CPE side there is none.

In Chapter 3 of this thesis, a MIMO IC is considered with each user having  $A_n$  transceivers. The problem is separated in signal and spectrum coordination parts and solved separately. We see on the remainder of this chapter that it is possible to apply the solution of Chapter 3 to the problem at hand.

Three alternative solutions have been proposed to the asynchronous problem [15,18,109], all of them considering the SISO IC situation. Some references have also focused on the modeling of the ICI effect [18,66,74,75]. In this section we provide both an accurate characterization of the MIMO asynchronous transmission and a solution for the signal and spectrum coordination problem.

## 5.3 Proposed Solution

In Chapter 3, a solution for the synchronous DMT MIMO IC is proposed that achieves good results and is polynomial time solvable. The problem is divided in signal and spectrum coordination parts and these two parts are solved iteratively and independently. The algorithm in Chapter 3 is of special interest here, because it forms the basis of the general algorithm that is presented in this chapter.

The solution of Chapter 3 begins with an equation of the received signal similar to (5.3). The difference is that for the general, possibly asynchronous case with any kind of groupings on both sides of the network we use the channel matrices  $\mathbf{A}_{n,j}^{k,s}$  and  $\mathbf{B}_{n,j}^{k,s}$ , whereas in Chapter 3 there is a restriction that  $\mathbf{A}_{n,j}^{k,k} = \mathbf{H}_{n,j}^k \forall n, j, k$ ,  $\mathbf{A}_{n,j}^{k,s} = \mathbf{0} \forall n, j, k \neq s$  and  $\mathbf{B}_{n,j}^{k,s} = \mathbf{0} \forall n, j, k, s$ . The main insight of this chapter is that independently of what channel matrix is used, the solution

method of Chapter 3 still applies. In the following, we derive the main parts of the algorithm while emphasizing the main differences between the current problem and that of Chapter 3.

We begin by writing the Lagrangian of (5.7) as

$$L(\mathcal{T}, \mathbf{P}, \boldsymbol{\mu}, \boldsymbol{\lambda}) = \sum_{n \in \mathcal{N}} \sum_{k \in \mathcal{K}} u_n b_n^k - \sum_{n \in \mathcal{N}} \lambda_n \left( \sum_{k \in \mathcal{K}} p_n^k - P_n^{\max} \right) - \sum_{n \in \mathcal{N}} \sum_{k \in \mathcal{K}} \mu_n^k \left( \text{tr} \{ \mathbf{T}_n^k (\mathbf{T}_n^k)^{\text{H}} \} - p_n^k \right) \quad (5.8)$$

Here  $\boldsymbol{\lambda} = [\lambda_1 \ \dots \ \lambda_N]^{\text{T}} \in \mathbb{R}_+^N$  and  $\boldsymbol{\mu} = [\mu_1^1 \ \dots \ \mu_1^k \ \mu_2^1 \ \dots \ \mu_N^K]^{\text{T}} \in \mathbb{R}^{NK}$  are Lagrange multipliers associated respectively with the per-user PCs and the per-user and per-tone trace constraint on the transmit matrices.

In our approach, we separate the problem in two parts. First, we solve for the transmit matrices while keeping the power allocation matrix fixed, then we solve for the power allocation matrix while keeping the transmit matrices fixed. Towards this end, we write (5.8) as a function of  $\mathcal{T}$  and  $\boldsymbol{\mu}$ ; and  $\mathbf{P}$  and  $\boldsymbol{\lambda}$ , respectively as

$$L(\mathcal{T}, \boldsymbol{\mu}) = \sum_{n \in \mathcal{N}} \sum_{k \in \mathcal{K}} u_n b_n^k - \sum_{n \in \mathcal{N}} \sum_{k \in \mathcal{K}} \mu_n^k \left( \text{tr} \{ \mathbf{T}_n^k (\mathbf{T}_n^k)^{\text{H}} \} - p_n^k \right) \quad (5.9)$$

$$L(\mathbf{P}, \boldsymbol{\lambda}) = \sum_{n \in \mathcal{N}} \sum_{k \in \mathcal{K}} u_n b_n^k - \sum_{n \in \mathcal{N}} \lambda_n \left( \sum_{k \in \mathcal{K}} p_n^k - P_n^{\max} \right) \quad (5.10)$$

For the following argument, we decompose the transmit matrices as  $\mathbf{T}_n^k = \sqrt{p_n^k} \bar{\mathbf{T}}_n^k$ , where  $\text{tr} \{ \bar{\mathbf{T}}_n^k (\bar{\mathbf{T}}_n^k)^{\text{H}} \} = 1$ . While solving for  $\mathbf{P}$  we keep  $\bar{\mathbf{T}}_n^k$  for all  $n$  and  $k$  fixed and while solving for  $\mathcal{T}$  we keep  $\mathbf{P}$  fixed.

The important thing to notice about (5.9) is that now each tone has its PC fixed for all the users, which simplifies the problem significantly. However, unlike the synchronous situation discussed in Chapter 3, the problem cannot be solved for each tone separately. The asynchronous transmission couples the optimization through the tones.

The important thing about (5.10) is that it is a pure spectrum coordination problem, just like [17, 59, 73, 96, 105, 110]. It is, however, a MIMO spectrum coordination problem, whereas all the references just cited treat a SISO situation. The problem in  $\mathbf{P}$  is coupled through frequency by the PCs.

### 5.3.1 Solving for $\mathcal{T}$

To solve (5.9), we follow the weighted MMSE (WMMSE) approach [22, 83] and Chapter 3. This approach establishes a way to maximize rate by minimizing the weighted minimum mean squared error (MMSE) of symbol detection. To use this method, for all users and tones we first calculate (5.6) and calculate a weighting matrix  $\mathbf{W}_n^k \in \mathbb{C}^{A_n \times A_n}$  as

$$\mathbf{W}_n^k = u_n (\mathbf{E}_n^k)^{-1} \quad (5.11)$$

Here

$$\mathbf{E}_n^k = ((\mathbf{T}_n^k)^H (\tilde{\mathbf{H}}_{n,n}^k)^H (\mathbf{M}_n^k)^{-1} \tilde{\mathbf{H}}_{n,n}^k \mathbf{T}_n^k + \mathbf{I}_{A_n})^{-1} \quad (5.12)$$

is the MSE matrix of symbol detection. The weighting matrix  $\mathbf{W}_n^k$  is the key to making the connection between the WRS maximization and the MSE minimization [22, 62, 83].

To solve for  $\mathbf{T}_n^k$  we formulate the weighted MMSE minimization problem subject to per-user and per-tone PCs. If the weighting matrix is calculated with (5.11), then a stationary point of the weighted MMSE minimization problem is also a stationary point of the WRS maximization problem. We solve the former because it is a convex problem. The solution for  $\mathbf{T}_n^k$  is given by

$$\begin{aligned} \mathbf{T}_n^k = & \left( (\tilde{\mathbf{H}}_{n,n}^k)^H (\mathbf{R}_n^k)^H \mathbf{W}_n^k \mathbf{R}_n^k \tilde{\mathbf{H}}_{n,n}^k + \sum_{\substack{j \in \mathcal{N} \\ j \neq n}} \sum_{s \in \mathcal{K}} (\mathbf{A}_{j,n}^{s,k})^H (\mathbf{R}_j^s)^H \mathbf{W}_j^s \mathbf{R}_j^s \mathbf{A}_{j,n}^{s,k} + \right. \\ & \left. (\mathbf{B}_{j,n}^{s,k})^H (\mathbf{R}_j^s)^H \mathbf{W}_j^s \mathbf{R}_j^s \mathbf{B}_{j,n}^{s,k} + \mu_n^k \mathbf{I}_{A_{\mathcal{G}_i^{\text{tx}}}} \right)^{-1} \times (\tilde{\mathbf{H}}_{n,n}^k)^H (\mathbf{R}_n^k)^H \mathbf{W}_n^k, \quad n \in \mathcal{G}_i^{\text{tx}} \end{aligned} \quad (5.13)$$

Here, the Lagrange multiplier  $\mu_n^k$  should be chosen such that the PC is respected.

The main difference between (5.11) and (5.13) and the equivalent equations in Chapter 3 is that the channel matrices  $\mathbf{A}_{n,j}^{k,s}$  and  $\mathbf{B}_{n,j}^{k,s}$  replace the MIMO IC matrices  $\mathbf{H}_{n,j}^k$ . Notice that these matrices take into account both any grouping on both the transmitter and receiver sides and possibly asynchronous transmission. Because of the extra dimensions offered by coordination of different users on the transmitter side, transmit matrices  $\mathbf{T}_n^k$  are larger or at least as large as the ones in Chapter 3.

### 5.3.2 Solving for $\mathbf{P}$

To solve for  $\mathbf{P}$ , we take a per-user approach, i.e. we solve for each user separately while keeping power for all other users fixed. To solve for user  $n$  in (5.10), we first notice that  $L(\mathbf{p}_n, \lambda_n)$  has a difference of convex (DC) programming structure, i.e. it is the difference of convex functions in  $p_n^k$ : while  $b_n^k$  is concave in  $p_n^k$ ,  $b_j^s$ ,  $j \neq n$ , is convex.<sup>3</sup> To more easily solve the problem, we first approximate  $b_j^s$ ,  $j \neq n$ , by its first order Taylor expansion. With these approximations, we write

$$\tilde{L}(\mathbf{p}_n, \lambda_n) = \sum_{k \in \mathcal{K}} u_n b_n^k + \sum_{\substack{j \in \mathcal{N} \\ j \neq n}} \sum_{s \in \mathcal{K}} u_j \left( b_j^s \left|_{\bar{\mathbf{P}}} (p_n^k - \bar{p}_n^k) \frac{\partial b_j^s}{\partial p_n^k} \right|_{\bar{\mathbf{P}}} \right) - \lambda_n p_n^k,$$

which is now concave in  $p_n^k$ . Here  $\bar{\mathbf{P}}$  and  $\bar{p}_n^k$  represent values from a previous iteration. To solve this concave problem, we take the derivative in  $p_n^k$  and set it to zero. We obtain

$$\frac{\partial \tilde{L}(\mathbf{p}_n, \lambda_n)}{\partial p_n^k} = u_n \text{tr} \left\{ \left( p_n^k \mathbf{S}_n^k + \mathbf{I}_{A_n} \right)^{-1} \mathbf{S}_n^k \right\} - \lambda_n - \tau_n^k = 0, \quad (5.14)$$

where  $\mathbf{S}_n^k = (\bar{\mathbf{T}}_n^k)^{\text{H}} (\tilde{\mathbf{H}}_{n,n}^k)^{\text{H}} (\mathbf{M}_n^k)^{-1} \tilde{\mathbf{H}}_{n,n}^k \bar{\mathbf{T}}_n^k$  and  $\tau_n^k$  is given by

$$\begin{aligned} \tau_n^k \triangleq & \sum_{\substack{j \in \mathcal{N} \\ j \neq n}} \sum_{s \in \mathcal{K}} \frac{u_j \partial b_j^s}{\partial p_n^k} = \sum_{\substack{j \in \mathcal{N} \\ j \neq n}} \sum_{s \in \mathcal{K}} u_j \text{tr} \left\{ \mathbf{E}_j^s (\mathbf{T}_j^s)^{\text{H}} (\mathbf{H}_{j,j}^s)^{\text{H}} (\mathbf{M}_j^s)^{-1} \right. \\ & \left. \left( \mathbf{A}_{j,n}^{s,k} \bar{\mathbf{T}}_n^k (\bar{\mathbf{T}}_n^k)^{\text{H}} (\mathbf{A}_{j,n}^{s,k})^{\text{H}} + \mathbf{B}_{j,n}^{s,k} \bar{\mathbf{T}}_n^k (\bar{\mathbf{T}}_n^k)^{\text{H}} (\mathbf{B}_{j,n}^{s,k})^{\text{H}} \right) (\mathbf{M}_j^s)^{-1} \mathbf{H}_{j,j}^s \mathbf{T}_j^s \right\} \end{aligned} \quad (5.15)$$

Here,  $\mathbf{E}_j^k$  is given by (5.12).

It may not look like so at first sight, but (5.14) is a kind of waterfilling equation. Eq. (5.14) is a generalization of the classical waterfilling in several directions: whereas the classical formula considers a single user synchronous SISO transmission, (5.14) works for a multi-user (possibly) asynchronous MIMO transmission with any kind of coordination on the transmitter and the receiver sides. In (5.14),  $\tau_n^k$  works by distorting the water level so that tones of user  $n$  that cause excessive interference to other users and tones are punished and hence are allocated less power. The water level is thus not constant, but frequency selective.

---

<sup>3</sup>There is one exception to this, namely the case of the MAC with equal weights for all users. See e.g. [113]

It can be shown that (5.14) has at most one nonnegative root and that this equation can be simplified to a polynomial form (see Chapter 3). For solving it, we need but to solve the polynomial and pick the largest root.

The polynomial is of degree  $A_n$ . When  $A_n$  is large, it may be too costly to solve the polynomial and pick the largest root. Since  $A_n - 1$  roots should be discarded anyway, in Chapter 3 the power method has been proposed to obtain the largest root of the polynomial. Here we exploit the fact that (5.14) is the derivative of a concave function, and thus it can have only one zero. To find its zero, we can use e.g. the Newton method.

### 5.3.3 Algorithm

We are now ready to write a general algorithm that applies to any number of users, to any number of transceivers, to any number of tones, to any kind of coordination on both the transmitter and on the receiver sides, and to synchronous/asynchronous transmission. Because of the general framework containing the BC, MAC, IC or any combination of them, the WMMSE approach to solve the signal coordination problem and the generalized DSB [62, 96] approach to solve the spectrum coordination part, we call it general framework WMMSE-GDSB (GF-WMMSE-GDSB).

In the algorithm, we first solve for the power matrix and then for the transmit matrices. In lines 3 and 4 we calculate the per-tone penalties and the  $\mathbf{S}_n^k$  matrix for all tones and users. The interference plus noise covariance matrix is given by (5.2.2).

In line 7 we solve for  $p_n^k$  for a given Lagrange multiplier. As mentioned in Chapter 3 and also earlier in this chapter, this can be done by solving a polynomial and picking the largest root. Other possibilities include using the power method or the Newton method. The next step in the algorithm is to adjust the Lagrange multiplier so that the PCs are satisfied.

The next step is to solve for the matrices  $\mathbf{T}_n^k$  for fixed  $\mathbf{P}$ . As mentioned before, this implies solving  $K$  problems with fixed PCs, one for each tone. We solve first for  $\mathbf{R}_n^k$  and for  $\mathbf{W}_n^k$  in lines 13-14. The loop that follows calculates  $\mathbf{T}_n^k$  with (5.13) and finds the appropriate Lagrange multiplier. We remark that when solving for  $\mathbf{T}_n^k$ , we are solving a problem with an equality constraint given by  $\text{tr}\{\mathbf{T}_n^k(\mathbf{T}_n^k)^H\} = p_n^k$ . This means that the Lagrange multipliers  $\mu_n^k$  can be negative.

The computational complexity of the proposed algorithm is estimated as follows: The computational complexity of the spectrum coordination part is

---

**GF-WMMSE-GDSB**


---

```

1 Initialize  $\mathbf{T}_n^k \forall n, k$  and  $\mathbf{P}$ ;
2 repeat
3   Calculate  $\tau_n^k$  with (5.15)  $\forall n, k$ ;
4   Calculate  $\mathbf{S}_n^k \triangleq (\overline{\mathbf{T}}_n^k)^H (\tilde{\mathbf{H}}_{n,n}^k)^H (\mathbf{M}_n^k)^{-1} \tilde{\mathbf{H}}_{n,n}^k \overline{\mathbf{T}}_n^k \forall n, k$ ;
5   for  $n = 1, \dots, N$  do
6     repeat
7       Solve (5.14) to obtain  $p_n^k$ ;
8       if  $\sum_k p_n^k > P_n^{\max}$  then
9         | increase  $\lambda_n$ ;
10      else
11        | decrease  $\lambda_n$ ;
12    until  $\lambda_n |\sum_k p_n^k - P_n^{\max}| < \epsilon$ 
13   Calculate  $\mathbf{R}_n^k$  with (5.6)  $\forall n, k$ ;
14   Calculate  $\mathbf{W}_n^k$  with (5.11)  $\forall n, k$ ;
15   for  $n = 1, \dots, N$  do
16     for  $k = 1, \dots, K$  do
17       repeat
18         Calculate  $\mathbf{T}_n^k$  with (5.13);
19         if  $\text{tr}\{\mathbf{T}_n^k (\mathbf{T}_n^k)^H\} > p_n^k$  then
20           | increase  $\mu_n^k$ ;
21         else
22           | decrease  $\mu_n^k$ ;
23       until  $|\text{tr}\{\mathbf{T}_n^k (\mathbf{T}_n^k)^H\} - p_n^k| < \epsilon$ 
24 until convergence

```

---

dominated by the calculation of  $\tau_n^k$ . For each user, the calculation of  $\tau_n^k$  for one user entails complexity of the order  $K^2 N (A_n)^3$ , where the term  $(A_n)^3$  is due to matrix inversions and multiplications. This should be repeated for all users, which implies a complexity of  $O(K^2 N^2 \max_n((A_n)^3))$ . For the special case of synchronous transmission, this is reduced to  $O(KN^2 \max_n((A_n)^3))$ . Computational complexity of the signal coordination part is dominated by the calculation of  $\mathbf{T}_n^k$ . For one user, calculation of this matrix entails complexity of the order of  $K^2 N (A_n)^3$ . This should be repeated for all users, which implies a complexity of  $O(K^2 N^2 \max_n((A_n)^3))$ . For the special case of synchronous transmission this is reduced to  $O(KN^2 \max_n((A_n)^3))$ .

The algorithm has been extensively experimented with and has always been observed to produce a monotonically increasing objective function. Hence it

has always been observed to converge. Because we are explicitly solving the stationary conditions of the problem, at convergence we reach at least a local optimum of the problem.

We remark that the GF-WMMSE-GDSB generalizes some established previously proposed algorithms, most of them being well-known in the field and some of them with proved convergence. For the synchronous DMT SISO IC case, the proposed algorithm is equivalent to the DSB [96]. For the asynchronous DMT SISO IC case, it boils down to the MIW [109]. For synchronous DMT MIMO IC, it is equivalent to the algorithm in Chapter 3. For the MIMO IC and MIMO BC, it is equivalent to the algorithms in [22, 83].

We also remark that the DMT-WMMSE algorithm proposed in Chapter 3 could be eventually used for the same purpose of the GF-WMMSE-GDSB. The difference between these two algorithms is that, in the former, signal and spectrum coordination are done jointly, while for the later the two types of coordination are done iteratively. Although the two algorithms have similar performance, in this chapter we opt for the GF-WMMSE-GDSB for two reasons. First, it is observed from experiments that the GF-WMMSE-GDSB converges in a significantly smaller number of iterations, which leads in most scenarios to lower time complexity. Second, these two algorithm can possibly be implemented with message passing between users. Given the large number of iterations needed for the DMT-WMMSE to converge, a higher price is paid for such message passing, which in practice means a higher share of channel capacity sacrificed for the sake of messages.

## 5.4 Simulation Results

### 5.4.1 Downstream ADSL

The first of our simulation scenarios is the ADSL downstream near-far scenario shown in Fig. 5.5. There are in total five users, each with two transceivers (two direct modes), i.e.  $A_n = 2 \forall n$ . Referring to the figure, we define the line lengths in the vector  $\mathbf{l} = [l_1 \dots l_5]^T$ . We similarly define  $\mathbf{d} = [d_1 \dots d_5]^T$ . The channel gains are calculated according to the model of [92]. The system has cables of 0.5 mm (AWG 24) and an SNR gap of 12.8 dB. Carrier spacing is given by  $\Delta_f = 4.3125$  kHz and the symbol rate is 4 KHz. Each user has a PC of 23.4 dBm. For each line, noise model ANSI A is adopted.

Our aim is to assess the impact of asynchronous transmission in the performance of our algorithm. Towards this end, we do three experiments with this scenario. In the three of them we simulate a MIMO IC, i.e.

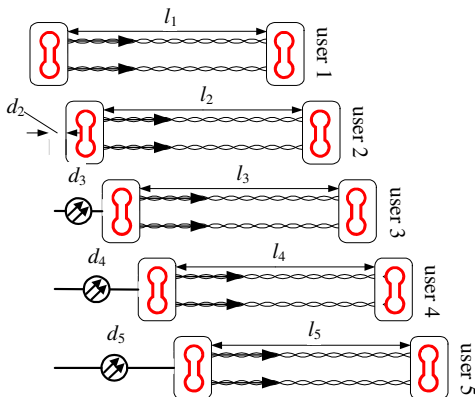


Figure 5.5: Downstream ADSL scenario.

$\mathcal{G}_n^{\text{tx}} = \mathcal{G}_n^{\text{rx}} = \{n\}$ ,  $n = 1, \dots, 5$  with both synchronous and asynchronous transmission.

In the first experiment, we keep only users 1 and 2 active. We use an offset  $\beta_{1,2} = \beta_{2,1} = 0.5$ . We set  $\mathbf{l} = [4 \ 3]^T$  km and  $\mathbf{d} = [0 \ 3]^T$  km. In this scenario the user with the short lines has to avoid excessive interference to the user with the long lines. By changing the values of the user weights  $w_n$ , we find the two rate regions for the synchronous and asynchronous cases with the GF-WMMSE-GDSB. They can be seen in Fig. 5.6. We notice that the asynchronous transmission incurs a rate loss of up to 10 %.

In the second experiment, we want to assess the rate loss incurred by asynchronous transmission as the number of users in the network increases. Referring to Fig. 5.5, we set  $\mathbf{l} = [4 \ 3.75 \ 3.5 \ 3.25 \ 3]^T$  km and  $\mathbf{d} = [0 \ 2.25 \ 2.5 \ 2.75 \ 3]^T$  km. We simulate the scenario four times, first with users 1 and 2 active, then users 1, 2 and 3 active, etc. We set  $w_1 = 0.8$  and set the remaining weights to be of equal values (they sum to 1 at the end)—given that user 1 suffers more from crosstalk, we assign higher preference to it.. The result of this experiment is depicted in Fig. 5.7, where we show the number of active users versus the WRS for the GF-WMMSE-GDSB for both synchronous and asynchronous cases. Not surprisingly, asynchronous transmission takes a greater toll on the capacity of the network as the number of users increases. For example, the difference in WRS between synchronous and asynchronous cases for two active users is 0.2 Mbps. For 5 active users, this value is more than 5 times greater.

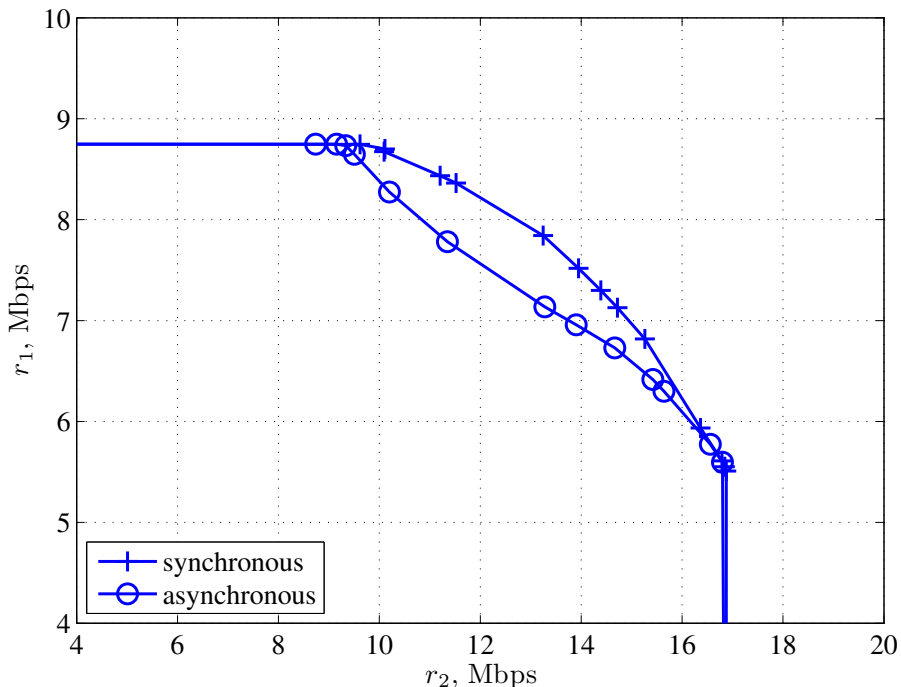


Figure 5.6: Rate region for the downstream ADSL scenario with two active users. Referring to Fig. 5.5, we use  $\mathbf{l} = [4 \ 3]^T$  km and  $\mathbf{d} = [0 \ 3]^T$  km.

In the third experiment, we go back to only two active users. This time we do a Monte-Carlo simulation in order to assess the impact of asynchronous transmission in different instantiation of the network. Referring to Fig. 5.5, we define  $l_1 = \text{unif}(4, 6)$  km,  $l_2 = \text{unif}(4, 6)$  km and  $d_2 = \text{unif}(3, l_1)$  km. Here we define  $\text{unif}(a, b)$  to be a uniformly distributed random variable between  $a$  and  $b$ . We also set  $\beta_{1,2} = \beta_{2,1} = 0.5$ . We simulate the GF-WMMSE-GDSB for both synchronous and asynchronous transmission for 100 instantiations of this scenario. For every scenario, we set the user weights as  $w_1 = 0.8$  and  $w_2 = 0.2$ —given that user 1 suffers more from crosstalk, we assign higher preference to it. We plot the histogram of the variable  $(\text{WRS}_{\text{syn}} - \text{WRS}_{\text{asyn}})/\text{WRS}_{\text{syn}}$  in Fig. 5.8. In this simulation we see that the impact of asynchronous transmission can be up to 7 %. Here we see the effectiveness of the GF-WMMSE-GDSB algorithm in the asynchronous case. In 45 % of the cases, there is almost no rate loss in relation to the synchronous case.

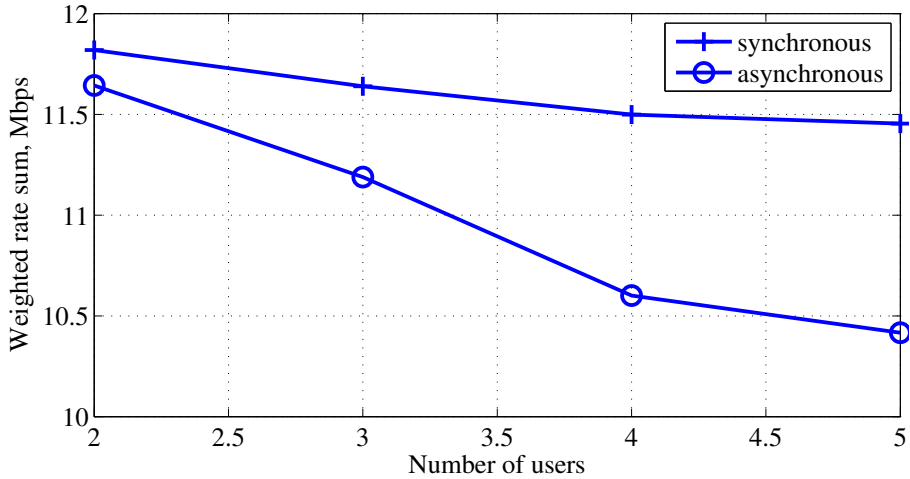


Figure 5.7: Weighted rate sum vs. number of active users for the GF-WMMSE-GDSB algorithm for both synchronous and asynchronous cases. Referring to Fig. 5.5, we set  $\mathbf{l} = [4 \ 3.75 \ 3.5 \ 3.25 \ 3]^T$  km and  $\mathbf{d} = [0 \ 2.25 \ 2.5 \ 2.75 \ 3]^T$  km.

### 5.4.2 Upstream G.fast

We simulate the upstream G.fast scenario depicted in Fig. 5.9. Here, there are 8 users. The 6 users at the top of the figure have each two transceivers, while the two users at the bottom of the figure have each 4 transceivers (all direct modes). We use a maximum power of 4 dBm for each transceiver, which means that the users with two transceivers have a PC of 7 dBm and the users with 4 transceiver have a PC of 10 dBm. The SNR gap is set to 9.45 dB, the carrier spacing is 51.75 KHz and the symbol rate is 48 KHz. The bandwidth of the G.fast standard starts at 2.2 MHz and goes up to 106 MHz—there is a total of  $K = 2047$  tones. For this scenario, we use measured channels.

For this experiment, we are interested in assessing the impact of added coordination on the receiver side. There is already some coordination on the transmitter side between the different transceivers of the users. We first simulate an *IC*, i.e. the situation when there is only one user in every group on both sides of the network. As mentioned before, this is the situation with the minimum amount of inter-user coordination. We also simulate a *partial MAC*, where there are three groups on the receiver side, as follows:  $\mathcal{G}_1^{\text{rx}} = \{1, 2, 3\}$ ,

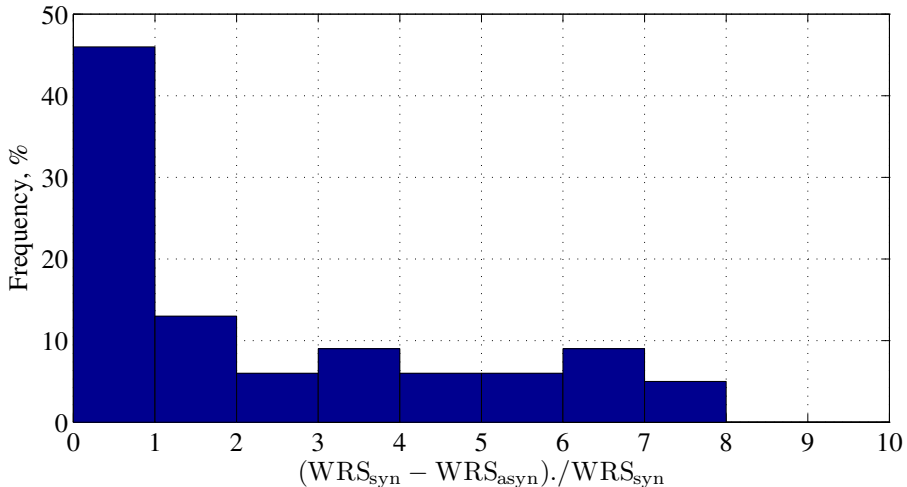


Figure 5.8: Histogram for the downstream ADSL scenario with two active users.. Referring to Fig. 5.5, we set  $l_1 = \text{unif}(4, 6)$  km,  $l_2 = \text{unif}(4, 6)$  km and  $d_2 = \text{unif}(3, l_1)$  km.

$\mathcal{G}_2^{\text{rx}} = \{4, 5, 6\}$  and  $\mathcal{G}_1^{\text{rx}} = \{7, 8\}$ . This grouping could for example indicate that the grouped users belong to the same service provider. Other possibilities would be a sub-loop unbundled scenario, where it is typical to have only a fraction of the end-customers on the signal coordination group or simply that grouped users are all connected to the same box on the CO side of the network. Lastly, we simulate a *full MAC*, i.e. with full receiver coordination. In this case, there is one group on the receiver side, i.e.  $\mathcal{G}_1^{\text{rx}} = \{1, \dots, 8\}$ . In Fig. 5.10, we depict these three respective rate regions. For these rate regions, we always set  $w_1 = w_2 = w_3 = w_4$  and  $w_5 = w_6 = w_7 = w_8$ . By changing the weights, we map the rate regions.

It should come as no surprise that more coordination translates into larger data rates. We remark that signal coordination over all the transceivers provides a substantial improvement compared to partial signal coordination.

In order to be able to assess the performance of our proposal, we also simulate previous solutions. Specifically, we simulate the DSB algorithm [96], the ZF algorithm [13, 14] and the SVD algorithm [47]. We details the implementation of these solutions in the following paragraphs.

The DSB algorithm is a pure spectrum coordination algorithm. It restricts  $\mathbf{R}_n^k$

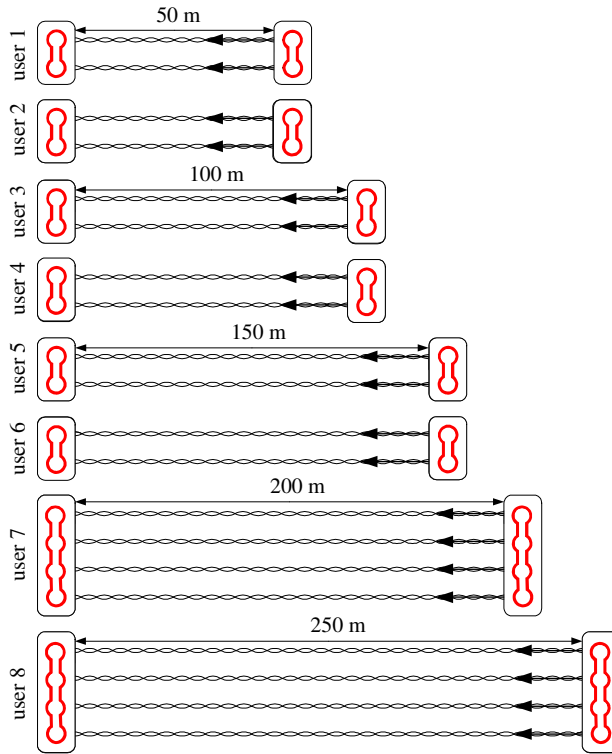


Figure 5.9: Upstream G.fast scenario. Here we show the IC scenario.

and  $\mathbf{T}_n^k$  to be diagonal. The DSB algorithm does not exploit the intra-user coordination that is possible in this scenario, and it performs poorly.

The ZF algorithm sets  $\mathbf{R}_n^k = (\tilde{\mathbf{H}}_{n,n}^k)^{-1}$  and restricts  $\mathbf{T}_n^k$  to be diagonal. To calculate the diagonal elements of  $\mathbf{T}_n^k$ , it performs power loading on the transmitter side with a waterfilling algorithm. We run the ZF algorithm for the IC and the full MAC cases—notice that for the partial MAC case the matrices  $\tilde{\mathbf{H}}_{n,n}^k$  are not square, so they have no inverse. For the IC case, inter-user interference is considered Gaussian noise. In this case, the ZF algorithm performs poorly because inter-user interference is unaccounted for. For the full MAC case, the ZF algorithm performs almost optimally. Still the use of ZF receivers causes noise enhancement, which translates itself in a slight rate loss in comparison to the GF-WMMSE-GDSB.

The SVD algorithm sets  $\mathbf{R}_n^k = (\mathbf{U}_{n,n}^k)^H$  and  $\mathbf{T}_n^k = \mathbf{V}_n^k$ , where  $\mathbf{U}_n^k$  and  $\mathbf{V}_n^k$  are



maximization problem in a multi-user system. Our framework includes systems with any number of users, any number of transceivers, any number of tones, any kind of coordination on both the transmitter and on the receiver sides, and synchronous or asynchronous transmission. In what concerns the coordination, we construct channel matrices from all transmitters to all receivers that have as building blocks the channel matrices relating to the MIMO IC and that depend on the kind of coordination on the transmitter and receiver sides. The algorithm divides the problem into two parts, one dealing with the spectrum coordination (i.e. power allocation) and the other dealing with signal coordination (i.e. the spatial separation typical of MIMO systems).

Some extensions that would be interesting to explore would be per-transceiver PCs and non-linear receivers. Per-transceiver PCs are the focus of Chapter 4 in this thesis. They are more realistic than the per-user PCs used in this chapter, but they also lead to more complex problems.

## Chapter 6

# Conclusion

The broadband access market is evolving fast. Optical fiber is expanding in a steady rhythm towards the CPEs, new DSL standards are being developed and research on DSM has gained momentum in the past decade. It is difficult to predict how this huge market will evolve in the coming decades. However, whatever broadband access turns into, for the next couple of decades DSL looks like a safe bet.

Mainly due to the ubiquitousness of the telephone network, DSL has had a head start in the competition in the sense that most of the infrastructure needed for this technology is already in place for hundreds of millions of users. DSL has been able to make good profit of this head start, and is currently the market leader by some margin.

DSL's demise has been predicted a number of times. In the past, it was expected that optical fiber would connect the users directly to the network backbone, thus rendering DSL obsolete. Contrary to these predictions, DSL stubbornly continues not only to dominate the market but also to grow faster than the competition. The continuation of this dominance in the future hinges a lot on the adaptability of DSL standards for the next generation of broadband access. This adaptability involves two factors.

First, new DSL standards suited to operate on shorter lines should be developed. As the fiber network expands, DSL technology will be responsible to bridge a short distance between the last fiber-fed terminal and the user. DSL standards are evolving accordingly. VDSL is designed to connect users from a fiber-fed

cabinet. The G.fast standard is now under development, and it is expected to operate on lines that are up to couple of hundred meters long. The joint operation of fiber-DSL looks to be a very promising and cost-effective way to deliver high quality broadband to a mass market.

The second factor is the intelligent management of multi-user interference, i.e. crosstalk. The techniques to deal with crosstalk are collectively known as dynamic spectrum management (DSM), and they are the unifying topic on this thesis. With the use of signal and spectrum coordination, DSM techniques intelligently use the power, frequency and space dimensions in the multi-user DSL channel to significantly increase performance. The gains in performance achieved with leave network operators and users salivating.

In this thesis, we focus on this second factor. We develop state-of-the-art DSM techniques that use both signal and spectrum coordination. These techniques have low complexity, are practical and provide excellent gains in performance.

With these two factors evolving hand in glove, DSL is perfectly poised to continue to be a major player in the broadband market. The technology is thus a safe bet. It is after all possible to achieve something in the neighborhood of 1 Gb/s on short DSL lines, i.e. the same data rate as some fiber connections. If such data rates are possible, in the next decades many users and service providers will wonder why switch to FTTH at all.

The main contributions of this thesis are:

### **The development of two algorithms that use spherical coordinates for the spectrum coordination problem.**

In Chapter 2, spherical coordinates are used to represent the power allocation vectors for every tone of the spectrum coordination problem, whereas the classical way to do so is with a Cartesian vector. The use of spherical coordinates allows us to find a surprising amount of structure in the problem, which we use in two algorithms. In the first proposed algorithm, called OSB-SC, we exploit concavity in the radial dimension to reduce the computational complexity in a very significant way. When comparing the OSB-SC to the relevant previous algorithm, the OSB, we find that the OSB-SC can be up to 60 times faster. As a welcome bonus, we find that the OSB-SC is more precise in its power allocation than the OSB.

The second algorithm, called TaSSO, uses spherical coordinates in taxicab geometry. This coordinate system makes it easier to solve the problem in a block coordinate descent method, where we first solve for the radius and subsequently solve for each of the angles. This algorithm uses structure in

three ways. First, the problem is concave on the radial dimension. Second, there is some limited structure to be found on the angle dimensions. In this thesis, we have established sufficient conditions for the problem to be convex and concave in each of the angle dimensions. And, third, after the solution for the radius there is a sum power constraint for every tone. When solving for a given angle, it can be that this sum power is already exhausted. We see from the experiments that TaSSO can be from 2-15 times faster than the previously proposed ISB.

Of the three ways we exploit structure in TaSSO, we believe that the second (i.e. the structure in the angle dimensions) is both the most important and the most surprising. It is the most important because we see from the experiments that it is the one that accounts for the largest savings in computational complexity. It is the most surprising because it conveys the message that the spectrum coordination problem has more structure than we previously imagined.

With this facts in hand, we believe that spherical coordinates provide a better way to represent the spectrum coordination problem than Cartesian coordinates. Spherical coordinates are used extensively in Physics in, for example, electromagnetics because they provide an easier and more economic way of representing some situations. For the spectrum coordination problem, we believe something similar happens. Spherical coordinates make it possible to easily uncover hidden structure that helps us solve the problem in a much more efficient way.

### **The development of algorithms that use combined signal and spectrum coordination for the DMT MIMO IC**

Research in DSM has been classically divided in signal and spectrum coordination. Both these directions evolved rapidly in the last 10-15 years. However most of the progress has been in parallel, with only timid attempts at combining the two types of coordination. In Chapter 3, we focus on a scenario that we call DMT MIMO IC. In this scenario a users has a set of transceivers to which it can apply two-sided signal coordination. However, signal coordination among all users in the cable binder is not possible. In this scenario, coordination involves both the signal and the spectrum levels.

We propose two algorithms for the weighted rate sum maximization problem in the DMT MIMO IC. In the first one, called DMT-WMMSE, we build on the recently suggested equivalence between the weighted rate sum maximization problem and the weighted minimum mean squared error (WMMSE) minimization problem for the (single tone) MIMO IC. We show that a simple adjustment on the single tone algorithm is sufficient to adapt it to the multitone case. The

resulting multitone algorithm solves the signal and spectrum coordination parts of the problem simultaneously and is guaranteed to reach a stationary point. We remark our paper [64] was one of the first to correctly adapt the initial idea of Ref. [22] to the MIMO IC case.

In the second algorithm, called WMMSE-GDSB, we separate the signal and spectrum coordination parts and solve each of them independently. The advantage here is that many options are possible for solving these two separate parts. We end up with many independent single tone MIMO IC's. In this way, we can rely on previous work on this topic and select any of the available solutions. For the spectrum coordination part, one of the interesting outcomes of our analysis is a generalization of the distributed spectrum balancing (DSB) power allocation formula for the DMT MIMO IC scenario. We show that the power allocation equation is a generalization of the waterfilling formula, but, in contrast to the classical waterfilling, there is a penalty for causing too much interference to other users and the matrix structure of the problem is taken into account. We also show some sufficient conditions for convergence of the WMMSE-GDSB.

Simulation results show good performance with both algorithms. We notice, however, that the WMMSE-GDSB converges much faster.

### **The development of algorithms that use combined signal and spectrum coordination for the DMT MIMO IC with per-transceiver power constraints**

In Chapter 4 we focus again on the DMT MIMO IC, but this time we use per-transceiver PCs. The optimization problem with per-transceiver PCs is more difficult than the one with per-user PCs in Chapter 3. There are more variables and more constraints to be satisfied. We adapt the two algorithms proposed in Chapter 3 to the per-transceiver PC case. First, we derive a new version of the DMT-WMMSE algorithm. The difference with the algorithm with per-user PCs proposed in Chapter 3 is that several Lagrange multipliers have to be found simultaneously. Second, we derive an adaptation of the WMMSE-GDSB algorithm. For the spectrum coordination part, we observe that a simple extension of the algorithm presented in Chapter 3 fails to produce a functioning algorithm. We propose to optimize the power allocation of all the transceivers of user  $n$  on tone  $k$  by first doing a change of variables. We represent the power allocation for the different transceivers of a given user with spherical coordinates in taxicab geometry. This coordinate system allows us to exploit structure on the radial dimension and solve the angles iteratively and sequentially. Simulation results show good performance with the two proposed

algorithms. The WMMSE-GDSB again has an advantage in that it is seen to converge much faster than the DMT-WMMSE.

### **Development of a unified framework and algorithm for the a general situation that includes everything as a special case**

Even if the DMT MIMO IC is an interesting scenario that should be very often found in the field, it does not capture the whole complexity of DSL networks. In Chapter 5, we develop a general system framework that includes every other previously studied situation as a special case. We also accurately model asynchronous transmission for the MIMO case. We propose an algorithm, called GF-WMMSE-GDSB, that works for all cases, including any number of users, any number of transceivers, any number of tones, any kind of coordination on both the transmitter and on the receiver sides, and synchronous or asynchronous transmission. Simulation results show that performance is excellent and computational complexity is polynomial.

## **Further research**

This thesis leaves space for many improvements. We now outline some directions for future research.

### **Search for further structure with spherical coordinates**

In Chapter 2 we found a surprising amount of structure on the spectrum coordination problem with the use of spherical coordinates. However, we probably do not exploit all structure there is. The regions of concavity and convexity obtained with Propositions 2.3 and 2.4 are quite large, but they do not cover the whole “real” regions. Easy to compute larger regions are an interesting direction for future research. Also, we remark that in this thesis we did not focus on *joint* concavity or convexity between angles. To establish joint concavity/convexity, we would need to look at the Hessian matrix. Perhaps there is also some structure to be found there.

### **DC programming with spherical coordinates**

Previous work has focused on branch-and-bound algorithms for spectrum coordination in DSL. Branch-and-bound uses the difference of convex (DC)

structure of the spectrum coordination problem. In [100, 108], algorithms are provided that reach the same results as the OSB with much smaller computational complexity. The DC structure can probably be used with spherical coordinates as well. Because of the concavity in the radial dimension, an algorithm exploiting the DC structure with spherical coordinates could theoretically be faster than the ones in [100, 108], which use Cartesian coordinates.

### **Use of different algorithms for the signal coordination part in the DMT MIMO IC**

In Part II of this thesis, we have used the WMMSE algorithm to compute the transmit matrices in the DMT MIMO IC weighted rate sum maximization problem in the WMMSE-GDSB algorithm. There are other interesting options as well that deserve to be investigated. For example, the concept of interference alignment (IA) has recently been proposed for the MIMO IC. IA algorithms have no direct way to distribute power through a multitone channel, so they should make a good pair with the GDSB.

### **Non-linear transmitters and receivers**

In Part II of this thesis, we focused on MIMO transmission in a multi-user channel. Throughout this thesis, we have only focused on linear transmitters and receivers. Another interesting direction for research is the inclusion of non-linear transmitters and receivers. These can be combined with the linear strategies we use in this thesis and can theoretically provide more gains in performance.

# Appendix A

## Appendices to Chapter 2

### A.1 $N$ -dimensional Sphere Formulas

To re-write  $\mathbf{p}^k \in \mathbb{R}^N$  as (2.6) for the general case, we write  $\mathbf{p}_n^k = \rho_n^k \mathbf{d}_n^k$ , where

$$d_1^k = \prod_{j=1}^{N-1} \cos \theta_{[j]}^k \quad (\text{A.1})$$

$$d_i^k = \prod_{j=1}^{N-i} \cos \theta_{[j]}^k \sin \theta_{[N-i+1]}^k, \quad i = 2, \dots, N-1 \quad (\text{A.2})$$

$$d_N^k = \sin \theta_{[1]}^k \quad (\text{A.3})$$

Here  $\theta_{[i]}^k \in [0, \pi/2]$ ,  $i = 1, \dots, N-1$ .

To re-write  $\mathbf{p}^k$  as (2.17) for the general case, we have  $\mathbf{p}^k = \eta^k \mathbf{v}^k$ , where

$$v_1^k = \prod_{j=1}^{N-1} (1 - \phi_{[j]}^k) \quad (\text{A.4})$$

$$v_i^k = \prod_{j=1}^{N-i} (1 - \phi_{[j]}^k) \phi_{[N-i+1]}^k, \quad i = 2, \dots, N-1 \quad (\text{A.5})$$

$$v_N^k = \phi_{[1]}^k \quad (\text{A.6})$$

Here  $\phi_{[i]}^k \in [0, 1]$ ,  $i = 1, \dots, N-1$ .

Transforming between Cartesian coordinates on the one hand and  $N$ -spherical coordinates in both Euclidean and taxicab geometry on the other hand is straightforward in both directions.

## A.2 Proof of Proposition 2.2

To arrive at (2.14) and (2.15), we consider  $Q$  even. Without loss of generality, we consider  $\bar{P}^{\min} = 0$ . For (2.14), we decorrelate the per-tone variables. We can then focus on the point  $\mathbf{y} = [0 \ 0]^T$  and the area enclosed by the dotted square close to it. See Fig. 2.2 for an illustration. Eq. (2.14) becomes

$$\mathbb{E} [d_{\text{points}}^2] \leq \mathbb{E} \left[ \frac{1}{K} \sum_{k \in \mathcal{K}} (\bar{p}_1^k)^2 + (\bar{p}_2^k)^2 \right] = 2\mathbb{E} [(\bar{p}_1^1)^2] = \frac{\bar{P}}{6(Q-1)^2} \quad (\text{A.7})$$

Here, we use the fact that the decorrelated per-tone random variables are equally distributed. We can calculate the expected value in  $\bar{p}_1^1$  and multiply it by 2. The variable  $\bar{p}_1^1$  is uniformly distributed in  $(0, \bar{P}/2(Q-1))$ . Reaching (A.7) is then straightforward.

To arrive at (2.15), we define

$$G(\mathbf{d}, \bar{\mathbf{p}}^k) = \left\| (\mathbf{d}^T \bar{\mathbf{p}}^k) \mathbf{d} - \bar{\mathbf{p}}^k \right\|_2^2 = (\bar{\mathbf{p}}^k)^T \bar{\mathbf{p}}^k - \mathbf{d}^T \bar{\mathbf{p}}^k (\bar{\mathbf{p}}^k)^T \mathbf{d} \quad (\text{A.8})$$

and

$$\mathbb{E} [d_{\text{lines}}^2] = \mathbb{E} \left[ \frac{1}{K} \sum_{k \in \mathcal{K}} \min_{\mathbf{d} \in \mathcal{D}} G(\mathbf{d}, \bar{\mathbf{p}}^k) \right] \quad (\text{A.9})$$

In (A.8), we use  $\|\mathbf{d}\|_2^2 = \mathbf{d}^T \mathbf{d} = 1$ . The most important steps in the derivation are shown in (A.10)-(A.15).

$$\mathbb{E} [d_{\text{lines}}^2] = \underbrace{\int \cdots \int}_{\mathcal{R}_1} \underbrace{\int \cdots \int}_{\mathcal{R}_2} \frac{1}{K} \left( \sum_{k \in \mathcal{K}} \min_{\mathbf{d} \in \mathcal{D}} G(\mathbf{d}, \bar{\mathbf{p}}^k) \right) f(\bar{\mathbf{p}}_1) f(\bar{\mathbf{p}}_2) d\bar{\mathbf{p}}_1 d\bar{\mathbf{p}}_2 \quad (\text{A.10})$$

$$< \frac{1}{\bar{P}^{2K}} \int_{\bar{p}_1^1=0}^{\bar{P}} \cdots \int_{\bar{p}_1^K=0}^{\bar{P}} \int_{\bar{p}_2^1=0}^{\bar{P}} \cdots \int_{\bar{p}_2^K=0}^{\bar{P}} \frac{1}{K} \left( \sum_{k \in \mathcal{K}} \min_{\mathbf{d} \in \mathcal{D}} G(\mathbf{d}, \bar{\mathbf{p}}^k) \right) d\bar{\mathbf{p}}_1 d\bar{\mathbf{p}}_2 \quad (\text{A.11})$$

$$= \frac{1}{\bar{P}^{2K} K} \int_{r^1 \in \mathcal{A}^1} \int_{\theta^1=0}^{\pi/2} \cdots \int_{r^K \in \mathcal{A}^K} \int_{\theta^K=0}^{\pi/2} \left( \sum_{k \in \mathcal{K}} \min_{\mathbf{d} \in \mathcal{D}} G(\mathbf{d}, r^k, \theta^k) \right) \prod_{k \in \mathcal{K}} r^k dr d\theta \quad (\text{A.12})$$

$$= \frac{1}{\bar{P}^{2K} K} \sum_{k \in \mathcal{K}} \int_{r^1 \in \mathcal{A}^1} \int_{\theta^1=0}^{\pi/2} \cdots \int_{r^K \in \mathcal{A}^K} \int_{\theta^K=0}^{\pi/2} \min_{\mathbf{d} \in \mathcal{D}} G(\mathbf{d}, r^k, \theta^k) \prod_{j \in \mathcal{K}} r^j dr d\theta \quad (\text{A.13})$$

$$= \frac{1}{\bar{P}^2} \int_{r \in \mathcal{A}} \int_{\theta=0}^{\pi/2} \min_{\mathbf{d} \in \mathcal{D}} G(\mathbf{d}, r, \theta) r dr d\theta$$

$$< \frac{2}{A} \sum_{i=0}^{Q-2} \int_{r=0}^{\bar{P} \cos^{-1}((i+1)\pi/4(Q-1))} \int_{\theta=i\pi/4(Q-1)}^{(i+1)\pi/4(Q-1)} \min_{\mathbf{d} \in \mathcal{D}} G(\mathbf{d}, r, \theta) r dr d\theta \quad (\text{A.14})$$

$$= \frac{2}{A} \sum_{i=0}^{Q-2} \int_{r=0}^{\bar{P} \cos^{-1}((i+1)\pi/4(Q-1))} \int_{\theta=0}^{\pi/4(Q-1)} r^3 \sin^2 \theta dr d\theta \quad (\text{A.15})$$

The expectation in (A.9) is written in integral form as (A.10). Here the sets  $\mathcal{R}_1$  and  $\mathcal{R}_2$  represent the hypervolumes where the integration takes place. They are defined as  $\mathcal{R}_n = \{[\bar{p}_n^1 \cdots \bar{p}_n^K] \mid \bar{p}_n^k \geq 0 \forall k \text{ and } \sum_{k \in \mathcal{K}} 10^{\bar{p}_n^k/10} \leq P^{\max}\}$ ,  $n = 1, 2$ . The pdf's are represented by  $f(\bar{\mathbf{p}}_1)$  and  $f(\bar{\mathbf{p}}_2)$ . Also  $d\bar{\mathbf{p}}_n = d\bar{p}_n^1 \cdots d\bar{p}_n^K$ .

In the whole derivation, we do two relaxations. The first is that we decorrelate the per-tone variables, i.e. we define  $f(\bar{p}_n^k) = \text{unif}(0, \bar{P}) \forall n, k$  and  $\bar{P} = 10 \log_{10} P^{\max}$ . The corresponding integral is shown in (A.11). In (A.12), we change to spherical coordinates, i.e.  $\bar{p}_1^k = r^k \cos \theta^k$  and  $\bar{p}_2^k = r^k \sin \theta^k$ . We define

$$G(\mathbf{d}, r^k, \theta^k) = (r^k)^2 \left( 1 - \mathbf{d}^T \begin{bmatrix} \cos^2 \theta^k & \cos \theta^k \sin \theta^k \\ \cos \theta^k \sin \theta^k & \sin^2 \theta^k \end{bmatrix} \mathbf{d} \right) \quad (\text{A.16})$$

We write the integral in  $r^k$  in the area defined by  $\mathcal{A}^k = \{r^k | 0 \leq \theta^k \leq \frac{\pi}{2}, r^k = \min(\bar{P}(\cos \theta^k)^{-1}, \bar{P}(\sin \theta^k)^{-1})\}$  and  $d\mathbf{r}$  and  $d\boldsymbol{\theta}$  are defined similarly to  $d\bar{\mathbf{p}}_n$ . In (A.13), we put the summation in  $k$  outside the integrals and notice that, since now the tones are uncorrelated, for a given tone  $k$ , we can integrate in  $j$ ,  $j \neq k$  easily. After that, we arrive at the left hand side of (A.14). Here the superscripts are no longer necessary, so we omit them.

From the left hand side of (A.14) to the right hand side of (A.14), we do a second relaxation. The integration on the region  $\mathcal{A}$  is too difficult, so we extend it to include more points in the radial direction. The region we integrate on is denoted  $\mathcal{A}'$  and is given by  $\mathcal{A}' = \mathcal{A}_1 \cup \mathcal{A}_2$

$$\mathcal{A}_1 = \bigcup_{i=0}^{Q-2} \left\{ r, \theta \left| \frac{i\pi}{4(Q-1)} \leq \theta \leq \frac{(i+1)\pi}{4(Q-1)} \right., \right. \\ \left. r = \bar{P} \cos^{-1} \left( \frac{(i+1)\pi}{4(Q-1)} \right) \right\}$$

$$\mathcal{A}_2 = \bigcup_{i=0}^{Q-2} \left\{ r, \theta \left| \frac{\pi}{4} + \frac{i\pi}{4(Q-1)} \leq \theta \leq \frac{\pi}{4} + \frac{(i+1)\pi}{4(Q-1)} \right., \right. \\ \left. r = \bar{P} \sin^{-1} \left( \frac{\pi}{4} + \frac{i\pi}{4(Q-1)} \right) \right\}.$$

We illustrate this region in Fig. 2.2. It consists of the union of the angular sectors with angular width of  $\pi/4(Q-1)$ . The radii increase as we approach  $\pi/4$ . Notice that, as far as the integrals are concerned, the regions  $\mathcal{A}_1$  and  $\mathcal{A}_2$  are the same. We can thus integrate in  $\mathcal{A}_1$  and multiply the result by 2. This is what is shown in the right hand side of (A.14). The variables  $r$  and  $\theta$  are uniformly distributed in  $\mathcal{A}'$ , so their joint pdf is given by  $f(r, \theta) = 1/A$ , where

$$A = \frac{\pi \bar{P}^2}{4(Q-1)} \sum_{i=0}^{Q-2} \cos^{-2} \left( \frac{(i+1)\pi}{4(Q-1)} \right). \quad (\text{A.17})$$

To arrive at (A.15), we notice that all segments have the same volume if they have the same radius. To make the calculations easier, we consider the segment close to  $\mathbf{d} = [1 \ 0]^T$  (i.e.  $0 \leq \theta \leq \pi/4(Q-1)$ ) and calculate the integral repeatedly for different values of the radius. We thus re-write (A.16) as  $G(\mathbf{d}, r, \theta) = r^2 \sin^2 \theta$ . In (A.15), we see that

$$\int_{\theta=0}^{\pi/4(Q-1)} \sin^2 \theta d\theta = \frac{\pi}{8(Q-1)} - \frac{1}{4} \sin \left( \frac{\pi}{2(Q-1)} \right) \quad (\text{A.18})$$

and

$$\sum_{i=0}^{Q-2} \int_{r=0}^{\bar{P} \cos^{-1}\left(\frac{(i+1)\pi}{4(Q-1)}\right)} r^3 dr = \frac{\bar{P}^4}{4} \sum_{i=0}^{Q-2} \cos^{-4}\left(\frac{(i+1)\pi}{4(Q-1)}\right). \quad (\text{A.19})$$

By substituting (A.17), (A.18) and (A.19) in (A.15), we complete the proof.

### A.3 Proof of Propositions 2.3 and 2.4

In this appendix, we drop the superscript  $k$  for the sake of conciseness. We first establish some properties related to  $a_n$ ,  $D_n$ ,  $c_n$  and  $F_n$ , all of them consequences of the definition of these variables, as follows:

- (i)  $a_n \phi_{[i]} + D_n \geq 0$  and  $c_n \phi_{[i]} + F_n \geq 0$ ,  $\phi_{[i]} \in [0, 1] \forall n$ ;
- (ii)  $D_n \geq 0$  and  $F_n \geq 0 \forall n$ ;
- (iii)  $a_n + D_n \geq 0$  and  $c_n + F_n \geq 0 \forall n$
- (iv) either  $a_n/D_n = -1$  or  $a_n D_n = 0 \forall n$

Property (i) is due to the fact that by definition  $a_n \phi_{[i]} + D_n = \eta v_n^k$ , where the right hand side is non-negative. The same is valid for  $c_n \phi_{[i]} + F_n$ . Properties (ii) and (iii) are direct consequences of (i). Property (iv) is due to the fact that either  $a_n \phi_{[i]} + D_n = X(1 - \phi_{[i]})$  or  $a_n \phi_{[i]} + D_n = X\phi_{[i]}$ ,  $X$  is non-negative constant.

A sufficient condition for concavity of (2.21) in  $\phi_{[i]}$  is given by

$$\begin{aligned} \max_{\phi_{[i]} \in [0,1]} \left( \frac{\partial^2 L(\phi_{[i]}, \boldsymbol{\lambda})}{\partial(\phi_{[i]})^2} \right) &= \max_{\phi_{[i]} \in [0,1]} \left( \sum_{n \in \mathcal{N}} \frac{\partial^2 b_n}{\partial(\phi_{[i]})^2} \right) \leq \sum_{n \in \mathcal{N}} \max_{\phi_{[i]} \in [0,1]} \left( \frac{\partial^2 u_n b_n}{\partial(\phi_{[i]})^2} \right) \\ &= \sum_{n \in \mathcal{N}} \max \left( \frac{\partial^2 u_n b_n}{\partial(\phi_{[i]})^2}(0), \frac{\partial^2 u_n b_n}{\partial(\phi_{[i]})^2}(1) \right) \leq 0. \end{aligned} \quad (\text{A.20})$$

In the same vein, a sufficient condition for convexity of (2.21) in  $\phi_{[i]}$  is

$$\begin{aligned} \min_{\phi_{[i]} \in [0,1]} \left( \frac{\partial^2 L(\phi_{[i]}, \boldsymbol{\lambda})}{\partial(\phi_{[i]})^2} \right) &= \min_{\phi_{[i]} \in [0,1]} \left( \sum_{n \in \mathcal{N}} \frac{\partial^2 b_n}{\partial(\phi_{[i]})^2} \right) \geq \sum_{n \in \mathcal{N}} \min_{\phi_{[i]} \in [0,1]} \left( \frac{\partial^2 u_n b_n}{\partial(\phi_{[i]})^2} \right) \\ &= \sum_{n \in \mathcal{N}} \min \left( \frac{\partial^2 u_n b_n}{\partial(\phi_{[i]})^2}(0), \frac{\partial^2 u_n b_n}{\partial(\phi_{[i]})^2}(1) \right) \geq 0. \end{aligned} \quad (\text{A.21})$$

Define  $S_n(\phi_{[i]}) \triangleq \partial^2 u_n b_n / \partial (\phi_{[i]})^2 (\phi_{[i]})$ , and further define

$$S_n(\phi_{[i]}) = \frac{-u_n(a_n + c_n)^2}{\underbrace{((a_n + c_n)\phi_{[i]} + D_n + F_n)^2}_{\triangleq S_n^1(\phi_{[i]})}} + \frac{u_n(c_n)^2}{\underbrace{(c_n\phi_{[i]} + F_n)^2}_{\triangleq S_n^2(\phi_{[i]})}} \quad (\text{A.22})$$

To prove the equalities in (A.20) and (A.21), i.e. to prove that  $S_n(\phi_{[i]})$  is minimized/maximized either at 0 or 1, we have to show that  $S_n(\phi_{[i]})$  is either monotonically increasing or monotonically decreasing for all  $n$ .

To show monotonicity of  $S_n(\phi_{[i]})$ , four cases should be analyzed: (1)  $a_n + c_n \geq 0$  and  $c_n \leq 0$ ; (2)  $a_n + c_n \leq 0$  and  $c_n \geq 0$ ; (3)  $a_n + c_n \leq 0$  and  $c_n \leq 0$ ; and (4)  $a_n + c_n \geq 0$  and  $c_n \geq 0$ . Cases 1 and 2 are easy. For case 1, both  $S_n^1(\phi_{[i]})$  and  $S_n^2(\phi_{[i]})$  in (A.22) are monotonically increasing, which means that their sum also is. Similarly, for case 2 both  $S_n^1(\phi_{[i]})$  and  $S_n^2(\phi_{[i]})$  are monotonically decreasing, which means that their sum also is.

Cases 3 and 4 are more difficult because they are a sum of a monotonically increasing function and a monotonically decreasing function.

*Lemma A.1.* Consider a monotonically increasing function  $f_+ : [a, b] \mapsto f_+(x)$  and monotonically decreasing function  $f_- : [a, b] \mapsto f_-(x)$ . The sum  $f_+(x) + f_-(x)$  is monotonically increasing if

$$\left| \frac{\partial f_+(x)}{\partial x} \right| \geq \left| \frac{\partial f_-(x)}{\partial x} \right|, \quad x \in [a, b]$$

**Proof.** The sum is monotonically increasing if ( $\epsilon > 0$  is such that  $x + \epsilon \leq b$ )

$$\begin{aligned} f_+(x + \epsilon) + f_-(x + \epsilon) &\geq f_+(x) + f_-(x); \\ \lim_{\epsilon \rightarrow 0} \frac{f_+(x + \epsilon) - f_+(x)}{\epsilon} &\geq - \lim_{\epsilon \rightarrow 0} \frac{f_-(x + \epsilon) - f_-(x)}{\epsilon} \end{aligned} \quad (\text{A.23})$$

To complete the proof, it suffices to identify the definition of the derivatives and notice that both sides are positive. Hence we can add the absolute value operator without loss of meaning.  $\blacksquare$

For the sum  $f_+(x) + f_-(x)$  to be monotonically decreasing, we only need to invert the inequality in (A.23).

In the following, we analyze case 4, i.e. when  $S_n^1(\phi_{[i]})$  is monotonically increasing and  $S_n^2(\phi_{[i]})$  is monotonically decreasing (the analysis of case 3 is very similar). We identify three subcases to be treated separately, which we call 4.1, 4.2 and 4.3. As a consequence of (ii) and (iv), we have (4.1)  $a < 0$ ,

$a = -D_n$ ; (4.2)  $a_n > 0$ ,  $D_n = 0$ ; and (4.3)  $a_n = 0$ ,  $D_n > 0$ . For case 4.1, we write

$$\left| \frac{\partial S_n^1(\phi_{[i]})}{\partial \phi_{[i]}} \right| \leq \left| \frac{\partial S_n^2(\phi_{[i]})}{\partial \phi_{[i]}} \right|,$$

$$\frac{(a_n + c_n)^3}{((a_n + c_n)\phi_{[i]} + D_n + F_n)^3} \leq \frac{(c_n)^3}{(c_n\phi_{[i]} + F_n)^3}, \quad (\text{A.24})$$

which means that  $S_n(\phi_{[i]})$  is monotonically decreasing. For case 4.2, we write

$$\frac{(a_n + c_n)^3}{((a_n + c_n)\phi_{[i]} + F_n)^3} \geq \frac{(c_n)^3}{(c_n\phi_{[i]} + F_n)^3}, \quad (\text{A.25})$$

which means that  $S_n(\phi_{[i]})$  is monotonically increasing. For case 4.3, we write

$$\frac{(c_n)^3}{((c_n)\phi_{[i]} + D_n + F_n)^3} \leq \frac{(c_n)^3}{(c_n\phi_{[i]} + F_n)^3}, \quad (\text{A.26})$$

which means that  $S_n(\phi_{[i]})$  is monotonically decreasing. In (A.24), (A.25) and (A.26), we use Properties (ii) and (iii). Cases 3.1, 3.2 and 3.3 are defined similarly and the conclusions are basically the same. This completes the proof.

# Appendix B

## Appendix to Chapter 3

### B.1 Proof of Proposition 3.2

We analyze the  $N$  user case. In the following we focus on parallel updates, i.e. all users change their powers at the same time while taking into account the interference of the previous iteration. We write

$$\begin{aligned} \mathbf{S}_n^{k,(i+1)} &= (\overline{\mathbf{T}}_n^k)^H (\mathbf{H}_{n,n}^k)^H (\mathbf{M}_n^{k,(i)})^{-1} \mathbf{H}_{n,n}^k \overline{\mathbf{T}}_n^k \\ \mathbf{M}_n^{k,(i)} &= \mathbf{I} + \sum_{j \neq n} p_j^{k,(i)} \mathbf{H}_{n,j}^k \overline{\mathbf{T}}_j^k (\overline{\mathbf{T}}_j^k)^H (\mathbf{H}_{n,j}^k)^H, \end{aligned}$$

where the bracketed superscripts denote iteration. Also define  $[x]^+ = \max\{x, 0\}$  and  $[x]^- = \max\{-x, 0\}$ . For the  $2 \times 2$  case, the power allocation for user  $n$ , tone  $k$  on iteration  $i$  can be found in closed form. Taking into account the coefficients of the polynomial in (3.36), and defining  $\alpha_1 = -\nu_n^{k,(i)} |\mathbf{S}_n^{k,(i)}|$ ,  $\alpha_2 = 2u_n |\mathbf{S}_n^{k,(i)}| - \nu_n^{k,(i)} \text{tr}\{\mathbf{S}_n^{k,(i)}\}$  and  $\alpha_3 = u_n \text{tr}\{\mathbf{S}_n^{k,(i)}\} - \nu_n^{k,(i)}$ , the two roots are given by  $(-\alpha_2 \pm \sqrt{\alpha_2^2 - 4\alpha_1\alpha_3}) / (2\alpha_1)$ . Because of Corollary 1, we only need the largest root. If this roots is non-negative, we assign it to  $p_n^{k,(i)}$ , otherwise we set  $p_n^{k,(i)} = 0$ . Thus, we can write

$$p_n^{k,(i)} = \left[ \max \left\{ \frac{u_n}{\nu_n^{k,(i)}} - \frac{\text{tr}\{\mathbf{S}_n^{k,(i)}\}}{2|\mathbf{S}_n^{k,(i)}|} + \sqrt{\Delta}; \frac{u_n}{\nu_n^{k,(i)}} - \frac{\text{tr}\{\mathbf{S}_n^{k,(i)}\}}{2|\mathbf{S}_n^{k,(i)}|} - \sqrt{\Delta} \right\} \right]^+,$$

where  $\Delta = (u_n)^2/(\nu_n^{k,(i)})^2 + \text{tr}\{\mathbf{S}_n^{k,(i)}\}^2/4|\mathbf{S}_n^{k,(i)}|^2 - 1/|\mathbf{S}_n^{k,(i)}|$ . Without loss of generality, we consider that the power budget for every user is tight. If that is not the case, we can use the concept of the ‘‘virtual tone’’ [15].

With the high SNR assumption, we can write

$$\frac{\text{tr}\{\mathbf{S}_n^{k,(i)}\}^2}{4|\mathbf{S}_n^{k,(i)}|^2} - \frac{1}{|\mathbf{S}_n^{k,(i)}|} = \frac{|b|^2}{(a^2 - |b|^2)^2} \approx 0 \Rightarrow p_n^{k,(i)} = \left[ \frac{2u_n}{\nu_n^{k,(i)}} - \frac{\text{tr}\{\mathbf{S}_n^{k,(i)}\}}{2|\mathbf{S}_n^{k,(i)}|} \right]^+.$$

This assumption translates into considering that the diagonal elements of SNR matrix  $\mathbf{S}_n^{k,(i)}$  are much larger than the off diagonal elements. Now we write

$$\begin{aligned} & \max_n \left\{ \max \left\{ \sum_k [p_n^{k,(i+1)} - p_n^{k,(i)}]^+; \sum_k [p_n^{k,(i+1)} - p_n^{k,(i)}]^- \right\} \right\} \\ &= \max_n \left\{ \max \left\{ \sum_k \left[ \left[ \frac{2u_n}{\nu_n^{k,(i+1)}} - \frac{\text{tr}\{\mathbf{S}_n^{k,(i+1)}\}}{2|\mathbf{S}_n^{k,(i+1)}|} \right]^+ - \left[ \frac{2u_n}{\nu_n^{k,(i)}} - \frac{\text{tr}\{\mathbf{S}_n^{k,(i)}\}}{2|\mathbf{S}_n^{k,(i)}|} \right]^+ \right]^+; \right. \\ & \quad \left. \sum_k \left[ \left[ \frac{2u_n}{\nu_n^{k,(i+1)}} - \frac{\text{tr}\{\mathbf{S}_n^{k,(i+1)}\}}{2|\mathbf{S}_n^{k,(i+1)}|} \right]^+ - \left[ \frac{2u_n}{\nu_n^{k,(i)}} - \frac{\text{tr}\{\mathbf{S}_n^{k,(i)}\}}{2|\mathbf{S}_n^{k,(i)}|} \right]^+ \right]^- \right\} \right\} \quad (\text{B.1}) \end{aligned}$$

$$\begin{aligned} & \leq \max_n \left\{ \max \left\{ \sum_k \left[ \frac{2u_n}{\nu_n^{k,(i)}} - \frac{\text{tr}\{\mathbf{S}_n^{k,(i+1)}\}}{2|\mathbf{S}_n^{k,(i+1)}|} - \frac{2u_n}{\nu_n^{k,(i)}} + \frac{\text{tr}\{\mathbf{S}_n^{k,(i)}\}}{2|\mathbf{S}_n^{k,(i)}|} \right]^+; \right. \\ & \quad \left. \sum_k \left[ \frac{2u_n}{\nu_n^{k,(i)}} - \frac{\text{tr}\{\mathbf{S}_n^{k,(i+1)}\}}{2|\mathbf{S}_n^{k,(i+1)}|} - \frac{2u_n}{\nu_n^{k,(i)}} + \frac{\text{tr}\{\mathbf{S}_n^{k,(i)}\}}{2|\mathbf{S}_n^{k,(i)}|} \right]^- \right\} \right\} \quad (\text{B.2}) \end{aligned}$$

In (B.1), we substitute (B.1); in (B.2) we use  $[a^+ - b^+]^+ \leq [a - b]^+$  (and likewise for  $[a^+ - b^+]^-$ ) and Corollary 1 of [15]. In (B.2), note that

$$\begin{aligned} \frac{\text{tr}\{\mathbf{S}_n^{k,(i)}\}}{2|\mathbf{S}_n^{k,(i)}|} &= \frac{\text{tr}\{(\mathbf{M}_n^{k,(i-1)})^{-1}\overline{\mathbf{H}}_{n,n}^k\}}{2|(\mathbf{M}_n^{k,(i-1)})^{-1}\overline{\mathbf{H}}_{n,n}^k|} \\ &= \frac{\text{tr}\{\text{adj}\{\mathbf{M}_n^{k,(i-1)}\}\overline{\mathbf{H}}_{n,n}^k\}}{2|\mathbf{M}_n^{k,(i-1)}||\mathbf{M}_n^{k,(i-1)}|^{-1}|\overline{\mathbf{H}}_{n,n}^k|} \\ &= \frac{\text{tr}\{\text{adj}\{\mathbf{M}_n^{k,(i-1)}\}\overline{\mathbf{H}}_{n,n}^k\}}{2|\overline{\mathbf{H}}_{n,n}^k|}. \end{aligned}$$

Here we first use the definition of  $\mathbf{S}_n^{k,(i)}$  and then the definition of  $\overline{\mathbf{H}}_{n,j}^k$ ; notice that, since all matrices are square, we can write

$$|\mathbf{S}_n^{k,(i)}| = |(\overline{\mathbf{T}}_n^k)^{\mathbf{H}}(\mathbf{H}_{n,n}^k)^{\mathbf{H}}(\mathbf{M}_n^{k,(i-1)})^{-1}\mathbf{H}_{n,n}^k\overline{\mathbf{T}}_n^k| = |(\mathbf{M}_n^{k,(i-1)})^{-1}\overline{\mathbf{H}}_{n,n}^k|.$$

Then the adjugate formula for matrix inverses, i.e.

$$(\mathbf{M}_n^{k,(i-1)})^{-1} = \text{adj}\{\mathbf{M}_n^{k,(i-1)}\}|\mathbf{M}_n^{k,(i-1)}|^{-1};$$

and  $|\mathbf{A}^{-1}\mathbf{B}| = |\mathbf{A}|^{-1}|\mathbf{B}|$ . Consider  $\overline{\mathbf{H}}_{n,j}^k = \begin{bmatrix} d_{n,j}^{k,(i)} & (e_{n,j}^{k,(i)})^* \\ e_{n,j}^{k,(i)} & d_{n,j}^{k,(i)} \end{bmatrix}$  for all  $n, j$ . Then  $\text{adj}\{\mathbf{M}_n^{k,(i)}\}$  can be written as

$$\begin{aligned} \text{adj}\{\mathbf{M}_n^{k,(i)}\} &= \sum_{j \neq n} \begin{bmatrix} p_j^{k,(i)} d_{n,j}^k + 1 & -p_j^{k,(i)} (e_{n,j}^k)^* \\ -p_j^{k,(i)} e_{n,j}^k & p_j^{k,(i)} d_{n,j}^k + 1 \end{bmatrix} \\ &= \sum_{j \neq n} p_j^{k,(i)} \underbrace{\begin{bmatrix} d_{n,j}^k & -(e_{n,j}^k)^* \\ -e_{n,j}^k & d_{n,j}^k \end{bmatrix}}_{=\text{adj}\{\mathbf{H}_{n,j}^k\}} + \mathbf{I}. \end{aligned} \quad (\text{B.3})$$

Substituting (B.3) in (B.2), we obtain

$$\begin{aligned} &\max_n \left\{ \max_k \left\{ \sum_{j \neq n} \frac{\text{tr}\{\text{adj}\{\mathbf{H}_{n,j}^k\}\overline{\mathbf{H}}_{n,n}^k\}}{2|\overline{\mathbf{H}}_{n,n}^k|} (p_j^{k,(i-1)} - p_j^{k,(i)})^+; \right. \right. \\ &\quad \left. \left. \sum_k \left[ \sum_{j \neq n} \frac{\text{tr}\{\text{adj}\{\mathbf{H}_{n,j}^k\}\overline{\mathbf{H}}_{n,n}^k\}}{2|\overline{\mathbf{H}}_{n,n}^k|} (p_j^{k,(i-1)} - p_j^{k,(i)})^- \right] \right\} \right\} \\ &\leq \max_n \left\{ \max_k \left\{ \sum_{j \neq n} \frac{\text{tr}\{\text{adj}\{\mathbf{H}_{n,j}^k\}\overline{\mathbf{H}}_{n,n}^k\}}{2|\overline{\mathbf{H}}_{n,n}^k|} [p_j^{k,(i-1)} - p_j^{k,(i)}]^+; \right. \right. \\ &\quad \left. \left. \sum_{j \neq n} \frac{\text{tr}\{\text{adj}\{\mathbf{H}_{n,j}^k\}\overline{\mathbf{H}}_{n,n}^k\}}{2|\overline{\mathbf{H}}_{n,n}^k|} [p_j^{k,(i-1)} - p_j^{k,(i)}]^- \right\} \right\} \quad (\text{B.4}) \end{aligned}$$

$$\begin{aligned} &\leq (N-1) \max_{\substack{j,n,k \\ j \neq n}} \left\{ \frac{\text{tr}\{\text{adj}\{\mathbf{H}_{n,j}^k\}\overline{\mathbf{H}}_{n,n}^k\}}{2|\overline{\mathbf{H}}_{n,n}^k|} \right\} \\ &\times \max_n \left\{ \max_k \left\{ \sum_k [p_n^{k,(i-1)} - p_n^{k,(i)}]^+; \sum_k [p_n^{k,(i-1)} - p_n^{k,(i)}]^- \right\} \right\} \quad (\text{B.5}) \end{aligned}$$

In (B.4), we use  $\sum_k [\sum_j a_j^k b_j^k]^+ \leq \sum_k \sum_j a_j^k [b_j^k]^+$  for non-negative  $a_j^k$  (and likewise for  $\sum_k [\sum_j a_j^k b_j^k]^-$ ). In (B.5) we use

$$\sum_k \sum_j^{N-1} a_j^k b_j^k \leq \sum_j \max_k \{a_j^k\} \sum_k b_j^k \leq (N-1) \max_{j,k} \{a_j^k\} \max_j \left\{ \sum_k b_j^k \right\}$$

for non-negative  $a_j^k, b_j^k$ . In (B.5), the condition

$$(N-1) \max_{\substack{j,n,k \\ j \neq n}} \left\{ \frac{\text{tr} \{ \text{adj} \{ \mathbf{H}_{n,j}^k \} \overline{\mathbf{H}}_{n,n}^k \}}{2 |\overline{\mathbf{H}}_{n,n}^k|} \right\} < 1$$

completes the proof.

# Appendix C

## Appendices for Chapter 4

### C.1 General Formulas for $\rho_n^k$ , $\theta_{n,[i]}^k$ and $\eta_n^k$ , $\phi_{n,[i]}^k$

To re-write  $\mathbf{p}_n^k \in \mathbb{R}^{A_n}$  as (4.20) for the general case, we have  $\mathbf{p}_n^k = \rho_n^k \mathbf{d}_n^k$ , where

$$d_{n,[1]}^k = \prod_{j=1}^{A_n-1} \cos \theta_{n,[j]}^k \quad (\text{C.1})$$

$$d_{n,[i]}^k = \prod_{j=1}^{A_n-i} \cos \theta_{n,[j]}^k \sin \theta_{n,[A_n-i+1]}^k, \quad i = 2, \dots, A_n - 1 \quad (\text{C.2})$$

$$d_{n,[A_n]}^k = \sin \theta_{n,[1]}^k \quad (\text{C.3})$$

Here  $0 \leq \theta_{n,[i]}^k \leq \pi/2$ ,  $\forall i$ .

To re-write  $\mathbf{p}_n^k$  as (4.27) for the general case, we have  $\mathbf{p}_n^k = \eta_n^k \mathbf{v}_n^k$ , where

$$v_{n,[1]}^k = \prod_{j=1}^{A_n-1} (1 - \phi_{n,[j]}^k) \quad (\text{C.4})$$

$$v_{n,[i]}^k = \prod_{j=1}^{A_n-i} (1 - \phi_{n,[j]}^k) \phi_{n,[N-i+1]}^k, \quad i = 2, \dots, A_n - 1 \quad (\text{C.5})$$

$$v_{n,[A_n]}^k = \phi_{n,[1]}^k \quad (\text{C.6})$$

Here  $0 \leq \phi_{n,[i]}^k \leq 1 \forall i$ .

Transforming between Cartesian coordinates on the one hand and spherical coordinates in both Euclidean and taxicab geometry on the other hand is straightforward in both directions.

## C.2 Proof of Proposition 4.1

Since  $A_n = 2$  for all users, we can drop one of the subscripts for  $\phi_n^k$ . We will refer to  $\phi_1 = [\phi_1^1 \ \dots \ \phi_1^K]^T$  and  $\phi_2 = [\phi_2^1 \ \dots \ \phi_2^K]^T$ . For simplicity, we assume that  $\sum_{k \in \mathcal{K}} \eta_n^k = 2P$ ,  $n = 1, 2$  and that the per-transceiver PCs are given by  $P$ . The optimization to be solved in  $\phi_1$  and  $\phi_2$  is given by

$$\begin{aligned} & \max_{\phi_1, \phi_2} \sum_{n \in \mathcal{N}} \sum_{k \in \mathcal{K}} u_n b_n^k \\ & \text{subject to} \quad \sum_{k \in \mathcal{K}} \eta_1^k \phi_1^k \leq P, \quad 0 \leq \phi_1^k \leq 1 \\ & \quad \quad \quad \sum_{k \in \mathcal{K}} \eta_2^k \phi_2^k \leq P, \quad 0 \leq \phi_2^k \leq 1 \end{aligned}$$

As explained in Section 4.4.4, we solve this problem with a block coordinate descent method. These constraints are convex and the feasible set of the problem is now the Cartesian product  $\mathcal{B}_1 \times \mathcal{B}_2$ , where  $\mathcal{B}_n = \{\phi_n \mid \sum_{k \in \mathcal{K}} \eta_n^k \phi_n^k \leq P, \phi_n^k \in [0, 1]\}$ . We solve sequentially, i.e.  $n = 1$ ,  $n = 2$  and repeat until convergence, the following problem:

$$\phi_n = \operatorname{argmax}_{\phi_n \in \mathcal{B}_n} \sum_{n \in \mathcal{N}} \sum_{k \in \mathcal{K}} u_n b_n^k.$$

Because of the vanishing duality gap of multitone problems [53], the dual decomposition and the exhaustive search, each step returns the optimal solution. Since  $b_n^k$  is continuously differentiable and the feasible set of the problem is the Cartesian product of non-empty, convex subsets, the block coordinate descent with two blocks is guaranteed to converge to a critical point [33].

# Appendix D

## Appendix to Chapter 5

### D.1 Derivation of the ICI Matrices for Fixed $\beta_{n,j}$

In this appendix we ignore the subscripts denoting users. To evaluate the impact of the asynchronous transmission, we focus on one victim and one interfering user, as depicted in Fig. 1.4. The victim user, denoted as user 1, has its DMT symbol for its  $i$ th transceiver denoted by  $\mathbf{x}_i \in \mathbb{C}^K$  (unlike the remainder of this paper the subscript does not denote user). The interfering user, denoted as user 2, has its DMT symbol denoted by  $\mathbf{u}_i$ . There are a total of  $U + V$  transceivers in the network, where  $U$  is the number of transceivers for user 1 and  $V$  for user 2. We number them sequentially. E.g., if each of the users has two transceivers, we refer to the DMT symbols as  $\mathbf{x}_1, \mathbf{x}_2, \mathbf{u}_3$  and  $\mathbf{u}_4$ . Symbols  $\mathbf{u}_{i,(1)}$  and  $\mathbf{u}_{i,(2)}$ ,  $i = U + 1, \dots, U + V$ , interfere with the reception of user 1, where the bracketed subscripts denote time. Without loss of generality, we consider time instants (1) and (2).

Before proceeding, we define some variables. We assume that the CP, whose length is given by  $L_{\text{cp}}$ , is longer than both the direct and crosstalk channel impulse responses. The offset between the transmission of the two users is given by  $\beta$ ,  $0 \leq \beta \leq 1$ . We define  $\mathbf{F}$  and  $\mathbf{F}^H \in \mathbb{C}^{K \times K}$  as the DFT and IDFT



$\tilde{\mathbf{F}}\tilde{\mathbf{C}}\mathbf{G}_{i,j}\mathbf{C}\mathbf{F}^H$ ;  $\mathbf{G}_{i,j} \in \mathbb{C}^{(K+L_{\text{cp}}) \times (K+L_{\text{cp}})}$  is a Toeplitz matrix with first column  $[\mathbf{g}_{i,j}^T \mathbf{0}_{1 \times (K+L_{\text{cp}}-L_g)}]^T$  and first row  $[g_{i,j}(1) \mathbf{0}_{1 \times (K+L_{\text{cp}}-1)}]$ , where  $\mathbf{g}_{i,j} \in \mathbb{C}_g^L$  is the  $L_g$ -tap channel impulse response from the transmitter of transceiver  $j$  to the receiver of transceiver  $i$  of user 1 and is considered constant in time;  $\mathbf{A}, \mathbf{B} \in \mathbb{C}^{KU \times KV}$  have a block structure, where the  $(i, j - U)$ -th block,  $i = 1, \dots, U$  and  $j = U + 1, \dots, U + V$ , are given respectively as  $\tilde{\mathbf{F}}\tilde{\mathbf{C}}\mathbf{G}_{i,j}\mathbf{S}_{(1)}\mathbf{C}\mathbf{F}^H$  and  $\tilde{\mathbf{F}}\tilde{\mathbf{C}}\mathbf{G}_{i,j}\mathbf{S}_{(2)}\mathbf{C}\mathbf{F}^H$ . The matrix  $\mathbf{G}_{i,j}$  is, as before, Toeplitz with  $\mathbf{g}_{i,j} \in \mathbb{C}^L$  being the  $L$ -tap channel impulse response from the transmitter of transceiver  $j$  of user 2 to the receiver of transceiver  $i$  of user 1.

Because  $L \leq L_{\text{cp}}$ , the process of insertion and removal of the CP creates a square circulant matrix, which is in turn diagonalized by the DFT and IDFT operations. Hence the  $(i, j)$ -th block of  $\mathbf{H}$ , where  $i, j = 1, \dots, U$ , is given by  $\tilde{\mathbf{F}}\tilde{\mathbf{C}}\mathbf{G}_{i,j}\mathbf{C}\mathbf{F}^H = \text{diag}\{\mathbf{h}_{i,j}\}$ , where  $\mathbf{h}_{i,j} \in \mathbb{C}^K$  is the corresponding channel frequency response. Because of the offset represented by the matrices  $\mathbf{S}_{(1)}$  and  $\mathbf{S}_{(2)}$ , the operation  $\tilde{\mathbf{C}}\mathbf{G}_{i,j}\mathbf{S}_{(1)}\mathbf{C}$  and  $\tilde{\mathbf{C}}\mathbf{G}_{i,j}\mathbf{S}_{(2)}\mathbf{C}$  fail to produce a circulant matrix, and therein lies the effect of the asynchronicity.

The next step is to write a per-tone version of (D.1):

$$\mathbf{r}^k = \mathbf{H}^k \mathbf{x}^k + \sum_{s \in \mathcal{K}} \mathbf{A}^{k,s} \mathbf{u}_{(1)}^s + \mathbf{B}^{k,s} \mathbf{u}_{(2)}^s + \mathbf{z}^k.$$

Here  $\mathbf{x}^k, \mathbf{z}^k \in \mathbb{C}^U$ ,  $\mathbf{u}_{(1)}, \mathbf{u}_{(2)} \in \mathbb{C}^V$ . We define  $\mathbf{x}^k = [x_1^k \ \dots \ x_U^k]^T$ . Other vectors are defined similarly. We also have  $\mathbf{H}^k \in \mathbb{C}^{U \times U}$  and  $\mathbf{A}^{k,s}, \mathbf{B}^{k,s} \in \mathbb{C}^{U \times V}$ . The matrix  $\mathbf{H}^k$  is obtained from  $\mathbf{H}$  by substituting the block  $(i, j)$  by the  $(k, k)$  element of block  $(i, j)$ , with  $i, j = 1, \dots, U$  and  $k = 1, \dots, K$ . The matrices  $\mathbf{A}^{k,s}, \mathbf{B}^{k,s}$  are obtained from  $\mathbf{A}$  and  $\mathbf{B}$  by substituting the block  $(i, j - U)$  by the  $(k, s)$  element of block  $(i, j - U)$ , with  $i = 1, \dots, U$ ,  $j = U + 1, \dots, U + V$  and  $k, s = 1, \dots, K$ .

Substituting  $\mathbf{u}_{(1)}^s = \mathbf{T}_u^s \bar{\mathbf{x}}_u^s$  and  $\mathbf{u}_{(2)}^s = \mathbf{T}_u^s \mathbf{x}_u^s$ , we arrive at (5.5).



# Bibliography

- [1] BINGHAM, J. A. C. Multicarrier modulation for data transmission: An idea whose time has come. *IEEE Commmun. Mag.* 28, 5 (1990), 5–14.
- [2] BOCHE, H., NAIK, S., AND ALPCAN, T. Characterization of convex and concave resource allocation problems in interference coupled wireless systems. *IEEE Trans. Sig. Process.* 59, 5 (2011), 2382–2394.
- [3] BÖLCSKEI, H., GESBERT, D., PAPADIAS, C. B., AND VAN DER VEEN, A.-J. *Space-Time Wireless Systems: From Array Processing to MIMO Communications*. Cambridge University Press, 2006.
- [4] BÖLCSKEI, H., GESBERT, D., AND PAULRAJ, A. J. On the capacity of OFDM-based spatial multiplexing systems. *IEEE Trans. Commun.* 50, 2 (2002), 225–234.
- [5] BÖLCSKEI, H., AND PAULRAJ, A. J. *Multiple-input multiple-output (MIMO) wireless systems*. 2002, pp. 90.1–90.14.
- [6] BOURNE, J. Fiber to the home: practically a reality. In *IEEE Int. Conf. Commun.* (Philadelphia, USA, 1988).
- [7] BOYD, S., AND VANDENBERGHE, L. *Convex Optimization*. Cambridge University Press, 2004.
- [8] CADAMBE, V. R., AND JAFAR, S. A. Can 100 speakers talk for 30 minutes each in one room within one hour and with zero interference to each other’s audience? In *Allerton Conf. Comm., Control and Comput.* (Monticello, USA, 2007).
- [9] CADAMBE, V. R., AND JAFAR, S. A. Interference alignment and degrees of freedom of the  $K$ -user interference channel. *IEEE Trans. Inf. Theory* 54, 8 (2008), 3425–3441.

- [10] CAMPELLO, J. Discrete bit loading for DMT. In *Proc. IEEE International Conference on Communications* (Vancouver, Canada, 1999).
- [11] CARLEIAL, A. A case where interference does not reduce capacity (corresp.). *IEEE Trans. Inf. Theory* 21, 5 (1975), 569–570.
- [12] CENDRILLON, R. *Multi-User Signal and Spectral Coordination for Digital Subscriber Lines*. PhD thesis, KU Leuven, 2004.
- [13] CENDRILLON, R., GINIS, G., VAN DEN BOGAERT, E., AND MOONEN, M. A near-optimal linear crosstalk canceler for upstream VDSL. *IEEE Trans. Signal Process.* 54, 8 (2006), 3136–3146.
- [14] CENDRILLON, R., GINIS, G., VAN DEN BOGAERT, E., AND MOONEN, M. A near-optimal linear crosstalk precoder for downstream VDSL. *IEEE Trans. Commun.* 55, 5 (2007), 860–863.
- [15] CENDRILLON, R., HUANG, J., CHIANG, M., AND MOONEN, M. Autonomous spectrum balancing for digital subscriber lines. *IEEE Trans. Signal Process.* 55, 8 (2007), 4241–4257.
- [16] CENDRILLON, R., AND MOONEN, M. Iterative spectrum management for digital subscriber lines. In *IEEE Int. Conf. Commun.* (Seoul, Korea, 2005).
- [17] CENDRILLON, R., YU, W., MOONEN, M., VERLINDEN, J., AND BOSTOEN, T. Optimal multiuser spectrum balancing for digital subscriber lines. *IEEE Trans. Commun.* 54, 5 (2006), 922–933.
- [18] CHAN, V. M. K., AND YU, W. Multiuser spectrum optimization for discrete multitone systems with asynchronous crosstalk. *IEEE Trans. Signal Process.* 55, 11 (2007), 5425–5435.
- [19] CHANCLOU, P., CAPELLE, B., CHARBONNIER, B., COURANT, J.-L., DENIS, Y., GENAY, N., GOSSELIN, S., KURZ, D., LANDOUSIES, B., LE BRIS, E., LE GUYADER, B., PIZZINAT, A., AND SALIOU, F. France Telecom’s PON deployment, learnt lessons and next steps. In *Optical Fiber Commun. Conf. and Exposition* (Anaheim, USA, 2013).
- [20] CHIANG, M., HANDE, P., LAN, T., AND TAN, C. W. Power control in wireless cellular networks. *Found. Trends Netw.* 2, 4 (Apr. 2008), 381–533.
- [21] CHOWDHERY, A., AND CIOFFI, J. M. Dynamic spectrum management for upstream mixtures of vectored & non-vectored DSL. In *IEEE Global Telecomm. Conf.* (Miami, USA, 2010).

- [22] CHRISTENSEN, S. S., AGARWAL, R., DE CARVALHO, E., AND CIOFFI, J. M. Weighted sum-rate maximization using weighted MMSE for MIMO-BC beamforming design. *IEEE Trans. Wireless Commun.* 7, 12 (2008), 4792–4799.
- [23] CIOFFI, J. M., JAGANNATHAN, S., MOHSENI, M., AND GINIS, G. CuPON: The copper alternative to PON 100 Gb/s DSL networks. *IEEE Commun. Mag.* 45, 6 (2007), 132–139.
- [24] EL AYACH, O., PETERS, S. W., AND W. HEATH, JR., R. The feasibility of interference alignment over measured MIMO-OFDM channels. *IEEE Trans. Veh. Technol.* 59, 9 (2010), 4309–4321.
- [25] ESCHER, F., FOISEL, H.-M., TEMPLIN, A., NAGEL, B., AND ADAMY, M. Enabling broadband communication, Deutsche Telekom FTTH deployment architecture, plans, rollout. In *Optical Fiber Commun. Conf.* (Los Angeles, USA, 2012).
- [26] FOROUZAN, A. R., MOONEN, M., MAES, J., AND GUENACH, M. Joint level 2 and 3 dynamic spectrum management for upstream VDSL. *IEEE Trans. Commun.* 59, 10 (2011), 2851–2861.
- [27] FOROUZAN, A. R., MOONEN, M., MAES, J., AND GUENACH, M. Joint level 2 and 3 dynamic spectrum management for downstream VDSL. *IEEE Trans. Commun.* 60, 10 (2012), 3111–3122.
- [28] GESBERT, D., KOUNTOURIS, M., W. HEATH, JR., R., CHAE, C.-B., AND SÄLZER, T. Shifting the MIMO paradigm. *IEEE Signal Process. Mag.* 24, 5 (2007), 36–46.
- [29] GINIS, G., AND CIOFFI, J. M. Vectored transmission for digital subscriber line systems. *IEEE J. Sel. Areas Commun.* 20, 5 (2002), 1085–1104.
- [30] GOLDEN, P., DEDIEU, H., AND JACOBSEN, K. *Fundamentals of DSL Technology*. Taylor & Francis, 2005.
- [31] GOLUB, G. H., AND VAN LOAN, C. F. *Matrix Computations*, 3rd ed. The Johns Hopkins University Press, 1996.
- [32] GOMADAM, K., CADAMBE, V. R., AND JAFAR, S. A. Approaching the capacity of wireless networks through distributed interference alignment. In *IEEE Global Telecomm. Conf.* (New Orleans, USA, 2008).
- [33] GRIPPO, L., AND SCIANDRONE, M. On the convergence of the block nonlinear Gauss-Seidel method under convex constraints. *Operations Research Letters* 23, 3 (2000), 127–136.

- [34] GUENACH, M., LOUVEAUX, J., VANDENDORPE, L., WHITING, P., MAES, J., AND PEETERS, M. On signal-to-noise ratio-assisted crosstalk channel estimation in downstream DSL systems. *IEEE Trans. Signal Process.* 58, 4 (2010), 2327–2338.
- [35] HAN, T., AND KOBAYASHI, K. A new achievable rate region for the interference channel. *IEEE Trans. Inf. Theory*, 27, 1 (1981), 49–60.
- [36] HAYASHI, S., AND LUO, Z.-Q. Spectrum management for interference-limited multiuser communication systems. *IEEE Trans. Inf. Theory* 55, 3 (2009), 1153–1175.
- [37] HO, Z. K. M., AND GESBERT, D. Balancing egoism and altruism on the interference channel: The mimo case. In *IEEE Int. Conf. Commun.* (Cape Town, South Africa, 2010).
- [38] HONG, M., AND LUO, Z.-Q. Signal processing and optimal resource allocation for the interference channel. *CoRR abs/1206.5144* (2012).
- [39] JAGANNATHAN, S., POURAHMAD, V., CIOFFI, J. M., OUZZIF, M., AND TARAFI, R. Common-mode data transmission using the binder sheath in digital subscriber lines. *IEEE Trans. Commun.* 57, 3 (2009), 831–840.
- [40] JOHAM, M., KUSUME, K., GZARA, M. H., UTSCHICK, W., AND NOSSEK, J. A. Transmit Wiener filter. Tech. rep., Munich University of Technology, 2002.
- [41] KERPEZ, K. Near-end crosstalk is almost gaussian. *IEEE Trans. Commun.* 41, 5 (1993), 670–672.
- [42] KIM, S. J., AND GIANNAKIS, G. B. Optimal resource allocation for MIMO ad-hoc cognitive radio networks. In *Allerton Conf. Comm., Control and Comput.* (Monticello, USA, 2008).
- [43] KRAUSE, E. F. *Taxicab geometry: an adventure in non-Euclidean geometry*. New York (N.Y.): Dover, 1986.
- [44] LE NIR, V., MOONEN, M., VERLINDEN, J., AND GUENACH, M. Full vectoring optimal power allocation in xDSL channels under per-modem power constraints and spectral mask constraints. *IEEE Trans. Commun.* 57, 1 (2009), 194–202.
- [45] LE NIR, V., MOONEN, M., VERLINDEN, J., AND GUENACH, M. Optimal power allocation for downstream xDSL with per-modem total power constraints: broadcast channel optimal spectrum balancing (BC-OSB). *IEEE Trans. Signal Process.* 57, 2 (2009), 690–697.

- [46] LEE, B., CIOFFI, J., JAGANNATHAN, S., SEONG, K., KIM, Y., MOHSENI, M., AND BRADY, M. Binder mimo channels. *IEEE Trans. Commun.* 55, 8 (2007), 1617–1628.
- [47] LEE, B., CIOFFI, J. M., JAGANNATHAN, S., AND MOHSENI, M. Gigabit DSL. *IEEE Trans. Commun.* 55, 9 (2007), 1689–1692.
- [48] LESHEM, A., AND LI, Y. A low complexity linear precoding technique for next generation VDSL downstream transmission over copper. *IEEE Trans. Signal Process.* 55, 1 (2007), 5527–5534.
- [49] LINDQVIST, N., LINDQVIST, F., DORTSCHY, B., PELAES, E., AND KLAUTAU, A. Impact of crosstalk estimation on the dynamic spectrum management performance. In *IEEE Global Telecommun. Conf.* (New Orleans, USA, 2008).
- [50] LU, K., WOLFF, R., AND GRATZER, F. Installed first cost economics of fiber/broadband access to the home. In *IEEE Global Telecommun. Conf.* (Hollywood, USA, 1988).
- [51] LUENBERGER, D., AND YE, Y. *Linear and Nonlinear Programming*, third ed. Springer, 2008.
- [52] LUO, Z.-Q., AND ZHANG, S. Duality gap estimation and polynomial time approximation for optimal spectrum management. *IEEE Trans. Signal Process.* 57, 7 (2009), 2675 – 2689.
- [53] LUO, Z.-Q., AND ZHANG, S. Dynamic spectrum management: Complexity and duality. *IEEE Trans. Signal Process.* 2, 1 (2009), 57–73.
- [54] MAES, J., NUZMAN, C., VAN WIJNGAARDEN, A., AND VAN BRUYSEL, D. Pilot-based crosstalk channel estimation for vector-enabled VDSL systems. In *Annual Conf. Inf. Sciences and Syst.* (Princeton, USA, 2010).
- [55] MAGESACHER, T., ÖDLING, P., BÖRJESSON, P. O., HENKEL, W., NORDSTRÖM, T., ZUKUNFT, R., AND HAAR, S. On the capacity of the copper cable channel using the common mode. In *IEEE Global Telecomm. Conf.* (Taipei, Taiwan, 2004).
- [56] MAGESACHER, T., ÖDLING, P., BÖRJESSON, P. O., AND NORDSTRÖM, T. Exploiting the common-mode signal in xDSL. In *European Signal Process. Conf.* (Vienna, Austria, 2004).
- [57] MORAES, R., DORTSCHY, B., KLAUTAU, A., AND RIUS I RIU, J. Semi-blind power allocation for digital subscriber lines. In *IEEE Int. Conf. Commun.* (Beijing, China, 2008).

- [58] MORAES, R., DORTSCHY, B., KLAUTAU, A., ZAMPOLO, R., AND RIUS I RIU, J. Optimal solution for the fixed margin problem in digital subscriber lines. In *Int. Symp. Control, Commun. and Signal Process.* (St. Julians, Malta, 2008).
- [59] MORAES, R. B., DORTSCHY, B., KLAUTAU, A., AND RIUS I RIU, J. Semiblind spectrum balancing for DSL. *IEEE Trans. Signal Process.* 58, 7 (2010), 3717–3727.
- [60] MORAES, R. B., AND SAMPAIO-NETO, R. Bit error rate minimising pilot symbol arrangement in closed-loop orthogonal frequency division multiplexing systems. *IET Commun.* 5, 14 (2011), 1999–2008.
- [61] MORAES, R. B., TSIAFLAKIS, P., MAES, J., AND MOONEN, M. General framework and algorithm for data rate maximization in DSL networks. *Submitted for publication.*
- [62] MORAES, R. B., TSIAFLAKIS, P., MAES, J., AND MOONEN, M. DMT MIMO IC rate maximization in DSL with combined signal and spectrum coordination. *IEEE Trans. Signal Process.* 61, 7 (2013), 1756–1769.
- [63] MORAES, R. B., TSIAFLAKIS, P., MAES, J., AND MOONEN, M. DMT MIMO IC rate maximization in DSL with per-transceiver power constraints. *Submitted for publication* (2013).
- [64] MORAES, R. B., TSIAFLAKIS, P., MAES, J., VAN BIESEN, L., AND MOONEN, M. The rate maximization problem in DSL with mixed spectrum and signal coordination. In *European Signal Process. Conf.* (Barcelona, Spain, 2011).
- [65] MORAES, R. B., TSIAFLAKIS, P., AND MOONEN, M. Dynamic spectrum management in DSL with asynchronous crosstalk. In *IEEE Int. Conf. Acoust., Speech and Signal Process.* (Prague, Czech Republic, 2011).
- [66] MORAES, R. B., TSIAFLAKIS, P., AND MOONEN, M. Intercarrier interference in DSL networks due to asynchronous DMT transmission. In *IEEE Int. Conf. Acoust., Speech and Signal Process.* (Vancouver, Canada, 2013).
- [67] MORAES, R. B., TSIAFLAKIS, P., AND MOONEN, M. Reduced complexity dynamic spectrum management based on a polar coordinates formulation. In *IEEE Int. Conf. Commun.* (Budapest, Hungary, 2013).
- [68] MORAES, R. B., WOLKERSTORFER, M., TSIAFLAKIS, P., AND MOONEN, M. Dynamic spectrum management with spherical coordinates. *Submitted for publication.*

- [69] NEGRO, F., SHENOY, S. P., GHAURI, I., AND SLOCK, D. T. M. On the MIMO interference channel. In *Inf. Theory and Appl. Workshop* (San Diego, USA, 2010).
- [70] ÖDLING, P., MAGESACHER, T., HÖST, S., BÖRJESSON, P. O., BERG, M., AND AREIZAGA, E. Fourth generation broadband concept. *IEEE Commun. Mag.* 47, 1 (2009), 63–69.
- [71] OKSMAN, V., AND CIOFFI, J. M. Noise Models for VDSL Performance Verification. ANSI, ANSI-77E7.4/99.438R2, 1999.
- [72] PALOMAR, D. P., CIOFFI, J. M., AND LAGUNAS, M. A. Joint tx-rx beamforming design for multicarrier MIMO channels: A unified framework for convex optimization. *IEEE Trans. Signal Process.* 51, 9 (2003), 2381–2401.
- [73] PAPANDRIOPOULOS, J., AND EVANS, J. S. SCALE: a low-complexity distributed protocol for spectrum balancing in multiuser DSL networks. *IEEE Trans. Inf. Theory* 55, 8 (2009), 3711–3724.
- [74] PARK, M., KO, K., PARK, B., AND HONG, D. Effects of asynchronous MAI on average SEP performance of OFDMA uplink systems over frequency-selective Rayleigh fading channels. *IEEE Trans. Commun.* 58, 2 (2010), 586–599.
- [75] PARK, M., KO, K., YOO, H., AND HONG, D. Performance analysis of OFDMA uplink systems with symbol timing misalignment. *IEEE Trans. Commun.* 7, 8 (2003), 376–378.
- [76] PEETERS, M., AND VANHASTEL, S. The copper phantom, 2001.
- [77] PETERSEN, K. B., AND PEDERSEN, M. S. The matrix cookbook. Tech. rep., Technical University of Denmark, 2008.
- [78] PRESS, W. H., TEUKOLSKY, S. A., VETTERLING, W. T., AND FLANNERY, B. P. *Numerical Recipes 3rd Edition: The Art of Scientific Computing*, 3 ed. Cambridge University Press, 2007.
- [79] RAHMATALLAH, Y., AND MOHAN, S. Peak-to-average power ratio reduction in ofdm systems: A survey and taxonomy, 2013.
- [80] SADEK, M., TARIGHAT, A., AND SAYED, A. H. A leakage-based precoding scheme for downlink multi-user MIMO channels. *IEEE Trans. Wireless Commun.* 6, 5 (2007), 1711–1721.
- [81] SCUTARI, G., PALOMAR, D. P., AND BARBAROSSA, S. The MIMO iterative waterfilling algorithm. *IEEE Trans. Signal Process.* 57, 5 (2009), 1917–1935.

- [82] SHANG, X., CHEN, B., KRAMER, G., AND POOR, H. Noisy-interference sum-rate capacity of parallel gaussian interference channels. *IEEE Trans. Inf. Theory* 57, 1 (2011), 210–226.
- [83] SHI, Q., RAZAVIYAYN, M., LUO, Z.-Q., AND HE, C. An iteratively weighted MMSE approach to distributed sum-utility maximization for a MIMO interfering broadcast channel. *IEEE Trans. Signal Process.* 59, 9 (2011), 4331–4340.
- [84] SHIN, J., MOON, J., AND AHN, J. Weighted-sum-rate-maximizing linear transceiver filters for the  $K$ -user MIMO interference channel. In *Global Telecomm. Conf.* (Houston, USA, 2011).
- [85] SONG, K., CHUNG, S., GINIS, G., AND CIOFFI, J. M. Dynamic spectrum management for next-generation DSL systems. *IEEE Commun. Mag.* 40, 10 (2002), 101–109.
- [86] STARR, J., EL AYACH, O., AND W. HEATH, JR., R. Interference alignment with per-antenna power constraints. In *IEEE Int. Symp. Inf. Theory* (S. Petersburg, Russia, 2011).
- [87] STARR, T., CIOFFI, J. M., AND SILVERMAN, P. *Understanding Digital Subscriber Lines Technology*. Prentice Hall, 1999.
- [88] STARR, T., SORBARA, M., CIOFFI, J. M., AND SILVERMAN, P. *DSL Advances*. Prentice Hall, 1999.
- [89] TELATAR, I. E. Capacity of multi-antenna gaussian channels. *European Trans. Telecommun.* 10 (1999), 585–595.
- [90] BROADBAND FORUM. FTTx supercharges broadband deployment, 2013.
- [91] IEEE SPECTRUM WEBSITE. Copper at the speed of fiber?, 2011.
- [92] ETSI STD. TS 101 270-1. Transmission and multiplexing (TM); access transmission systems on metallic access cables; very-high bit-rate digital subscriber line transceivers (VDSL); part 1: Functional requirements, 2003.
- [93] TIMMERS, M., GUENACH, M., NUZMAN, C., AND MAES, J. G.fast: evolving the copper access network. *Communications Magazine, IEEE* 51, 8 (2013), 74–79.
- [94] TIMMERS, M., HOOGHE, K., GUENACH, M., AND MAES, J. Digital complexity in DSL: An extrapolated historical overview. In *Second Int. Conf. Access Networks (ACCESS)* (Luxembourg, 2011).

- [95] TSIAFLAKIS, P. *Resource Management and Optimization in Multi-user DSL Systems*. PhD thesis, KU Leuven, 2009.
- [96] TSIAFLAKIS, P., DIEHL, M., AND MOONEN, M. Distributed spectrum management algorithms for multiuser DSL networks. *IEEE Trans. Signal Process.* 56, 10 (2008), 4825–4843.
- [97] TSIAFLAKIS, P., AND GLINEUR, F. A novel class of iterative approximation methods for DSL spectrum optimization. In *IEEE Int. Conf. Commun.* (Ottawa, Canada, 2013).
- [98] TSIAFLAKIS, P., MORAES, R. B., AND MOONEN, M. A low complexity algorithm for joint spectrum and signal coordination in upstream DSL transmission. In *18th IEEE Symp. on Commun. Veh. Technol. Benelux* (Ghent, Belgium, 2011).
- [99] TSIAFLAKIS, P., TAN, C., YI, Y., CHIANG, M., AND MOONEN, M. Optimality certificate of dynamic spectrum management in multi-carrier interference channels. In *IEEE Int. Symp. on Inf. Theory* (Toronto, Canada, 2008).
- [100] TSIAFLAKIS, P., VANGORP, J., MOONEN, M., AND VERDILEN, J. A low complexity branch and bound approach to optimal spectrum balancing for digital subscriber lines. In *IEEE Global Telecomm. Conf.* (San Francisco, USA, 2006).
- [101] TSIAFLAKIS, P., VANGORP, J., VERLINDEN, J., AND MOONEN, M. Multiple access channel optimal spectrum balancing for upstream DSL transmission. *IEEE Commun. Lett.* 11, 4 (2007), 398–400.
- [102] VANBLEU, K. *Advanced Equalization Techniques for DMT-based systems*. PhD thesis, KU Leuven, 2004.
- [103] VENTURINO, L., PRASAD, N., AND WANG, X. Coordinated linear beamforming in downlink multi-cell wireless networks. *IEEE Trans. Wireless Commun.* 9, 4 (2010), 1451–1461.
- [104] WANG, Z., AND GIANNAKIS, G. B. Wireless multicarrier communications: where Fourier meets Shannon. *IEEE Signal Processing Magazine* 17, 3 (2000), 1–17.
- [105] WOLKERSTORFER, M., JALDÉN, J., AND NORDSTRÖM, T. Column generation for discrete-rate multi-user and multi-carrier power control. *IEEE Trans. Commun.* 60, 9 (2012), 2712–2722.

- [106] WOLKERSTORFER, M., STATOVCI, D., AND NORDSTRÖM, T. Robust spectrum management for DMT-based systems. *IEEE Trans. Signal Process.* 58, 6 (2010), 3238–3250.
- [107] WUNDER, G., FISCHER, R., BOCHE, H., LITSYN, S., AND NO, J.-S. The papr problem in ofdm transmission: New directions for a long-lasting problem. *Signal Processing Magazine, IEEE* 30, 6 (2013), 130–144.
- [108] XU, Y., LE-NGOC, T., AND PANIGRAHI, S. Global concave minimization for optimal spectrum balancing in multi-user DSL networks. *IEEE Trans. Signal Process.* 56, 7 (2008), 2875 – 2885.
- [109] YU, W. Multiuser water-filling in the presence of crosstalk. In *Inf. Theory and Appl. Workshop* (San Diego, USA, 2007).
- [110] YU, W., GINIS, G., AND CIOFFI, J. M. Distributed multiuser power control for digital subscriber lines. *IEEE J. Sel. Areas of Commun.* 20, 5 (2002), 1105–1115.
- [111] YU, W., KWON, T., AND SHIN, C. Multicell coordination via joint scheduling, beamforming and power spectrum adaptation. In *IEEE INFOCOM* (Shanghai, China, 2011).
- [112] YU, W., AND LUI, R. Dual methods for nonconvex spectrum optimization of multicarrier systems. *IEEE Trans. Commun.* 54, 7 (2006), 1310–1322.
- [113] YU, W., RHEE, W., BOYD, S., AND CIOFFI, J. M. Iterative water-filling for gaussian vector multiple-access channels. *IEEE Trans. Inf. Theory* 50, 1 (2004), 145–152.
- [114] ZIDANE, R., HUBERMAN, S., LEUNG, C., AND LE-NGOC, T. Vectors DSL: benefits and challenges for service providers. *Communications Magazine, IEEE* 51, 2 (2013), 152–157.
- [115] ZOU, W. Y., AND WU, Y. COFDM: an overview. *IEEE Trans. Broadcast.* 41, 1 (1995), 1–8.

# Curriculum Vitae



Rodrigo B. Moraes was born in Belém, Brazil, in 1982. He obtained the Bachelor degree at the Federal University of Pará, Belém, Brazil, in 2005 and the M.Sc. degree at the Pontifical Catholic University, Rio de Janeiro, Brazil, in 2009, both in Electrical Engineering. Since October 2009, he is working towards a Ph.D. degree at the department of Electrical Engineering at the KU Leuven, Leuven, Belgium.

He was a visiting researcher at Ericsson's Broadband Technologies laboratories, Stockholm, Sweden, in 2006 and at the FTW Vienna, Vienna, Austria, in 2013.

Mr. Moraes received the FAPERJ *Nota Dez* Scholarship by state of Rio de Janeiro, Brazil in 2008, the IEEE Travel Grants in 2008 and the Best Paper Award in the Selected Areas in Communications Symposium at the IEEE International Conference on Communications (ICC) 2013.



# Publications

## Journal Papers

- R.B. Moraes, B. Dortschy, A. Klautau and J. Rius i Riu, “Semiblind Spectrum Balancing for DSL,” *IEEE Transactions on Signal Processing*, vol. 58, no. 7, pp. 3717-3727, July 2010
- R.B. Moraes and R. Sampaio-Neto, “Bit error rate minimising pilot symbol arrangement in closed-loop orthogonal frequency division multiplexing systems,” *IET Communications*, vol. 5, no. 14, pp. 1999-2008, Sept. 2011
- R.B. Moraes, P. Tsiaflakis, J. Maes and M. Moonen, “DMT MIMO IC Rate Maximization in DSL With Combined Signal and Spectrum Coordination,” *IEEE Transactions on Signal Processing*, vol. 61, no. 7, pp. 1756-1769, April 2013
- R.B. Moraes, P. Tsiaflakis, J. Maes and M. Moonen, “DMT MIMO IC Rate Maximization in DSL with Per-Transceiver Power Constraints,” submitted for publication.
- R.B. Moraes, P. Tsiaflakis, J. Maes and M. Moonen, “General Framework and Algorithm for Data Rate Maximization in DSL Networks,” submitted for publication.
- R.B. Moraes, M. Wolkerstorfer, P. Tsiaflakis and M. Moonen, “Dynamic Spectrum Management with Spherical Coordinates“, submitted for publication.

## Journal Papers in Preparation

- R.B. Moraes, P. Tsiaflakis and M. Moonen, “Spherical Coordinates Based Dynamic Spectrum Management with Linear Approximations”.

## Conference Papers<sup>1</sup>

- R. Moraes, B. Dortschy, A. Klautau and J. R. i Riu, “Semi-Blind Power Allocation for Digital Subscriber Lines,” IEEE International. Conference on Communications. (ICC), Beijing, China, 2008.
- R.B. Moraes, B. Dortschy, A. Klautau , R. Zampolo and J. Rius i Riu, “Optimal Solution for the Fixed Margin Problem in Digital Subscriber Lines,” International Symposium on Communications, Control and Signal Processing (ISCCSP), St. Julians, Malta, 2008.
- R.B. Moraes, P. Tsiaflakis and M. Moonen, “Dynamic Spectrum Management in DSL with Asynchronous Crosstalk,” IEEE International Confence on Acoustics, Speech and Signal Processing (ICASSP), Prague, Czech Republic, 2011.
- R.B. Moraes, P. Tsiaflakis, J. Maes, L. Van Biesen and Marc Moonen, “The Rate Maximization Problem in DSL with Mixed Spectrum and Signal Coordination,” European Signal Processing Conference (EUSIPCO), Barcelona, Spain, 2011.
- P. Tsiaflakis, R.B. Moraes, and M. Moonen, “A Low-Complexity Algorithm for Joint Spectrum and Signal Coordination in Upstream DSL Transmission,” Symposium on Communications and Vehicular Technology Benelux (SCVT), Ghent, Belgium, 2011.
- R.B. Moraes, P. Tsiaflakis and M. Moonen, “Intercarrier Interference in DSL Networks due to Asynchronous DMT Transmission,” IEEE International Conference on Acoustics, Speech and Signal Processing (ICASSP), Vancouver, Canada, 2013.
- R.B. Moraes, P. Tsiaflakis and M. Moonen, “Reduced Complexity Dynamic Spectrum Management Based on a Polar Coordinates Formulation,” IEEE International Conference on Commun. (ICC), Budapest, Hungary, 2013.

---

<sup>1</sup>The paper “Reduced Complexity Dynamic Spectrum Management Based on a Polar Coordinates Formulation” received the *Best Paper Award* on the Selected Areas in Communications Symposium at the IEEE International Conference on Communications, Budapest, Hungary, 2013.

## Patents

- R.B. Moraes, A. B. R. Klautau, Jr., R. F. Zampolo, B. Dortschy and J. Rius i Riu, “Methods and arrangements in a digital subscriber line network,” published as WO2008118048A1, EP2137919A1 and US8295151.
- R.B. Moraes, A. B. R Klautau, Jr., R. F. Zampolo, B. Dortschy and J. Rius i Riu, “Methods and arrangements for power minimization in a multi-tone transmission-based communication system,” published as WO2008044975A1, EP2074776B1 and US8238545.





FACULTY OF ENGINEERING SCIENCE  
DEPARTMENT OF ELECTRICAL ENGINEERING  
STADIUS CENTER FOR DYNAMICAL SYSTEMS, SIGNAL PROCESSING AND DATA ANALYTICS  
Kasteelpark Arenberg 10 postbus 2440  
B-3001 Heverlee  
rodrigo.moraes@esat.kuleuven.be

